Comprehensive System-level Assessments of Non-combustion Products from Wastes and By-products of Oil Sands

by

Miguel Leonardo Baritto Loreto

A thesis submitted in partial fulfillment of the requirements for the degree of

Doctor of Philosophy

in

Engineering Management

Department of Mechanical Engineering

University of Alberta

Abstract

Non-combustion products, i.e., those not burned for energy production, have the potential to diversify and enhance the resilience of the oil sands industry in anticipation of reduced fuel demand due to the ongoing decarbonization of the economy. Despite the significance of this transition, there are very few economic and environmental performance assessments of the production processes at a commercial scale. Such information is crucial for the development of an industry centered around non-combustion products. The primary objective of this thesis is to evaluate the economic feasibility and greenhouse gas (GHG) emissions associated with the production of non-combustion products. Techno-economic and life cycle GHG emissions assessments were conducted for three non-combustion products derived from different wastes and by-products of the extraction and processing of oil sands bitumen. Vanadium, obtained from the spent catalysts and petcoke generated during bitumen upgrading, heavy minerals (zircon and titanium minerals) concentrated in froth treatment tailings, and carbon fiber made from asphaltene after bitumen deasphalting were analyzed.

Available experimental data was used to scale up the production processes from laboratory scale to commercial operation. First principles were applied to complete the material and energy balances of each relevant operation. The main equipment was sized, and energy consumption was estimated using empirical correlations and information from vendors and manufacturers. With this information, the capital cost of the production processes was calculated. Feedstock, utilities, labor-related, and facility-related costs make up the operating costs. A technoeconomic assessment was performed to estimate the production cost or the internal rate of return (IRR) of the processes. Plant capacities for a base case were defined

based on the current generation rate of wastes and by-products, and economies of scale benefits were assessed, among other scenarios.

The scope of the life cycle GHG emissions assessment was cradle-to-gate. The boundary system includes the upstream operations from bitumen extraction up to the generation of the waste of the by-product that feeds the production process of the non-combustion products; upstream emissions associated with the production of consumables and the electricity used in the process; and process emissions from the combustion of fuels to provide heat to the process and from the transformation of the feedstock into the final non-combustion product.

Recovering vanadium from hydroconversion spent catalyst would cost \$9.89/kg V_2O_5 and emit 10.3 kg CO_2eq/kg V_2O_5, while doing so from petcoke fly ash would cost \$18.77/kg V_2O_5 and generate 26.6 kg CO_2eq/kg V_2O_5. The production cost of asphaltene-based carbon fiber (ACF) was estimated to be \$10.16/kg ACF and life cycle GHG emissions to be 16.2 kg CO_2eq/kg ACF. Both metrics outperform those of polyacrylonitrile (PAN)-based carbon fiber, which represents about 90% of all the carbon fiber produced worldwide. The IRR of recovering heavy minerals from froth treatment tailings would be 9.8%, considering the current market price of zircon, titanium minerals, and residual bitumen recovered in the process. Life cycle GHG emissions would be 1,499 kg CO_2eq/t heavy minerals.

The models developed in this study are based on assumptions that introduce uncertainty into the estimated costs and GHG emissions, either because process data unavailability at a commercial scale or because the volatility of economic and GHG emissions factors over the life cycle of the products. Monte Carlo simulations were performed to calculate the more likely range of variation of the model's outputs considering the variability of the inputs. In addition, sensitivity analysis was conducted to identify those variables that should be

estimated more accurately to reduce the uncertainty of the results. This research provides valuable insights into the economic and environmental feasibility of targeted non-combustion products from oil sands, assisting stakeholders, including oil sands operators, waste management companies, researchers, government, and investors in making informed decisions on this activity in Alberta. The results of the study also provide information to the government for policy formulation. The study framework can be adapted to evaluate the performance of other non-combustion products from oil sands wastes and by-products.

Preface

This thesis is an original intellectual work by Miguel Baritto under the supervision of Dr. Amit Kumar.

Chapter 2 of this thesis was published as M. Baritto, A.O. Oni, A. Kumar. The development of a techno-economic model for the assessment of vanadium recovery from bitumen upgrading spent catalyst. Journal of Cleaner Production. 2022, 20:132376. I was responsible for the conceptualization, data curation, formal analysis, investigation, methodology, validation, and writing the original draft. A.O. Oni and A. Kumar provided guidelines in conceptualization, validation, formal analysis, and review and editing. A. Kumar was also responsible for funding acquisition and supervision.

Chapter 3 was submitted to Fuel (March 06, 2024) as M. Baritto, A.O. Oni, A. Kumar. Life cycle GHG emissions assessment of vanadium recovery from spent catalysts from bitumen upgraders. I was responsible for the conceptualization, methodology, formal analysis, and writing the original draft. A.O. Oni provided support on conceptualization, methodology, validation, and review and editing. A. Kumar was the supervisory author, provided resources, acquired funds, and reviewed and edited the final draft.

Chapter 4 was submitted to Waste Management (July 02, 2024) as M. Baritto, A.O. Oni, A. Kumar. Vanadium recovery from oil sands petcoke fly ash: a comprehensive techno-economic assessment. I was responsible for the conceptualization, methodology, formal analysis, and writing the original draft. A.O. Oni provided support on conceptualization, methodology, validation, and review and editing. A. Kumar was the supervisory author, provided resources, acquired funds, and reviewed and edited the final draft.

Chapter 5 was published as M. Baritto, A.O. Oni, A. Kumar. Life cycle GHG emissions assessment of vanadium recovery from bitumen-derived petcoke fly ash. Journal of Environmental Management. 2024, 363:121377. I was responsible for the conceptualization, methodology, formal analysis, and writing the original draft. A.O. Oni provided support on conceptualization, methodology, validation, and review and editing. A. Kumar was the supervisory author, provided resources, acquired funds, and reviewed and edited the final draft.

Chapters 6 and 7 have not been published.

Chapter 8 was published as M. Baritto, A.O. Oni, A. Kumar. The development of a techno-economic model for the assessment of asphaltene-based carbon fiber production. Journal of Cleaner Production 2023. 428:139489. I was responsible for the conceptualization, methodology, data curation, formal analysis, and writing the original draft. A.O. Oni provided support for conceptualization, methodology, validation, and review and editing. A Kumar supervised the study and was responsible for resources and funding acquisition.

Chapter 9 was published as M. Baritto, A.O. Oni, A. Kumar. Estimation of life cycle greenhouse gas emissions of asphaltene-based carbon fibers derived from oil sands bitumen. Sustainable Materials and Technologies 2023. 36:e00627. I was responsible for the conceptualization, methodology, data curation, formal analysis, and writing the original draft. A.O. Oni provided support for conceptualization, methodology, validation, and review and editing. A Kumar supervised the study and was responsible for resources and funding acquisition.

To Miguel Eduardo and Victor Miguel,

with love

Acknowledgements

I extend my sincere gratitude to my supervisor, Prof. Amit Kumar, for providing me with the opportunity to be part of his research group. His mentorship and guidance have been instrumental throughout my program.

I am deeply thankful to Dr. Abayomi Olufemi Oni for his support during this research journey. His insightful feedback and meticulous review of manuscripts and significantly enhanced the quality of the research. Beyond being a collaborator, Femi provided invaluable guidance throughout my experience as a PhD student.

I acknowledge the NSERC/Cenovus/Alberta Innovates Associate Industrial Research Chair in Energy and Environmental Systems Engineering and the Cenovus Energy Endowed Chair in Environmental Engineering for providing financial support for this study. The author is also grateful to NSERC Alliance Grant Program in Integrated Assessment of Energy Systems for the financial support. As a part of the University of Alberta's Future Energy Systems research initiative, this research was made possible in part thanks to funding from the Canada First Research Excellence Fund. Also, I thank Alberta Innovates for the financial support. The author is also grateful to the representatives from Cenovus Energy Inc., Suncor Energy Inc., Alberta Innovates Natural Resources Canada (NRCan), Alberta Energy and Minerals (AEM) and Environment and Climate Change Canada (ECCC) Energy for their inputs and comments during the course of this study. This research was undertaken, in part, thanks to funding from the Canada Research Chairs Program. This funding was provided in support of the Canada Research Chair in Assessment of Energy Systems (Tier-1).

Special thanks go to Dr. Eskinder Gemechu for his expert guidance in life cycle assessments and to Astrid Blodgett for her meticulous editing of my manuscripts and this thesis.

I am immensely grateful to my parents, Miguel Baritto and Magaly Loreto. Their constant belief in me and the education they provided enabled me to achieve one of my greatest academic goals. I would also like to express my appreciation to my aunt Aura Baritto for her support during my bachelor's and master's studies, and to my grandmother, Ela, for her prayers.

Finally, heartfelt thanks to my wife, Joanna Infante, whose constant support has been a presence since my undergraduate days. She has never doubted my success and continues to inspire me to become the best version of myself. Gracias por acompañarme en esta aventura.

Table of contents

List of tables

List of figures

List of abbreviations

ACF	asphaltene-based carbon fiber
ACN	Acrylonitrile
ADU	atmospheric distillation unit
AMV	ammonium metavanadate
AR	atmospheric residue
Asp.	Asphaltene
Capex	capital cost
CEPCI	Chemical Engineering Plant Cost Index
CF	carbon fiber
DAO	deasphalted oil
DCF	discounted cash flow
DOE	U.S. Department of Energy
DRU	diluent recovery unit
DVL	diluent volume lost per volume of bitumen produced
E&M	electrostatic and magnetic
EAF	electric arc furnace
ES	electrostatic separation
FCC	fluid catalytic cracking
FCI	fixed capital investment
FOB	free-on-board
FTT	froth treatment tailings
FU	functional unit

G&A	general and administrative cost
GF	green fiber
GHG	greenhouse gas
GREET	Greenhouse gases, Regulated Emissions, and Energy use in Technologies
HM	heavy minerals
HMC	heavy minerals concentrate
HMCP	heavy minerals concentration plant
HMSP	heavy minerals separation plant
HT	high temperature
IRR	internal rate of return
ISBL	inside battery limit
LCA	life cycle assessment
LF	location factor
LHSV	liquid hourly space velocity
LT	low temperature
Mbbl	millions of barrels
MDA	Mineral Development Agreement
MEA	Monoethanolamine
MHF	multiple hearth furnace
MRT	molecular recognition technology
MS	magnetic separation
M&S	Marshall and Swift equipment cost index

NFT	naphthenic froth treatment
NiMo	nickel molybdenum
NPV	net present value
NRU	naphtha recovery unit
O/A	organic solution to aqueous solution ratio
ORNL	Oak Ridge National Laboratory
OSBL	outside battery limit
PAN	Polyacrylonitrile
PAN-CF	PAN-based carbon fiber
PLS	pregnant leach solution
R&D	research and development
REE	rare earth elements
RUST	Regression, Uncertainty, and Sensitivity Tool
SAGD	steam-assisted gravity drainage
SCO	synthetic crude oil
SDA	solvent deasphalting
SELEX:-Asp	selective separation of asphaltenes
SP	softening point
TRL	technology readiness level
VDU	vacuum distillation unit
VGO	vacuum gas oil
Vis.	Visbreaking
VR	vacuum residue

VRFB	vanadium redox flow battery
VTM	vanadium titano-magnetite
WC	working capital
wppm	weight parts per million

Chapter 1: Introduction

1.1 Background

Oil sands are a mixture of sand, water, and bitumen, a highly viscous crude oil. The oil sands deposits are found primarily in Alberta, Canada. Other major oil sands deposits are found in Venezuela and Russia, and small reserves are found in the United States, Nigeria, Madagascar, Congo, and elsewhere. Alberta's oil sands deposits are located at the north of the province, near Athabasca, Cold Lake, and Peace River, and with 165 billion barrels, represent the third largest reserves of oil in the world (Government of Alberta 2017). The oil sands' value chain begins with the production of bitumen, either by surface mining and bitumen extraction or by in situ production through deep wells. The product of these operations is heavy sour bitumen which has high viscosity. It is combined with diluents to lower the viscosity which is named dilbit. Bitumen can be refined to produce fuel products in high-conversion refineries. Alternatively, and with the aim of adding value to bitumen, it can be upgraded to a light synthetic crude oil (SCO). Because of its higher quality, SCO can be refined in conventional refineries to produce fuels. Currently, about three million barrels of bitumen per day are produced in Alberta, 65% of it sold for refining and the remaining 35% upgraded to produce SCO (Alberta Energy Regulator 2018). Despite being one of the largest oil producers in the world, Alberta's bitumen costs more than conventional crude oils (Government of Alberta 2023) for three main reasons: quality (high sulfur content, low API gravity), marketability (scarcity of high-conversion refineries), and logistics (lack of pipelines for transportation). This situation represents an economic constraint for the oil sands industry.

Exploring high-potential, non-combustion products from the oil sands is relevant for Canada and Alberta. First, such products would diversify the province's economy, which currently relies on the production of bitumen that is converted into combustion products like gasoline, diesel, and other types of fuels; and second, non-combustion products would support the oil sands industry by increasing its ability to manage periods of increased bitumen production or offsetting a decrease in demand for fossil fuels driven by the decarbonization of the economy (Stantec Consulting Ltd. 2018), and ultimately, helping to overcome the price differential at which bitumen in currently sold. Because the production of these alternative products would be a side activity in the oil sands industry, the business case must unquestionably show the added value to oil sands operations. It is necessary, therefore, to evaluate the economic feasibility of the production processes and the potential benefits of the products. Bitumen production, upgrading, and refining, moreover, are greenhouse gas (GHG)-intensive activities (Bergerson et al. 2012; Nimana et al. 2015b; 2015a), contributing with about 11% of Canada's carbon footprint (Government of Canada 2023b). A comprehensive life cycle GHG assessment is required, therefore, to understand how the production of non-combustion products would contribute to increase or reduce the GHG impact of oil sands operations. This research addresses both issues through techno-economic analysis (TEA) and life cycle assessment (LCA) of the production of non-combustion products. Vanadium, titanium, and zirconium have been identified as non-combustion products from oil sands with moderate to high long-term market potential (Meisen 2017; Stantec Consulting Ltd. 2018). The production of bitumen-derived asphaltene-based carbon fiber is also considered to be of potential interest for industry. Therefore, the recovery of metals and valuable minerals from oil sands wastes and by-products, and the production of bitumen-derived asphaltene-based carbon fiber, are the focus of this study, but the framework developed can be used to assess the feasibility of other non-combustion products.

Vanadium, titanium, and zirconium are widely used in several industries, from construction to military, chemical, and energy. Vanadium is primarily obtained from ores, metallurgical slags, concentrates, and petroleum residues. A significant amount of vanadium is recycled from spent catalyst, fly ash, and steel scrap (Petranikova et al. 2020). About 90% of vanadium produced worldwide is used to obtain ferrovanadium, an additive employed in the manufacturing of steel alloys. The balance is used in the chemical industry, mainly in the form of vanadium pentoxide (V_2O_5) (2021). China controls the market, because it dominates not only the vanadium ores (largest reserves and imports), but also the supply of V_2O_5 and ferrovanadium. Rising demand for renewable intermittent energy, e.g., solar and wind, requires a subsequent growth in energy storage devices. In that sense, vanadium redox flow batteries (VRFBs) emerge as a potential reliable, cost-effective solution because of their great performance in long-duration applications and longevity. One of the challenges for VRFBs is the availability of vanadium, which, as mentioned above, is influenced by the steel industry. Moreover, despite the abundancy of vanadium in nature, the world’s resources are mainly concentrated in four countries (China, Russia, South Africa, and Australia) (U.S. Geological Survey 2022), suggesting a potential supply risk for traditional and emerging applications (Ciotola et al. 2021; Rodby et al. 2023).

Titanium metal is a strong lightweight structural material for aerospace, automotive, military and construction industries, as well as for medical and dental prostheses and implants, manufacturing of sport implements and jewelry, and electronic devices. Also, titanium is widely used as a catalyst in several chemical and industrial processes and is a common white pigment in paints, printing inks, soaps, plastics, cosmetics, and even food. Titanium is obtained from minerals such as rutile, ilmenite, anatase, sphene, and altered ilmenite (commonly called leucoxene). These minerals, especially rutile and ilmenite, are processed to obtain titanium dioxide (TiO_2), which is used as feedstock to manufacture pigments or to produce titanium metal and welding rods flux wire cord. Zirconium is used mainly as an opacifier in surface glazers and pigments, refractories, and metallurgical furnaces. It is also used in paper coatings, paint driers and catalysts, in the structure of nuclear reactor cores, steel production, and jewelry. The most important source of zirconium is the mineral zircon (ZrSiO4), which can be used directly to produce ceramics, or processed to obtain zirconium dioxide, or zirconia (ZrO_2). In general, titanium and zirconium minerals are co-produced by mining hard-rock deposits or processing mineral sands. Titanium is an abundant material in nature; however, about 64% of the world reserves are in Australia, China, and India. South Africa and Australia produce the most titanium minerals, closely followed by China (U.S. Geological Survey 2022). Unlike titanium, zirconium is scarce. Australia (70%) and South Africa (21%) control the world reserves (U.S. Geological Survey 2022). Demand for zirconium is increasing because of the growing use of zircon in foundries and refractories (Mordor Intelligence 2018; Perks and Mudd 2019), as well as in the telecommunication and energy sectors (Zhu et al. 2023).

Vanadium is found in the bitumen phase of oil sands, whereas titanium and zirconium minerals are in the sand phase. With 2.4 million tonnes of mined oil sands and a total production of 3 million barrels of bitumen per day (Alberta Energy Regulator 2023a), Alberta’s oil sands have the potential to produce 33,000 tonnes of vanadium, 282,000 tonnes of zirconium, and 3.1 million tonnes of titanium[1] , equivalent to 45%, 19%, and 46% of the world's mine production, respectively (U.S. Geological Survey 2022). Vanadium is distributed differently in the oil sands industry than titanium and zirconium are. Vanadium is carried in the bitumen and removed during upgrading, and therefore it is concentrated in the wastes and by-products of that process, such as petcoke and hydroconversion spent catalysts. The other two are concentrated in the centrifuge tailings of the bitumen extraction process, in which bitumen is separated from the sand.

Carbon fiber is a material with a high strength-to-weight ratio that can potentially replace aluminum and steel as structural material, for example in lightweight vehicles. Carbon fiber is obtained from a carbon precursor. Currently, about 90% of the carbon fiber produced in the world is made from polyacrylonitrile (PAN), and the balance is obtained from rayon or petroleum pitch (Morgan 2005; Bajpai 2021a). The United States, Western Europe, China, and Japan are the principal producers of carbon fiber (Das et al. 2016). The high cost of carbon fiber is a barrier for massive implementation (Bajpai 2021b). PAN production accounts for about half the production cost, and the conversion from PAN to carbon fiber makes up the rest (Warren 2014). The development of low-cost precursors is key to achieve the cost reduction required to increase the use of carbon fiber. Asphaltenes are the heavy fraction of bitumen and crude oil that is not soluble in n-heptane (Redelius 2011). Asphaltenes are complex molecules that impart high viscosity to bitumen and crude oil; therefore, they are removed during upgrading and refining to improve the quality of the final

---

[1] Based on concentrations of 190 wppm of vanadium [27], 0.35 wt.% of titanium, and 0.032 wt.% of zirconium [56] in oil sands.

product. Asphaltenes can also be removed from bitumen in the field to match pipeline specifications while lowering the requirement of diluent for transportation to downstream upgraders and refineries (Gray 2019). This approach is called partial upgrading, and its implementation is under research in Alberta's oil sands industry (Keeson and Gieseman 2018; Gray 2019). Currently, asphaltene derived from oil sands bitumen has very limited use, therefore it is seen as a low-value by-product or even as a waste. Because of its high carbon content (>80 wt.%) and relatively low cost, asphaltenes are considered as a potential raw material for carbon fiber production (Stantec Consulting Ltd. 2018). With an asphaltene content between 14 and 17 wt.% (Gray 2015; Gray 2019), and a production near of 3 million barrels per day (Alberta Energy Regulator 2023a), Alberta oil sands bitumen has the potential to become the principal supplier of asphaltene-based carbon fiber.

1.2 Literature review and research gap

Several processes for the recovery of metals and heavy minerals from oil sands by-products and wastes are reviewed or described in the literature. For instance, Feng (Feng 2017) proposed a process for the recovery of vanadium directly from oil sands petcoke, while Jack et al. (Jack et al. 1979; 1980), McCorriston (McCorriston 1984), Griffin and Etsell (Griffin and Etsell 1984), Holloway and Etsell (Holloway and Etsell 2004; 2005), Holloway et al. (Holloway et al. 2005), Gomez-Bueno et al. (Gomez-Bueno et al. 1981), and Lakshmanan et al. (Lakshmanan et al. 1989) developed hydrometallurgy routes for the recovery of vanadium from fly ash produced by the combustion of oil sands bitumen-derived petcoke. The results of those studies suggest that only traces of vanadium can be extracted directly from the petcoke generated in the upgrading of oil sands bitumen, irrespective of the extraction method used. On the other hand, vanadium in petcoke fly ash is leachable with a proper combination of roasting additives and leaching agents. Although the technical feasibility of recovering vanadium from petcoke fly ash has been proven, little can be said about the economic feasibility and GHG emissions of the process. Holloway and Etsell developed a process flow sheet for vanadium recovery from delayed coker petcoke fly ash (Holloway and Etsell 2005). The process is based on roasting with sodium chloride followed by water leaching, precipitation of ammonium metavanadate, and production of vanadium pentoxide by calcination. The proposed process also includes the decarbonization of the ash prior to roasting, a desilication step to reduce the silicon content in the final vanadium product, the recovery and recycling of sodium chloride to the roasting operation, and the treatment of the off-gases from the decarbonization and roasting to obtain diverse chloride by-products that improve the economics of the process. These studies present a preliminary economic analysis of the process and conclude that the activity is potentially profitable. However, few details on the economic assumptions were included, so it is hard to determine the validity of the conclusions for the current market conditions. The GHG emissions of the proposed process were not considered in that study. No other study found in the literature review considered the economics or carbon footprint of the process in its scope.

Recovering vanadium from spent catalyst generated in oil refining has been widely studied. Furimsky, Marafi et al., and Zeng and Cheng provide comprehensive reviews on this topic (Furimsky 1996; Zeng and Cheng 2009a; 2009b; Akcil et al. 2015; Marafi et al. 2017), and details of commercial processes are provided by Marafi et al., Akcil et al., Llanos and Deering, and Berrebi et al. (Berrebi et al. 1993; Llanos and Deering 1998; Akcil et al. 2015; Marafi et al. 2017). Published studies on the recovery of vanadium from oil spent catalyst tend to generate experimental data at the laboratory scale, mainly for the central operations, and include a process flowsheet based on the results. However, there is very limited discussion on the feasibility of the whole process. General ideas on the economics of these processes are found in the literature. Marafi et al. (Marafi and Stanislaus 2003) and El-Nady et al. (El-Nadi et al. 2009) mention that the metal content on the spent catalyst and world metal prices affect the feasibility of the recovery process, but they do not provide any information on the assessment of these processes. For catalysts with high vanadium content, recovery processes could be economically attractive, as suggested by Dufresne (Dufresne 2007), but the conditions for that, specifically from bitumen upgrading operations, have not been discussed, nor has the recovery cost estimate been assessed. In addition, there is limited discussion on the processes at an industrial scale and their GHG emissions. In this regard, the Greenhouse gases, Regulated Emissions, and Energy use in Technologies (GREET) model includes a module for the treatment of spent catalysts (Wang et al. 2015). The considered feedstock is a blend of Mo/Ni/Al spent catalyst from different refineries. The process for metal recovery includes roasting, grinding, vanadium and molybdenum recovery, the fusing of alumina, and water pretreatment. The estimated GHG emissions using that model are 3.04 kg CO_2/kg spent catalyst, which includes direct emissions from coke burn-off. The GREET model offers results at a high level but not at the process level. AMG Vanadium, a spent catalyst processor based in the United States, runs a pyrometallurgy process to obtain ferrovanadium from refinery spent catalyst. The company reports process emissions of 12.6 kg CO_2/kg FeV and claims a reduction of 80% compared with the emissions from primary production (AMG Vanadium). No details on the recovery process nor the methods used for GHG emissions estimation are provided on AMG Vanadium's website.

Diverse processes for the recovery of heavy minerals from FTT have been developed over the years, but only a few have been subjected to tecno-economic analysis. Ciu et al. review processes for the recovery of zirconium and titanium minerals from oil sands tailings (Ciu et al. 2013). Earlier studies considered deoiling by burning off the residual bitumen from FTT, whether as-received (Baillie et al. 1976; Trevoy et al. 1978) or after a first stage of concentration (H.A. Simons Ltd. 1996; Owen and Tipman 1999; Bulatovic 2000; Oxenford et al. 2001; Chachula and Liu 2003). The drawbacks of this deoiling method are twofold. First, the physical characteristics of the heavy minerals (e.g., magnetic susceptibility) may be altered during roasting, affecting the downstream separation processes and altering the grade of the concentrate (Ciu et al. 2013). Second, the generation of emissions: burning the residual bitumen produces greenhouse gases (GHG), and thermal decomposition of secondary minerals such as pyrite would generate SO_2 emissions. More recent studies implement a combination of gravity separation and solvent extraction (attritioning and settling) for deoiling (Reeves 2008; Erasmus et al. 2010; Moran and Chachula 2014)). This deoiling method does not present the inconveniences of tailing roasting, but it does increase the complexity of the process because of the solvent handling. Schutte [cited in (Ityokumbul et al. 1987)] estimated the capital and production costs of a recovery plant with recovery efficiencies of 70%, 80%, and 33% of Ti, Zr, and Fe minerals, respectively. However, the breakdown of this recovery cost was not reported.

Alberta's 1996 Mineral Development Agreement (MDA) final report includes details, drawings and flowsheets of a plant sized to recover heavy minerals from centrifuge tailings of Suncor and Syncrude 1994 operations (H.A. Simons Ltd. 1996). Capital, operating, and production costs were estimated. In addition to the production of concentrates, that study considered the production of high-value products like synthetic rutile and pigments. Besides the outdated information, the main drawback of the MDA report is the recovery process considered, which considers roasting as the means for deoiling. This deoiling route is unlikely to be used on a commercial scale given the global efforts to reduce GHG emissions. Titanium Corporation (now CVW Cleantech Inc.) has developed a commercial-ready technology for the recovery of bitumen, solvent, water, titanium, zirconium, and rare earth elements from oil sands FTT, and is planning to operate a concentrator plant and a mineral separation plant in the Horizon site operated by Canadian Natural Resources Ltd. (Titanium Corporation Ltd. 2019). Moran et al. estimated the expected revenues and capped the operating cost of the project (Moran et al. 2016), while, in a recent study, CVW Cleantech Inc. present the expected revenue, capital, and operating cost of a mineral recovery plant at the commercial scale (CVW Cleantech Inc. 2023). Other than this corporate study, there are no studies on the economics of recovering heavy minerals from FTT.

Tailing ponds are a significant source of GHG emissions, mainly methane via microbial methanogenesis (Holowenko et al. 2000). Carbon dioxide is also found in the gas bubbling up from tailing ponds. Mechanisms like aerobic biodegradation and the catabolic process occurring in the bitumen film on the ponds' surface are the reasons for the CO_2 emissions (Burkus 2014a; Small et al. 2015). Inhibiting methanogenesis in situ is one option to reduce the GHG emissions from tailing ponds (Allam et al. 2023). Another option is to remove part of the residual diluent and bitumen in the tailings before entering the tailing ponds, which can be achieved as a side benefit of recovering titanium and zirconium minerals from FTT (Moran et al. 2016). CVW Cleantech Inc. estimated the GHG reduction from diverting diluent and bitumen from tailing ponds, as well as the process GHG emissions from the recovery of heavy minerals from FTT (CVW Cleantech Inc. 2023). However, there is limited data on the net effect of these activities on the GHG emissions, especially from a life cycle perspective.

Regarding the production of bitumen-derived ACF, the technology is in a very early stage of research, so a few published studies focus on process development and the generation of laboratory-scale data. Limited information about expected production costs and GHG emissions on a commercial scale is available in the public domain. Regardless of the origin of the asphaltene, the general process to produce ACF is essentially the same: asphaltene modification (thermal or chemical treatment), melt spinning, stabilization, and carbonization (Leal and Penaloza 2002; Ni et al. 2019; Qin et al. 2019; Leistenschneider et al. 2021; Zuo et al. 2021a; Zuo et al. 2021b). The process resembles that of producing pitch-based carbon fiber, which is currently at a commercial scale. The research efforts concentrate on solving the following challenges in the production of carbon fiber from bitumen-derived asphaltenes: low concentration of asphaltenes in bottoms from solvent deasphalting operations (Zachariah and De Klerl 2017; Saad et al. 2022), poor spinnability and low softening point of asphaltenes (Yadav et al. 2021; Zuo et al. 2021b; De Crisci et al. 2022; Chacón-Patiño et al. 2023), lengthy stabilization process and tendency of the fiber to fuse during this operation (Leistenschneider et al. 2021; Zuo et al. 2021a), and low mechanical properties compared to PAN-CF (Chen 2021; Saad et al. 2022).

Based on the price of asphaltene sold at a market price of coal and on a very rough estimation of capital and operation costs, Stantec Consulting Ltd. (2018) presented a business case for the production of bitumen-derived ACF in Alberta. Arya (2020) estimated a production cost of \$5.03/kg CF using capital and operation costs available for PAN-CF production and an asphaltene-carbon fiber conversion efficiency of 45%. These studies make the idea of bitumen-derived ACF production compelling; however, they were based on generic assumptions and are not process-specific. In a recent study, Al Bari et al. (2023) presented an economic and environmental assessment of ACF, based on their own laboratory-scale data. They estimated a production cost of \$6.64/kg for a 2,000 tonnes per year line. However, the capital cost estimate was based on PAN-CF lines rather than more suitable equipment for ACF. Also, the effect of the plant size on the production cost was not assessed in that study. Bisheh and Abdin (2023) discussed the market potential of bitumen-derived ACF as an alternative to other fiber-reinforced composites. In the analysis, the authors assumed an ACF production cost lower than PAN-CF and Kevlar fiber, and comparable to glass fiber; however, no details were provided. More detailed cost estimation is required to determine the potential profitability of this activity.

Regarding the environmental impact of bitumen-derived ACF, Arya (2020) developed a high-level life cycle assessment to estimate the GHG emissions of a carbon fiber plant. Arya's results showed an ACF GHG emissions value of 29.1 kg CO_2/kg CF. However, this result can be misleading because the author used the emission factors of PAN-based carbon fiber as proxy data to estimate the GHG emissions of ACF production. Furthermore, Arya reported upstream emissions associated with bitumen production and asphaltene separation but did not define the system boundary nor enumerate the unit operations involved in the processes. Al Bari et al. (2023) performed a cradle-to-gate LCA of bitumen-derived ACF and estimated GHG emissions between 7.46 and 14.71 kg CO_2eq/kg CF. The main drawbacks of that study are not accounting for off-gas emissions and the exclusion of an off-gas abatement system. Also, some simplifications could lead to underestimating the emissions; for instance, considering the constant specific heat of materials and gases coming out stabilization and carbonization operations, which are performed in a wide range of temperatures, and assuming a nitrogen-to-carbon fiber ratio of 1.0 kg N_2/kg CF in the carbonization operation, when for commercial equipment such a ratio can be as high as 6.0 to 12 kg N_2/kg CF (Stry 2012; Harper International N.d.).

In summary, studies on the production of non-combustion products from oil sands tend to generate experimental data at a laboratory scale, mainly for the core unit operations. However, the feasibility of the whole process is often left out. Aspects like recovery cost, including capital and operating costs, are not included, or, in the best case, are outdated or aggregated; or the financial assumptions are not clear. The effect of the plant capacity on the expected production cost is another important aspect that has not been well addressed in the available literature. The assessment of the environmental impact of the production processes is very limited in the public domain. The estimation of GHG emissions for some of the considered processes can be found in non-peer reviewed literature. The information from such sources is not comprehensive and usually does not include detailed results, therefore it is not possible to identify the main GHG sources, which is critical to optimize/modify the process and reduce emissions at a commercial scale. In addition, an assessment of the GHG emissions from a life cycle perspective is needed to compare the production of non-combustion products from oil sands with the incumbent pathways and understand potential tradeoffs and benefits of such activities. The aim of this research was to bridge these research gaps.

1.3 Research objectives

The general objective of this research is to develop data-intensive techno-economic and LCA models to evaluate the economic and environmental feasibilities of the production of non-combustion products, e.g., vanadium, heavy minerals, and carbon fiber, from wastes and by-products of the extraction and processing of oil sands bitumen. The specific objectives of this research are to:

- Identify suitable processes for the production of the targeted non-combustion products;
- Develop mathematical models of the identified production processes;
- Evaluate the economic feasibility of the targeted non-combustion products by estimating either the production cost or the internal rate of return;
- Evaluate the economies of scale benefits of the production processes for a wide range of plant capacities;
- Develop material and energy inventories for all the cradle-to-gate life cycle stages of the production of the targeted non-combustion products;
- Estimate the net cradle-to-gate life cycle GHG emissions of the production of the targeted non-combustion products;
- Perform sensitivity and uncertainty analyses to identify key input parameters and provide a likely range of production costs and GHG emissions.

1.4 Scope and limitations

The focus of this study is the production of vanadium, heavy minerals, i.e., zircon and titanium minerals, and carbon fiber from wastes and by-products of bitumen extraction and processing. Where applicable, the effect of co- and by-products of the production process were included in the techno-economic and GHG emissions assessments.

The oil sands waste and by-products considered in this study are centrifuge tailings from bitumen extraction operations as source of heavy minerals; delayed petcoke from bitumen thermal conversion operations and spent catalyst from bitumen hydroconversion units as sources of vanadium; and residue from bitumen deasphalting operations as source of asphaltenes for carbon fiber production.

The production cost of each non-combustion product was estimated using the discounted cash flow (DCF) method. The annual cash flow calculation includes capital and operation costs and revenues from products and co-products of the processes. The system boundary for the LCA includes all operations from bitumen production and extraction to bitumen process to production of non-combustion products. The production of consumables, electricity, and natural gas combustion was also included in the system boundary.

The developed process models are based on process flow diagrams and limited to available data from the literature. Some data regarding equipment cost and energy consumption was retrieved from published sources or provided by vendors and manufacturers. For low technology readiness level (TRL) technology, e.g., asphaltene-based carbon fiber production, proxy processes and deemed suitable commercial equipment were used to model the production process at a commercial scale. Emission factors related to upstream operations, e.g., raw material and consumable, electricity, and natural gas, and material and energy costs, were taken from the literature as well.

The considered production processes were compared with incumbent and primary production processes to assess their feasibility. Cost and GHG emissions data related to those processes were taken from published sources.

This study considers Alberta, Canada as the location of the production plants; however, the developed framework is still valid for other jurisdictions after adjustment of location factor, energy costs, and emission factors.

1.5 Organization of the thesis

This paper-based thesis has ten chapters. Because each paper is self-contained, some assumptions, methods, process descriptions, and data are repeated. A summary of each chapter is found below.

Chapter 2 presents a techno-economic assessment of the recovery of vanadium from the spent hydroconversion catalyst generated during bitumen upgrading. The reference process is based on roasting, water leaching, and selective precipitation. The recovery of molybdenum, nickel, and alumina from the leaching cake was also considered in the estimation of vanadium recovery cost. Chapter 3 describes the life cycle GHG emissions estimation of vanadium recovery from the spent hydroconversion catalyst generated during bitumen upgrading. In addition to upstream and process emissions, the avoided emissions by displacing molybdenum and alumina from their primary production processes are taken account.

Chapter 4 examines the economic feasibility of recovering vanadium from delayed petcoke. Salt roasting followed by water leaching and selective precipitation were considered as the reference process. The vanadium recovery cost was estimated for different plant capacities.

Chapter 5 presents a cradle-to-gate life cycle GHG emissions estimation of the considered process, including oil sands mining, bitumen extraction, atmospheric and vacuum distillation, and delayed coking as the upstream operations to obtain petcoke, the feedstock for the vanadium recovery process.

Chapter 6 discusses the economic and environmental feasibility of recovering heavy minerals from froth treatment tailings that originate during bitumen extraction. The reference process comprises two stages: heavy mineral concentration and heavy minerals separation. Different production scenarios were considered based on whether the two stages are performed in a single plant or in different plants. The economic attractiveness of the activity was calculated for a given set of co-product market prices, including the revenue from recovering bitumen from the tailings. Chapter 7 presents a net cradle-to-gate life cycle GHG emissions assessment, considering upstream and process emissions, as well as avoided emissions by diverting tailings from tailing ponds.

Chapters 8 and 9 are dedicated to the production of bitumen-derived asphaltene-based carbon fibers. In the former, a techno-economic assessment was performed to estimate the production cost and compare it with that of PAN-based carbon fibers, the most common product in today's market. The effect of the plant capacity and tow size on the production cost were addressed. In the latter, the cradle-to-gate life cycle GHG emissions from the production of ACF were evaluated.

Chapter 10 gives conclusions and provides recommendations for future work.

Chapter 2: The development of a techno-economic model for the assessment of vanadium recovery from bitumen upgrading spent catalyst[2]

2.1 Introduction

About 90% of the vanadium produced worldwide is used in the manufacturing of ferrous and non-ferrous alloys (Perles 2014) and the balance as catalysts and oxidizers in a number of chemical processes (Inokawa et al. 2017; Li et al. 2019), in the production of glass coatings and ceramics (Hashim et al. 2019; Sharma et al. 2019), and as electrolyte in vanadium redox flow batteries (VRFB) (L'Abbate et al. 2018; Lourenssen et al. 2019). Global vanadium reserves are about 20 million tonnes and are concentrated in China (47%), Russia (25%), South Africa (17%) and Australia (10%); the world's mine production reached 73,000 tonnes in 2018 (U.S. Geological Survey 2019). Besides from ores, vanadium is recovered from petroleum residues, spent catalysts, fly ash, and slags from the iron industry (Moskalyk and Alfantazi 2003), increasing the world vanadium resources to about 63 million tonnes (U.S. Geological Survey 2019).

Vanadium demand for steel production is expected to keep growing (Perles 2014; Prophecy Development Corp. 2019), and the growth of the VRFB market is an additional demand for vanadium (Adroit Market Research 2019). Alberta is a western Canadian province and is one of the largest hydrocarbon base in North America. It has huge oil sands deposit. Oil sands

---

[2] A version of this chapter has been published as M. Baritto, A.O. Oni, A. Kumar. The development of a techno-economic model for the assessment of vanadium recovery from bitumen upgrading spent catalyst. Journal of Cleaner Production. 2022, 20:132376.

have the potential to be a major source of vanadium, helping to avoid a shortage of this material. With the vanadium content in bitumen averaging 190 wppm (Gray 2015) and a production of 3 Mbbl of bitumen per day (480,000 m^3/d) (Alberta Energy Regulator 2018), the potential for vanadium production from Alberta's oil sands is about 33,000 t/y, equivalent to 45% of the vanadium mined worldwide in 2018. Vanadium is distributed across diverse streams in the oil sands industry and is concentrated in different wastes and by-products such as petcoke (Hill et al. 2014a), spent catalyst (Gray et al. 2000; Gray 2015) and fly ash (Gomez-Bueno et al. 1981). Given the promising potential of the oil sands industry as vanadium supplier, the recovery of vanadium at the industrial scale merits consideration. In this regard, a techno-economic assessment would allow stakeholders to make informed decisions on developing this activity in regions with bitumen deposits around the world.

Catalysts are used to promote reactions in upgrading bitumen in hydroconversion and hydrotreating units; NiMo supported on alumina is the most common catalyst (Gray 2015). Because of the process conditions and the metal content in the crude oil feed, catalyst deactivates over time through coke formation and metal deposition (Marafi et al. 2017) and must be replaced by fresh catalysts. Particularly, the vanadium content in bitumen upgrading spent catalyst is high compared with spent catalyst generated during the refining of conventional oil, as shown in Table 2-1. This characteristic depicts the potential of bitumen upgrading spent catalyst as an important source of vanadium.

Table 2-1. Vanadium content in spent catalyst for processing of different crude oils

Catalyst application	Crude oil	V content (wt.%)	Reference
Hydrodesulfurization of AR	Conventional	1.50	(Lee et al. 1992)
Hydroprocessing	Conventional	0.05	(Berrebi et al. 1993)
Hydrodesulfurization	Conventional	4.04	(Zhang and Inoue 1995)
Hydrodesulfurization of AR	Conventional	6.50	(Marafi et al. 1996)
Hydrodesulfurization	Conventional	5.36	(Mulak et al. 2006)
Hydrodesulfurization of AR	Heavy oil	14.9	(Marafi and Stanislaus 2003)
Refining	Heavy oil	27.3[a]	(Villarreal et al. 1999)
Hydroconversion	Bitumen	20.8	(Gray et al. 2000)

a. Vanadium pentoxide.

There are many studies on the recovery of vanadium from oil spent catalysts, but not from bitumen upgrading catalyst. The two main routes are pyrometallurgy and hydrometallurgy. Marafi et al., Furimsky, and Zeng and Cheng provide comprehensive reviews on this topic (Furimsky 1996; Zeng and Cheng 2009a; Akcil et al. 2015; Marafi et al. 2017), and details of commercial processes are provided by Marafi et al., Akcil et al., Llanos and Deering, and Berrebi et al. (Berrebi et al. 1993; Llanos and Deering 1998; Akcil et al. 2015; Marafi et al.

2017). Pyrometallurgy routes are used mainly to produce metal alloys while hydrometallurgy routes are more suitable to obtain vanadium oxides. Among the different hydrometallurgy routes, salt-roasting and water leaching has the advantage of a low-cost leaching medium and avoid handling acid solutions than increase the complexity, cost, and environment impact of the recovery process. Published studies on the recovery of vanadium from oil spent catalyst tend to generate experimental data at the laboratory scale, mainly for the central operations, and include a process flowsheet based on the results. However, there is very limited discussion on the feasibility of the whole process. Whether to recover vanadium from the spent catalyst depends greatly on the recovery cost. However, there are very scarce information in the literature on this aspect.

General ideas on the economics of these processes are found in the literature. Marafi et al. (Marafi and Stanislaus 2003) and El-Nady et al. (El-Nadi et al. 2009) mention that the metal content on the spent catalyst and world metal prices affect the feasibility of the recovery process, but they do not provide any information on the assessment of these processes. For catalysts with high vanadium content, recovery processes could be economically attractive, as suggested by Dufresne (Dufresne 2007), but the conditions for that, specifically from bitumen upgrading operations, have not been discussed, nor has the recovery cost estimate been assessed. Sometimes the ideas are contradictory: several authors state that for hydrotreating spent catalyst, recovering metals is not profitable because the processing cost exceeds the revenue by selling the metals (Furimsky 1996; Marafi and Stanislaus 2003; Dufresne 2007). Other author claims that the high metal content in hydrodesulfurization spent catalyst makes the recovery of vanadium economically viable (Jafarinejad 2017). None of these studies provide details on the cost estimates. Moreover, in the studies related to the development of recovery routes, it is common to find claims about the economics of the proposed processes; however, no data supporting the statements are provided (Zhang and Inoue 1995; Chen et al. 2007; Mohapatra and Park 2007; Singh et al. 2018), or only rough or partial estimates are presented. For instance, Pathak et al. used experimental data from other studies to estimate the reagent costs to leach one kilogram of vanadium, nickel, and molybdenum from spent catalyst (Pathak et al. 2020). Although this study showed that sulfuric leaching is more economical than organic leaching in terms of consumables cost, little insight on the recovery cost or on the profitability of the process is included in the results. Cibati et al. developed process flowsheets for the recovery of vanadium from spent hydrotreating catalyst by acid leaching and by bioleaching (Cibati et al. 2015). They performed an economic assessment to compare both methods and found that the payback period for acid leaching is significantly shorter than that for bioleaching. Although this study provides a general idea about the economics of the recovery process, the authors acknowledged that the assessment was preliminary and had been conducted only for process comparison. Some cost components that could affect the profitability of the process were not included, for instance, process water, decoking the raw spent catalyst, and utility costs.

Stakeholders need the vanadium recovery cost estimates from different sources to understand the economics of the processes or to benchmark specific processes for the recovery of vanadium from bitumen spent catalyst. Prophesy Development Corp. reported the operating cost of producing vanadium pentoxide from ore extracted in Nevada, USA, to be $10.60 per kilogram through a heap leaching process followed by solvent extraction and precipitation (Prophecy Development Corp. 2019). Of that price, $0.85 is mining cost, which is not part of the recovery of vanadium from spent catalyst. Bushveld Minerals reported a cost of around

$8.89 per kilogram of vanadium (Bushveld Minerals 2020). The big issue with data from corporate reports is that it is not clear which cost components were included, nor what the financial assumptions were; therefore, taking these values as references is not straightforward. In a recent study, Gao et al. estimated the operating cost of producing vanadium pentoxide from vanadium slag leachate (Gao et al. 2020). In that study, the authors evaluated three processes and found operating costs of $7.71-$11.73 per kilogram of V_2O_5. Although the study included the breakdown of the cost estimate, it did not include the capital cost or the unit operations for producing the leachate. That study is not useful to stakeholders in projects for the recovery of vanadium from bitumen upgrading spent catalyst, first because the required plant would be greenfield, so a capital cost estimate is required, and second because the spent catalyst needs to be pre-treated to produce the leachate from which vanadium would be recovered. In the current study these gaps in the literature were addressed.

Efforts have been made to estimate the recovery cost of vanadium from oil sands from sources other than upgrading spent catalyst. Holloway and Etsell developed a process for the recovery of vanadium from oil sands fly ash and estimated a recovery cost of $4.57 per kilogram of V_2O_5 (Holloway and Etsell 2005). The proposed process comprises unit operations similar to those used for the recovery of vanadium from spent catalyst; however, some issues hinder the extrapolation of the results to the latter case. The recovery cost is broken down into capital and operating costs, but no details on the equipment purchase, raw material, or utility costs are presented. Also, the vanadium content in fly ash is considerably lower than in bitumen upgrading spent catalyst, therefore the unit recovery cost from the former is likely to be higher than from the latter, given the similarities in recovery processes.

In an another study, the authors performed a high-level analysis of the potential revenue from the recovery of vanadium from oil sands fly ash (Stantec Consulting Ltd. 2018). Based on the bitumen production rate, vanadium content, and ash yield, and assuming a vanadium recovery efficiency of 90%, a revenue of $13 M per year with a selling price of $12.92 per tonne of vanadium was estimated. That study provides the economic motivation for developing this activity, but since a cost estimate was not performed, it is not possible to comment on its feasibility.

Finally, decision-makers can get a sense of the cost of recovery processes by examining related studies. Marafi et al. developed a process for the rejuvenation of refinery spent catalyst (Marafi et al. 2008). Although the process is not intended for recovering metals, some of the spent catalyst pre-treatment operations are common to rejuvenation and metal reclamation. For instance, the spent catalyst is deoiled, sieved, and leached to produce a metals-rich stream suitable for metal recovery (not included in the economic assessment) and a stream for catalyst rejuvenation. Unfortunately, detailed cost estimates were not provided, so it is not possible to extract information on the operations of interest for metal recovery. Other studies provide some insight on the cost of recovery metals from oil spent catalyst including Ferella et al. (Ferella et al. 2019) (recovery of REEs from FCC spent catalyst by hydrometallurgy), Arroyo et al. (Arroyo et al. 2015) (recovery of germanium from coal fly ash by hydrometallurgy), and Yang et al. (Yang et al. 2011) (recovery of nickel from hydrogenation spent catalyst by hydrometallurgy). None of these studies conduct a techno-economic assessment of the whole value chain. In this research, these gaps in the literature were addressed as well.

The available literature on the recovery cost is insufficient to estimate the feasibility of recovering vanadium from upgrading spent catalyst. Most of the studies are incomplete techno-economic analyses of recovery processes and excludes the cost components that could affect the profitability of the activity. Other studies are based on different vanadium sources, which make their results not directly applicable to bitumen upgrading spent catalyst. Moreover, the few studies that include economic assessments report outdated costs or are not tailored to oil sands specific processes. In light of these research gaps, the recovery of vanadium from spent catalyst generated in bitumen upgrading was investigated from a techno-economic perspective. The recovery process is based on salt roasting, water leaching, and selective precipitation. First, a data-intensive process model was developed that included the recovery of main products, co-products and by-products, and emissions and effluent treatment. Then, capital and operating costs were estimated, and the recovery cost of vanadium was determined through development of a techno-economic model. The economies of scale and options for the management of solid residues from the leaching operation are discussed in this paper as well. The specific objectives of this research are to:

- Develop a techno-economic model to estimate the cost of vanadium recovery from bitumen-upgrading spent catalyst;
- Evaluate the influence of the plant capacity, as well as co-products and by-products, on the vanadium recovery cost;
- Conduct sensitivity and uncertainty analyses to assess the influence of input variations on the vanadium recovery cost;
- Conduct a case study for Alberta, a western province in Canada and a large oil sands base in the world.

2.2 Methods

2.2.1 Feedstock description

Spent catalyst is generated at diverse points along the bitumen value chain. Bitumen is produced by mining or by in situ techniques, depending on the depth of the reservoir. Regardless of the production method, the product is a diluted bitumen called dilbit, which is either sold to high-conversion refineries or upgraded to a synthetic crude oil to improve its quality before refining it. Among the existing upgrading technologies, delaying coking, hydroconversion, or a combination of both, are currently used worldwide, including Alberta. Figure 2-1 shows a simplified schematic of the bitumen upgrading process. In hydroconversion, a combination of hydrogen, heat, and catalysts is used to breakdown heavy fractions like vacuum residue, into lighter fractions. The role of hydrogen is to suppress coking, while catalysts promote hydrogenation reactions. For the hydroconversion of heavy fractions with high metal content, the catalyst must be replaced frequently because of quick deactivation and poisoning. Hydrotreating is used to remove impurities from distillates and to hydrogenate olefins and aromatics. This operation also combines temperature, hydrogen, and catalysts, but it is less severe than hydroconversion, thus the life of hydrotreating catalyst is considerably larger than hydroconversion catalyst life.

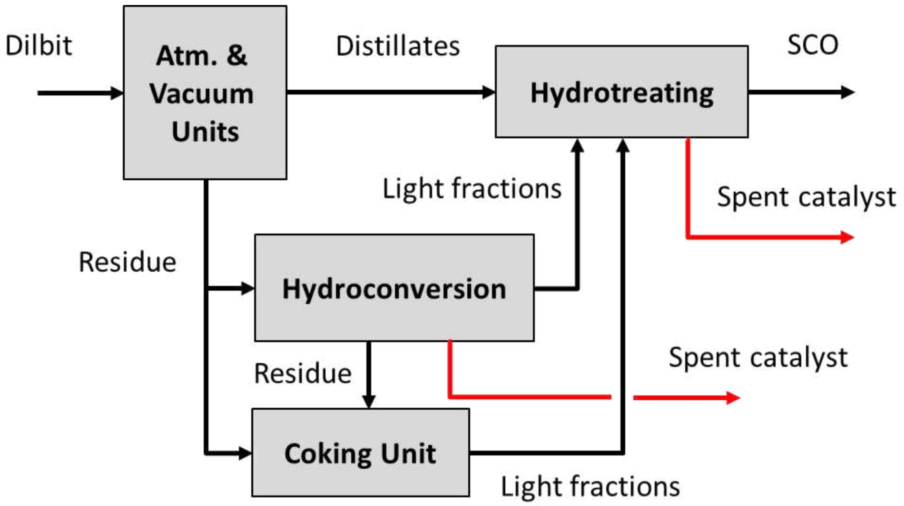

Figure 2-1. Simplified schematic of bitumen upgrading process

Hydroconversion spent catalyst is considered as feedstock in this study. This consideration relies on the availability of the resource, which is related to the catalyst replacement rate at the upgraders. Based on a liquid hourly superficial velocity (LHSV) of 0.5 h^{-1} (Ancheyta and Speight 2007) and a replacement rate of 1 wt.% daily (Gray 2015), the spent catalyst generation was estimated in this study to be 36,285 t/y from hydroconversion upgraders in Alberta. Of these, 16,353 t/y are generated at the Scotford upgrader and 14,176 t/y at the Mildred Lake upgrader. Details of the estimation are presented in Table 2-2, while the location of the upgraders in Alberta is shown in Figure 2-2.

Table 2-2. Spent catalyst generated per year in Alberta hydroconversion upgraders. Estimation is based on a LHSV of 0.5 h^{-1} (Ancheyta and Speight 2007) and a replacement rate of 1 wt.% daily (Gray 2015)

Upgrader	Configuration	Reactor feed[a]	Spent catalysts
Shell – Scotford	Hydroconversion	14,950 m^3/d VR	16,353 t/y

Upgrader	Configuration	Reactor feed[a]	Spent catalysts
Syncrude – Mildred Lake	Hydroconversion + Fluid coking	12,960 m^3/d VGO	14,176 t/y
NWR – Sturgeon	Hydroconversion + Delayed coking	2,930 m^3/d VGO	3,206 t/y
Husky – Lloydminster	Hydroconversion	2,330 m^3/d VR	2,550 t/y

a. Based on plant SCO capacity (Oil Sands Magazine), a SCO/bitumen ratio equal to 1.037 (from our research group collagues (Nimana et al. 2015c)), and a yield of 24 vol.% VGO and 38 vol.% VR (Netzer 2006).

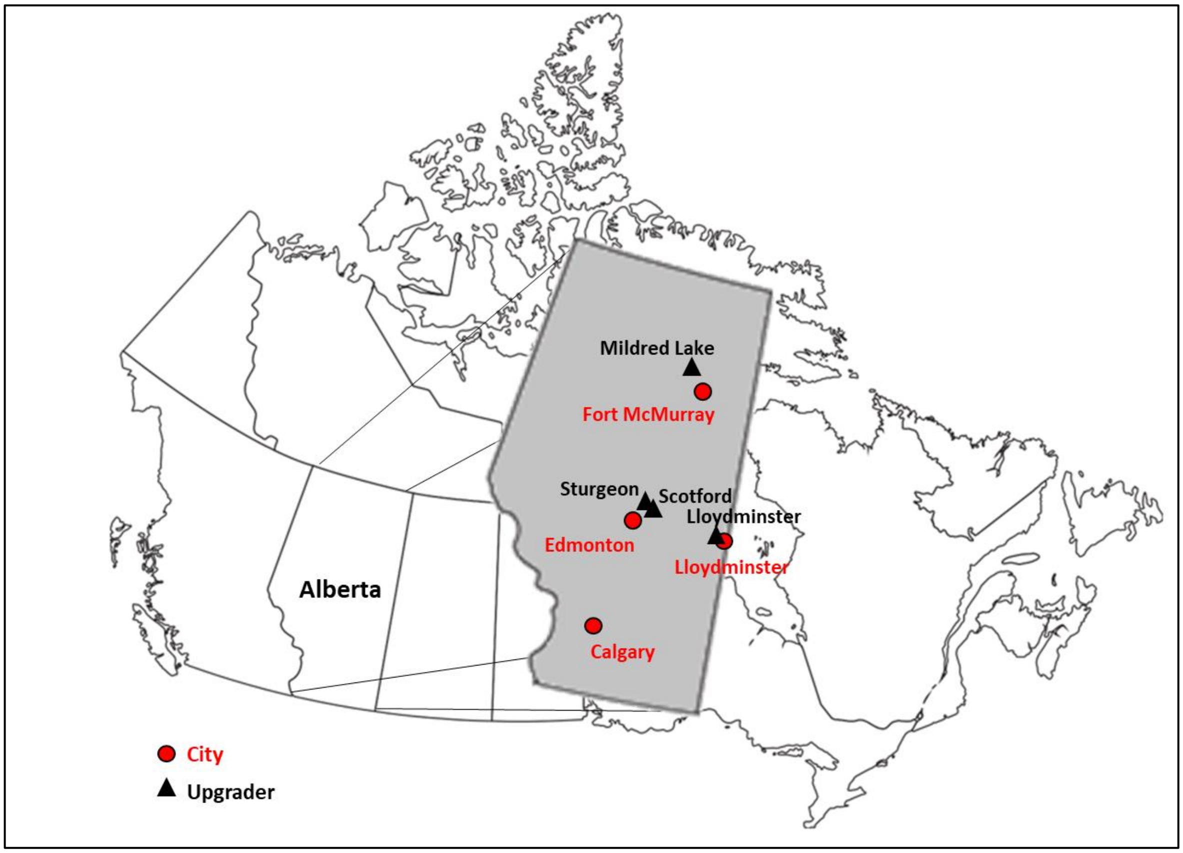

Figure 2-2. Location of Alberta's hydroconversion upgraders considered in this study

A comprehensive composition of spent catalyst from Alberta's bitumen upgrading is provided by Gray et al. (Gray et al. 2000). They analyzed samples withdrawn from the LC-Fining unit at Syncrude's Mildred Lake upgrader. Based on that data, and assuming that metals are presented in their sulfide form, the composition of the spent catalyst considered in this study is 13.2 wt.% V_2S_3, 7.1 wt.% V_2O_5, 6.8 wt.% MoS_2, 3.7 wt.% Ni_3S_4, 12.9 wt.% C (coke), 53.8 wt.% Al_2O_3.

2.2.2 Process description

Figure 2-3 shows a conceptual flowsheet for the recovery of vanadium from bitumen upgrading spent catalyst by salt roasting followed by water leaching, based on Llanos et al. (Llanos et al. 1997). This hydrometallurgy route was selected because it has been successfully implemented at industrial scale for processing of oil refining spent catalyst (Berrebi et al. 1993; Llanos and Deering 1998). The red arrows in the flowsheet indicate the main product, co-products, and by-products, representing potential revenue streams.

The oil-free spent catalyst is roasted in air at 600^{o}C to oxidize the vanadium and molybdenum sulfides and burn off the coke deposits present in the feedstock. Then it is roasted with Na_2CO_3 at 700^{o}C to convert the metal oxides into water soluble salts (Ferella et al. 2011). Other compounds in the roasted spent catalyst do not react with Na_2CO_3 at the roasting temperature (Llanos and Deering 1998; Chen et al. 2004; Chen et al. 2006; Mohapatra and Park 2007; Al-Sheeha et al. 2013). The first step of the roasting operation is exothermic, and the reaction energy is enough to keep the required temperature. The second stage is endothermic; therefore, the required energy is supplied by combustion of natural gas. Roasting is performed in a multiple hearth furnace (MHF). The generated gases are exhausted through the top of the equipment, and SO_2 is removed by wet scrubbing with slurry lime.

Gypsum is a by-product of gas cleaning that can be disposed of or sold. Table 2-3 presents the reactions that were considered to occur during roasting of spent catalysts.

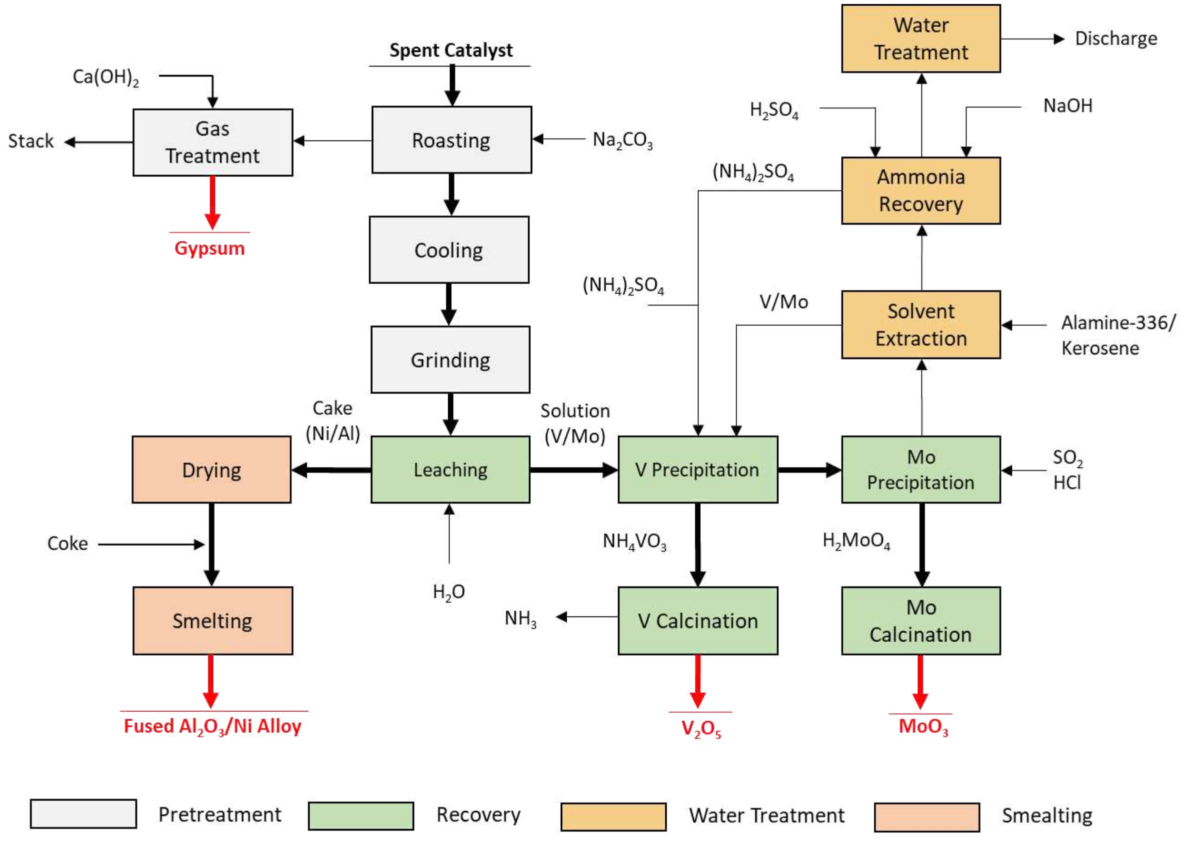

Figure 2-3. Conceptual flowsheet for the recovery of vanadium by salt roasting and water leaching

The roasted spent catalyst is cooled down in a bulk solids heat exchanger, using water at ambient temperature, and then ground in a ball mill. Vanadium and molybdenum are leached out of the ground spent catalyst with water at 90ºC. The percentage of leached vanadium is between 85% and 99%, and that of molybdenum is expected to be between 91% and 99% (Toda 1989; Chen et al. 2004; Chen et al. 2006; Al-Sheeha et al. 2013). The pregnant solution is treated with $(NH_4)_2SO_4$ for the precipitation of vanadium in the form of ammonium metavanadate (AMV) (Biswas 1985; Llanos et al. 1997; Nkosi et al. 2017).

The precipitate is separated from the mother liquid by filtration and directed to the vanadium calcination unit. The precipitated AMV is thermally decomposed into granular V_2O_5 and ammonia by calcination. According to an earlier study, the purity of vanadium pentoxide obtained through this route is greater than 99%, with 0.2% Mo (Llanos and Deering 1998). Off-gases are treated for ammonia removal before being released to the atmosphere. The mother liquid from the vanadium precipitation operation is acidified by treating it with SO_2 and HCl, and molybdic acid is precipitated. Molybdenum trioxide is produced by calcination of molybdic acid [99% MoO_3, 0.2% V] (Llanos and Deering 1998).

Residual vanadium and molybdenum remaining in the barren liquid is recovered by solvent extraction and recycled back to the vanadium precipitation operation. The aqueous solution is brought into contact with an organic solution consisting of Alamine-336 diluted on kerosene. Vanadium and molybdenum are stripped from the organic solution using NH_4OH. The raffinate is treated with NaOH to raise its pH, heated to near its boiling temperature, and contacted with air in a packed column to strip off the ammonia in the solution. The gaseous ammonia is scrubbed with a solution of H_2SO_4 to produce $(NH_4)_2SO_4$ which is recycled back to the vanadium precipitation operation. Finally, the ammonia-free stream is treated for pH and temperature control, and removing of suspended solids, before being discharged.

The underflow from the leaching operation is a cake consisting of about 70% of insoluble solids and residual V and Mo, and 30% of moisture (Llanos and Deering 1998). The cake is dried, mixed with metallurgical coke and smelted at about 2,000ºC to recover fused alumina and a nickel alloy.

Table 2-3. Reactions occurring during roasting of spent catalyst

Unit operation	Reactions	Comments
Roasting (first stage)	$2V_2S_{3(s)} + 11O_{2(g)} = 2V_2O_{5(s)} + 6SO_{2(g)}$	Oxidation of vanadium sulfide in air
	$2MoS_{2(s)} + 7O_{2(g)} = 2MoO_{3(s)} + 4SO_{2(g)}$	Oxidation of molybdenum sulfide in air
	$2Ni_3S_{2(s)} + 7O_{2(g)} = 6NiO_{(s)} + 4SO_{2(g)}$	Oxidation of nickel sulfide in air
	$C_{(s)} + O_{2(g)} = CO_{2(g)}$	Coke burning
Roasting (second stage)	$V_2O_{5(s)} + Na_2CO_{3(s)} = 2NaVO_{3(s)} + CO_{2(g)}$	Conversion of vanadium pentoxide into soluble salt
	$MoO_{3(s)} + Na_2CO_{3(s)} = Na_2MoO_{4(s)} + CO_{2(g)}$	Conversion of molybdenum trioxide into soluble salt
Vanadium calcination	$2NH_4VO_{3(s)} \rightarrow V_2O_{5(s)} + 2NH_{3(g)} + H_2O_{(g)}$	Calcination of AMV. Thermal decomposition in ammonia, vanadium pentoxide, and water
Molybdenum calcination	$H_2MoO_{4(s)} \rightarrow MoO_{3(s)} + H_2O_{(g)}$	Calcination of molybdic acid. Thermal decomposition in molybdenum trioxide and water
Smelting	$NiO_{(s)} + C_{(s)} \rightarrow Ni_{(s)} + CO_{(g)}$	Reduction of nickel oxide

2.2.3 Material and energy balance

A spreadsheet-based process model was developed to estimate metal recovery rate, consumables rates, emission and effluent composition and generation rate, and energy requirements.

Separation efficiencies were used to estimate outputs to model leaching, solvent extraction, and ammonia recovery operations. The output of precipitation operations was estimated from the expected concentration of metals in the mother liquor. The consumable requirements were calculated based on known ratios (e.g., the liquid-to-solid ratio for leaching), stoichiometric reactions (roasting, calcination) or known excess percentage of reactants (precipitation, smelting). The specific values of the parameters used in this study are provided in Table 2-4.

The energy requirement to meet process temperatures was estimated through energy balance. Heat transfer and the energy of reaction were considered. For instance, in roasting and calcination operations, stoichiometric reactions along with the heat of formation were considered to include the energy of reaction in the energy balance. Energy consumption in the smelting operation, and the electricity required to drive the MHF, and rotary kilns were estimated from similar processes (Brown et al. 1996). Electricity consumption in the grinding process was calculated with the Bond equation, using the work index of alumina as representative of spent catalyst (Bond 1961).

Table 2-4. Process conditions used for model development

Variable	Value	Source	Comments/Remarks
Roasting			
First step roasting temperature	600ºC	(Ferella et al. 2011)	
Second step roasting temperature	700ºC	(Ferella et al. 2011)	
Na_2CO_3-to-spent catalyst ratio	0.24	[43]	
Cooling			
Final temperature	30ºC		
Cooling water temperature	10ºC		Ambient temperature
Grinding			
Final size	500 µm	(Al-Sheeha et al. 2013)	To estimate power requirement
Leaching			

Variable	Value	Source	Comments/Remarks
Residence time	6 h	(Al-Sheeha et al. 2013)	To size tanks
Leaching temperature	90ºC	(Al-Sheeha et al. 2013)	To estimate heat requirement
Liquid-to-solid ratio	1.5 L/kg	(Al-Sheeha et al. 2013)	To estimate water requirement
Wash ratio	2.0	(Haug 2000)	To estimate water for filtration
Vanadium precipitation			
Vanadium concentration in mother liquid	0.5 g/L	(Llanos et al. 1997)	To estimate NH_4VO_3 precipitation
Ammonia concentration in mother liquid	12 g/L	(Llanos et al. 1997)	To estimate $(NH_4)_2SO_4$ requirement

Variable	**Value**	**Source**	**Comments/Remarks**
Residence time	2 h	(Llanos et al. 1997)	To size tanks
Wash ratio	2.0	(Haug 2000)	To estimate water for filtration
Vanadium calcination			
Calcination temperature	500ºC	(Chen et al. 2006)	To estimate heat duty
Molybdenum precipitation			
pH of the solution	1.1	(Llanos et al. 1997)	To estimate HCl requirement
Molybdenum concentration in effluent	0.5 g/L	(Llanos et al. 1997)	To estimate H_2MoO_4 precipitation
Residence time	2 h	(Llanos et al. 1997)	To size tanks

Variable	Value	Source	Comments/Remarks
Wash ratio	2.0	(Haug 2000)	To estimate water for filtration
Molybdenum calcination			
Calcination temperature	500ºC	(Llanos et al. 1997)	To estimate heat duty
Residual V and Mo solvent extraction			
Extractant	Alamine-336		
O/A ratio	1:5	(Kim et al. 2014)	To estimate the rate of organic solution
Extraction rate	99% V, Mo	(Kim et al. 2014)	To estimate extracted V and Mo
Stripping agent	NH_4OH		
O/A ratio	2:1	(Chen et al. 2006)	To estimate ammonium hydroxide

Variable	Value	Source	Comments/Remarks
Stripping ratio	99.8% V, Mo	(Chen et al. 2006)	To estimate V and Mo stripped
Ammonia recovery			
Stripping temperature	90ºC		Near ammonia solution boiling point
NH_3 removal efficiency	85%	(Kinidi et al. 2018)	To estimate ammonia removal
Cake drying			
Initial moisture content	30 wt.%	(Llanos et al. 1997)	To estimate heat duty
Final moisture content	2 wt.%	(Llanos et al. 1997)	To estimate heat duty
Cake smelting			
Coke requirement	30% excess	(Llanos et al. 1997)	To ensure complete reduction of oxides

Variable	Value	Source	Comments/Remarks
Temperature	2,072ºC	(Llanos et al. 1997)	To ensure smelting of all metals in the cake

2.2.4 Equipment sizing and evaluation of utility demand

Material and energy balances provide the information required to size equipment and estimate utility demand. Table 2-5 shows a list of the major equipment and the parameters of interest for sizing and cost estimation. Besides the major equipment, ancillary equipment was sized and is included in the cost estimation.

Equipment sizing also facilitates the estimation of utility demand. The power required is the sum of the power consumption for driving pumps, conveyors, compressors, air coolers, ball mill, and rotational equipment like the kilns for calcination and the MHF for roasting.

Natural gas is used as a heat source, either by direct combustion in equipment like rotational kilns and a multiple-hearth furnace or by steam generation in a boiler. The heat requirement is a direct result of the energy balance, and the equivalent energy content in the natural gas was estimated assuming burners and boiler efficiencies of 0.88 (Cengel and Boles 2015).

2.2.5 Development of techno-economic assessment model

The techno-economic assessment model of the vanadium recovery plant considered detailed technical parameters and economic parameters including capital and operating cost, co-product and by-product revenue, and vanadium recovery cost estimates. Figure 2-4 shows the upgrading catalyst life cycle. Spent catalyst generated in bitumen upgraders is transported by logistic companies to the metal recovery plant, where vanadium, molybdenum, alumina, and nickel are recovered from the waste. The recovered metals are used by catalyst manufacturers to produce fresh catalyst or as raw material for other products. In this study, the costs of transportation of spent catalyst, and those incurred within the metal recovery plant were considered.

Table 2-5. List of major equipment and corresponding sizing parameters

Equipment	Operation	Parameter	Comments/remarks
Multiple hearth furnace	Roasting	Number of hearths	Estimated as a function of solid capacity (Pennington 1959)
Spray tower	Roasting	Gas flow rate	From the material balance. Used for gas cleaning
Bulk solid heat exchanger	Cooling	Heat duty	From the energy balance
Ball mill	Grinding	Power	Depends on solid capacity and product size (Ulrich and Vasudevan 2004)
Stirred tank	Leaching, precipitation, solvent extraction, ammonia recovery	Volume	Estimated from feed flow and residence time
Stripping column	Solvent extraction, ammonia recovery	Liquid flow	From the material balance
Rotary kiln	Calcination	Heat duty	From the energy balance
Flash dryer	Drying	Evaporation rate	From the material balance
Electric arc furnace	Smelting	Heat duty	From the energy balance
Water treatment plant	Water treatment	Liquid flow	From the material balance

Another key assumption in the techno-economic assessment model relates to the feedstock cost. Often, upgraders provide the spent catalyst to the metal recovery plant free of charge, or the metal recovery plant charges an environmental fee to dispose of the spent catalyst. In this study, a free-of-charge feedstock scenario was considered for the base case, thus the estimated vanadium recovery cost is a conservative value. The effect of the feedstock cost on the vanadium recovery cost was study as one of the scenarios defined in Section 2.2.6.

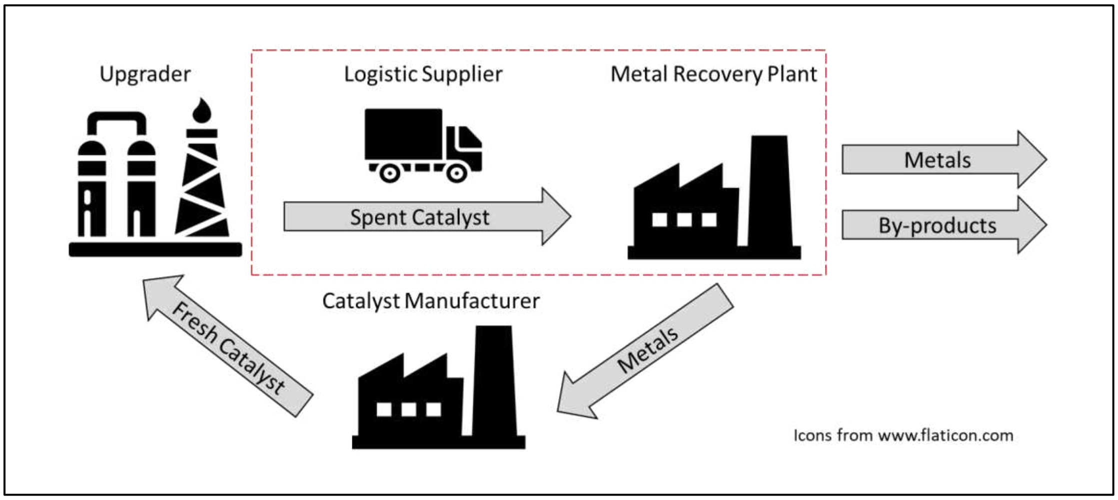

Figure 2-4. Upgrading catalyst life cycle. The system studied is within the dashed lines.

2.2.5.1 Capital cost

Capital cost is the sum of the fixed capital investment (FCI) and the working capital. The FCI includes the inside battery limit (ISBL) investment, the outside battery limit (OSBL) investment, engineering and construction cost, and contingency charges. The ISBL is the sum of the free-on-board cost (FOB) of the equipment multiplied by the respective factors to consider installation cost and materials, dimensions, and conditions other than those for which the FOBs are provided in several textbooks [61, 65, 66]. All FOBs were updated to the

Chemical Engineering Plant Cost Index (CEPCI) of 776.9, and a location factor of 1.43 (Towler and Sinnot 2008) was used for Alberta, Canada. Table 2-6 summarizes the general assumptions for capital cost estimation.

Table 2-6. Assumptions for capital cost estimation

Item	Value	Comments/remarks
CEPCI	776.9	Corresponding to 2021 USD
Location factor (LF)	1.43[a]	For Fort McMurray, Alberta
Fixed capital investment (FCI)		
Inside battery limit investment (ISBL)	Depends on the equipment	Found in cost curves
Outside battery limit investment (OSBL)	40% ISBL	Site conditions not specified
Engineering and construction cost	30% (ISBL + OSBL)	For small projects
Contingency	15% (ISBL + OSBL)	Typical value for general projects
Working capital (WC)	15% (ISBL + OSBL)	Typical value for general plants
Total capital cost	LF (FCI) + WC	

a. Based on 2003 location factor (1.60) and rate exchange (1.40 CAD/USD) and updated with 2021 rate exchange (1.25 CAD/USD) (Towler and Sinnot 2008).

2.2.5.2 Operating cost

Operating cost includes feedstock, consumables, utilities, labor, maintenance, operating supplies, laboratory charges, property insurance, plant overhead, and transportation of spent catalyst to the metal recovery plant. Consumables prices were obtained from vendors. Electricity and natural gas prices correspond to typical values for industrial consumers in Alberta. Cooling water and water treatment costs were obtained from the literature. Transport cost, including containment of spent catalyst, was estimated as a fraction of the cost of fresh catalyst, according to data in Valeri et al. (Valeri et al. N.d.). The remaining cost components were estimated through factors suggested by Peters et al. (Peters et al. 2003). Table 2-7 presents the utility cost and other operating costs assumed in this study.

2.2.5.3 Vanadium recovery cost

The vanadium recovery cost was calculated through development of a discounted cash flow (DCF) analysis model. Future cash flows were calculated considering the escalation of operating cost. The model also estimated the co-products and by-products revenues. Their market prices were obtained from vendors. Usually, the co-products and by-products are sold at a discount relative to the market price. For metals, this discount could be in the range 15-40% (Baddour and Snowden-Swan 2019). In this study, the selling price considered is 20% of the market price (Table 2-8). The vanadium recovery cost is the vanadium selling price at a fixed internal rate of return [IRR]). The basic assumptions for the techno-economic analysis are shown in Table 2-9. Details of the method is presented in Appendix A.

Table 2-7. Operating costs assumed in this study

Category	Item	Cost/value	Reference
Feedstock cost	Spent catalyst	0	Assumption for the base case
Utility cost	Electricity from the grid	\$0.042/kWh	(Canada Energy Regulator 2017)
	Natural gas	\$1.32/GJ	(Canada Energy Regulator 2017)
	Cooling water	\$0.08/t	(Peters et al. 2003)
	Water treatment	\$56/1000 m^3	(Turton et al. 2012)
Transport cost	Containment and transportation	9% fresh catalyst cost \$6/kg fresh catalyst	(Valeri et al. N.d.) (Marafi et al. 2008)
Other operating costs	Operating labor	\$30/h; 1,960 h/y; 4.5 operators/shift; 2 operators/operation	(Turton et al. 2012)
	Supervisorial and clerical labor	15% of operating labor	(Peters et al. 2003)

	Maintenance and repairs	10% of fixed capital investment	(Peters et al. 2003)
	Operating supplies	15% of maintenance and repairs	(Peters et al. 2003)
	Laboratory charges	20% of operating labor	(Peters et al. 2003)
	Property insurance	1% of fixed capital investment	(Peters et al. 2003)
	Plant overhead	50% of total labor and maintenance	(Peters et al. 2003)

Table 2-8. Co-product and by-product selling prices assumed in this study

Co- or by-product	Selling price	Reference
Molybdenum trioxide	$22,000/t	(Trading Economics 2020)
Fused alumina	$276/t	(Focus Economics 2019)
Nickel alloy	$1,210/t	(iScrap App 2020)
Gypsum	$24/t	(Statista 2019)

Table 2-9. Economic assumptions for the techno-economic assessment

Item	Value
Plant lifetime	20 years
On-stream factor	0.95
Operating cost escalation	2%
Internal rate of return	10%

2.2.5.4 Sensitivity and uncertainty analysis

Sensitivity analysis helps to identify the influence of the inputs on the model outputs, providing insight on which variables should be estimated more accurately to reduce variability in the results. This is important for models that use data from published/industry sources rather than experimental data, and in economic assessments depending on the price of consumables, utilities, and products with high volatility.

In this study, the RUST toolbox was used for sensitivity analysis (Di Lullo et al. 2019). The Morris method was used to study the sensitivity of vanadium recovery cost on 26 inputs. An overview of the method is shown in Appendix B. The inputs considered included process variables, like the percentage of vanadium and molybdenum leached and precipitated, and the wash ratio used in filtration operations. The maximum and minimum values of those variables were selected from typical values found in the literature (Toda 1989; Chen et al. 2004; Chen et al. 2006; Zeng and Cheng 2009a; Yang et al. 2011; Al-Sheeha et al. 2013; Gao et al. 2020).

Also, economic variables were considered, i.e., co-product and by-product selling prices, the specific cost of each consumable, and the specific cost of each utility. All the economic inputs were varied by ±30% of the base case values. This range of variation was selected to include the maximum and minimum market price in the last ten years of the main co-products and consumables.

The model used for this study was developed based on several assumptions, which introduces uncertainties into the process model. One way to deal with uncertainties is by performing a Monte Carlo simulation. In this study, the RUST toolbox was used for uncertainty analysis (Di Lullo et al. 2020). The inputs used for uncertainty analysis were the twelve identified as relevant following the sensitivity analysis. For the 5,000 runs performed for the analysis, the inputs were populated using a uniform probability distribution within those ranges.

2.2.6 Definition of scenarios

2.2.6.1 Base case scenario

For the base case scenario, a recovery plant with a capacity of 30,000 tonnes of spent catalyst per year (annual output of 5,400 t V_2O_5 and 1,720 t MoO_3) was considered. This is a typical capacity of existing commercial plants (Akcil et al. 2015); however, the economies of scale were investigated by changing the plant capacity from 2,000 to 50,000 t/y. Thus, plants with the capacity to process spent catalyst from upgraders located in Alberta were included in the analysis.

2.2.6.2 Disposal scenario

The base case scenario was compared with a disposal scenario in which the solid residues from the leaching process are simply dried and disposed of instead of being further processed for the recovery of Ni and Al_2O_3. For this scenario, a cost of $55/t of solid residues was considered (Towler and Sinnot 2008).

2.2.6.3 Feedstock cost

The feedstock cost, e.g., spent catalyst, is an agreement between the refinery/upgrader where the spent catalysts is generated and the metal recovery plant. For the base case of this study, it was assumed that the spent catalyst is provided for free to the recovery plant. This scenario is valid if the generator of spent catalysts considers zero value for such waste, or if the metal recovery plant is run by the generator of the spent catalyst, e.g., upgrader integrated operation.

In some cases, the metal recovery plant charges an environmental fee for the treatment of hazardous solids (Ferella et al. 2019). Spent catalysts are considered a hazardous waste. One of the reasons of such classification is the elevated leachability of some metals presented in the spent catalysts, including vanadium (Furimsky 1996). After disposal of spent catalyst in landfills, the leached metals could percolate the soil and reach groundwaters. Processing spent catalyst to recover metals diverts such waste from landfills and eliminates the risk of groundwater contamination. The environmental fee is a revenue stream for the recovery plant.

On the other hand, the metal recovery plant can purchase spent catalyst at a price that depends on the concentration of valuable metals in the raw material. The vanadium recovery cost was estimated for the described scenarios and considering typical feedstock costs as per a spent catalyst recycling plant in North America (A. Orr, personal communication, April 17, 2020).

2.3 Results and discussion

2.3.1 Base case scenario

2.3.1.1 Material and energy balance

For a processing capacity of 30,000 tonnes of spent catalyst per year, about 0.70 t/h of V_2S_3 and V_2O_5 are present in the feed to the roasting operation. Vanadium reacts with sodium carbonate to produce 0.88 t/h of sodium metavanadate, which is leached out with water from the catalyst support. After $(NH_4)_2SO_4$ is added to the pregnant solution, 0.84 t/h of vanadium precipitates as ammonium metavanadate (AMV), which is decomposed by calcination into 0.65 t/h of granular V_2O_5, the principal product of the process. Besides V_2O_5, molybdenum is recovered. About 0.23 t/h of molybdic acid precipitates, and, after calcination, 0.21 t/h of MoO_3 is recovered as a co-product. About 1.84 t/h of fused alumina and 0.09 t/h of nickel alloy are recovered by drying the solid residue from leaching operation and smelting the remaining solids. Gypsum is a by-product of cleaning the roasting off-gases and produced at a rate of 1.68 t/h. Table 2-10 shows the material balance for each unit operation considered in the process.

About 9,195 kWh per hour is required, of these, 70.3% corresponds to electricity. Cake smelting is the operation with the highest electricity consumption. Roasting is the operation with the second highest electricity consumption, mainly to drive the ramble arms of the multiple hearth furnace. Grinding is the third highest electricity consumer. Electricity is also used for ancillary equipment like pumps, conveyors, and fans, but they consume far less electricity. Natural gas is consumed directly in burners as well as in the steam used as heat source in different operations. In total, 9.28 GJ/h are required. Table 2-11 shows the utilities consumption for each unit operation.

Table 2-10. Material balance for the base case scenario

Unit operation	Input (t/h)		Output (t/h)	
Roasting	Spent catalyst	3.42	Roasted spent catalyst	3.23
	Sodium carbonate	1.08	Off-gases	9.93
	Air	9.32	Unreacted sodium carbonate	0.54
Off-gases cleaning	Off-gases	9.93	Gypsum	1.68
	Calcium hydroxide	0.720	Water	0.175
	Water	0.351	Clean gasses	9.31
	Oxygen	0.156		
Cooling	Roasted spent catalyst	3.77	Cooled spent catalyst	3.77
Grinding	Cooled spent catalyst	3.77	Ground spent catalyst	3.77
Leaching	Ground spent catalyst	3.77	Solution	7.30
	Leching water	4.55	Cake	2.82
	Wash water	1.75		

Unit operation	Input (t/h)		Output (t/h)	
V precipitation	Solution	7.30	V reduced mother liquor	9.29
	Ammonium sulfate	0.345	Ammonium metavanadate	0.838
	Ammonium sulfate recycled from ammonium recovery	0.469	Water in cake	0.279
	Solution recycled from solvent extraction	1.73		
	Wash water	0.559		
V calcination	Ammonium metavanadate	0.838	Vanadium pentoxide	0.652
	Water in cake	0.279	Ammonia	0.122
			Water	0.344
Mo precipitation	V reduced mother liquor	9.29	Mo reduced mother liquor	9.21
	Chloric acid	0.0612	Molybdic acid	0.233
	Sulfur dioxide	0.00920	Water in cake	0.0778
	Wash water	0.156		

Unit operation	Input (t/h)		Output (t/h)	
	Mo recycled from solvent extraction	0.00379		
Mo calcination	Molybdic acid	0.233	Molybdenum trioxide	0.207
	Water in cake	0.0778	Water vapor	0.104
Solvent extraction	Mo reduced mother liquor	8.45	Residual V/Mo	0.007
	Alamine-336	0.00252	Extract solution	8.667
	Kerosene	0.0120		
	Ammonium hydroxide	0.0679		
Ammonia recovery	Extract solution	8.667	Ammonium sulfide	1.526
	Sodium hydroxide	0.0248	Effluent	8.545
	Sulfuric acid	0.348		
	Ammonia from V calcination	0.122		
Drying	Cake	2.82	Residual solids	1.97
			Water vapor	0.789

Unit operation	Input (t/h)		Output (t/h)	
			Water in cake	0.0564
Smelting	Residual solids	1.97	Fused alumina	1.84
	Metallurgical coke	0.0189	Nickel alloy	0.162
	Water in solids	0.0564	Carbon dioxide	0.0440

Table 2-11. Utility consumption for the base case scenario

Unit operation	Electricity (kWh/h)	Natural gas (GJ/h)	Cooling water (t/h)
Roasting	496	1.14	-
Cooling	105.5	-	21.8
Grinding	66.6	-	-
Leaching	5.04	3.47	-
V precipitation	1.25	-	-
V calcination	7.67	2.04	-
Mo precipitation	10.0	-	-
Mo calcination	7.63	0.28	-
Solvent extraction	1.76	-	-
Ammonia recovery	3.14	0.15	-
Drying	0.218	2.20	-
Smelting	5,398	-	-

2.3.1.2 Recovery cost

The summary of costs and revenues for the base case scenario is present in Table 2-12. The total inside battery limit (ISBL) is $33.4 M. Operations involving thermal processes contribute the most to the ISBL; roasting (28.8%), vanadium calcination (19.0%), smelting (14.9%), and molybdenum calcination (9.8%) are the top four operations in the ISBL. This is because furnaces and kilns are considerably more expensive than tanks and agitators, the main equipment used in the remaining operations. The FCI for the base case is $67.8 M and the total capital cost is $74.8 M.

The operating cost totalize $46.1 M/y, including consumable, utility labor, facility dependent cost, plant overhead, and transport of spent catalyst to the metal recovery plant. The total consumables cost is $6.29 M/y (13.6% of operating cost). Sodium carbonate and lime account for 39.5% and 19.4% of this cost, respectively. Ammonium sulfate for AMV precipitation and sulfuric acid for ammonia recovery correspond to 14.5% and 14.4% of the total consumable cost, respectively. Since the ammonia is recovered as ammonium sulfate, which is recycled back to the vanadium precipitation operation, it can be said that roughly one-third of the consumables cost is related to this operation. The use of alternative reagents for vanadium precipitation (e.g., other ammonium salts or sulfide precipitation) or a different separation operation (e.g., solvent extraction or ion exchange) could be explored for more cost-effective options. Details of these and other options are found in Zeng and Yong (Zeng and Cheng 2009b).

The utility cost represents 5.00% of the operating cost. The cost of electricity at year one of operation is $2.09 M/y and of natural gas is $0.10 M/y, and of cooling water and water treatment is $0.11 M/y for a plant processing 30,000 tonnes of spent catalyst per year., Labor-dependent cost, plant overhead and facility-dependent cost, account for 20.9%, 14.9% and 10.4%, of the operating cost, respectively.

Transport cost, which includes containment and transportation of spent catalyst, is $16.2 M/y, representing 35.2% of the operating cost.

The co-products and by-products revenue is \$8.88 M/y, and MoO_3 makes up 85% of the total, despite the relatively low amount recovered, because of its high market price. On the other hand, alumina, which is not as valuable as MoO_3, contributes 10% to the total revenue, because of the relatively high amount found in the catalyst support. Nickel alloy contributes 4.2% to the total revenue, while gypsum's contribution is negligible.

Table 2-12. Summary of costs and revenues for a plant processing 30,000 tonnes of spent catalysts per year

Cost/revenue	Value
Capital cost	\$74.8 M
Operating cost[a]	
Consumable cost	\$6.29 M/y
Electricity	\$2.09 M/y
Natural gas	\$0.10 M/y
Cooling water	\$0.01 M/y
Water treatment	\$0.09 M/y
Labor dependent	\$9.63 M/y
Facility dependent	\$4.77 M/y
Plant overhead	\$6.88 M/y
Spent catalyst transport cost	\$16.2 M/y
Total	\$46.1 M/y
Co-product and by-product revenue	\$8.88 M/y
Vanadium revenue[b]	\$53.6 M/y

a. At year one of operation; b. For breakeven.

The vanadium recovery cost calculated through the techno-economic analysis is \$9.90/kg V_2O_5, i.e., the selling price in order to break even in the plant life span. This cost is significantly lower than the production costs of vanadium ores reported by industry (Prophecy Development Corp. 2019; Bushveld Minerals 2020). Although a direct comparison with these costs is not possible, the probable causes of the cost difference can be inferred by examining each process. First, recovering vanadium from spent catalyst avoids the costs of exploration, mining, and beneficiation in the production of vanadium from ores. Second, this assessment assumes that the feedstock is free of charge, which is valid for recovery plants integrated to upgrader operations. Should vanadium be recovered in a third-party plant, the supply of spent catalyst from the upgrader to the plant could be subject to a charge, increasing the recovery cost. Finally, selling the by-products and co-products has an important effect on the vanadium recovery cost. As can be seen in the recovery cost breakdown shown in Figure 2-5, the co-products and by-products revenue is \$1.64/kg V_2O_5, which offsets the capital cost. This revenue stream, especially the selling of molybdenum, is not present in the production of vanadium from ores.

The feasibility of the recovery process was determined by comparing the V_2O_5 market price and the recovery cost. The market price of V_2O_5 depends on the product's purity and the location of the market. The current price of V_2O_5 98 wt.% purity is about \$22.80/kg in Europe (Vanadium Price 2020). V_2O_5 with a purity higher than 99.5 wt.% was sold for around \$50/kg in China (Gao et al. 2020). Market volatility is another factor affecting profitability in the long term. In the last 40 years, the historical low price of 98 wt.% V_2O_5 has been \$2.44/kg (Vanadium Price 2020); however, the mean before 2000 was around \$6/kg and afterwards it was around \$12.00/kg. Unless the market price falls to historical lows, the recovery process assessed in this study is potentially profitable. In fact, for a market price of \$12.0/kg, the recovered V_2O_5 could be sold at a discount of up to 18%, generating profit.

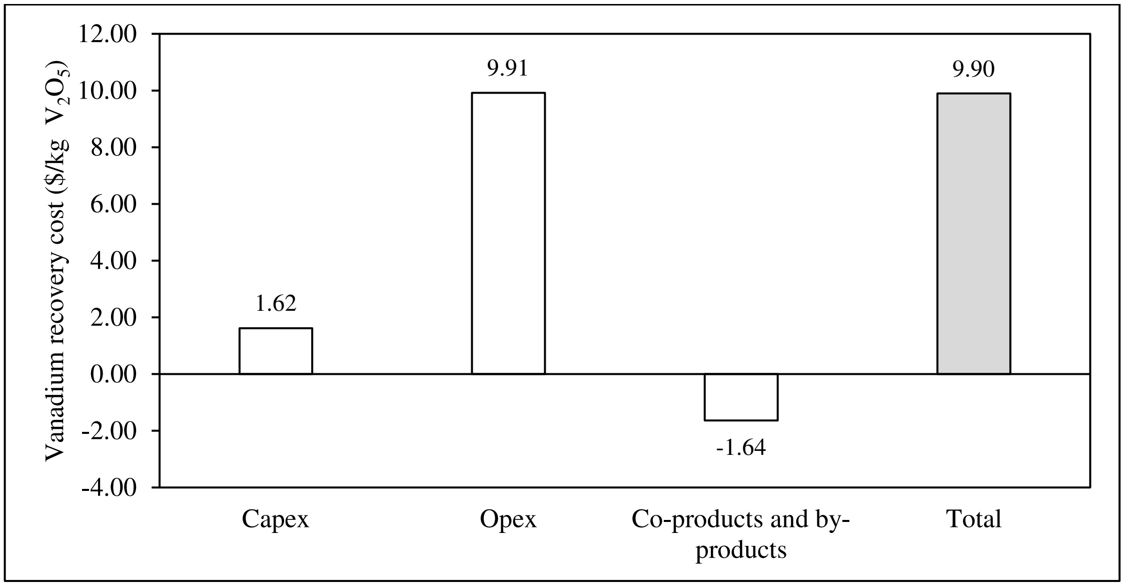

Figure 2-5. Breakdown of vanadium recovery cost for the base case

2.3.2 Economies of scale and the effect of plant capacity on vanadium recovery cost

The capital cost was calculated for different plant capacities to examine economies of scale. The results are shown in Figure 2-6. This type of plant exhibits economies of scale with a scale factor of 0.46. The results suggest that a centralized plant for processing spent catalyst coming from multiple upgraders is more competitive than a plant dedicated solely to one upgrader.

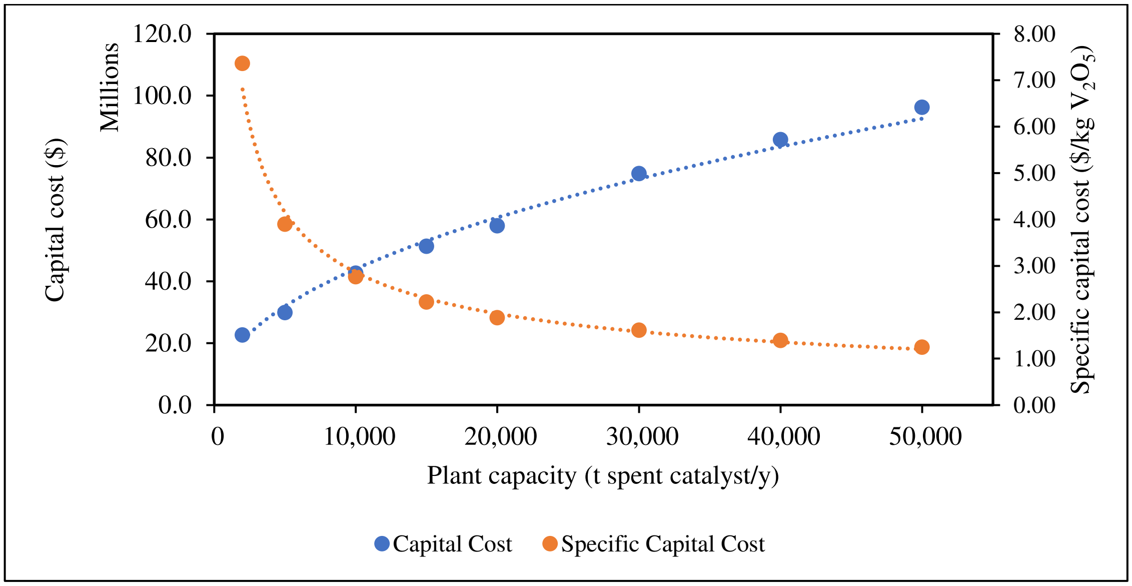

Figure 2-6. Capital cost and specific capital cost for different plant capacities

The effect of plant capacity on vanadium recovery cost was also studied. The results are shown in Figure 2-7. It is observed that the vanadium recovery cost decreases with the plant capacity. This is a consequence of the economies of scale exhibited by the capital cost. Considering a market price of \$12.00/kg V_2O_5, the minimum profitable capacity is about 22,400 t/y. Based on this value, and taking Alberta's upgraders as a case study, it is concluded that standalone plants for processing spent catalyst are not economically feasible. To increase the profitability of the project, a centralized plant for processing spent catalyst coming from multiple plants can be considered. For instance, the vanadium recovery cost for a 36,000 t/y plant would be \$9.05/kg V_2O_5. Referring again to the Alberta case study, such capacity would be achieved by combining the spent catalyst originating in the Mildred Lake, Scotford, Sturgeon, and Lloydminster plants.

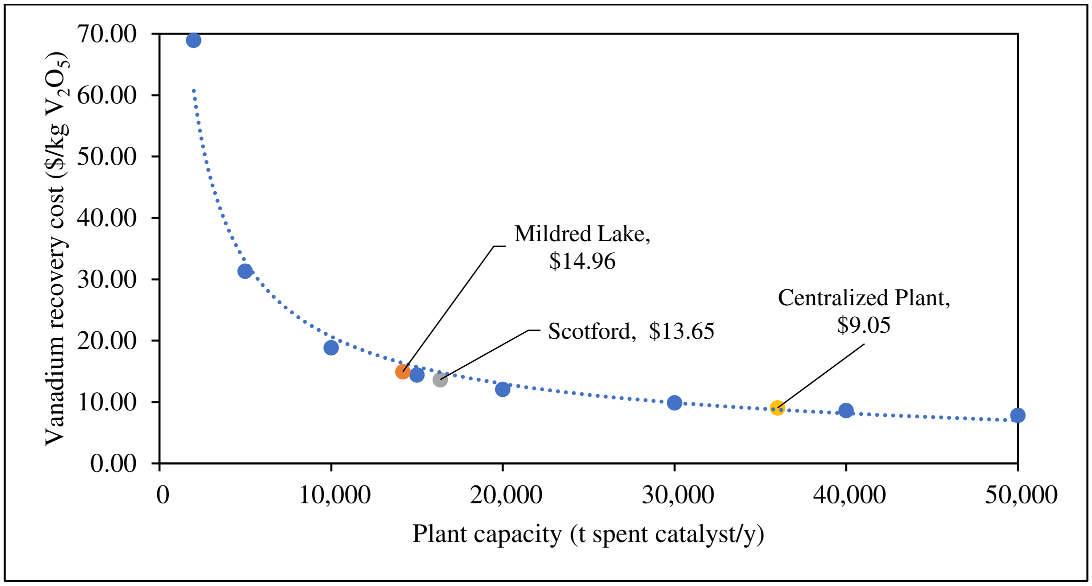

Figure 2-7. Vanadium recovery cost vs. plant capacity

2.3.3 Sensitivity analysis

The results of the sensitivity analysis are shown in Figure 2-8. This Morris plot ranks the influence of the parameters on the model output, i.e., the vanadium recovery cost, based on the position of the absolute mean value and standard deviation in the plot. The high sensitivity and high non-linear parameters are located at the top right of the plot. The vanadium recovery cost is most sensitive to the transport cost, the wash ratio, the MoO_3 selling price, the percentage of molybdenum and vanadium leached, and the price of Na_2CO_3. Because the efficiency of the vanadium precipitation operation is high, the amount of vanadium recovered in the whole process is determined by the percentage of vanadium leached, which explains the sensitivity of the recovery cost to this parameter. As noted in Section 2.3.1.2, MoO_3 contributes to more than 80% of the co-products and by-products revenue, and because this is an important component of the vanadium recovery cost, the sensitivity to the price of MoO_3 and percentage of molybdenum leached was expected. The same can be said about the transport cost, which represents about 35% of the operating cost. Finally, the wash ratio determines the quantity of water used in the filtering operations. Since the same wash ratio was assumed for all three filtering operations, even small variations in this parameter significantly change the process water use, which not only affects the operating cost but also the capital cost because the size of most of the equipment depends on the volume of the solution.

The consumables with the greatest influence on the vanadium recovery cost are Na_2CO_3 and H_2SO_4, and electricity is the utility whose price has the most impact. The eighteen inputs near the origin have little influence on vanadium recovery cost. These results suggest that more experimental leaching and filtration data for this specific feedstock is needed in order to obtain a more likely estimate of the vanadium recovery cost.

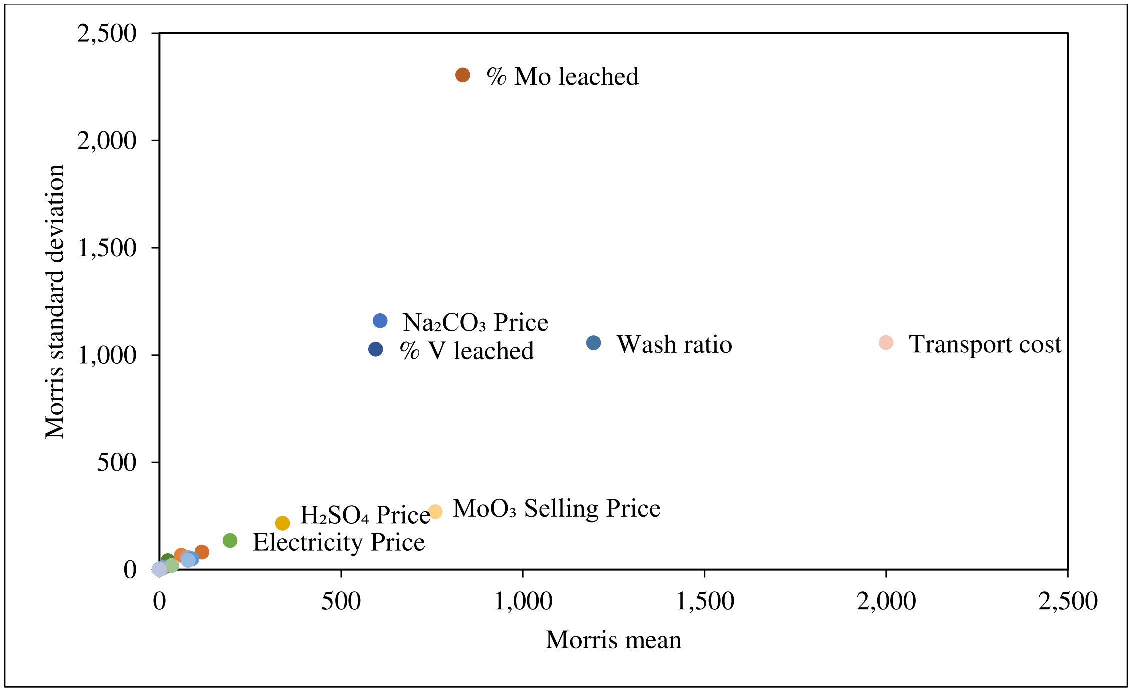

Figure 2-8. Analysis of elementary effects related to vanadium recovery cost and plant capacity of 30,000 t/y

2.3.4 Uncertainty analysis

Figure 2-9 shows the effect of the inputs on the vanadium recovery cost. The central axis of the tornado plot represents the mean of the entire sample generated by the Monte Carlo simulation (\$10.93/kg V_2O_5), while the ends represent how that mean would change if the value of each input is moved to its minimum and maximum values. For all the considered inputs, the vanadium recovery cost is lower than the reference market price. The MoO_3 selling price, the transport cost, the wash ratio, and the percentage of vanadium and molybdenum leached are the inputs with the most variation between ends in the tornado plot, which coincides with the results of the sensitivity analysis.

The influence of the selling price of MoO_3 on the vanadium recovery cost suggests that negotiating the discount at which this co-product is sold would be more beneficial than negotiating the bulk price of most of the consumables. The accuracy of the transport cost estimation should be carefully considered, given the great influence of this cost component on the vanadium recovery cost. Because the transport cost directly depends on the location of the metal recovery plant, a case dependent analysis is required.

That the wash ratio has great effect on the recovery cost is not surprising given that this variable is not only related to the consumables cost and utility cost, but also to the capital cost since the tank size depends on the flow rate, which is affected by the amount of water used in filtration. With respect to the percentage of vanadium and molybdenum leached, the output of the recovery process directly depends on these variables, thus any variation in their values would be reflected on the expected vanadium recovery cost.

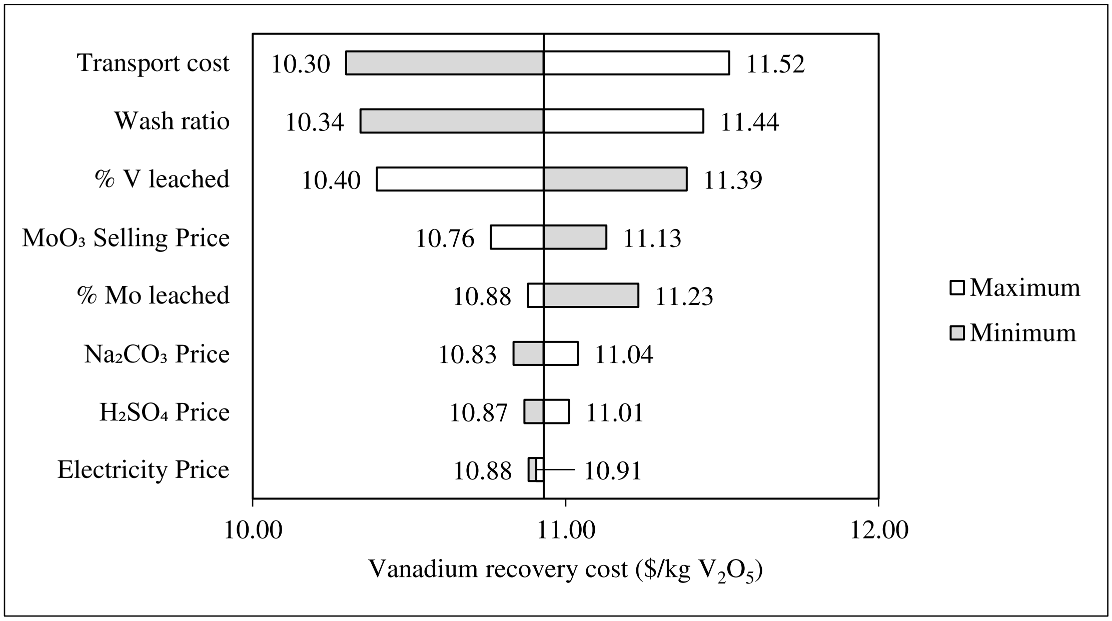

Figure 2-9. Changes in the Monte Carlo simulation mean value as each input is moved to its maximum and minimum value compared to the base case

Figure 2-10 shows summarizes the results of the Monte Carlo simulation. The median of the vanadium recovery cost is $10.92. The worst case, i.e., the 90th percentile, is above the market price of $12.00/kg. In fact, for 15% of the runs the vanadium recovery cost was higher than the reference market price. A more detailed analysis is required, especially for those inputs with the greater effect on the model output, in order to narrow the uncertainties and obtained a more accurate cost estimation, before concluding on the economic feasibility of this activity.

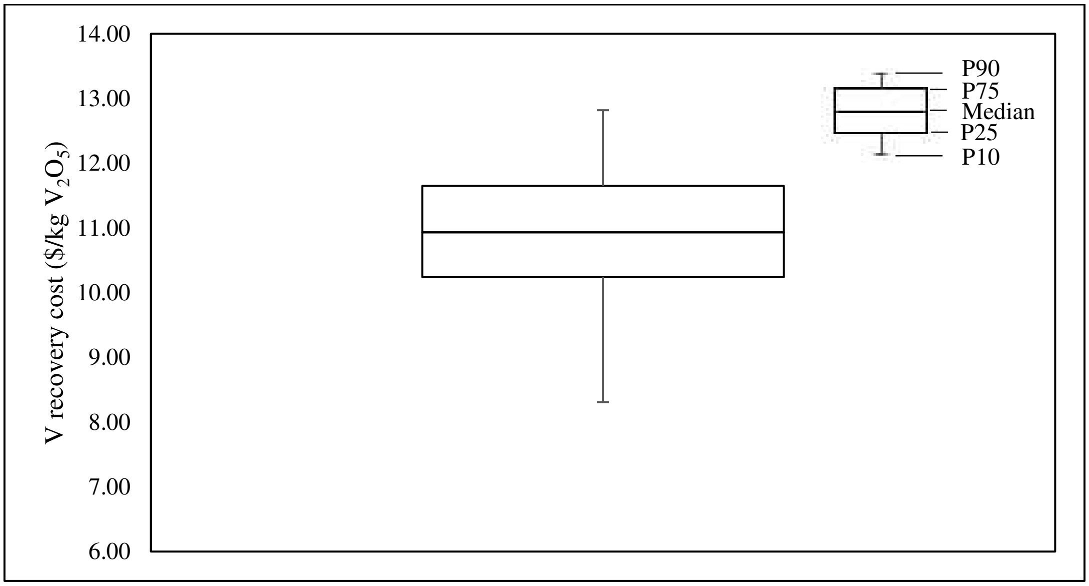

Figure 2-10. Monte Carlo simulation results

2.3.5 Disposal scenario

The definition of the disposal scenario was driven by the results in Section 2.3.1.2 that suggest that MoO_3 is the only co-product worth selling. The capital and operating costs and the vanadium recovery cost for both scenarios are presented in Table 2-13. It is shown that it is not worth further processing the solid residues from the leaching operation to recover fused alumina and nickel alloy, since the capital investment and operating cost of the smelting operation surpass the revenue from selling those co-products. In fact, disposing the solid residues reduces the vanadium recovery cost by \$0.66/kg V_2O_5. The difference decreases as the selling prices of the by-products and co-products increase, as depicted in Figure 2-11. Recovering alumina and nickel alloy is justified if the by-products and co-products are sold at more than 80% of their market price. The difference between scenarios could be higher if environmental taxes are considered, since the smelting operation consumes the highest amount of electricity, generating a significant amount of greenhouse gas (GHG) emissions and leading to a higher vanadium recovery cost.

Table 2-13. Economic analysis of vanadium recovery from spent catalysts. IRR 10%

Scenario	**Capital cost**	**Operating cost**	**Co and by-products revenue**	**Vanadium recovery cost**
Base case	\$74.8 M	\$46.1 M/y	\$8.88 M/y	\$9.89/kg V_2O_5
Disposal	\$63.7 M	\$43.0 M/y	\$7.66 M/y	\$9.23/kg V_2O_5

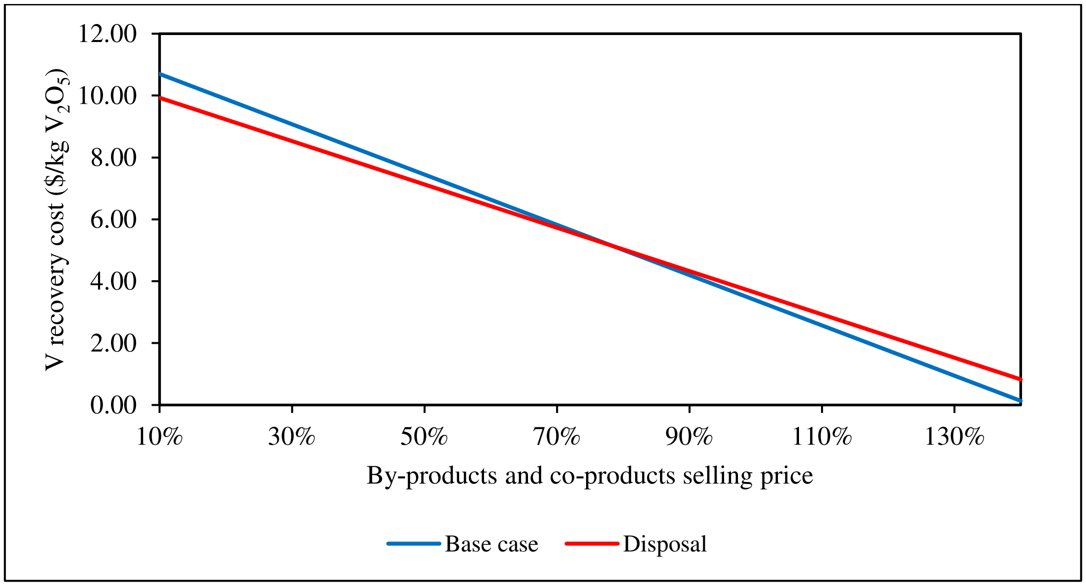

Figure 2-11. Effect of co-product and by-product selling price on the vanadium recovery cost

2.3.6 Effect of the feedstock cost

Figure 2-12 shows the variation of the vanadium recovery cost with the cost of feedstock, e.g., spent catalyst, for a plant capacity of 30,000 t/y spent catalyst. Negative feedstock costs represent a fee charged by the metal recovery plant to the upgrader for management and processing of hazardous solids, thus it is a revenue stream. It is observed that the vanadium recovery cost could be reduced \$3.23/kg V_2O_5 for a fee of \$500/t spent catalyst, a reasonable value for spent catalyst processing plants in North America. On the other hand, if the metal recovery plant purchases spent catalyst to the upgrader, the cost should not exceed \$300/t spent catalyst in order to keep the vanadium recovery cost below the reference market price of \$12.00/kg V_2O_5. These results show that negotiating the feedstock cost is key for the economic feasibility of this kind of activity.

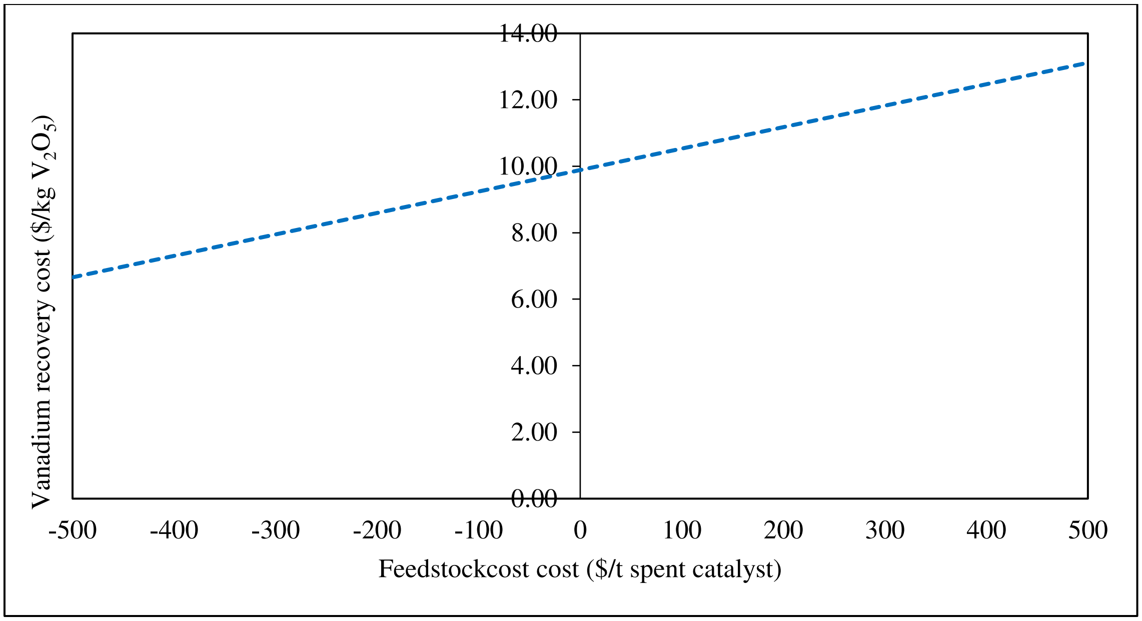

Figure 2-12. Variation of vanadium recovery cost with the feedstock cost

2.4 Conclusions

A data-intensive techno-economic model was developed to estimate the vanadium recovery cost from bitumen spent catalyst. A process based on salt roasting followed by water leaching and hydroconversion spent catalyst as feedstock was considered. Material and energy balances were performed to estimate equipment sizes and capital and operating costs. The vanadium recovery cost was estimated through development of techno-economic models.

For a capacity of 30,000 tonnes of spent catalyst per year, the vanadium recovery cost is (\$9.90 per kg of V_2O_5) lower than both the projected production cost of mining projects and the current vanadium market price. The vanadium recovery cost decreases with plant capacity due to economies of scale. For this reason, a centralized plant for processing spent catalyst generated in multiple hydroconversion upgraders is potentially feasible. Also, the feasibility of implementing pyrometallurgy operations for the recovery of alumina and nickel from the solid residues generated in the leaching operation depends on the selling price of those co-products; applying a discount of 20% of the current market price, for instance, does not justify the investment in such operations.

The recovery cost of vanadium is more sensitive to the transport cost, the wash ratio implemented in filtration operations, the percentage of vanadium and molybdenum leached out from the catalyst support, and the selling price of MoO_3. The uncertainty analysis shows that variations in those parameters could affect the economic feasibility of the activity.

The results of this research can be used by oil sands operators, waste processing companies, and policymakers to shape projects on the recovery of vanadium from spent catalyst.

Chapter 3: Life cycle GHG emissions assessment of vanadium recovery from spent catalysts from bitumen upgraders[3]

3.1 Introduction

Vanadium is used mainly to produce steel and non-ferrous alloys, but it is also used to manufacture glass coating, ceramics, and catalysts for several industrial processes, and to produce electrolytes for vanadium redox flow batteries (VRFB). Vanadium consumption in the steel industry is projected to increase (Kelley et al. 2017; Prophecy Development Corp. 2019), and the increasing adoption of VRFB places additional pressure on the vanadium market (Adroit Market Research 2019). Global vanadium reserves are about 22 million metric tons, concentrated in China (43%), Russia (22%), Australia (18%), and South Africa (16%), while the world mine production was 86,800 metric tons in 2019 (U.S. Geological Survey 2021). Vanadium is typically mined along with titano-magnetite ore and obtained as a by-product of steel manufacturing. Additionally, it is present in uranium ores. The production of vanadium extends beyond traditional mining methods, with sources including fly ash, spent catalysts, and slag from the steel industry, as well as petroleum residues (Moskalyk and Alfantazi 2003).

Alberta, a province in western Canada, has one of the world's largest petroleum reserves, in the form of oil sands (a mixture of bitumen, water, sand, and clay). Thanks to the high vanadium content in bitumen (190 wppm in average (Gray 2015)) and substantial production

---

[3] A version of this chapter has been submitted to Fuel as M. Baritto, A.O. Oni, A. Kumar. Life cycle GHG emissions assessment of vanadium recovery from spent catalysts from bitumen upgraders.

of bitumen (about 3 million barrels daily (Alberta Energy Regulator 2018)), Alberta's oil sands could become one of the major sources of vanadium. At the current bitumen production rate, about 33,000 metric tonnes of vanadium per year could be produced, representing 31% of the world total mine production in 2021 (U.S. Geological Survey 2022). Considering the potential of the oil sands in the vanadium market, scaling vanadium production to industrial levels merits consideration. However, incorporating this process into the bitumen value chain represents an additional pressure on the already high environmental burden of oil sands operations. For this reason, besides the economic feasibility of such activity, its environmental impact should be addressed.

Vanadium is found in different wastes and by-products of the oil sands industry, including petroleum coke (Hill et al. 2014a) and its ashes (Gomez-Bueno et al. 1981), and spent catalyst (Gray et al. 2000; Gray 2015) . In this study, the vanadium source considered is spent catalysts from bitumen upgrading. In operations like hydroconversion and hydrotreating, chemical reactions are facilitated using catalysts. Because of coke formation and the deposition of metals, primarily vanadium and nickel, catalysts lose their effectiveness over time (Marafi et al. 2017). The spent catalysts are replaced by fresh ones to ensure the continuity of the process.

The recovery of vanadium from oil spent catalysts has been extensively studied. Pyrometallurgy and hydrometallurgy are the most commons routes. The latter usually involves salt-roasting spent catalysts. Detailed reviews of the processes have been conducted by Zeng and Cheng (Zeng and Cheng 2009a; 2009b), Furimsky (Furimsky 1996), and Marafi et al. (Marafi et al. 2017). Commercial processes are described by Llanos and Deering (Llanos and Deering 1998), Marafi et al. (Marafi et al. 2017), Berrebi et al. (Berrebi et al.

1993), and Akcil et al. (Akcil et al. 2015) . Characteristics of these studies are the generation of data at laboratory scale and a proposed process flowsheet. However, there has been limited discussion on the scaling of the process for commercial operations and its implications on greenhouse gas (GHG) emissions. The Greenhouse gases, Regulated Emissions, and Energy use in Technologies (GREET) model has a module for the treatment of spent catalysts (Wang et al. 2015). The process feedstock is a mixture of Mo/Ni/Al spent catalyst from different refineries, with 7.0 wt.% vanadium and 15.0 wt.% residual coke. The process for metal recovery includes roasting, grinding, vanadium and molybdenum recovery, the fusing of alumina, and water pretreatment. The estimated GHG emissions using that model are 3.04 kg CO_2/kg spent catalyst, which includes direct emissions from coke burn-off. The GREET model offers results at a high level but not at the process level. AMG Vanadium, a spent catalyst processor based in the United States, runs a pyrometallurgy process to obtain ferrovanadium from refinery spent catalyst. The company reports process GHG emissions of 12.6 kg CO_2/kg FeV and claims a reduction of 80% compared with the GHG emissions from primary production (AMG Vanadium). No details on the recovery process nor the methods used for GHG emissions estimation are provided on AMG Vanadium's website.

A sense of the GHG emissions from vanadium recovery from bitumen upgrading spent catalysts can be obtained by examining similar processes used for the recovery of different metals from spent catalysts. Roccheti et al. developed a process to recover vanadium, nickel, and other metals from petrochemical spent catalysts, specifically from hydrodesulphurization units (Roccheti et al. 2013). They also performed a life cycle assessment (LCA) of the process. The process includes leaching with ferric iron and sulfuric acid followed by precipitation with sodium hydroxide. The product is a metal mixture used in the iron alloy sector. The authors reported 0.42 kg CO_2eq/kg product from their study system boundary, which includes the production of process electricity, ferric sulfate, sulfuric acid, and sodium hydroxide. The operation with the highest contribution to the GHG emissions is sodium hydroxide production (68%), followed by sulfuric acid (7%), ferric sulfate (22%), and energy production (3%). The advantage of the proposed process is that it avoids thermal operations like roasting with salt and thus the upstream emissions contribute more GHG emissions than the process itself. However, the system boundary does not include the removal of any residual coke on the spent catalysts, which may imply the need for heat treatment to burn off the coke and, thus, the generation of direct emissions. Alonso-Fariñas et al. conducted an LCA of a process for recovering lanthanum from spent catalysts generated by the fluid catalytic cracking (FCC) of heavy fuel oil (Alonso-Fariñas et al. 2020). The process is comprised of acid leaching and sequential precipitation to recover $LaCl_3$ followed by $Al(OH)_3$. Both compounds can directly feed FCC catalyst production. Also, the solid cake from leaching can be dried and ground to be used as a cement substitute. The authors found that the production of Na(OH) for the precipitation of $Al(OH)_3$ makes up 60% of the overall GHG emissions and lanthanum recovery 23%. Most of these emissions are due to the consumption of heat to maintain the leaching temperature. About 40.6 kg CO_2eq/kg $LaCl_3$ are saved by the displacement of cement and $Al(OH)_3$ from their primary production processes. This shows the positive effect of the by-products in the total GHG emissions from the process. The upstream emissions represent a gross part of the share, given that there is no need for thermal operations like roasting or smelting of solid residues performed during the process. Therefore, using this process as a reference for the recovery of vanadium from bitumen upgrading spent catalyst can be misleading. Yang et al. estimated the GHG emissions from nickel recovery from hydrogenation spent catalyst (Yang et al. 2011). The process includes two-stage acid leaching, acid separation, and electrowinning. The system boundary includes the production of consumables, energy consumption, and transportation. About 15.53 kg CO_2eq/kg Ni are generated; of these, 81% corresponds to electricity production. Finally, Le and Lee reviewed hydrometallurgy routes for recovering metals from spent catalysts (Le and Lee 2021). They recognized the need for an LCA and the scarcity of available information. In fact, the only two LCA studies on the recovery of metals from spent catalyst cited in that review were those by Roccheti et al. and Yang et al.

It was concluded that the available literature on GHG emissions from metal recovery from spent catalyst is inadequate to assess the environmental impact of recovering vanadium from bitumen upgrading spent catalysts. The drawbacks of the cited studies are incompleteness, lack of detail and breakdown of results, the recovery of metals other than vanadium, and the consideration of other sources of spent catalysts rather than bitumen upgrading. Considering these gaps, the recovery of vanadium from spent catalysts generated during bitumen upgrading was studied from a GHG emissions point of view. The results will support informed decision-making on the development of economic activity near bitumen upgraders. The objectives of this study were to:

- Develop a data-intensive process model of a hydrometallurgy route for recovering vanadium from the spent catalyst;
- Conduct a life cycle GHG emissions assessment of the vanadium recovery process;
- Evaluate the effect of inputs variations on GHG emissions through sensitivity and uncertainty analyses;
- Conduct a case study for Alberta, Canada.

3.2 Methods

3.2.1 Feedstock description

In Alberta, four upgraders use hydroconversion technology: Scotford, Mildred Lake, Sturgeon, and Lloydminster. The location of these upgraders is shown in Figure 2-2. Based on the data shown in Table 2-2, the generation rate of spent catalyst was estimated at about 36,000 t/y. Then, a capacity of 30,000 t/y was assumed for the vanadium recovery plant.

Spent catalyst composition depends on the properties of the reactor feed, which vary with the properties of the upgraded bitumen. For this study, the data of fresh catalyst fed and spent catalyst removed from the LC-Fining unit at the Mildred Lake upgrader (Table 3-1) was used to estimate the spent catalyst composition. The composition of the spent catalyst was estimated as 13.2 wt.% V_2S_3, 7.1 wt.% V_2O_5, 6.8 wt.% MoS_2, 3.7 wt.% Ni_3S_4, 12.9 wt.% C (coke), 53.8 wt.% Al_2O_3, after assuming metals in their sulfide form.

3.2.2 Recovery process description

Hydrometallurgy routes have been successfully implemented to recover metals from spent catalyst at the industrial scale (Berrebi et al. 1993; Llanos and Deering 1998). Llanos et al. presented a hydrometallurgy process comprised of salt roasting and subsequent water leaching and selective precipitation (Llanos et al. 1997). Through this process, vanadium pentoxide is recovered as the main product, and molybdenum trioxide is co-produced. In addition, nickel alloy and alumina are recovered if a pyrometallurgy process is coupled to the main process. Figure 2-3 shows the process flow considered in this study, and the process description is presented in Section 2.2.2. The products of the process are vanadium pentoxide and molybdenum trioxide. A pyrometallurgy route is included to recover alumina and nickel from the leaching cake.

Table 3-1. Metal and carbon content in fresh and spent catalyst (Gray et al. 2000)

Compound/element	**Content**
Fresh catalyst	
NiO	2-4 wt.%
MoO_3	10-15 wt.%
Spent catalyst, elemental composition	
C (coke)	0.24 g/g alumina
V	0.26 g/g alumina
Ni	2.8 g/ g initial
Others	0.026 g/g alumina

3.2.3 Estimation of life cycle GHG emissions

In Alberta, bitumen is produced either in situ using deep wells or by mining . The production method depends on the depth of the oil sands deposit. Diluted bitumen, named dilbit, is then directly sold to high-conversion refineries or upgraded into SCO. Upgraders are fed mostly with dilbit from oil sands mining. Because spent catalysts are generated from upgrading operations, mining was considered as the bitumen production method in this study.

Hydroconversion and hydrotreating operations are two sources of spent catalyst in the bitumen upgrading process, as shown in Figure 2-1. Both operations combine heat, hydrogen, and catalysts to promote reactions that improve feed quality. As discussed in Section 2.2.1, because of the high metal content and the ability to continuously feed a plant for metal recovery, hydroconversion spent catalysts was considered as the feedstock for vanadium recovery in this study.

The scope of the life cycle assessment performed in this analysis was cradle-to-gate, i.e., from bitumen production to the recovery of metals, prior to transportation to final use. The GHG emissions are classified as indirect emissions and direct emissions. Indirect GHG emissions include those from the upstream operations required to obtain the spent catalyst to feed the vanadium recovery process; GHG emissions associated with the production of the consumables required by the vanadium recovery process; and GHG emissions from the production of electricity used by said process. Direct GHG emissions are those generated on site and include emissions from the combustion of fuels to provide heat to the process as well as those generated during chemical reactions. The system boundary includes the unit operations shown in Figure 3-1. Unless stated otherwise, electricity is obtained from the grid and natural gas is used as fuel. The energy consumption data were segregated into electricity and heat, and the associated GHG emissions were calculated using the emission factors in Table 3-2.

Indirect GHG emissions from bitumen production, atmospheric and vacuum distillation, and hydroconversion were estimated from published energy consumption and process GHG emissions data and allocated to vanadium in spent catalysts. A mass allocation approach, using the method presented by Wang et al. (Wang et al. 2004), was considered in this study. The compiled data is shown in Table 3-3. Indirect GHG emissions from the production of consumables were obtained from the literature (Argonne National Laboratory 2020), as summarized in Table 3-4. The indirect GHG emissions associated with construction and maintenance were excluded. The disposal of wastes and by-products of the recovery process was excluded as well. For the direct GHG emissions, natural gas consumption and emissions from chemical reactions were estimated through process modeling. Details of the developed model are presented in Section 2.2.3

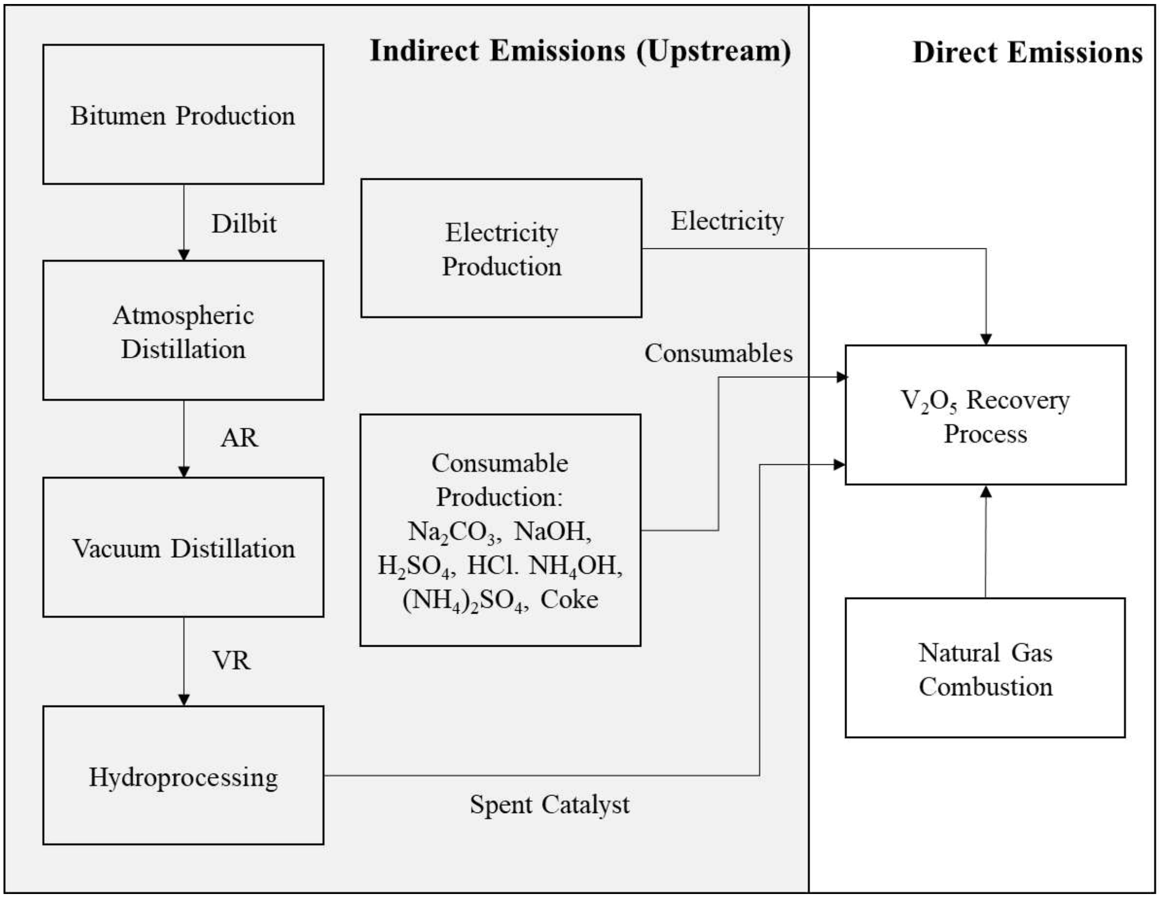

Figure 3-1. System boundary for life cycle GHG emissions

3.2.4 Model development

The material and energy balances of each unit operation were performed using first principles and correlations implemented in spreadsheet-based models. The main process conditions used to develop the process model are presented in Table 2-4. The electricity consumption of screw conveyors, pumps, compressors, and agitators, as well as the heat losses from reactors and stirred tanks, were also included in the model. The amount of soluble salts and the composition of the off-gases from the roasting operation were obtained from the stoichiometric reactions shown in Table 2-3. The energy balance includes the sensible heat of the feed and product, the enthalpy of reaction, and off-gases energy. The electricity required to drive the multiple hearth furnace shaft and the feeding belt conveyer was also considered.

The calculated heat duty of the cooling heat exchanger enabled estimation of the electricity consumption of the refrigerator unit. The energy required for grinding the spent catalysts was calculated using the Bond equation (Ulrich and Vasudevan 2004), assuming a work index equal to alumina's, the base material of the catalysts.

The outputs of leaching, solvent extraction, and ammonia recovery operations were estimated using separation ratios or operation efficiencies. The output of the precipitation operations was estimated from the metal concentration in the spent liquor reported by Llanos et al. (Llanos et al. 1997). The energy balance for those operations included heating the involved streams up to the required temperature and the electricity consumed by stirring, if required.

Table 3-2. Emission factors used in this study (Government of Alberta 2019b)

Energy type	Emission factor
Electricity production (grid)	530 kg CO_2eq/MWh
Natural gas combustion	188 kg CO_2eq/MWh[a]
Diesel combustion	3.0 kg CO_2eq/L

a. Considering emissions of 1.954 kg CO_2eq/m^3 (Government of Alberta 2019b) and a heat content of 10.37 kWh/m^3 (Government of Canada 2015).

Table 3-3. Data for the estimation of indirect emissions associated with bitumen production and processing

Operation	Electricity	Fuel	Reference[b]
Bitumen production	80.4 kWh/m^3 bitumen	74.4 m^3 natural gas/m^3 bitumen 6.2 L diesel/m^3 bitumen	(Nimana et al. 2015a)
Atmospheric distillation	0.90 kWh/bbl dilbit	30.5 kWh/bbl dilbit	(Nimana et al. 2015b)
Vacuum distillation	0.30 kWh/bbl AR	52.2 kWh/bbl AR	(Nimana et al. 2015b)
Hydroconversion	8.0 kWh/bbl VR	51.8 kWh/bbl VR	(Nimana et al. 2015b)
Hydrogen production[a]	-	0.0398 m^3 natural gas/m^3 H_2	(Nimana et al. 2015b)

a. For the hydroconversion of vacuum residue.

b. From studies by my research group.

Table 3-4. Data for the estimation of indirect GHG emissions associated with consumable production

Consumable	**Carbon intensity (kg CO_2eq/kg consumable)**	**Reference**
Coke (metallurgical)	0.15	(Li et al. 2020)
HCl	1.84	(Argonne National Laboratory 2020)
H_2SO_4	0.14	(City of Winnipeg)
Na_2CO_3	1.01	(Argonne National Laboratory 2020)
NaOH	0.46	(City of Winnipeg)
NH_4OH	1.16	(Argonne National Laboratory 2020)
$(NH_4)_2SO_4$	0.63	(Argonne National Laboratory 2020)

The calcination of vanadium and molybdenum was modeled in the same way as roasting. The sensible heat of the feed, the enthalpy of reaction, and the energy carried by the off-gases and products were included in the energy balance, assuming stochiometric reactions (Table 2-3). The electricity required to drive the rotary kiln used in each operation was included.

Regarding the recovery of metals from the leaching cake, the drying operation was modeled as the simple evaporation of water to reduce the moisture content up to a suitable value for the upcoming smelting operation. Stochiometric reactions for the oxidation of nickel contained in the dried cake were assumed to determine off-gases composition (Table 2-3), while the energy consumption was obtained through a correlation with similar processes.

3.2.5 Sensitivity and uncertainty analyses

The Regression, Uncertainty, and Sensitivity Tool (RUST) (from our research group colleagues (Di Lullo et al. 2019)) was used for sensitivity and uncertainty analyses. The sensitivity of the estimated GHG emissions per kg of recovered V_2O_5 was evaluated using the Morris method. An overview of the method is shown in Appendix B. Fifty-one inputs were varied for the analysis. The inputs included process variables like excess air for roasting and the liquid-to-solid ratio used in leaching; equipment performance factors like the specific energy consumption of furnaces, the coefficient of performance (COP) of the refrigeration system, the efficiency of boilers, furnaces, and burners, the work index for grinding, and the heat transfer coefficients to estimate heat losses from vessels; and emission factors. Eight inputs identified following the sensitivity analysis were used for uncertainty analysis. Five thousand runs were performed for the Monte Carlo simulation, implemented in RUST as well. The same variation ranges used for the sensitivity analysis were considered in the uncertainty analysis. A uniform probability distribution was considered to populate the samples.

3.2.6 Treatment of co-products

The studied process is a multifunctional product system. Besides vanadium, molybdenum, alumina, and nickel alloy can be recovered from the spent catalyst. Thus, the allocation of GHG emissions among co-products is required. In the metal industry, this allocation is usually performed in proportion to the mass or economic value of the co-products (Norris and Weidema 2002). For the system considered in this study, mass-based allocation can be misleading since the largest co-product is alumina, which constitutes the support of the catalyst, but V_2O_5 is the product of interest. Moreover, recovering alumina and nickel does not drive the process. As shown in Chapter 2, the production cost of V_2O_5 is insensitive to the revenue for selling recovered alumina and nickel alloy. Conversely, the authors noted in their earlier study that recovering MoO_3 is necessary for the profitability of the process (Baritto et al.).

As indicated by the International Organization for Standardization (ISO) in standard 14040, system expansion is preferred over allocation. System expansion implies expanding the system boundary to include displaced processes and any further processing of the co-products (International Organization for Standardization 2006). The recovered MoO_3 is usually recycled back to the catalyst's manufacturers, while the fate of alumina and nickel alloy is in the steel industry. Considering V_2O_5 as the main product of the process, the co-produced MoO_3 and Al_2O_3 would displace the primary production of molybdenum and alumina towards different applications or even reduce the primary production. That said, the V_2O_5 product system was expanded to include primary routes to produce alumina and molybdenum trioxide. The displaced GHG emissions are accredited to the V_2O_5 product system. The recovered nickel alloy is considered scrap, a by-product of alumina recovery. For this reason, displaced processes, if any, are not considered in the expansion of the system.

Figure 3-2 depicts the system expansion considered in this study. Subsystem A is the original system boundary, which is considered a V_2O_5 product system. Subsystems B and C are the displaced primary production routes of alumina and MoO_3, respectively. The GHG emissions from subsystems B and C are subtracted from the GHG emissions from subsystem A to obtain the GHG emissions associated with the recovery of V_2O_5 through the process considered in this study.

The estimated carbon intensity of MoO_3 is 10.8 kg CO_2eq/kg MoO_3 (Snowden-Swan et al. 2016), based on the International Molybdenum Association's product inventory, which includes mining the ore and refining the molybdenum. Regarding the primary production of alumina, the GREET model estimates 3.52 kg CO_2eq/kg Al_2O_3 (Argonne National Laboratory 2020), while Nunez and Jones reported 2.00 kg CO_2eq/kg Al_2O_3 (Nunez and Jones 2015). For this study the average of those values (2.75 kg CO_2eq/kg Al_2O_3) was used.

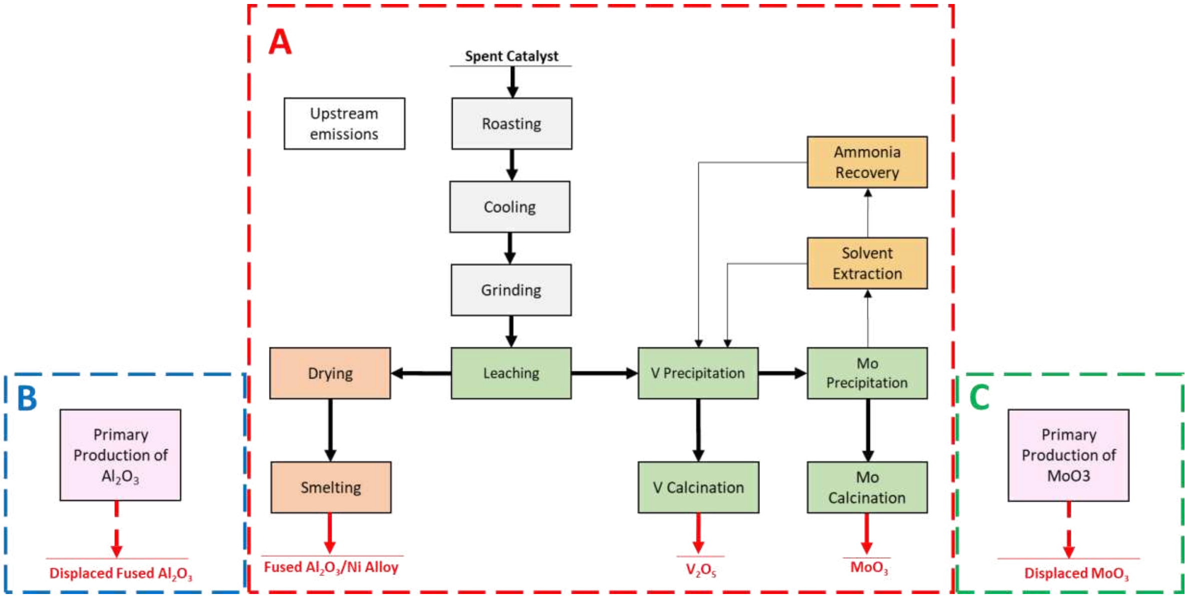

Figure 3-2. System expansion. Subsystem A: V_2O_5 product system; Subsystem B: Displaced Al_2O_3 production process; Subsystem C: Displaced MoO_3 production process

3.3 Results and discussion

3.3.1 Material and energy balance

A plant processing 30,000 tonnes of spent catalyst per year would generate about 0.65 t/h of granular V_2O_5. Besides V_2O_5, about 0.21 t/h of MoO_3 is co-produced. By incorporating a pyrometallurgy treatment to the leaching cake, 1.84 t/h of fused alumina and 0.36 t/h of nickel alloy are recovered as well. Table 2-10 shows the material balance, on a V_2O_5 basis, for each unit operation considered in the process.

Figure 3-3 shows the energy consumption per kg of V_2O_5. In total, 13.3 kWh/kg V_2O_5 are required. Of this, 70.3% corresponds to electricity and 29.7% to natural gas. Operations involving thermal processes are the main consumers. Electricity for cake smelting consumes the most energy (62.2%), leaching accounts for 11.2%. The leaching operation uses natural gas to raise the temperature of the leaching water. The large amount of natural gas used in this case is due to the high liquid-to-solid ratio and the high temperature required for heating water. In roasting, the consumption of both natural gas and electricity is significant, making up 9.4% of the total energy consumption, the former to provide heat for the second stage of roasting and the latter mainly to drive the center shaft of the furnace and the fan to provide air to the operation. Vanadium calcination contributes 6.7% of the energy consumption in the form of natural gas. Electricity is also used by the ball mill and the refrigeration system for cooling, as well as by auxiliary equipment like conveyors, pumps, and agitators, but they consume considerably less electricity than smelting and roasting. The consumption of natural gas to provide heat to the remaining operations is marginal.

As Figure 3-3 shows, the recovery of nickel and alumina represents 69% of the total energy consumption; the recovery includes cake drying and smelting. Should only vanadium and molybdenum be recovered, the energy consumption would be 4.10 kWh/kg V_2O_5, or 31% of the energy required for the whole process. Whether to recover nickel and alumina is an economic consideration. In Chapter 2, it was concluded that the breakeven recovery cost of vanadium strongly depends on the co-production of molybdenum; the contribution of the other metals is not significant (Baritto et al. 2022).

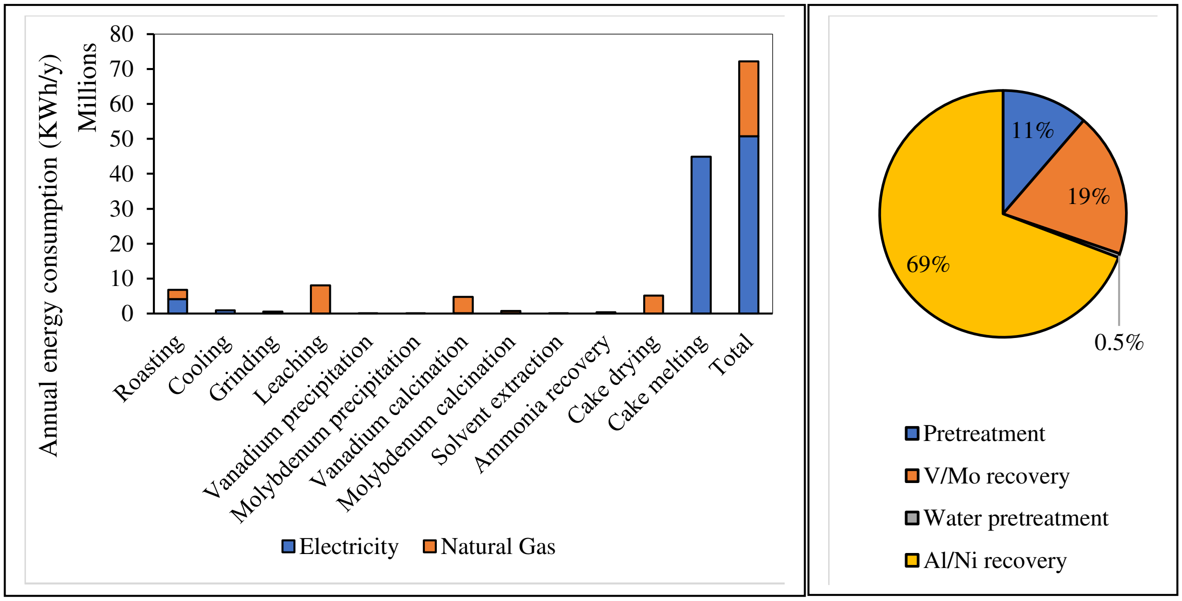

Figure 3-3. Energy consumption of vanadium recovery from bitumen upgrading spent catalysts. Left: annual energy consumption. Right: breakdown of annual energy consumption

3.3.2 Indirect emissions

Indirect emissions comprise bitumen production and processing and the production of consumables and electricity consumed by the recovery process. These emissions total 6.31 kg CO_2eq/kg V_2O_5 with 73.1% coming from the production of electricity for the recovery process, 25.6% from the production of consumables, and 1.3% from the upstream operations required to generate the feedstock.

Table 3-5 shows the indirect GHG emissions from bitumen production and processing. For the upstream operations associated with the generation of the feedstock, the GHG emissions were calculated from the collected data and from these determined the cumulative GHG emissions as far as the hydroconversion operation. For multiproduct operations, the cumulative GHG emissions were allocated to the streams carrying vanadium. The results are expressed per barrel of produced bitumen and per kg of vanadium pentoxide. It is observed that the cumulative GHG emissions from the hydroconversion operation are lower than the cumulative GHG emissions from the other operations. The low value is a result of the allocation method applied. The content of vanadium in the hydroconversion feed is in the order of 200 wppm, and this operation removes about 71 wt.% of vanadium (Gray 2015). As a result, the allocation weight assigned to vanadium in spent catalysts is 1.5 x 10^{-4}, reducing the cumulative GHG emissions to practically zero.

Table 3-5. Indirect emissions associated with the generation of the feedstock

Operation	**Process GHG emissions (kg CO_2/bbl bit.)**	**Cumulative GHG emissions (kg CO_2/bbl bit.)**	**Cumulative GHG emissions (kg CO_2/V_2O_5)**	**Comments**
Bitumen production	31.7	31.7	531	-
Atmospheric distillation	8.87	28.0	469	Allocated to AR
Vacuum distillation	8.88	24.0	401	Allocated to VR
Hydroconversion	8.70	0.005	0.085	Allocated to vanadium

The indirect emissions associated with the production of consumables are 1.50 kg CO_2/kg V_2O_5, while those from the generation of the electricity used in the recovery process are 5.04 kg CO_2eq/kg V_2O_5. The distribution of these indirect emissions among the related operations in the vanadium recovery process is shown in Table 3-6. Sodium carbonate for the roasting of the spent catalyst is the consumable with the greatest GHG emissions. Cake smelting is the operation that consumes the most electricity; thus, it has the greatest GHG emissions related to electricity production.

3.3.3 Direct emissions

Direct emissions include those from burning natural gas to supply heat to the process, and process emissions, i.e., those generated during the transformation of the feedstock into the final product. Direct emissions total 3.62 kg CO_2eq/kg V_2O_5; 79.6% corresponds to process emissions and 20.4% to the combustion of natural gas. The largest source of direct emissions is the roasting operation (78.2%), mainly because burning the residual coke out of the spent catalyst releases 13.5 million kg CO_2eq/y. Leaching is the operation with the largest GHG emissions from the combustion of natural gas (7.73% of direct emissions) because the high amount of heat required to increase the temperature of process water used in this operation.

Table 3-6. Indirect emissions associated with the production of consumables and electricity

Related operation in vanadium recovery process	**Consumable**	**GHG emissions from consumable production (kg CO_2eq/kg V_2O_5)**	**GHG emissions from electricity production (kg CO_2eq/kg V_2O_5)**
Roasting	Na_2CO_3	1.01	0.40
Cooling			0.09
Grinding			0.05
Leaching			0.001
Vanadium precipitation	$(NH_4)_2SO_4$	0.34	0.01
	H_2SO_4	0.07	0.001
Molybdenum precipitation	HCl	0.06	0.01
Vanadium calcination			0.01
Molybdenum calcination			0.01
Solvent extraction	NH_4OH	0.12	0.001
Ammonia recovery	NaOH	0.02	0.003
Cake drying			0.0002
Cake melting	Coke	0.002	4.39

3.3.4 Life cycle GHG emissions

The life cycle GHG emissions are 10.3 kg CO_2eq/kg V_2O_5. Of these, 35% are direct GHG emissions and 65% indirect GHG emissions. Electricity production contributes 48% to the life cycle GHG emissions, while 16% correspond to the production of consumables, with Na_2CO_3 making up 10% of the life cycle GHG emissions. The production and processing of bitumen to produce feedstock only account for about 1% of the life cycle GHG emissions. The complete breakdown is shown in Figure 3-4.

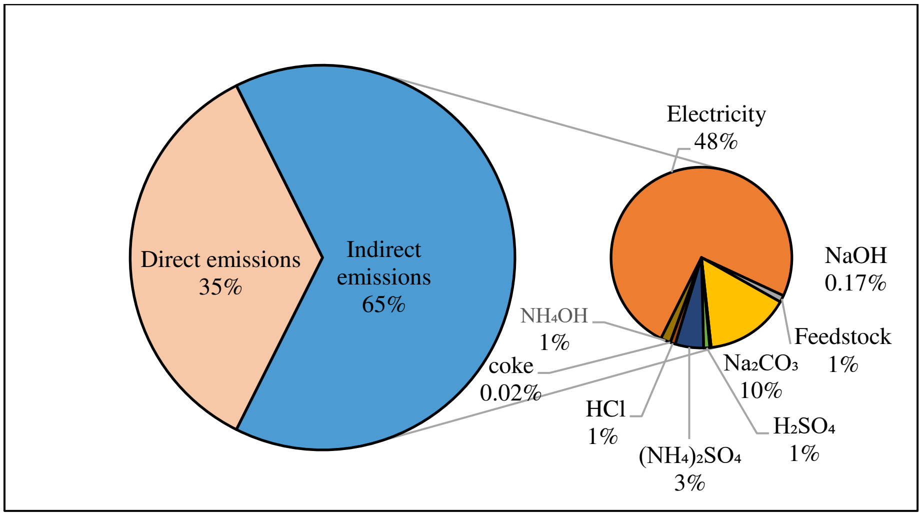

Figure 3-4. Breakdown of life cycle GHG emissions

Figure 3-5 presents the contribution of each operation of the recovery process to the life cycle GHG emissions. The indirect GHG emissions from the production of electricity and consumables were distributed among the operations responsible for the consumption of each resource. To account for all the GHG emission categories in the same figure, the GHG emissions associated with the feedstock were allocated to the roasting operation.

Cake melting and roasting are the operations that contribute the most to the life cycle GHG emissions, with 4.44 and 4.42 kg CO_2eq/kg V_2O_5, respectively, corresponding to 86.6% of the total emissions. GHG emissions from the roasting operation are mostly process GHG emissions from the burning of residual coke on the spent catalyst surface, but also those associated with the production of Na_2CO_3 (the consumable with the largest contribution to the life cycle GHG emissions) and the production of electricity (the electricity consumed by this operation is the second largest in the process). The GHG emissions associated with the cake melting operation are mainly from the production of the electricity required in this operation. As seen in Figure 3-5, the pretreatment of the spent catalysts, which includes roasting, represents 45% of the life cycle GHG emissions. The same percentage is shared by the operations involved in the recovery of nickel and aluminum from the leaching cake. The life cycle GHG emissions would be 4.62 kg CO_2eq/kg V_2O_5 lower if these materials were not recovered.

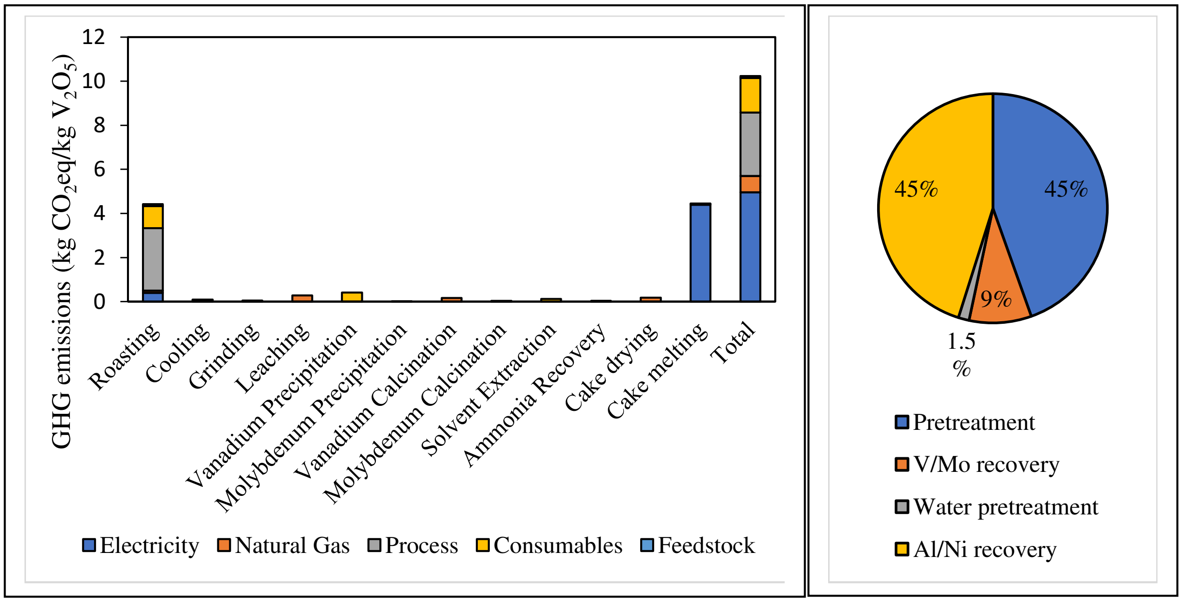

Figure 3-5. Contribution of each operation of the vanadium recovery process on the life cycle GHG emissions

3.3.5 Sensitive inputs and effect of uncertainties on the estimated process emissions

Figure 3-6 shows the results of the sensitivity analysis. The inputs with higher influence on the output (i.e., their variation leads to large variations in the output mean) are found on the right side. Also, the higher the vertical coordinate, the greater the standard deviation of the output relative to one specific input, which means that the model's output is a non-linear function on that parameter. It is observed that the GHG emissions from the studied process are more sensitive to the emission factor of electricity production by the grid and the specific energy consumption in the electric arc furnace used for smelting the leaching cake and separating nickel alloy from fused alumina. This result is not surprising given the high electricity consumption in the smelting operation. Also, a group of inputs with a much lower effect on the model's output than the two mentioned above but significantly higher effect than the rest of the considered inputs is identified. The Na_2CO_3-to-spent catalyst ratio, used in the second stage of roasting, is the input with the third highest sensitivity. This result is because the upstream GHG emissions from the production of the salt are directly added to the GHG emissions from the recovery process. Therefore, a small change in this input, as well as in the carbon intensity of the Na_2CO_3 production process, would make a significant change in the output of the model. The GHG emissions associated with heat production account for about 9% of the total GHG emissions and directly depend on the emission factor of natural gas combustion, hence the sensitivity of the output to this input. The solid fraction in cake indicates the amount of water that should be removed during the drying process. The GHG emissions associated with the generation of heat for this operation are about 2% of the total; however, the interaction of this input with the GHG emission factor of natural gas combustion may be responsible for the sensitivity of this input. Finally, the liquid-to-solid ratio in leaching is the amount of water used, and therefore heated, in the process, and ammonium sulfate has a high carbon intensity and consumption per kg of V_2O_5. The rest of the inputs have little influence on the output of the model.

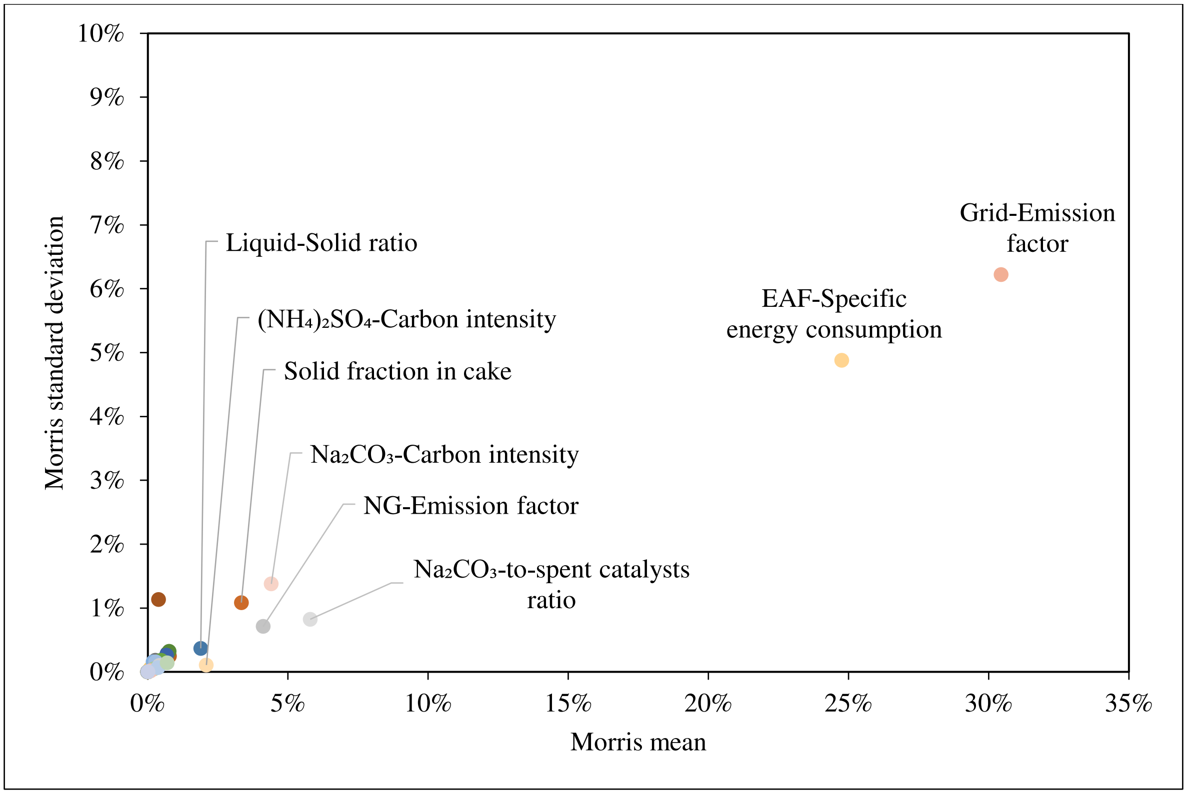

Figure 3-6. Results of the sensitivity analysis

Figure 3-7 presents the results of the Monte Carlo simulation, considering the variation in the eight inputs that influence the output of the model. The life cycle GHG emissions from the recovery process range from 8.21 kg CO_2eq/kg V_2O_5 to 12.1 kg CO_2eq/kg V_2O_5, with a confidence of 90%. The mean value is 10.0 kg CO_2eq/kg V_2O_5, with a standard deviation of 1.19 kg CO_2eq/kg V_2O_5.

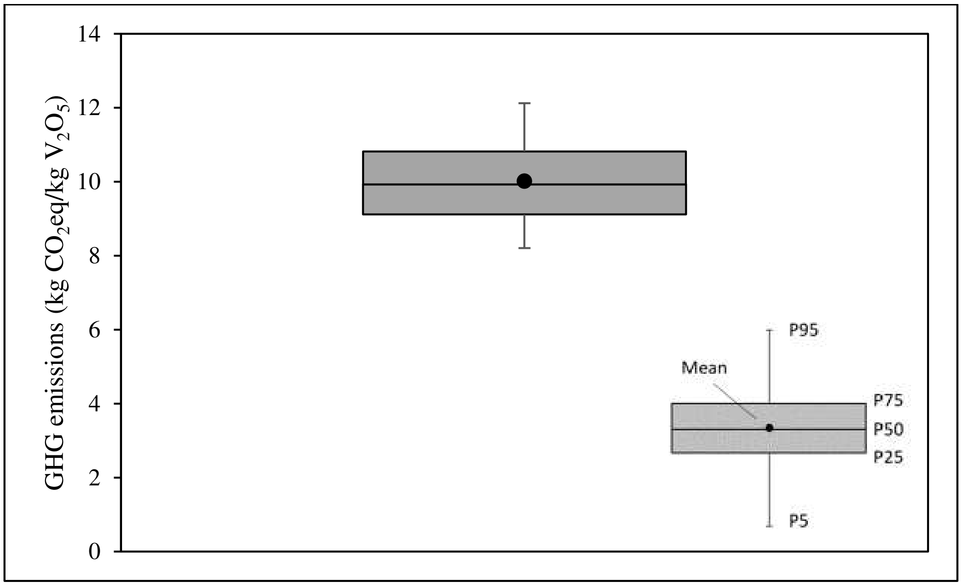

Figure 3-7. Results of the uncertainty analysis

3.3.6 Comparison with other processes

Figure 3-8 presents the GHG emissions from the production of vanadium pentoxide from different sources. The aim is to compare the GHG emissions from the studied process with those from one of the primary processes to produce V_2O_5. Vanadium pentoxide is usually produced from a vanadium-bearing slag obtained as a by-product of steel production from a vanadium titano-magnetite (VTM) ore. Energy consumption and GHG emissions data for this process were used to estimate the GHG emissions of this pathway (Chen et al. 2015). GHG emissions from mining and dressing, sintering and pelletization, the blast furnace, and the basic oxygen furnace, as well as from the co-production of ilmenite, and the production of coke, coal, lime, quicklime, and electricity used in those operations, were considered as upstream GHG emissions associated to the generation of vanadium slag, i.e., the feedstock to produce V_2O_5. Such GHG emissions were allocated to vanadium, ilmenite, and steel in a mass basis. GHG emissions from the production of electricity and consumables used in the vanadium production process complete the indirect GHG emissions. Those emissions from the vanadium production process were considered direct emissions.

Recovering vanadium pentoxide from spent catalysts generates lower GHG emissions than the primary production process. One of the advantages of using spent catalyst as a source of V_2O_5 is the considerably reduced upstream GHG emissions from the extraction and processing of bitumen allocated to vanadium in the spent catalyst (1% of life cycle GHG emissions), compared to those from VTM mining and processing to vanadium slag (23% of the life cycle GHG emissions)

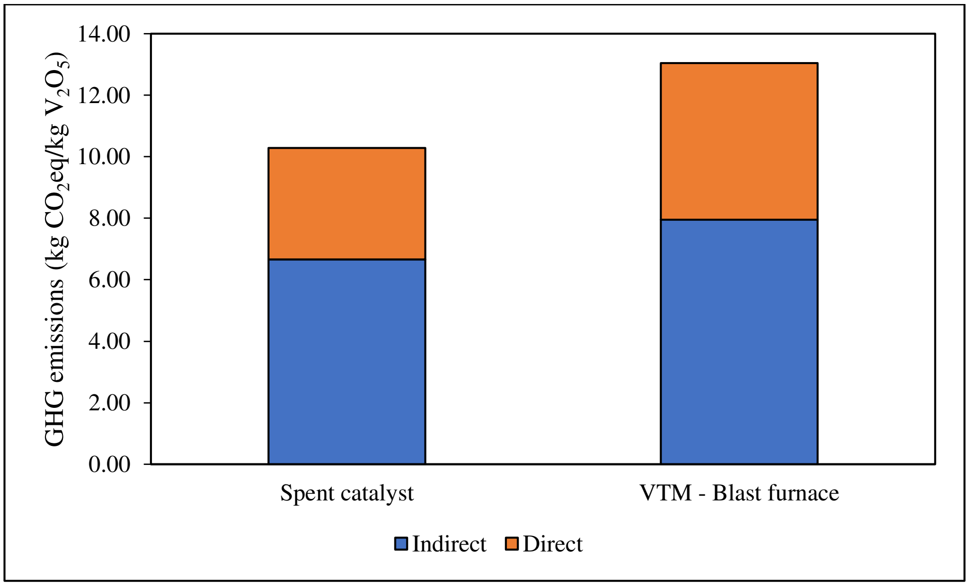

Figure 3-8. GHG emissions comparison between different vanadium sources. Spent catalyst vs titano-vanadium magnetite

Producing ferrovanadium (FeV) is an alternative means of processing spent catalyst. The process includes roasting the spent catalysts and oxidation-reduction in an electric arc furnace to produce FeV. A ferrovanadium manufacturer in the US reports process GHG emissions of 12.6 kg CO_2eq/kg FeV (AMG Vanadium). A direct comparison between the results of this study and the US manufacturer's process is not possible because the product functions are not the same. However, insight into the performance of the processes can be gained by rewriting the process GHG emissions in terms of vanadium content in a product. The results, shown in Figure 3-9, indicate that recovering vanadium from spent catalyst in the form of V_2O_5 would generate about 42% fewer process GHG emissions than doing so in the form of FeV.

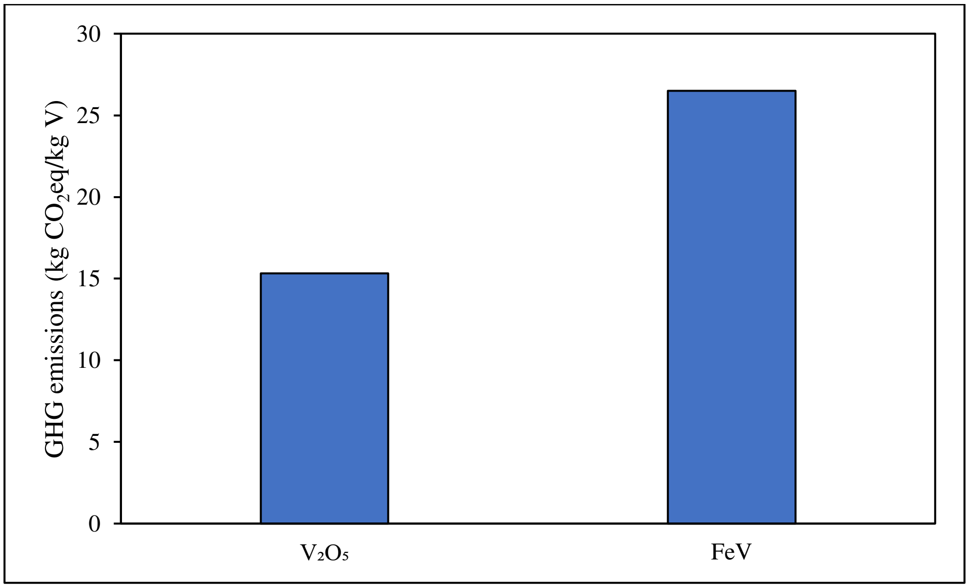

Figure 3-9. GHG emissions per kg of recovered vanadium. Production of V_2O_5 vs production of FeV

3.3.7 Emissions associated to vanadium pentoxide

The life cycle GHG emissions results are expressed per kg of recovered vanadium pentoxide and acredited to the V_2O_5 product system as explained in Section 3.2.6. As shown in Figure 3-10, the GHG emissions from subsystem A, i.e., the recovery process, are 10.3 kg CO_2eq/kg V_2O_5. This number is equivalent to allocating all the GHG emissions solely to vanadium pentoxide without considering system expansion. The co-production of alumina displaces from its primary production process the equivalent of 2.83 kg Al_2O_3 per kg of recovered V_2O_5, which represents 7.78 kg CO_2eq/kg V_2O_5 accredited to the V_2O_5 product system. In the case of molybdenum trioxide, about 0.32 kg MoO_3 is recovered per kg of recovered V_2O_5, enough to accredit 3.44 kg CO_2eq/kg V_2O_5 to the V_2O_5 product system. In summary, the displacement of alumina and molybdenum trioxide by the co-produced metals would offset all of emissions from the recovery process and generate a credit of 0.94 kg CO_2eq/kg V_2O_5. Besides the obvious environmental benefit, this result also could represent an economic advantage if a carbon tax is in place, as is the case in Alberta, Canada.

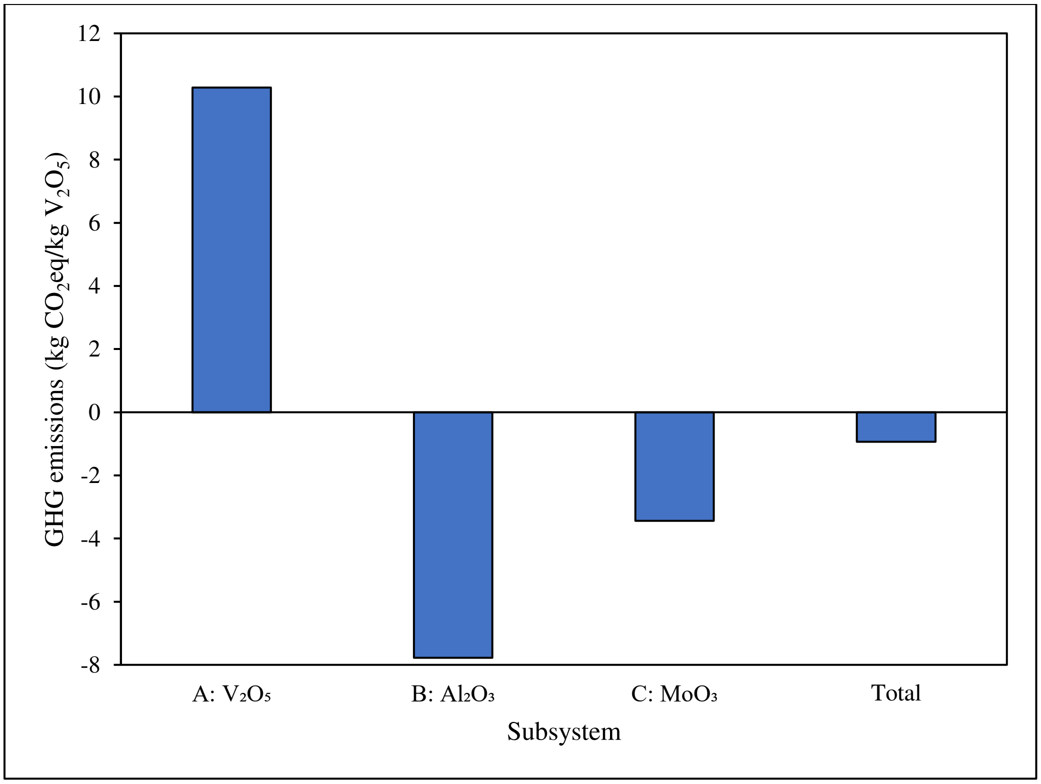

Figure 3-10. Allocation of GHG emissions to the V_2O_5 product system

3.4 Conclusions

The life cycle GHG emissions from the recovery of V_2O_5 from bitumen hydroconversion spent catalysts through hydrometallurgy were estimated. Upstream GHG emissions, including bitumen production and processing, and the production of consumables were calculated based on energy consumption and direct emissions data. To estimate the GHG emissions from the recovery process, a data-intensive spreadsheet-based model was developed.

Life cycle GHG emissions are 10.3 kg CO_2eq/kg V_2O_5. Of these, 35% are direct emissions and 65% indirect (upstream) GHG emissions. The greatest contributor to indirect GHG emissions is Na_2CO_3 production, with 1.01 kg CO_2eq/kg V_2O_5, while bitumen production and processing contribute 0.085 kg CO_2eq/kg V_2O_5. Regarding the direct GHG emissions, spent catalyst roasting is by far the greatest source of GHG, with 80% of the share.

The grid emission factor and the specific energy consumption in the electric arc furnace are the inputs with greater effect on the life cycle GHG emissions. The carbon intensity of Na_2CO_3 production and the salt-to-spent catalyst ratio have a moderate influence on the model output. According to the uncertainty analysis results, by considering the variation of the relevant inputs, the likely values of life cycle GHG emissions are between 8.21 kg CO_2eq/kg V_2O_5 and 12.1 kg CO_2eq/kg V_2O_5. These values are lower than the GHG emissions from the production of vanadium pentoxide from vanadium titano-magnetite.

Considering only the process GHG emissions, recovering vanadium from spent catalysts in the form of V_2O_5 generates fewer emissions than doing so in the form of FeV, in terms of kg CO_2eq per kg of vanadium in the product.

Besides vanadium pentoxide, the study considered the recovery of alumina and molybdenum trioxide. The displacement of these by-products from their primary production processes represents GHG emissions savings of about 11.2 kg CO_2eq/kg V_2O_5. These savings are enough to offset the GHG emissions from the recovery process and generate a credit of 0.94 kg CO_2eq/kg V_2O_5.

Diverse stakeholders, like oil sands operators, policymakers, and catalyst recycling companies, can use the results of this study to frame projects on the recovery of vanadium from spent catalyst.

Chapter 4: The techno-economic assessment of vanadium recovery from bitumen-derived petcoke fly ash[4]

4.1 Introduction

Petroleum coke, or petcoke, is a solid by-product of the upgrading and refining of crude oils. During the coking operation, the feed, e.g., the heavy residues of crude oil distillation, is subjected to high temperatures to thermally crack the long-chain hydrocarbons into light products. Petcoke is composed of the heavy molecules left behind in the coking operation, including sulfur and metals carried along with the fed bitumen. The commercial value of petcoke depends on its grade and morphology, and it can be used as fuel for power generation and cement kilns and in the manufacturing of aluminum, steel, and glass. However, petcoke from heavy and sour crude oils is mainly stockpiled because the oils' metal and sulfur content limit its use as raw material or fuel. This issue is observed worldwide as refineries evolve to process heavy petroleum feedstock that produces petcoke (Edwards 2015). Recovering the vanadium trapped to the petcoke is a way to create value from this by-product, given the ramping demand of the metal for steel production but also for the manufacturing of redox flow batteries. The purpose of this study is to explore the economic feasibility of vanadium recovery at a large scale, considering the petcoke from the upgrading of Alberta's oil sands bitumen as a case study.

---

[4] A version of this chapter has been submitted to Waste Management as M. Baritto, A.O. Oni, A. Kumar. Vanadium recovery from oil sands petcoke fly ash: a comprehensive techno-economic assessment.

Alberta, a western province of Canada, has one of the largest deposits of crude oil in the world. The deposits are mainly in the form of oil sands, a mixture of bitumen, water, and inorganic material. Alberta's oil sands bitumen has a high sulfur and metal content compared to conventional crude oil. These elements concentrate in the petcoke derived from both delayed and fluid coking; the coking technologies used in bitumen upgrading in Alberta. The metal and ash content in bitumen petcoke exceeds the specifications of anode-grade coke, and the high level of sulfur in petcoke limits its use as fuel-grade coke (Gray 2015). Therefore, this by-product is either stockpiled, sold as a low-value fuel, or combusted in situ to provide heat to the upgrading process. Currently, the production of petcoke is about 11.4 million metric tons per year, and the amount of stockpiled petcoke is to 132 million metric tons (Alberta Energy Regulator 2020). With such inventory and a vanadium content in petcoke of 0.11 to 0.13 wt.% (Gray 2015), Alberta's oil sands have the potential to become an important supplier of vanadium worldwide.

The technical viability of vanadium recovery from petcoke derived from different crude oils has been established. Diverse hydrometallurgy and pyrometallurgy routes have been proposed to recover vanadium in the form of ferrovanadium alloys or vanadium pentoxide, along with other metals like nickel and molybdenum The metals can be recovered directly from the petcoke with or without previous modification or from the residue of the combustion or gasification of petcoke. In general, leaching vanadium directly from petcoke exhibits poor yield (water or alkali leaching) or low selectivity (acid leaching) that increases the complexity of the process because of the additional purification steps. The modification of petcoke prior to leaching appears to increase the extraction efficiency. Zhang et al. tested different types of surfactants in the leaching of vanadium with a solution of NaOH and Na_2CO_3 (Zhang et al.

2015). The vanadium content in the leaching solution increased up to 39% relative at the case without surfactant; the increase depends on the temperature and surfactant amount.

Haas et al. patented a process to recover vanadium from ash that originates from the gasification of petcoke (Haas and Hesse 1981). Because the gasification process uses an alkali catalyst, such as sodium carbonate or potassium carbonate, the produced ash contains vanadium salts that are readily soluble in water, which ease the recovery of the metals. Queneau et al. patented a process to selectively recover vanadium and nickel from petcoke by slurrying the material in a sodium carbonate solution and digesting the slurry at a moderately elevated temperature in a pressurized oxidating atmosphere, producing a sodium vanadate liquor and a digestion residue (Queneau et al. 1984). The residue is leached with an alkali solution to extract residual vanadium. The nickel remaining in the leaching residue can be recovered in a further acid leaching step. Davila Armas studied the extraction of vanadium and nickel from Venezuelan petcoke generated during the refining of conventional crude oil (Davila Armas 1988). Following leaching with different reagents, only traces of metals were recovered from the as received petcoke. However, after grinding, heating, and treatment with hydrogen chloride, the recovery of vanadium and nickel from flexicoke was greater than 85% and 80%, respectively. Gardner patented a process to recover vanadium from flexicoke directly from the material or from fly ash (Gardner 1987). The process comprises mixing the material with an alkali metal compound, burning off the carbon and producing water-soluble vanadium salts, water leaching, and vanadium precipitation with ammonium sulfate.

The salt-roasting treatment to recover vanadium was proven at laboratory scale using Syrian petcoke (Shlewit and Alibrahim 2006). Roasting the petcoke with Na_2CO_3 and leaching with water extracted 60 wt.% of the vanadium and more than 90 wt.% of the sulfur in the petcoke.

Reppas and Spitz proposed a method to obtain a methane-rich gas by hydromethanation of carbonaceous feedstocks, including petcoke, in the presence of an alkali metal catalyst, carbon monoxide, hydrogen, and steam (Rappas and Spitz 2013). A vanadium-rich char is obtained as a by-product of the gasification process. Vanadium is recovered from the char through a sequence of aqueous quenching, ion exchange or solvent extraction, and ammonium vanadate precipitation.

Vanadium oxides can be recovered from petcoke using pyrometallurgy processes. For instance, petcoke can be melted in an iron bath with severe oxidizing atmosphere. Under such conditions, nickel is dissolved in the melt, while molten vanadium metal is oxidized to form a slag (Holcombe and Malone 2001) or dust (Malone and Holcombe 2001), which is withdrawn from the reactor.

Regarding the recovery of vanadium and other metals from petcoke derived from bitumen oil sands, a few processes have been proposed. Jack et al. studied the leaching of metals from petcoke, ashed petcoke, and fly ash using different leachates and petcoke produced via delayed coking, fluid coking, and flexicoking. They found that only traces of vanadium and nickel can be extracted directly from delayed coker and fluid coker petcoke, irrespective of the leachate used, while about 34 wt.%, vanadium, 35 wt.% iron, and 43 wt.% nickel were recovered from flexicoker petcoke using a 2 N H_2SO_4 solution (Jack et al. 1980). The extraction efficiency of vanadium decreases but its selectivity increases when a Na_2CO_3 solution is used as leachate (Jack et al. 1979). Also, the authors concluded that the leachability and selectivity of vanadium and nickel improve if the petcoke is ashed at temperatures below 500°C. However, the efficiency of vanadium and nickel extraction drops 40% and 70%, respectively, for acid leaching using fly ash from the combustion (above 1,000°C) of delayer coker petcoke (Jack et al. 1979). McCorriston patented a process to recover vanadium from petcoke and fly ash by mixing the material with an alkali metal carbonate, heating the mixture in an oxidative atmosphere, and contacting the resulting solid with water to extract the vanadium, which is recovered as ammonium vanadate by precipitation with ammonia (McCorriston 1984). This author reported vanadium recovery efficiency as high as 91-96.2 wt.% from delayed coker petcoke, 79.1-88.0 wt.% from delayed coker petcoke fly ash, 88.0 wt.% from ashed (at 540°C) delayed coker petcoke, and 76.4-76.9 wt.% from ashed (at 560°C) fluid coker petcoke. Griffin and Etsell characterized the fly ash from the combustion of delayed coker petcoke, determined the leachability of vanadium and nickel for different extraction procedures, and optimized the leaching conditions (Griffin and Etsell 1984). Direct leaching did not extract any significant quantity of vanadium, while the highest vanadium extraction was obtained by roasting the ash with sodium chloride followed by water leaching. For a roasting temperature of 905°C with 14 wt.% NaCl and subsequent leaching with water at 97°C with a liquid-to-solid ratio of 1 ml/g, about 95% of vanadium was extracted into an aqueous solution. After acidification of the solution and the addition of the stoichiometric quantity of ammonium chloride, about 70% of vanadium was precipitated as ammonium metavanadate. Holloway and Etsell developed a process flow sheet for vanadium recovery from delayed coker petcoke fly ash (Holloway and Etsell 2005). The process is based on roasting with sodium chloride followed by water leaching, precipitation of ammonium metavanadate, and production of vanadium pentoxide by calcination. The proposed process also includes the decarbonization of the ash prior to roasting, a desilication step to reduce the silicon content in the final vanadium product, the recovery and recycling of sodium chloride to the roasting operation, and the treatment of the off-gases from the decarbonization and roasting to obtain diverse chloride by-products that improve the economics of the process. These authors present a preliminary economic analysis of the process and conclude that the activity is potentially profitable. However, limited details on the economic assumptions were included, so it is hard to determine the validity of the conclusions for the current market conditions.

Feng explored the recovery of vanadium directly from fluid coke after chemical activation (Feng 2017). In the proposed process, the fluid coke is chemically activated by treatment with NaOH or KOH to convert vanadium into a water-soluble species. After sequential washing with water, about 92 wt.% of vanadium leached out. Further washing is required to remove impurities from the activated petcoke, producing a clean activated carbon with commercial value. The precipitation of the dissolved vanadium as calcium vanadate by adding $Ca(OH)_2$ to the aqueous solution is currently being researched.

From the literature review, technology for recovering vanadium from bitumen petcoke, particularly from its fly ash, is available. However, little can be said about the economic feasibility of the process. Such information is key for stakeholders to make informed decisions on the development of a vanadium industry around bitumen production and upgrading. To bridge this gap, the recovery of vanadium from petcoke fly ash was studied from a techno-economic perspective, considering Alberta’s oil sands industry as a case study. The specific objectives of the research are to:

- Develop a techno-economic model to estimate the cost of vanadium recovery from bitumen-derived petcoke fly ash;
- Determine the effect of plant capacity on vanadium recovery cost;

- Assess the influence of input variations on the estimated recovery cost, through sensitivity and uncertainty analyses.

4.2 Methods

4.2.1 Feedstock description

Table 4-1 presents the composition of the fly ash used in this study. This compositions was reported by Gomez-Bueno et al. (Gomez-Bueno et al. 1981) and corresponds to fly ash from the combustion of delayed coking petcoke from Suncor operations, one of the major oil sands operators in Alberta; it is consistent with the composition reported in other studies (Griffin and Etsell 1984; Holloway 2003).

Table 4-1. Fly ash composition (wt.%) (Gomez-Bueno et al. 1981)

V_2O_5	NiO	Fe_2O_3	Al_2O_3	SiO_2	S	C
3.58	1.74	6.66	15.6	33.1	2.48	26.0

4.2.2 Process description

The conceptual flow sheet for the recovery of vanadium from combustion fly ash is shown in Figure 4-1. The decarbonation, roasting, leaching, and desilication steps are based on experimental data from Holloway and Etsell's studies (Holloway and Etsell 2004; 2005; Holloway et al. 2005), while precipitation and effluent treatment are based on work by Llanos et al. (Llanos et al. 1997).

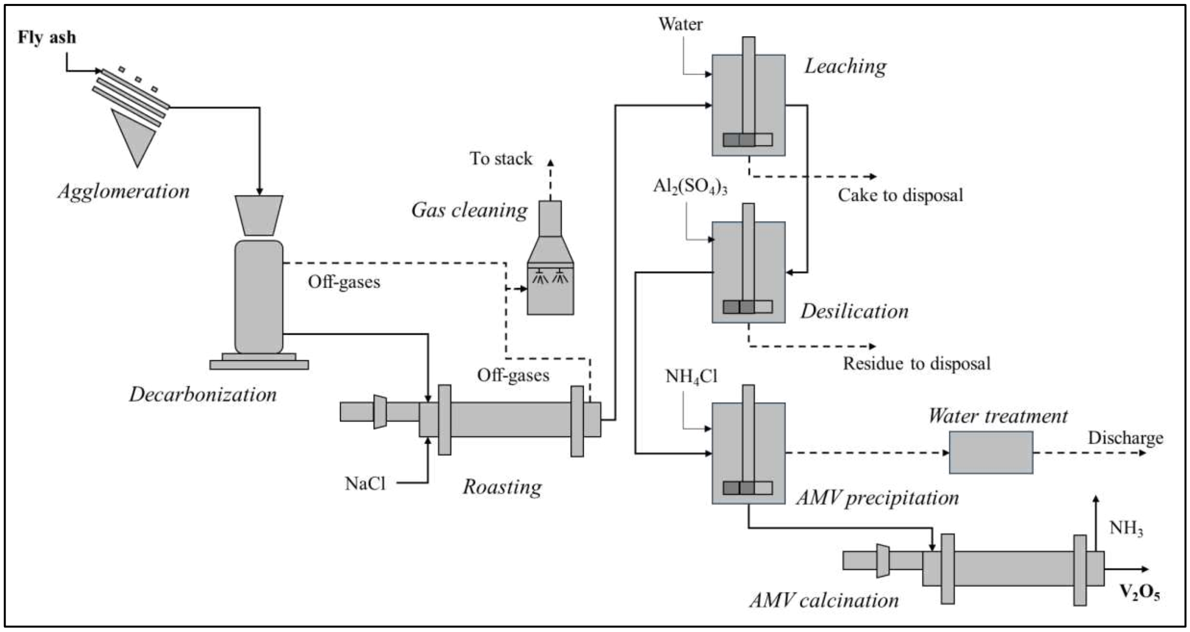

Figure 4-1. Conceptual flow sheet for the recovery of vanadium from petcoke combustion fly ash

With a mean size ranging between 4 and 45 μm (Gomez-Bueno et al. 1981; Griffin and Etsell 1984), the as-received fly ash is too fine to be handled by decarbonization equipment. An agglomeration operation is included to enlarge the size of the feedstock to avoid operational issues in downstream operations. The fly ash is mixed with water to produce pellets with a diameter greater than 10 mm.

The fly ash pellets are roasted in air at 500ºC to burn off the residual carbon and sulfur. Holloway determined that a total decarbonization may not be required since vanadium extraction is affected until the fly ash contains more than 15 wt.% unburnt carbon (Holloway 2003). The partial decarbonization not only reduces the size of the decarbonization oven, but also reduces the heating requirement during the downstream roasting operation, by burning the remaining carbon. In this study the total decarbonization of the fly ash was assumed as the worst-case scenario.

The off-gas from the decarbonization operation is cooled and treated to remove SO_2 and CO_2 before being released to the atmosphere. A wet-limestone scrubbing system can be used for desulfurization, generating gypsum as a by-product that can be disposed of or sold. The removal of CO_2 can be performed through an amine scrubbing operation. The decarbonated fly ash is further roasted with NaCl at 850ºC to convert vanadium oxide into sodium metavanadate, which is a water-soluble salt. More vanadium (85 wt.%) is extracted by adding 30 wt.% NaCl (Holloway 2003). At 850ºC, the other compounds in the fly ash do not react with sodium chloride.

The roasted fly ash is quenched in water to recover energy and leach out the vanadium. During the operation, the water is heated to 97ºC, the leaching temperature. Any excess water above the required leaching temperature is evaporated during quenching. After washing and filtration, the residue cake is disposed of, while the pregnant solution is purified with aluminum sulfate for the precipitation of the silicon that was leached along with the vanadium. The purified vanadium-rich solution is concentrated by evaporation, treated with ammonium sulfate, and cooled to room temperature for the precipitation of ammonium metavanadate (AMV). The barren liquor is directed to a water treatment plant before discharge. The precipitated AMV is thermally decomposed into granular V_2O_5 and NH_3 by calcination.

4.2.3 Material and energy balance

Spreadsheet-based process models were developed to estimate vanadium pentoxide production, consumables, and energy requirements, as well as solid residue, emissions, and effluent generation rates, based on data reported in the literature.

Extraction efficiencies were used to estimate outputs to model leaching, desilication, and AMV precipitation. Known process requirements were used to complete the material balance of each operation. For instance, water addition for agglomeration, salt addition for roasting, solids concentration for leaching, Al-to-Si for desilication, and NH_4Cl excess for AMV precipitation. Also, energy balances were completed to estimate energy requirements to meet process temperatures and supply endothermic reactions. Table 4-2 presents the process conditions and data input for completing the material and energy balances.

4.2.4 Equipment sizing and estimation of utility demand

The major equipment was sized based on the results of material and energy balances, according to the parameters presented in Table 4-3. Equipment sizing facilitates the estimation of the equipment cost and utility demand. The electricity requirement is for power consumption by rotary kilns and ancillary equipment such as agitators, fans, conveyors, and drum filters. Driver efficiency was considered as a function of the power requirement. The heat and cooling requirement are direct results of the energy balance. Natural gas is used as a heat source, either by direct combustion in kilns or by steam generation in a boiler. The equivalent energy content in the natural gas was estimated assuming the typical thermal efficiency of rotary kilns and boilers. Cooling water at 25°C was considered to be available for cooling purposes.

Table 4-2. Data input for material and energy balances

Operation	Equipment	Item	Value	References/Comments
Agglomeration	Disk agglomerator	Water use	0.20 kg H_2O/kg fly ash	For disk agglomerators (Ulrich and Vasudevan 2004)
		Energy consumption	3.5 kW-s/kg	Between 3 and 4 for disk agglomerators (Ulrich and Vasudevan 2004)
Decarbonization	Shaft furnace	Power consumption by air fan	0.0025*air volume flow	For 8 kPa total pressure (Engineering Toolbox 2003)
		Heat consumption	N/A	Heat is provided by the combustion of the carbon in fly ash. Excess air is calculated to match the required temperature.
Roasting	Rotary kiln (direct)	Power consumption	0.15*internal volume	Correlation from Ulrich and Vasudevan (Ulrich and Vasudevan

Operation	Equipment	Item	Value	References/Comments
				2004). Internal volume is a function of the solid mass flow and density, filling factor (12%), and residence time (3 h).
		Heat loss	40% heat input	(Ulrich and Vasudevan 2004)
		Combustion efficiency	70%	(Ulrich and Vasudevan 2004)
		Air-to-fuel ratio	15	(Ulrich and Vasudevan 2004)
Leaching and desilication	Reactor	Tank volume	Leaching time*volume flow	Tank is sized assuming a diameter-to-height ratio of 1.0
		Heat transfer coefficient for heat loss in leaching reactor	395 W/m^{2}K	Natural convection for agitated tank (Perry et al. 2018)
		Agitator diameter and power number	0.2*tank diameter and 1.2	For power consumption. Turbine-type agitator (Perry et al. 2018)

Operation	Equipment	Item	Value	References/Comments
	Drum filter	Power consumption	4.6x10^{-4}*mass flow of solids in cake	For drum filter (Ulrich and Vasudevan 2004)
AMV precipitation	Falling film evaporator	Steam temperature	212°C	Medium pressure steam
		Heat transfer coefficient	3,750 W/m^2K	(Ulrich and Vasudevan 2004)
	Reactor	Tank volume	Leaching time*volume flow	Tank is sized assuming a diameter-to-height ratio of 1.0
		Heat transfer coefficient for heat loss in leaching reactor	395 W/m^2K	Natural convection for agitated tank (Perry et al. 2018)
		Agitator diameter and power number	0.2*tank diameter and 1.2	For power consumption. Turbine-type agitator (Perry et al. 2018)

Operation	Equipment	Item	Value	References/Comments
	Heat exchanger for cooling	Cooling water temperature change	5ºC	
		Heat transfer coefficient	2,000 W/m^{2}K	(Ulrich and Vasudevan 2004)
	Cooling system	Coefficient of performance	5-6.1	The coefficient of performance depends on the cooling duty. Typical values for industrial applications.
AMV calcination	Rotary kiln (indirect)	Power consumption	6*(internal diameter)^2	(Ulrich and Vasudevan 2004)
		Furnace efficiency	50%	(Ulrich and Vasudevan 2004)
		Air-to-fuel ratio	15	(Ulrich and Vasudevan 2004)

Operation	Equipment	Item	Value	References/Comments
Gas treatment	Gas treatment unit	CO_2 removal efficiency	90%	Typical value for a MEA-based gas treatment unit (International Energy Agency 2021a)

Table 4-3. Sizing parameters and energy consumption of the major equipment

Operation	Equipment	Sizing parameter	Heat and power consumption	Comments
Agglomeration	Disk agglomerator	Solid mass flow from material balance.	Specific power consumption: 3.5 kW-s/kg (Ulrich and Vasudevan 2004)	Able to convert dusty feeds, such as fly ash, into spherical pellets.

Operation	Equipment	Sizing parameter	Heat and power consumption	Comments
Decarbonization	Shaft furnace	Internal volume calculated based on the solid mass flow and density, residence time, and filling factor (0.55) (Ulrich and Vasudevan 2004).	Thermal efficiency: Power consumption by forced flow fan. Calculated as a function of the air volume flow for and pressure drop (Ulrich and Vasudevan 2004; Perry et al. 2018).	This equipment provides the required residence time and can handle the size of the fly ash pellets.
Roasting	Rotary kiln	Internal volume calculated based on the solid mass flow and density, residence time, and filling factor (0.12)	Thermal efficiency: 0.70 Power consumption proportional to internal	Like the equipment used for ore roasting in the processing of minerals.

Operation	Equipment	Sizing parameter	Heat and power consumption	Comments
		(Ulrich and Vasudevan 2004).	volume (Ulrich and Vasudevan 2004).	
Leaching, desilication, and AMV precipitation	Reactor	Volume calculated from the residence time and the volume flow rate of the solution. The diameter (D) and height (H) of the reactor were calculated under the D:H=1.0 assumption.	Turbine type agitator. Power calculated from assumed power number, rotational speed, and agitator diameter (Perry et al. 2018).	

Operation	**Equipment**	**Sizing parameter**	**Heat and power consumption**	**Comments**
AMV calcination	Rotary calciner	Internal volume calculated based on the solid mass flow and density, residence time, and filling factor (0.10) (Ulrich and Vasudevan 2004).	Thermal efficiency: 0.50. Power consumption proportional to the square diameter (Ulrich and Vasudevan 2004).	Indirect type

4.2.5 Economic assessment model

The economic assessment corresponds solely to the vanadium recovery process. Petcoke combustion costs are not included because they are allocated to the upgrader operation. Moreover, the present study is gate-to-gate; this means the handling and transportation costs of fly ash from the upgrader to the recovery plant are not considered, nor is the transportation cost of vanadium pentoxide to the end user.

4.2.5.1 Capital cost

Capital cost is comprised of the fixed capital investment (FCI) and working capital (WC). The FCI includes the inside battery limit (ISBL) investment (i.e., the procuring and installing costs of process equipment), the outside battery limit (OSBL) investment (i.e., additions to the site infrastructure and ancillary equipment), engineering cost, and contingency charges. The ISBL is the sum of the free-on-board (FOB) cost of the equipment multiplied by the respective installation, material, dimension, and process condition factors, all of which are found in several textbooks (Peters et al. 2003; Ulrich and Vasudevan 2004; Turton et al. 2012; Towler and Sinnot 2013). The FOBs were updated to the Chemical Engineering Plant Cost Index (CEPCI) of 776.9 (2021), and a location factor (LF) of 1.43 was used for Alberta, Canada. Table 4-4 shows the main assumptions for the estimation of cost estimation.

Table 4-4. Assumptions for capital cost estimation

Item	Value	Comments/remarks
Fixed capital cost (FCI)		

Inside battery limit investment (ISBL)	Depends on the equipment	Found in cost curves as a function of the sizing parameter shown in Table 4-3
Outside battery limit investment (OSBL)	40% ISBL	Site conditions not specified
Engineering cost	10% (ISBL + OSBL)	For small projects
Contingency	10% (ISBL + OSBL)	For general projects
Working capital (WC)	15% (ISBL + OSBL)	For general plants
Total capital cost	FCI + WC	

4.2.5.2 Operating cost

Operating cost includes feedstock, consumables, utilities, waste treatment, labor, maintenance, insurance, and plant overhead. Consumable prices were obtained from vendors. Electricity and natural gas prices correspond to typical values for industrial consumers in Alberta (Canada Energy Regulator 2020). Cooling water and waste treatment costs were obtained from the literature. The remaining cost components were estimated as suggested by Towler and Sinnot and are shown in Table 4-5.

Table 4-5. Assumptions for operating cost estimation

Category	Item	Cost	Comments
Feedstock	Fly ash	\$50/t	The price of coal fly ash for the cement industry was used as reference (Shwekat 2015)
Consumable	NaCl	\$0.26/kg	(Wasajja et al. 2020)
	$Al_2(SO_4)_3$	\$0.18/kg	(Gill et al. 2016)
	NH_4Cl	\$0.20/kg	(ChemAnalyst 2022)
	Process water	\$0.53/m^3	(Peters et al. 2003)
Utility	Electricity	\$0.042/kWh	(Canada Energy Regulator 2017)
	Natural gas	\$1.32/GJ	(Canada Energy Regulator 2017)
	Chilled water	\$0.08/m^3	(Peters et al. 2003)
Labor	Labor	Based on average salary in Alberta's chemical industry (Chemistry Industry Association of Canada 2021), number of workers per shift per unit per operation (Ulrich and Vasudevan 2004), three 8 h/shifts, 7 days/week, and 48 weeks/year	
	SO_2 removal	\$540/t	Wet-limestone scrubbing. (Chichanowicz 2010)

Waste treatment	HCl removal	\$570/t	
	CO_2 removal	\$50/t	Ammine absorption. Diluted stream (International Energy Agency 2021a)
	Solid disposal	\$55/t	(Peters et al. 2003)
	Wastewater treatment	\$1.50/m^3	(Peters et al. 2003)
Other costs	Maintenance	5% ISBL	(Towler and Sinnot 2013)
	Rent	2% (ISBL+OSBL)	(Towler and Sinnot 2013)
	Insurance	1% ISBL	(Towler and Sinnot 2013)
	Plant overhead	1% revenue (R&D) + 65% labor (G&A)	(Towler and Sinnot 2013)

4.2.5.3 Vanadium recovery cost

A discounted cash flow (DCF) analysis was performed to estimate the vanadium recovery cost. The vanadium recovery cost represents the vanadium selling price to break even over the plant life span. For such a selling price, the net present value (NPV) is zero at the known discount rate (e.g., the internal rate of return [IRR]). The basic assumptions for the DCF analysis are presented in Table 4-6. See Appendix A for details about the DCF used in this research.

Table 4-6. Assumptions for estimation of vanadium recovery cost through discounted cash flow analysis

Item	Value
Plant lifetime	20 years
On-stream factor	0.95
Operating cost escalation	2%
IRR	10%

4.2.6 Sensitivity and uncertainty analyses

A sensitivity analysis was performed to identify the inputs whose variation most impacts the model output. The Morris method, implemented in our research group colleague's Regression, Uncertainty, and Sensitivity Tool (RUST) (Di Lullo et al. 2019), was used to assess the model sensitivity on twenty-five inputs, including equipment performance, material and energy consumption, and consumable, utility, and feedstock prices. First, the Morris method was run considering variations in the inputs of ±10%, ±30%, and ±50%

relative to the values considered for the base case. Based on the results, insensitive inputs were discarded for further analysis. Then, the variation range of the identified sensitive inputs was refined, according to typical values, and current and forecasted market prices. Table 4-7 shows the refined variation range of the identified inputs used in the final sensitivity analysis. Appendix B presents an overview of the Morris method.

A Monte Carlo simulation implemented in RUST was used for the uncertainty analysis. Considering the same input variation range presented in Table 4-7, five thousand runs were performed, and the inputs were populated assuming a uniform probability distribution.

Table 4-7. Refined variation range of the identified sensitive inputs for sensitivity analysis

Input	Min	Max	Comments
SO_2 removal efficiency	90%	99%	For wet scrubbing (Sorrels et al. 2021)
CO_2 removal efficiency	90%	95%	For ammine capture systems (International Energy Agency 2021a)
HCl removal efficiency	90%	99%	For wet scrubbing (Macleod 2018)
Solid fraction in leaching cake	0.5	0.7	For cakes obtained from drum filters (Ulrich and Vasudevan 2004)

Input	**Min**	**Max**	**Comments**
Wash ratio of leaching cake	1.5	2.0	For drum filters (Perry et al. 2018)
Solid disposal cost	\$55/t	\$100/t	Maximum from typical landfill fees of industrial wastes in Alberta
SO_2 removal cost	\$250/t	\$600/t	(Chichanowicz 2010)
CO_2 removal cost	\$40/t	\$120/t	(International Energy Agency 2021a)
HCl removal cost	\$250/t	\$600/t	(Chichanowicz 2010)
NaCl price	\$50/t	\$110/t	Average values from the market (alibaba.com 2022b)
Feedstock price	\$35/t	\$70/t	Average market values (alibaba.com 2022a)
Natural gas price	\$0.88/GJ	\$7.87/GJ	Industrial consumer in Alberta. Minimum price in the last 10 years and maximum forecasted price in the next 10 years (Canada Energy Regulator 2020)

4.2.7 Definition of scenarios

The base case scenario for combustion fly ash was defined based on the current rate of petcoke burned in Suncor's plant. According to data from Alberta Energy Regulator, 11% of petcoke produced in Suncor upgraders, about 49,000 metric tons monthly, were used as fuel in the plant between January 2019 and August 2020 (Alberta Energy Regulator 2019; 2020). This amount is equivalent to 588,000 t/y of petcoke. Considering an ash content of 4.2% (Gray 2015), and that around 65% of the ash is fly ash (Griffin and Etsell 1984), the generation rate of fly ash is about 16,000 t/y. The base case scenario for this residue considered a plant capacity matching that generation rate. However, the stockpiled ashes by Suncor in ash ponds could be used as feedstock for vanadium recovery. This assumption was used in the economies of scale analysis for considering plant capacities beyond the ash generation rate.

4.3 Results and discussion

4.3.1 Base case scenario

4.3.1.1 Material and energy balance

In the base case, about 404 metric tons of vanadium pentoxide are recovered. Table 4-8 shows the material inventory per unit mass of produced V_2O_5. This inventory was obtained after performing the material balance for each unit operation in the recovery process.

Table 4-8. Material inventory for the base case scenario. All quantities expressed in kg/kg V_2O_5

Operation	Material	Input	Output
Agglomeration	Fly ash	36.4	
	Water	9.1	
	Fly ash pellets		45.5
Decarbonization	Fly ash pellets	45.5	
	Air	112.6	
	Decarbonized fly ash		26.0
	Off-gas		132
Roasting	Decarbonized fly ash	26.0	
	NaCl	11.2	
	Air	20.7	
	Roasted fly ash		35.5
	Off-gas		22.5
Leaching	Roasted fly ash	35.5	

Operation	Material	Input	Output
	Quenching water	40.4	
	Washing water	20.5	
	Vanadium-rich solution		57.1
	Condensate		5.0
	Cake		34.2
Desilication	Vanadium-rich solution	57.1	
	$Al_2(SO_4)_2$	0.36	
	Wash water	0.03	
	Purified solution		58.1
	Cake		0.051
AMV precipitation	Purified solution	58.1	
	NH_4Cl	2.35	
	Wash water	0.86	
	NH_4VO_3		1.29

Operation	Material	Input	Output
	Evaporated water		21.8
	Water in cake		0.43
	Wastewater		36.6
AMV calcination	NH_4VO_3	1.29	
	Water in cake	0.43	
	NH_3		0.19
	Water vapor		0.53
	V_2O_5		1.00

Electricity and natural gas are the source of energy supply to the process. Figure 4-2 presents the energy inventory obtained from the energy balance, including the power required to run the main and ancillary equipment. About 0.43 kWh electricity and 0.14 GJ heat are required per kg of vanadium pentoxide produced. Decarbonization consumes 25% of the total electricity, mostly to run the forced flow fan that supplies air to the operation. AMV calcination, roasting, and agglomeration require respectively 33%, 25%, and 8% of the electricity consumption to drive the rotary equipment involved in the operations. The share of the remaining operations is less than 5%, used to run agitators and drum filters. Regarding natural gas, AMV precipitation consumes 42% of the total, to concentrate the vanadium-rich solution by evaporation. Roasting consumes 41%, to provide the heat for the reaction at the required temperature. Although quenching the roasted fly ash allows energy recovery to heat the water for leaching, the leaching operation still consumes 15% of the total natural gas to provide the heat of reaction and make up the heat loses. The natural gas consumption by AMV calcination is low (2%) because of the relatively small amount of material to be calcinated. The requirement of natural gas could be lowered significantly by recovering heat from the off-gases of decarbonization.

4.3.1.2 Vanadium recovery cost

The estimated capital cost for a plant with a capacity of 16,000 metric tons per year is $7.6 M, and the operating cost at year one is $5.7 M. The breakdown of the capital cost is presented in Figure 4-3. The ISBL corresponds to 53% of the capital cost. Equipment for roasting and AMV calcination account for 23% of the ISBL, because the rotary kilns are considerably more expensive than the remaining equipment.

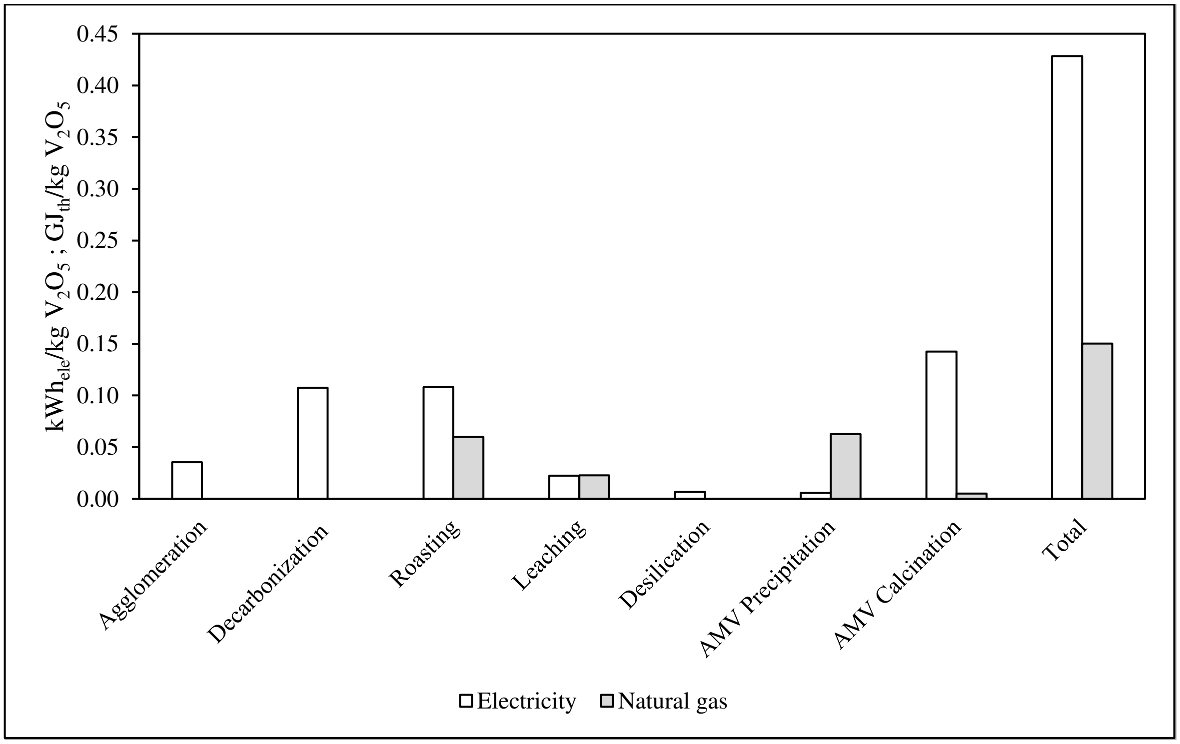

Figure 4-2. Energy consumption by operation

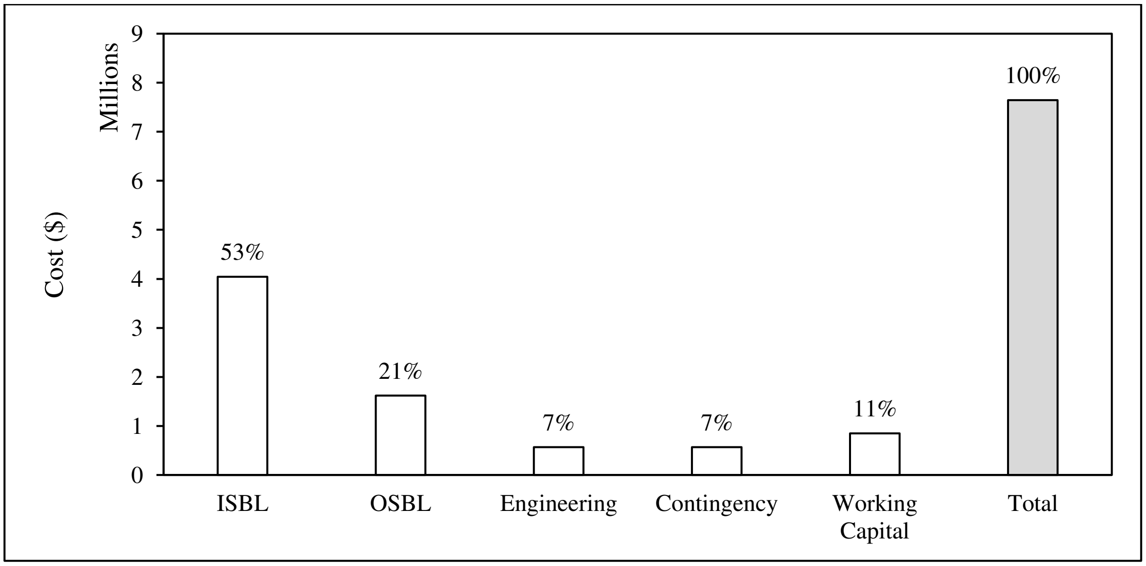

Figure 4-3. Breakdown of capital cost for the base case scenario

As shown in Figure 4-4, waste treatment represents the greatest operating cost, at about 29% of the total cost. Of this, 67% corresponds to off-gas cleaning (38% to CO_2 removal, 22% to

SO_2 removal, and 7% to HCl removal), and 32% to disposal of the solid residue from leaching (32%) and desilication (0.1%). Consumables make up 16% of operating cost. Sodium chloride for roasting corresponds to 75% of the consumables cost, 21% to ammonium chloride for AMV precipitation. The costs of aluminum sulfate for desilication and of process water contribute 3% and less than 2% of the consumable cost, respectively. Feedstock cost, i.e., fly ash cost, is another important contributor to the operating cost, with 14% of the share.

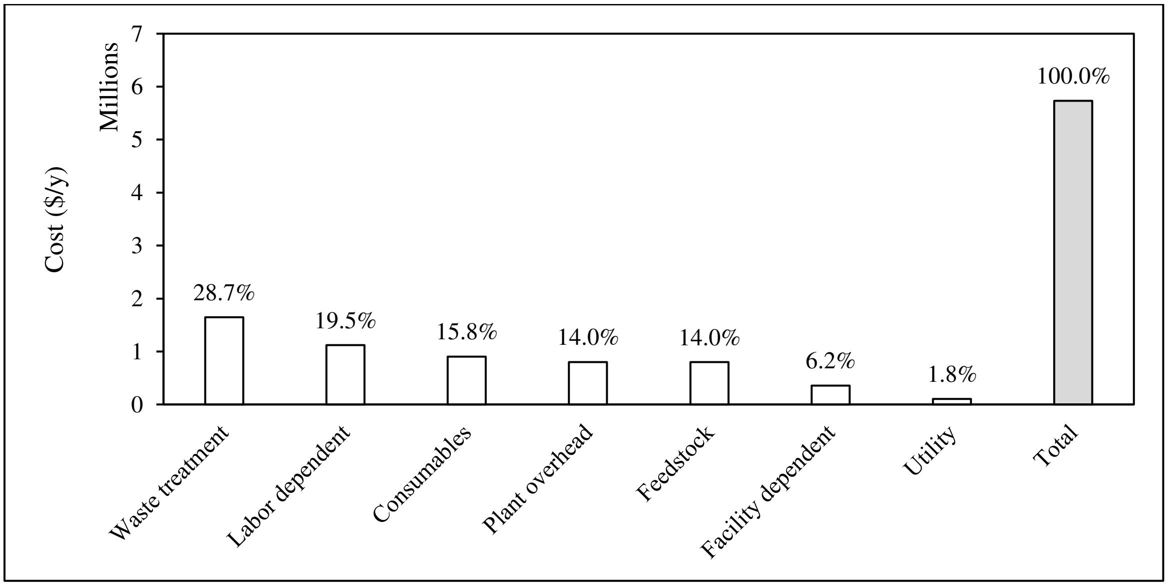

Figure 4-4. Breakdown of operating cost at year one of operations for the base case scenario

The vanadium recovery cost calculated through a DCF analysis is \$18.77/kg V_2O_5 for the base case; \$2.22/kg V_2O_5 correspond to capital cost and \$16.55/kg V_2O_5 to operating cost. This cost is higher than the current market price of \$16.00/kg V_2O_5 (October 2022 (vanadiumprice.com 2022)) and the average price over the last 20 years, around \$12.00/kg V_2O_5. To compete in the vanadium global market, the main cost components of the recovery cost need to change.

Figure 4-5 shows the breakdown of the recovery cost. About 81% of the recovery cost is concentrated in six components of the operating cost. Labor and overhead could be reduced with a higher degree of automation of the processes and through corporate decisions that affect investment in administrative and research activities. Gas treatment makes up 17% of the recovery cost (\$3.18/kg V_2O_5), from all the CO_2 and SO_2 that must be removed from the off-gases generated in the decarbonization operation. It is worth considering other means of decarbonating the fly ash or even a different approach that does not require that operation. For instance, the removal of unburned carbon from fly ash by froth flotation (Stemerowicz et al. 1976; Walker and Wheelock 2006; Zhang et al. 2020), gravity separation (Zhang et al. 2020), or electrostatic separation (Tao et al. 2015) has been proven with different degrees of success. In addition, Sakuma and Kobori patented a process that combines the generation of a fly ash slurry and a magnetic separation step to recover vanadium without decarbonization of the feed (Sakuma and Kobori 2018). Consumables make up 14% of the recovery cost. Holloway and Etsell explored the possibility of recovering NaCl and a cake containing NH_4Cl and NH_4VO_3 by the evaporation and cooling of the barren liquor remaining after vanadium precipitation (Holloway and Etsell 2005). The salt recovery would reduce the requirement of sodium chloride for roasting, as well as optimize the use of NH_4Cl and increase the vanadium precipitation yield if the cake is recycled back to the AMV precipitation operation. The cost of feedstock makes up 12.3% of the recovery cost (\$2.31/kg V_2O_5). However, this cost would be avoided if the recovery plant is integrated to the bitumen upgrading facility and run by the same operator. In such a case, the fly ash would be available at no cost. Finally, the disposal of solid residues, mainly the leaching cake, makes up 8.2% of the recovery cost (\$1.54/kg V_2O_5); therefore, diverting this material from the landfill would not only avoid the disposal cost but generate value. Holloway and Etsell suggested using the leaching cake as an alumina source for the glass and ceramic industry or as an aggregate for road construction or concrete manufacturing. In either case, the cost of further processing should be assessed to determine whether it exceeds the commercial value of the final product (Holloway and Etsell 2005).

4.3.2 The effect of plant capacity on capital cost and vanadium recovery cost

Figure 4-6 presents the capital cost and the specific capital cost, i.e., capital cost per kg of recovered vanadium pentoxide, for different plant capacities. It is observed that the process benefits from economies of scale with a scale factor of approximately 0.54, which represents a reduction of the specific capital cost as the plant capacity increases.

Figure 4-7 shows the vanadium recovery cost for different plant capacities. Considering a market price of \$16.00/kg V_2O_5, the minimum profitable capacity is 45,100 t fly ash/y. For the Suncor upgraders, this minimum profitable capacity represents 2.8 times the current generation rate of fly ash, equivalent to burning 1.6 M metric tons of petcoke per year. Considering the 20 year-average price of vanadium of \$12.00/kg V_2O_5, the minimum profitable capacity rises to 155,100 t fly ash/y, which would be achieved if 5.6 million tonnes of petcoke per year, slightly above the current generation rate, is burned. Should the combustion of petcoke be halted, through migration to a less carbon-intensive fuel like natural gas to produce heat for upgrading for example, the ash that has stockpiled in ponds since operations began could be used as feedstock in the vanadium recovery plant. Further studies on the amount of stockpiled ash available, its composition, and additional costs from handling and conditioning the ash for feedstock, are required and are beyond the scope of this study.

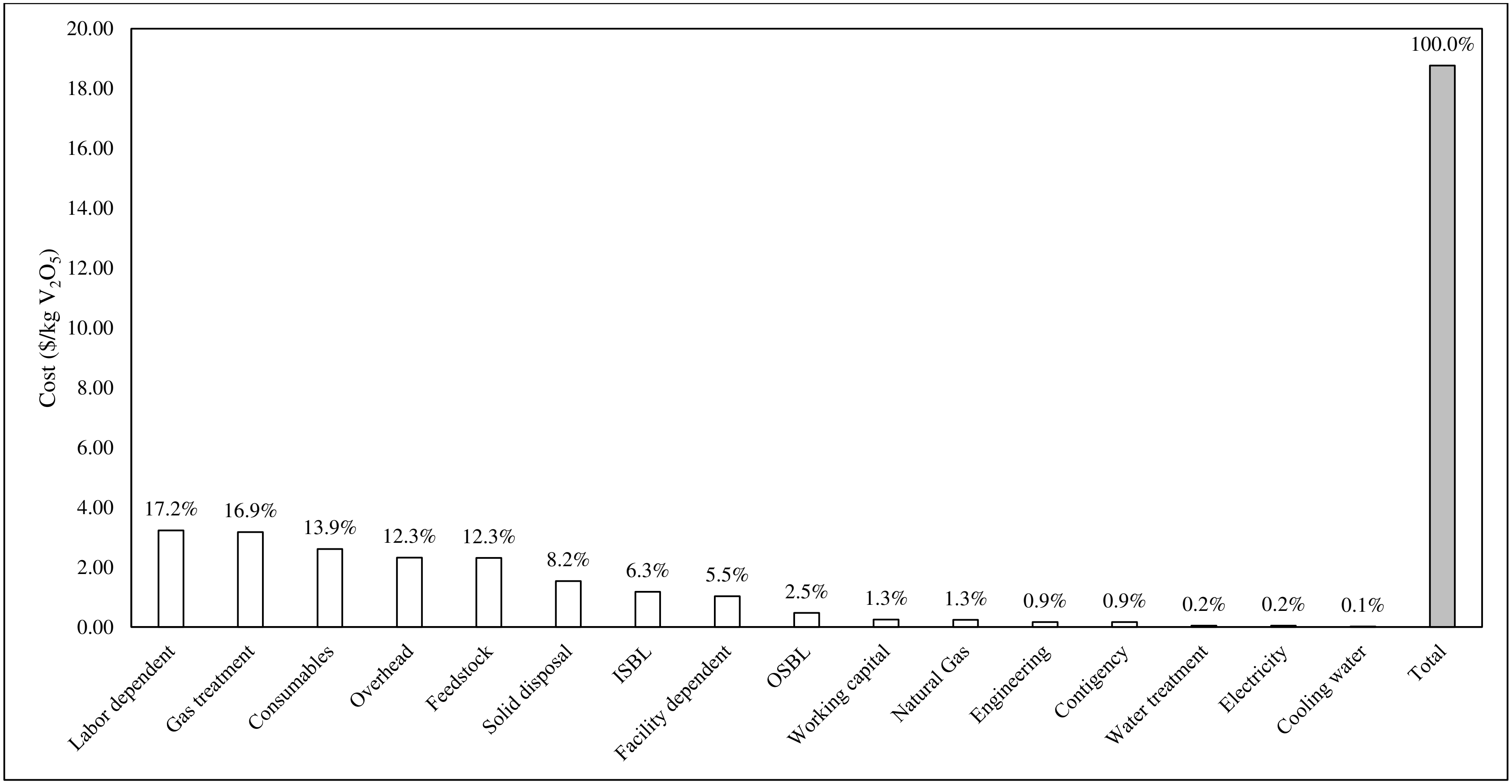

Figure 4-5. Breakdown of V_2O_5 recovery cost for the base case scenario

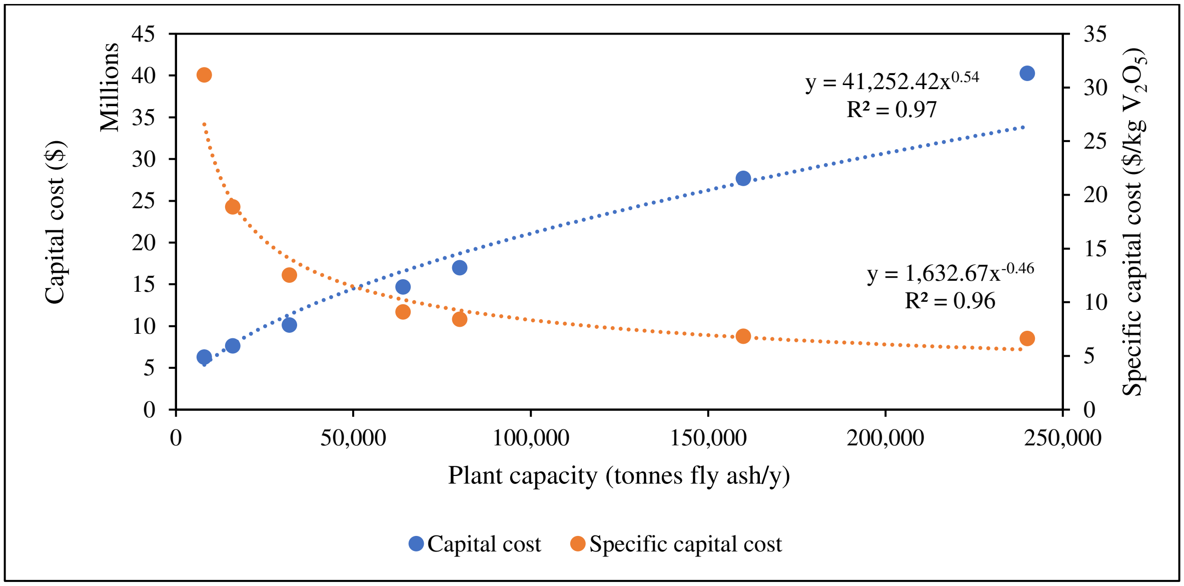

Figure 4-6. Variation of capital cost with plant capacity

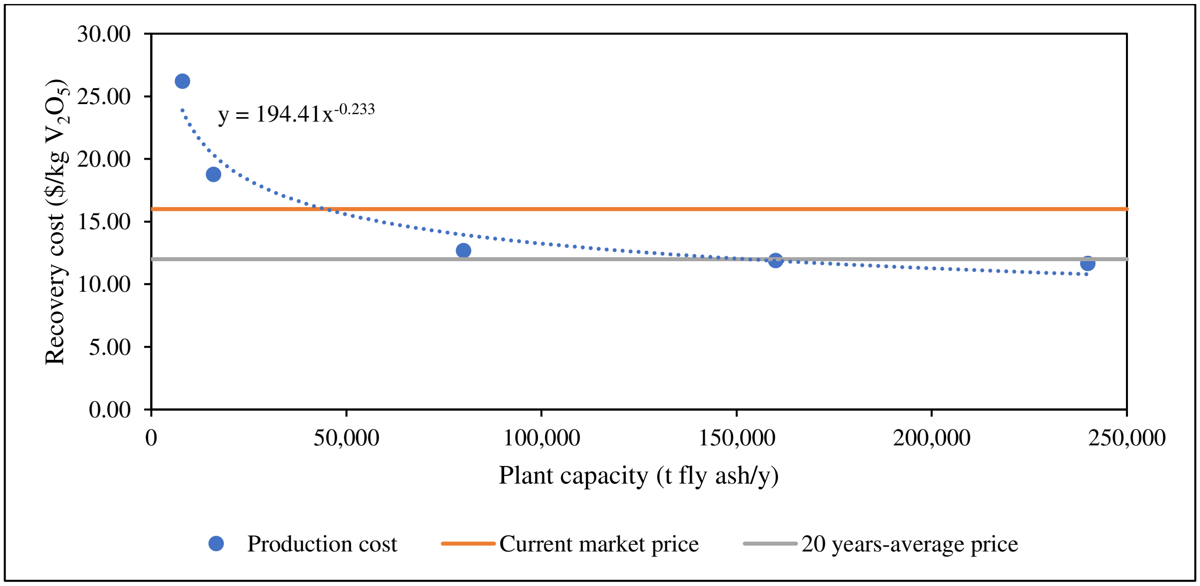

Figure 4-7. Vanadium recovery cost v. plant capacity

4.3.3 Sensitive inputs and results of Monte Carlo simulation

Figure 4-8 presents the results of the sensitivity analysis, after refining the variation range of the sensitive inputs previously identified. The cost of CO_2 removal is the input with most sensitivity; therefore, selecting a tailored method for carbon capture at the early stages of the project is recommended for accurate cost estimates. The feedstock cost and the disposal cost of the solid residues are other inputs with high sensitivity. Differences in the price of fly ash considered for the estimate affect the recovery cost; therefore, early negotiation with the oil sands operator supplying the feedstock is key for a proper project shaping. In the same way, the characterization of the solid residue is needed to determine the landfill disposal fee or, alternatively, the commercial value of the residue, thus narrowing the variation of the model output. The price of natural gas exhibits high non-linearity. Given the interaction of this input with other parameters, the use of reliable forecasts is recommended to develop a business case for the project. The remining inputs were included in the uncertainty analysis, even though their variations influence the model output less than the discussed inputs.

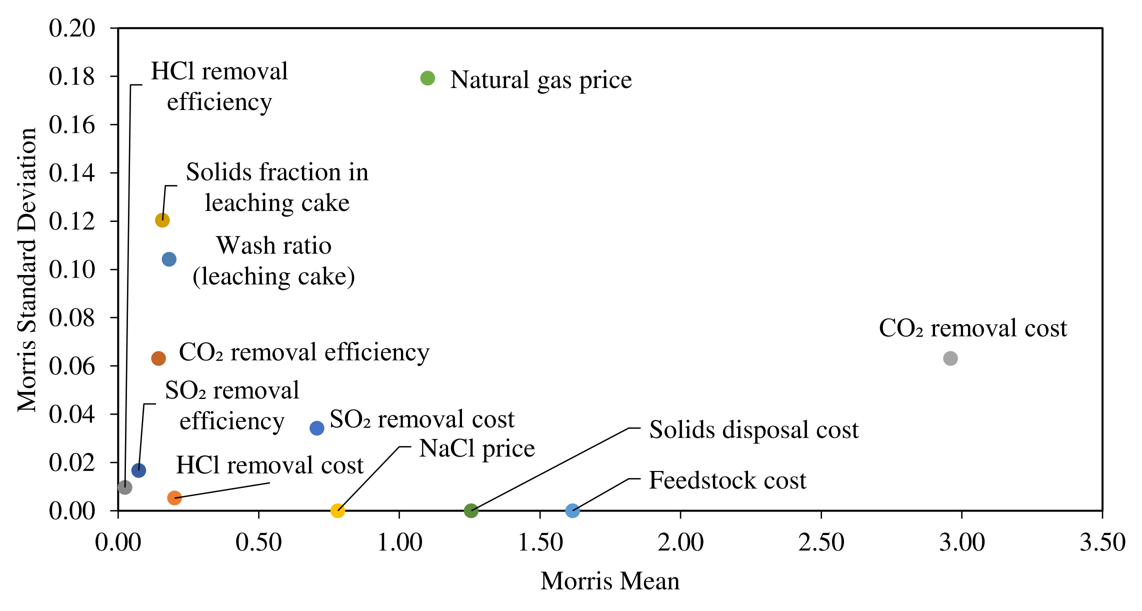

Figure 4-8. Sensitivity analysis results

Figure 4-9 presents the mean, minimum, and maximum recovery cost values for a 16,000 metric ton per year plant, obtained through Monte Carlo simulations. The 25th, 50th, and 75th percentiles are included in the figure. All the values are above the current market price of vanadium pentoxide, hence the uncertainties in the model do not change the conclusion that the process is profitable under the current market conditions and fly ash generation rate. The uncertainty analysis also reaffirms the need for the suggested process modifications and improvements in order to develop this activity in Alberta.

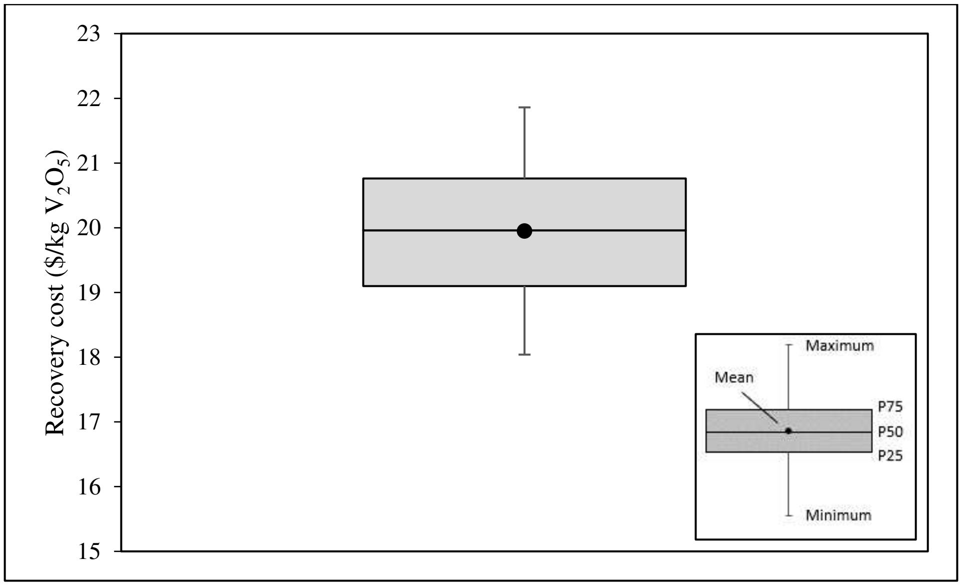

Figure 4-9. Summary of Monte Carlo simulations results for uncertainty analysis

4.4 Conclusions

The feasibility of vanadium recovery from bitumen-derived petcoke fly ash was investigated through a data-intensive techno-economic assessment. The fly ash obtained from the combustion of delayed petcoke generated during bitumen upgrading was considered as a case study, and Alberta, Canada, as the location of the recovery plant. A capacity of 16,000 metric tons of fly ash per year, corresponding to the current generation of fly ash by a major oil sands operator in Alberta, was defined as base case, and the effect of scale on recovery cost was also examined.

For such a capacity, about 404 metric tons of vanadium pentoxide are recovered at a cost of \$18.77/kg V_2O_5. This cost is higher than the current market price of vanadium (\$16.00/kg V_2O_5), thus some modifications to the process are required to compete with other primary production processes. The costs of off-gas cleaning and consumables are among the greater contributors to the vanadium recovery cost, therefore alternatives to fly ash decarbonization and incorporating a salt recycling loop would significatively affect recovery cost. Larger plant capacities lead to lower recovery costs. For plant capacities greater than 45,100 metric tons of fly ash per year, the estimated recovery cost is below the current market price.

Sensitivity and uncertainty analyses were performed to identify sensitive inputs and the range of variation in the recovery cost. The model output is sensitive to the cost of removing CO_2 from the off-gases, the feedstock price, and the solid waste disposal cost. Considering the uncertainties in the model, for a plant capacity of 16,000 metric tons per year, the recovery costs range from \$18.04 to \$21.86 per kg V_2O_5, with a mean value of \$19.95/kg V_2O_5.

Chapter 5: Life cycle GHG emissions assessment of vanadium recovery from bitumen-derived petcoke fly ash[5]

5.1 Introduction

Vanadium is typically obtained as a by-product of steel manufacturing from titano-magnetite ores. Petroleum residues, fly ash from the combustion of fuels, and spent catalysts, especially from sulfuric acid production and crude oil refining, are secondary sources of vanadium. This metal also concentrates in petroleum coke, or petcoke, a solid by-product of petroleum refining and upgrading of heavy crude oils and bitumen obtained after the thermal cracking of residues from distillation. Usually, petcoke is used as fuel for power generation and as raw material, additive, or reagent in the steel, glass, aluminum, and cement industries. However, the commercial value of petcoke from heavy crude oils is limited because of the high sulfur and metal content of the residue. Therefore, petcoke from bitumen is mainly stockpiled. Recovering vanadium from petcoke would create value as demand for steel production and redox flow batteries increases.

The oil sands industry in Alberta, Canada, has the potential to supply vanadium, given the increase in the petcoke produced from refined and upgraded bitumen and the high vanadium content. With 11.4 million metric tons of petcoke generated per year (Alberta Energy Regulator 2020) and a vanadium content of about 0.12 wt.% (Gray 2015), the maximum

---

[5] A version of this chapter has been published as M. Baritto, A.O. Oni, A. Kumar. Life cycle GHG emissions assessment of vanadium recovery from bitumen-derived petcoke fly ash. Journal of Environmental Management. 2024, 363:121377.

production of vanadium from this source is estimated in 13,680 metric tons, 16% of all the vanadium mined worldwide (U.S. Geological Survey 2021).

Diverse routes for the recovery of the vanadium present in petcoke have been proposed. Depending on the nature of the petcoke, vanadium and other metals can be recovered directly from petcoke (Queneau et al. 1984; Gardner 1987; Davila Armas 1988; Zhang et al. 2015), or from fly ash and slags originating from the combustion and gasification of petcoke (Haas and Hesse 1981; Gardner 1987; Shlewit and Alibrahim 2006; Xiao et al. 2010). Among the proposed processes, the roasting of petcoke/fly ash with an alkali metal compound followed by water leaching appears to increase the yield and selectivity of vanadium extraction. Regarding oil sands bitumen-derived petcoke, direct leaching does not extract any significant amount of vanadium (Griffin and Etsell 1984), at least for delayed coking petcoke and fluid coke, the two coking technologies in place in Alberta's upgraders. On the other hand, using petcoke fly ash to feed a roasting and leaching route appears to be a plausible route, as shown by Jack et al. (Jack et al. 1979; 1980), McCorriston (McCorriston 1984), Griffin and Etsell (Griffin and Etsell 1984), Holloway and Etsell (Holloway and Etsell 2004; 2005), and Holloway et al. (Holloway et al. 2005) Using fly ash as vanadium source is compatible with current operations in the oil sands industry because a significant part of the generated petcoke is already combusted to provide heat and produce power for the operations. The entire pathway to get fly ash from bitumen is shown in Figure 5-1. Oil sands are mined from open pits using shovels and trucks that use diesel as fuel and transported to bitumen extraction facilities through slurry pipelines. There, bitumen is separated from sand using a series of water-based flotation processes. The resulting froth is subjected to a solvent-based gravity separation process to remove the remaining water and fine solids, producing a diluted bitumen, called dilbit, which is pumped to upgrading facilities to improve its quality. As part of the upgrading process, dilbit is fractionated in the atmospheric and vacuum distillation units, and the resulting heavy residue is mostly processed using thermal cracking in the coking units. A fraction of the generated petcoke is combusted to provide energy to the operations, producing fly ash that is stockpiled in ponds, but it could be used for vanadium recovery. For instance, about 5.3 million metric tons of petcoke are produced annually by Suncor, one of the major oil sands operators in Alberta, and 11% of it is used as fuel in the plant (Alberta Energy Regulator 2020). With an ash content of 4.2 wt.% (Gray 2015) and 65% generation of fly ash (Griffin and Etsell 1984), the production rate of fly ash is about 16,000 metric tons, containing around 570 metric tons of vanadium pentoxide.

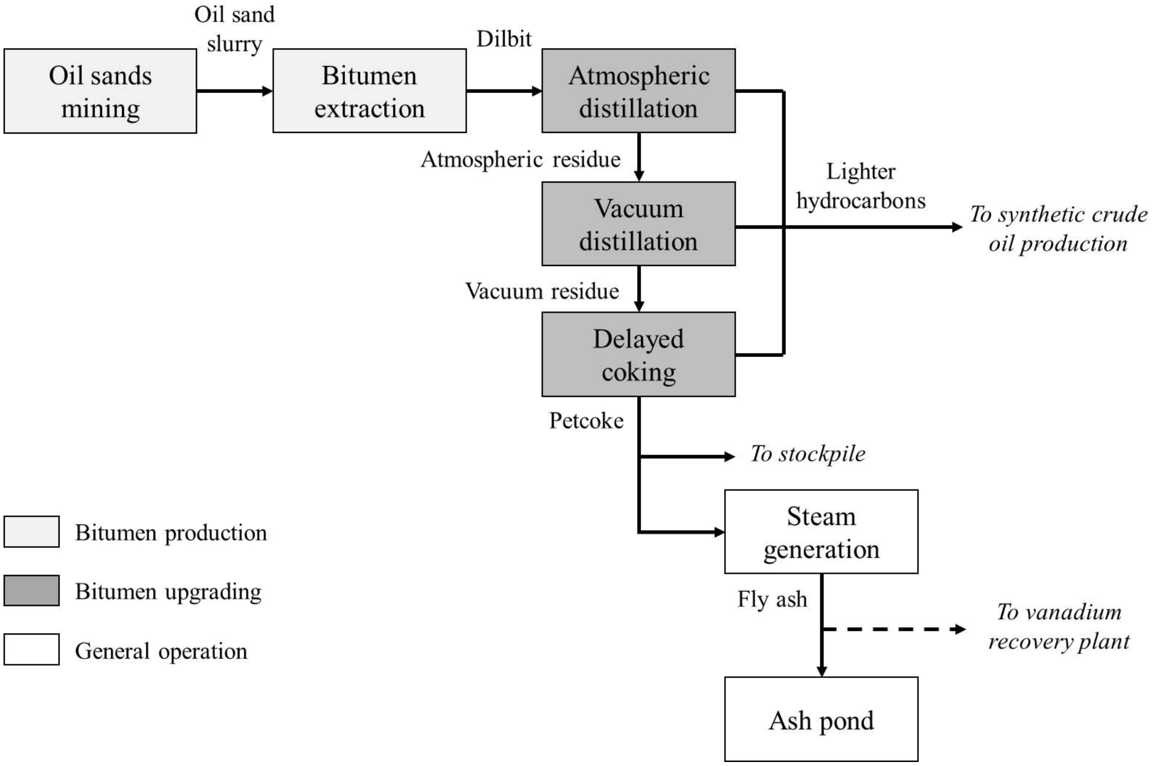

Figure 5-1. Pathway to obtain fly ash from oil sands bitumen

Although the technical feasibility of recovering vanadium from petcoke fly ash has been proven, the environmental impact of the processes has not been compared with primary production processes (e.g., vanadium titano-magnetite [VTM] ore) and alternative sources (e.g., spent catalysts) of vanadium. This research was focused on greenhouse gas (GHG) emissions because both petcoke combustion and the processing of fly ash for vanadium recovery release carbon to the atmosphere that would otherwise remain in stable form in stockpiled petcoke. It is, therefore, necessary to estimate the life cycle GHG emissions from the petcoke fly ash pathway to compare them with benchmark and alternative pathways to produce vanadium pentoxide. Information on GHG emissions from the recovery of vanadium from petcoke fly ash is very limited. The studies cited above developed process flowsheets but did not discuss the GHG emissions from the processes at commercial scale. Bjerknes et al. give a sense of the environmental impact in their evaluation of a plant for the recovery of vanadium from Venezuelan flexicoke using a salt roasting and water leaching process (Bjerknes et al. 1995). However, those authors focused on emissions of suspended particulate and SO_2, rather than GHG emissions, perhaps because the studied process used decarbonized fly ash as feedstock. Also, the vanadium content in Venezuelan petcoke is higher than in bitumen-derived petcoke, and, because flexicoke technology is not implemented in Alberta's upgraders, the recovery process is not directly transferable.

Considering the identified research gap, the recovery of vanadium from bitumen-derived petcoke fly ash was investigated from a GHG emissions perspective. The results will support informed decision-making on the development of economic activity near bitumen upgraders. The specific objectives of this research are to:

- Develop a process model of a hydrometallurgy route for recovering vanadium from fly ash;
- Conduct a life cycle GHG emissions assessment of the vanadium recovery process;
- Conduct sensitivity and uncertainty analyses to assess the influence of input variations on GHG emissions;
- Conduct a case study for Alberta, a western province in Canada and one of the largest oil sands bases in the world.

5.2 Methods

5.2.1 Process for recovering vanadium from petcoke fly ash

For this study, fly ash from the combustion of delayed petcoke derived from bitumen oil sands was considered as the feedstock for the vanadium recovery plant. The fly ash composition is shown in Table 4-1 and corresponds to Suncor operations.

The vanadium recovery process used as reference for the assessment is a hydrometallurgy route based on research by Holloway and colleagues (Holloway and Etsell 2004; 2005; Holloway et al. 2005). The flowsheet of the process is shown in Figure 4-1.

The process begins with the agglomeration of the received fly ash by mixing with it water. The goal is to enlarge the size of the material and avoid operational issues in the subsequent operations. The resulting pellets are decarbonized by burning in air and then mixed with NaCl and roasted to produce readily water-soluble vanadium salts. The roasted fly ash is quenched in water and the vanadium salts are dissolved. The solid residue is sent to disposal, while the pregnant solution is treated with $Al_2(SO_4)_3$ to precipitate traces of silicon that are dissolved along with vanadium. The vanadium in solution is concentrated by evaporation, mixed with ammonium chloride, and cooled down to precipitate ammonium metavanadate (AMV), which is calcinated to obtain granular V_2O_5.

5.2.2 Process model

The process conditions shown in Table 4-2 were used to develop a spreadsheet-based model of the vanadium recovery process. The outputs of the model are the material and energy balances of each operation. Details of the model are provided in Chapter 4. Table 4-2 also summarizes the main assumptions used to calculate the energy consumption in the process. Electricity is provided by the grid, and natural gas (used to provide heat) comes from either direct combustion or steam generation. An efficiency of 88% for steam generation was used because it is a typical value for natural gas boilers (Ulrich and Vasudevan 2004), while the conversion efficiency of electricity into power is from 78% to 92% depending on the motor size (Engineering Toolbox 2009).

5.2.3 Estimation of life cycle GHG emissions

The objective of this assessment is to estimate the life cycle GHG emissions per kilogram of vanadium pentoxide recovered from bitumen-derived petcoke fly ash. The scope of the analysis is cradle-to-gate, i.e., from bitumen production to vanadium recovery, without considering its use and disposal. Unless otherwise stated, the emissions related to handling and treatment of wastes and by-products are not included. For the purposes of this analysis, GHG emissions are classified as indirect emissions and direct emissions, as shown in Figure 5-2. The indirect emissions include those from the upstream operations required to obtain the feedstock for the vanadium recovery process; emissions associated with the production of the consumables required by the vanadium recovery process; and emissions from the production of electricity used by said process. Direct emissions are those generated on-site and include emissions from the combustion of fuels to provide heat to the process and emissions generated during the transformation of the feedstock to obtain the final product. The following sections describe the methods used to estimate emissions in each category comprising the life cycle GHG emissions of the vanadium recovery process.

5.2.3.1 Feedstock production

Feedstock emissions are generated during the upstream operations required to get from oil sands to petcoke fly ash. Bitumen is produced through both surface mining and in situ methods. Because most upgraded bitumen in Alberta is from surface mining (Oil Sands Magazine N.d.), that method was considered for the analysis. Oil sands are mined using diesel-fueled shovels and trucks, crushed in rotary breakers and double roll crushers, mixed with hot water, and transported via a conditioning pipe to a bitumen extraction facility. There, bitumen is separated from sand through a series of flotation and deaeration stages, processes that consume significant amounts of water and steam. The remaining fines and water in the bitumen froth are removed via a solvent froth treatment, and the resulting diluted bitumen, called dilbit, is pumped to the upgrader.

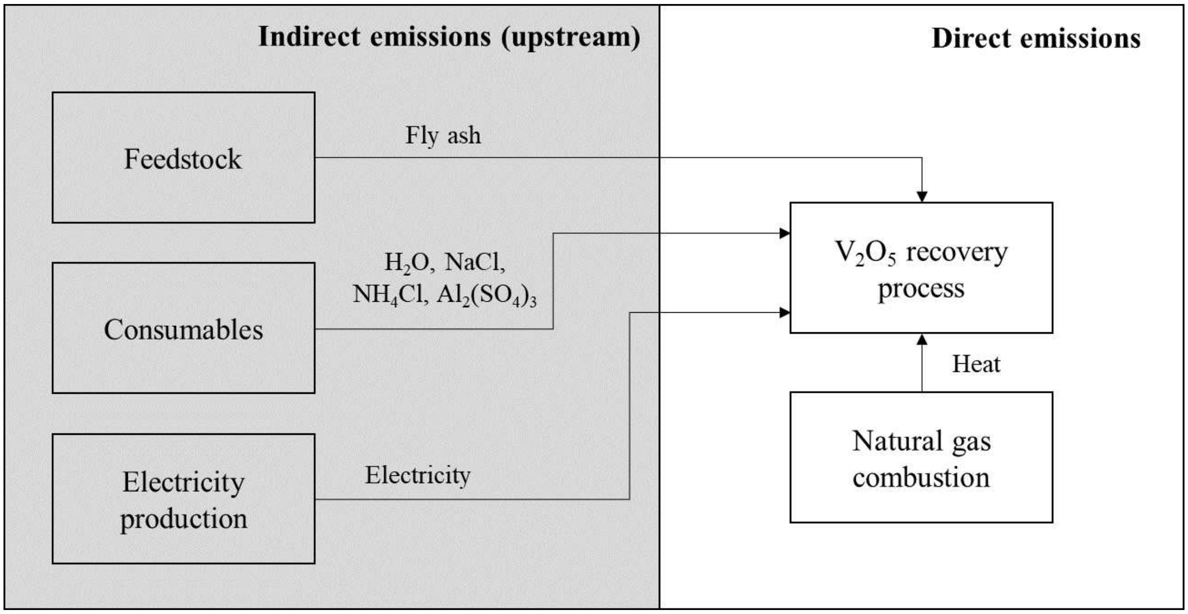

Figure 5-2. System boundary for the life cycle GHG emissions assessment

In the upgrader, dilbit is fed to an atmospheric distillation unit (ADU) where the solvent is recovered and recycled back to the bitumen extraction facility. Light fractions of bitumen, like naphtha and diesel, are obtained from this operation. The residue, i.e., heavy components with high distillation temperatures, are sent to the vacuum distillation unit (VDU) to increase the yield of the upgrader. Light and heavy vacuum gas-oil is also obtained from this unit. The energy consumption in the distillation units is in the form of heat to vaporize the feed, steam to strip the distillation products from the columns, and electricity to pump feeds and products. The bottom of the vacuum distillation operation is sent to delayed cokers, where it is thermally cracked into lighter liquid hydrocarbons. The gaseous light ends are treated in a plant fuel system to get fuel gas that is used to heat the feed to the diverse unit operations in the upgrader. The solid residue of the coking operation, i.e., petcoke, is either stockpiled or fed to coke-fired boilers to produce steam to run operations.

The energy consumption data for each of the upstream operations is from studies by my research group and others (shown in Table 5-1) and is used along with the emission factors shown in Table 5-2 to calculate the upstream emissions. For the purpose of this analysis, it was assumed that steam required for atmospheric distillation, vacuum distillation, and delayed coking is generated from natural gas boilers, in keeping with the assumptions made in the studies where this data was extracted from. Petcoke boilers are used to produce steam for other operations. Running natural gas and petcoke boilers is an industrial practice. For instance, about 57% of the steam required by Suncor's operations is generated from petcoke combustion and the balance from natural gas (Suncor Energy 2017).

Table 5-1. Energy consumption data for the estimation of upstream emissions

Operation	Electricity	Diesel	Natural gas	Fuel gas	Petcoke
Bitumen production[a]	80.4 kWh/bbl bitumen	6.2 l/m^3 bitumen	74.4 m^3/m^3 bitumen	-	-
Atmospheric distillation[b,f]	0.90 kWh/bbl dilbit	-	3.1 kWh/bbl dilbit	20.6 kWh/bbl dilbit	-
Vacuum distillation[c,f]	0.30 kWh/bbl AR	-	2.7 kWh/bbl AR	35.3 kWh/bbl AR	-
Delayed coking[d,f]	30 kWh/t petcoke	-	331 kWh/t petcoke	41.1 kWh/bbl VR	-

Steam generation[e]	4.8 kWh/t steam	-	-	-	100 kg petcoke/t steam

a. Energy consumption per barrel of product. Data from our research group colleagues Nimana et al. (Nimana et al. 2015b).

b. Energy consumption per barrel of feed. Electricity consumption data from Nimana et al. (Nimana et al. 2015b); natural gas and fuel gas consumption data from Abella and Bergerson (Abella and Bergerson).

c. Energy consumption per barrel of feed. Data from Abella and Bergerson (Abella and Bergerson).

d. Electricity consumption and natural gas consumption per metric ton of generated petcoke. Fuel gas consumption per barrel of feed. Data from Abella and Bergerson (Abella and Bergerson).

e. Data from Abella and Bergerson (Abella and Bergerson). Petcoke consumption based on 3.59 MJ/kg steam (5.2 MPa, 565°C) and petcoke heat value of 35.2 MJ/kg petcoke.

f. Natural gas consumption calculated from steam consumption and a natural gas boiler efficiency of 95%.

Table 5-2. Emission factors used to estimate GHG emission from the production of electricity and combustion of fuels

Energy type	Emission factor
Electricity production (grid)	530 kg CO_2eq/MWh[a]
Natural gas combustion	188 kg CO_2eq/MWh[b]
Fuel gas combustion	186 kg CO_2eq/MWh[c]
Diesel combustion	3.0 kg CO_2eq/l diesel[a]
Petcoke combustion	2.34 kg CO_2eq/kg coke[d]

a. From the Government of Alberta (Government of Alberta 2019a).

b. Based on 1.954 kg CO_2eq/m^3 (Government of Alberta 2019a) and 10.37 kWh/m^3 (Government of Canada 2015).

c. Based on 2.42 kg CO_2eq/kg (Nimana et al. 2015b) and a typical heat content of still gas from refinery (46.9 MJ/kg (Engineering toolbox 2008)).

d. The emission factors from the combustion of petcoke are 3494 g CO_2/l coke, 0.12 g CH_4/l coke, and 24 g N_2O /m^3 coke (Government of Canada 2022). Assuming a petcoke density of 1,500 kg/m^3 (Gray 2015), the equivalent Global Warming Potential for a 100-year time horizon was calculated.

Upstream operations can be considered a multiproduct system. The main products are the diverse bitumen fractions used to obtain synthetic crude oil and energy from the combustion of petcoke. The fly ash is now treated as a product as well, instead of a waste, because it will be used as feedstock in the vanadium recovery process. The upstream emissions calculated from the energy consumption data in Table 5-1 were allocated to the vanadium-containing streams through the upstream operations to quantify the emissions associated solely with the functional unit of this study, i.e., one kilogram of recovered vanadium pentoxide. The allocation method was based on the work by Wang et al. (Wang et al. 2004), and it is depicted in Figure 5-3. For any operation n, the emissions generated in that operation are added to the emissions from the previous operation n-1, allocated to the vanadium-containing stream. Then, an allocation factor is used to obtain the allocated cumulative emissions from operation n. This approach was repeated from the first operation (bitumen production) to the final operation (steam generation) in the upstream operations. The allocation was made on a mass basis, except for the steam generation operation, where an economic allocation was used. The selection of a different allocation factor responds to the different nature of the products obtained in the steam generation operation, steam (energy) and fly ash (material). The allocation factors used in this study are presented in Table 5-3.

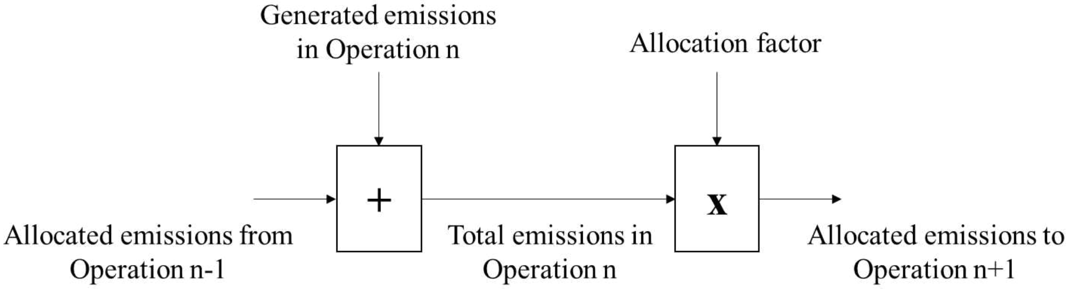

Figure 5-3. GHG emissions allocation method used in this study

Table 5-3. Allocation factors

Operation	Vanadium-contained stream	Allocation factor
Bitumen production	Dilbit	1.00
Atmospheric distillation	Atmospheric residue	0.69[a]
Vacuum distillation	Vacuum residue	0.65[b]
Delayed coking	Petcoke	0.26[c]
Steam generation	Fly ash	0.0285[d]

a. From the material balance presented by our research group colleagues Nimana et al. (Nimana et al. 2015b).

b. From feed and product data for the vacuum distillation of Athabasca bitumen provided by Gray (Gray 2015). Among the products, i.e., light ends, LVGO, HVGO, and VR, the latter represents 65 wt.% of the share.

c. From Gray's material balance of delayed coking of Athabasca bitumen (Gray 2015). Petcoke represents 26.1 wt.% of the products, which include light ends and liquid products.

d. The combustion of one kg of petcoke generates 9.80 kg of steam (5.2 MPa, 565°C), by supplying 35.2 MJ. If this amount of energy is supplied by the combustion of natural gas, the cost would be \$0.046/kg petcoke at a rate of \$1.32/GJ natural gas. This number is considered the economic value of the generated steam. Considering an ash content of 4.2 wt.% and that 65% of the generated ash corresponds to fly ash, the combustion of one kg of petcoke produces 0.027 kg of fly ash. For a price of \$50/t fly ash, the economic value of this product is \$0.00135/kg petcoke, which represents

2.85% of the total economic value of the products from the steam generation operation.

5.2.3.2 Process emissions

The decarbonization of fly ash involves burning the unreacted carbon present in the fly ash. Therefore, carbon dioxide is found in the off-gases from that operation. Emissions from the decarbonization of fly ash were computed assuming the stoichiometric oxidation of carbon and sulfur in the feedstock. Off-gases from fly ash decarbonization and roasting should be treated to remove carbon dioxide, sulfur, and hydrogen chloride before been released to the atmosphere. Wet scrubbing and amine gas treatment were assumed since this technology is widely used in the chemical industry. The operation of the gas treatment unit requires electricity and heat; therefore, their associated emissions are considered. Rosental et al. provide the energy consumption per kg of captured CO_2 for an amine treatment unit based on monoethanolamine (MEA) (Rosental et al. 2020). Using this data and the emission factors for electricity production and combustion of gas natural in Alberta, the carbon intensity of the gas treatment unit was estimated to be 0.173 kg CO_2e/kg captured CO_2. Grant et al. performed an LCA of a similar gas treatment unit, including the production of MEA and credits for material displacement due to by-products (e.g., gypsum) in the system boundary (Grant et al. 2014). They reported 0.232 kg CO_2e/kg captured CO_2. For this study, the average of the two values (0.203 kg CO_2e/kg captured CO_2) was used and the differences were considered in the sensitivity and uncertainty analysis. The mass flow of the off-gases per kg of recovered V_2O_5 was obtained from the process material balance, and, assuming a 90% capture efficiency (typical for MEA based gas treatment units (International Energy Agency 2021a)), the additional emissions due to gas treatment were calculated.

5.2.3.3 Consumables and electricity production and combustion of natural gas

The GHG emissions in these categories were estimated from the corresponding inventory obtained using the process model developed in this study and the associated emission factors found in a City of Winnipeg report. The data used to estimate the emissions from the production of consumables and electricity and the combustion of natural gas is shown in Table 5-4. The breakdown of the consumption of electricity and natural gas is discussed in Section 5.3.1

Table 5-4. Data for the estimation of upstream emissions associated with the production of consumables

Consumable/Energy source	Emission factor	Consumption[b]
Aluminum sulfate	0.50 kg CO_2eq/kg[a]	0.36 kg/kg V_2O_5
Sodium chloride	0.20 kg CO_2eq/kg[a]	11.2 kg/kg V_2O_5
Ammonium chloride	1.18 kg CO_2eq/kg[a]	2.35 kg/kg V_2O_5
Process water	0.03 kg CO_2eq/m^3[a]	0.07 m^3/kg V_2O_5
Electricity	See Table 5-2	0.43 kWh/kg V_2O_5
Natural gas	See Table 5-2	0.15 GJ/kg V_2O_5

a. City of Winnipeg report (City of Winnipeg).

b. This study.

5.3 Results and discussion

5.3.1 Process energy consumption

The salt roasting and water leaching process requires 0.43 kWh electricity and 0.15 GJ natural gas per kg of recovered V_2O_5. The breakdown of the energy consumed by each operation is shown in Figure 5-4. AMV calcination consumes 33% of the total energy to drive the rotary kiln used in this operation. Decarbonization and roasting consume 25% each. The electricity consumed in the former is to run the fan to provide air for the combustion of unreacted carbon in the fly ash. In the latter, electricity is used to drive the rotary kiln used for roasting. About 8% of the total electricity is required by the disk agglomerator, while 5% is used to drive the agitator in the leaching operation.

Regarding natural gas consumption, the AMV precipitation operation takes the largest share, over 42%. Natural gas is required in this operation to evaporate water from the pregnant liquor and concentrate vanadium in solution. About 41% of the total natural gas is burned to provide the sensible and reaction heat for roasting and make up heat losses. The leaching operation consumes 15% to provide reaction heat and make up heat losses. The natural gas consumption by AMV calcination is only 2% because of the relatively small amount of material to be calcinated. No heat recovery from the off-gases of decarbonization was considered in this analysis.

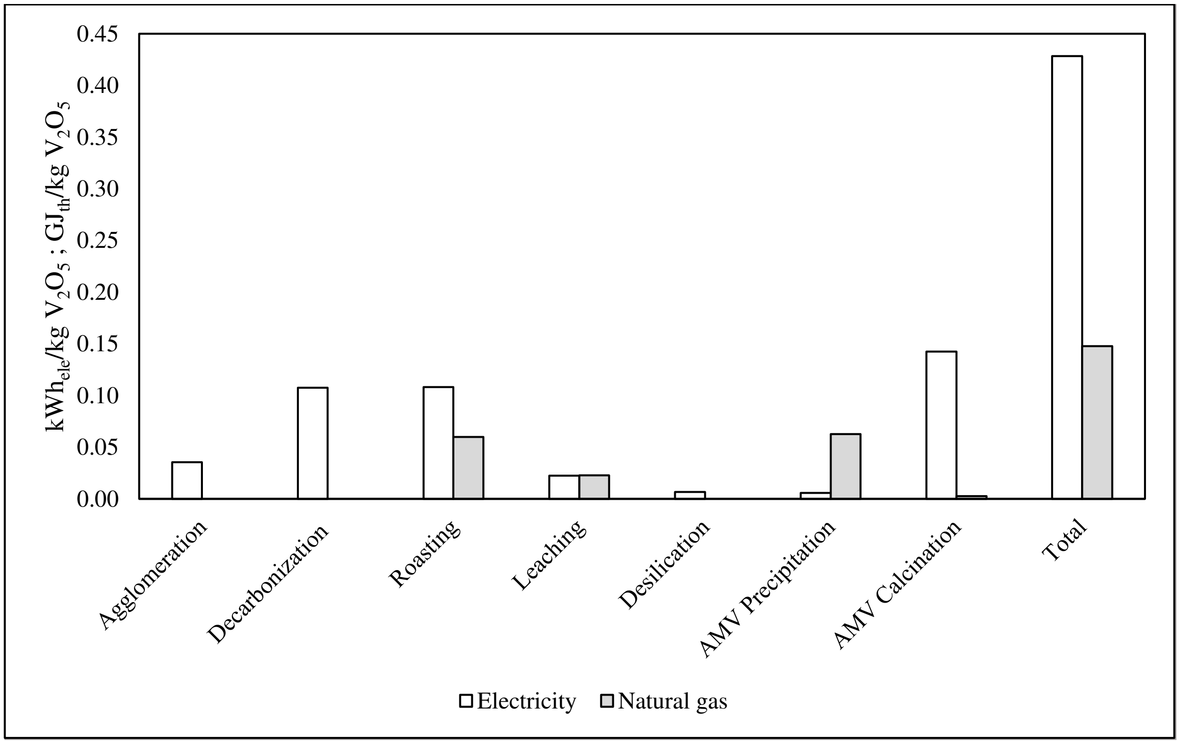

Figure 5-4. Energy consumption by operation

5.3.2 Life cycle GHG emissions

The life cycle GHG emissions were estimated to be 26.6 kg CO_2e/kg V_2O_5, of which 66% corresponds to direct emissions and 34% to indirect emissions. Regarding the indirect emissions, 3.53 kg CO_2e/kg V_2O_5 come from those stages related to the generation of fly ash (from bitumen production to steam generation), 5.19 kg CO_2e/kg V_2O_5 are emitted during the production of the consumables for the process, and 0.23 kg CO_2e/kg V_2O_5 are from the production of the consumed electricity in the vanadium recovery process. Direct emissions include 7.87 kg CO_2e/kg V_2O_5 from the combustion of natural gas and 9.79 kg CO_2e/kg V_2O_5 from the process. This breakdown is shown in Figure 5-5..

.

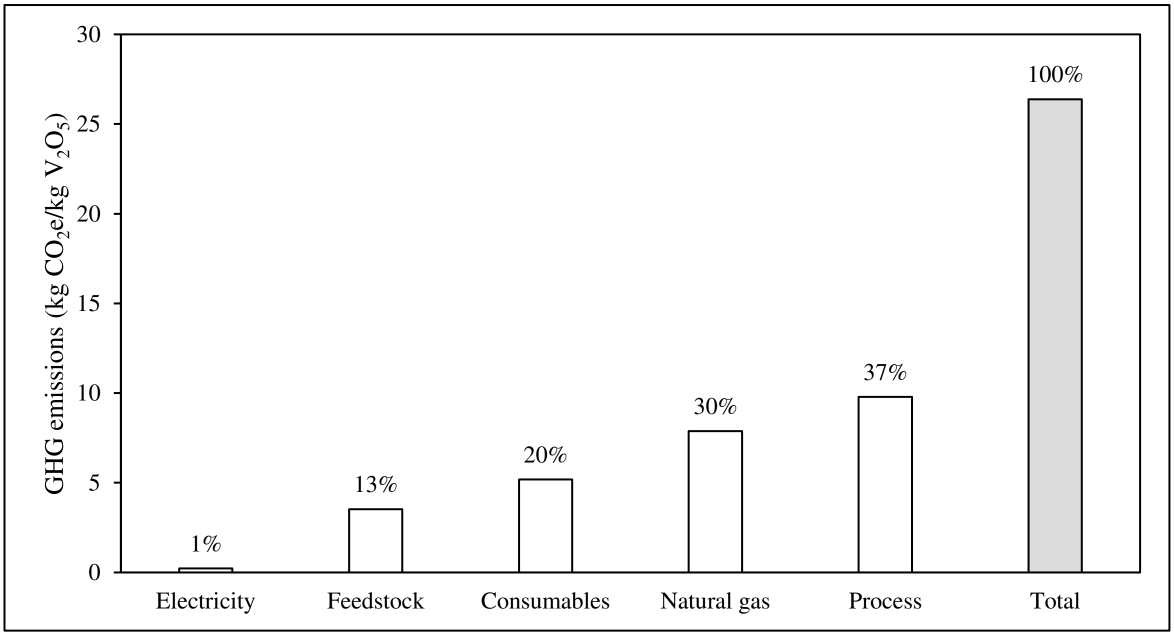

Figure 5-5. GHG emissions through the life cycle of vanadium recovery from petcoke fly ash

Figure 5-6 shows the contribution of each upstream operation in the feedstock generation stage. Steam generation is the greatest contributor with 92% of the emissions, or 12% of the life cycle GHG emissions. Bitumen production, atmospheric and vacuum distillation, and delayed coking are energy-intensive operations; however, their share of life cycle GHG emissions is very low (about 1% combined) because most of the emissions are allocated to the hydrocarbon products of each operation rather than to vanadium-containing streams.

The emissions related to steam generation come from the combustion of petcoke. Petcoke gasification could be an alternative to combustion that generates lower GHG emissions (National Energy Technology Laboratory N.d.). A metal-enriched slag is generated during petcoke gasification that could be used as feedstock to the vanadium recovery process. Some studies show the technical feasibility of bitumen-derived petcoke gasification (Watkinson et al. 1989; Furimsky 1998; Duchesne 2012; Hill et al. 2014b) and the characterization of the generated slag (Duchesne et al. 2016; Duchesne et al. 2017; Cousins et al. 2018). No particular process for the recovery of vanadium from the slag generated during gasification of such petcoke was found in the literature; however, processes applied to generic gasification slag have been proposed (Haas and Hesse 1981; Rappas and Spitz 2013). Those processes are based on the solubilization of vanadium oxides by reacting with alkali metals, followed by water leaching and vanadium separation, as in the process considered in this study. Further research on the suitability of gasification slag for vanadium recovering and tailoring the recovery process is worthy of consideration.

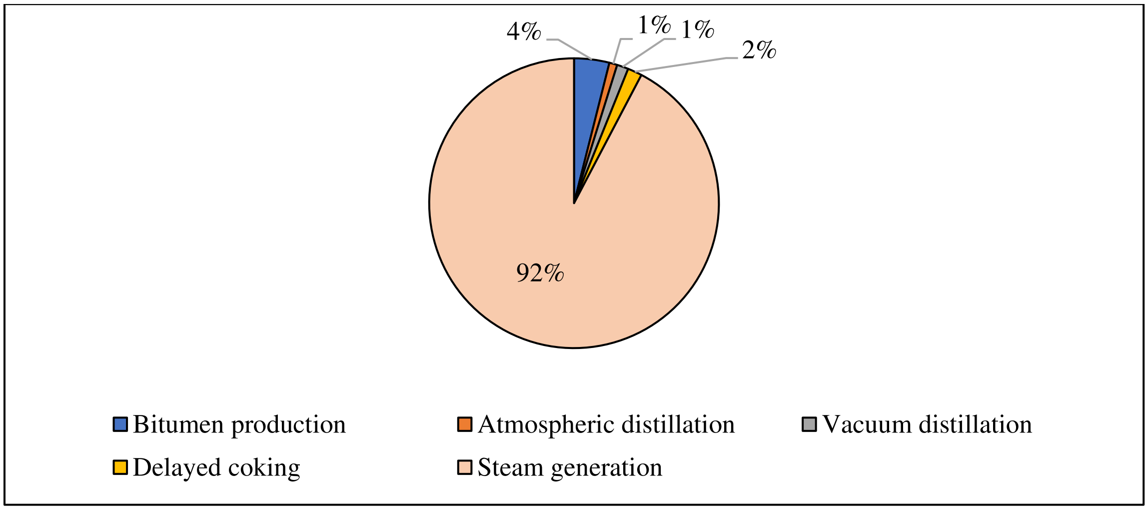

Figure 5-6. Breakdown of the GHG emissions from the feedstock generation stage

As shown in Figure 5-7., the consumables that contribute the most to the upstream emissions are sodium chloride and ammonium chloride. Reducing their consumption in the process would reduce GHG emissions. Holloway and Etsell considered the recovery of NaCl and a cake containing NH_4Cl and NH_4VO_3 by the evaporation and cooling of the barren liquor remaining after vanadium precipitation (Holloway and Etsell 2005). In this way, the consumption of sodium chloride for roasting is reduced and the use of NH_4Cl is optimized, leading to lower emissions associated with those consumables.

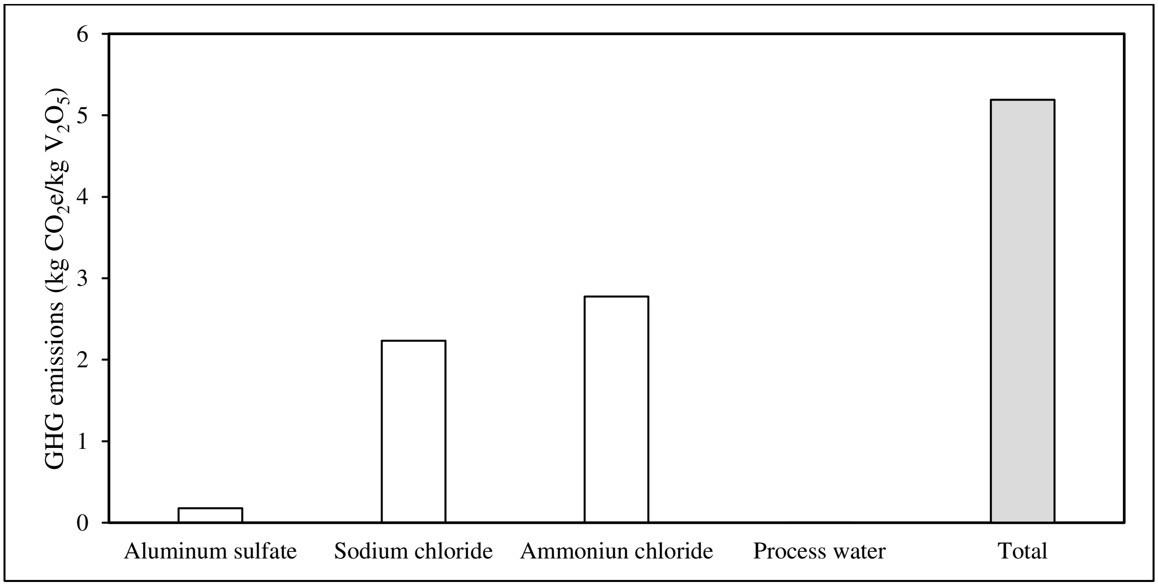

Figure 5-7. Contribution of consumable production to the life cycle GHG emissions

Figure 5-8 presents the contribution of each operation in the recovery process to the life cycle GHG emissions. The emissions associated with the production of electricity and consumables and with the combustion of natural gas were distributed to the operations responsible for the consumption of each resource. To account for all the emission categories in the same figure, the emissions associated with the feedstock were allocated to the agglomeration operation.

Fly ash decarbonization is the operation that contributes the most to life cycle GHG emissions, with 9.8 kg CO_2e/kg V_2O_5. This number represents 37% of the total emissions. Almost all the emissions from fly ash decarbonization are process emissions from the combustion of carbon in the feedstock, even if a gas treatment unit is implemented to remove CO_2 from the off-gases. Those emissions were estimated to be 34.7 kg CO_2e/kg V_2O_5 without considering off-gas treatment. In such a scenario, the life cycle GHG emissions would be

51.5 kg CO_2e/kg V_2O_5. Given the substantial contribution of the process emissions to the total emissions, a gas treatment operation to capture the carbon dioxide found in the off-gases was included. With an MEA-based ammine gas treatment unit, the operation avoids releasing 31.2 kg CO_2e/kg V_2O_5 to the atmosphere; therefore, the process emissions are cut down to 3.47 kg CO_2e/kg V_2O_5. The operation of the gas treatment unit generates additional emissions that are allocated to the decarbonization operation. For the mentioned amount of carbon captured, the additional emissions are about 6.32 kg CO_2e/kg V_2O_5, so the net reduction in the GHG emissions by implementing the off-gas treatment operation is 24.9 kg CO_2e/kg V_2O_5, the direct emissions are reduced to 17.7 kg CO_2e/kg V_2O_5, and the life cycle GHG emissions total 26.6 kg CO_2e/kg V_2O_5, as indicated in the previous section. Ammine gas treatment is a suitable solution to the direct emissions from the process; however, it can impact the vanadium recovery cost. In Chapter 4, the authors determined that with amine gas treatment, the cost of vanadium recovery is 21% higher than the cost without (Baritto et al. 2023b). A better approach to reduce process emissions while maintaining a low recovery cost could be to avoid generating GHG emissions through other means of decarbonizing the fly ash. For instance, the removal of unburned carbon from fly ash by froth flotation (Stemerowicz et al. 1976; Walker and Wheelock 2006; Zhang et al. 2020), gravity separation (Zhang et al. 2020), and electrostatic separation (Tao et al. 2015) has been proven with different degrees of success. Another approach is to omit the decarbonization operation. To that end, Sakuma and Kobori patented a process that combines the generation of a fly ash slurry and a magnetic separation step to recover vanadium without decarbonizing the feed (Sakuma and Kobori 2018).

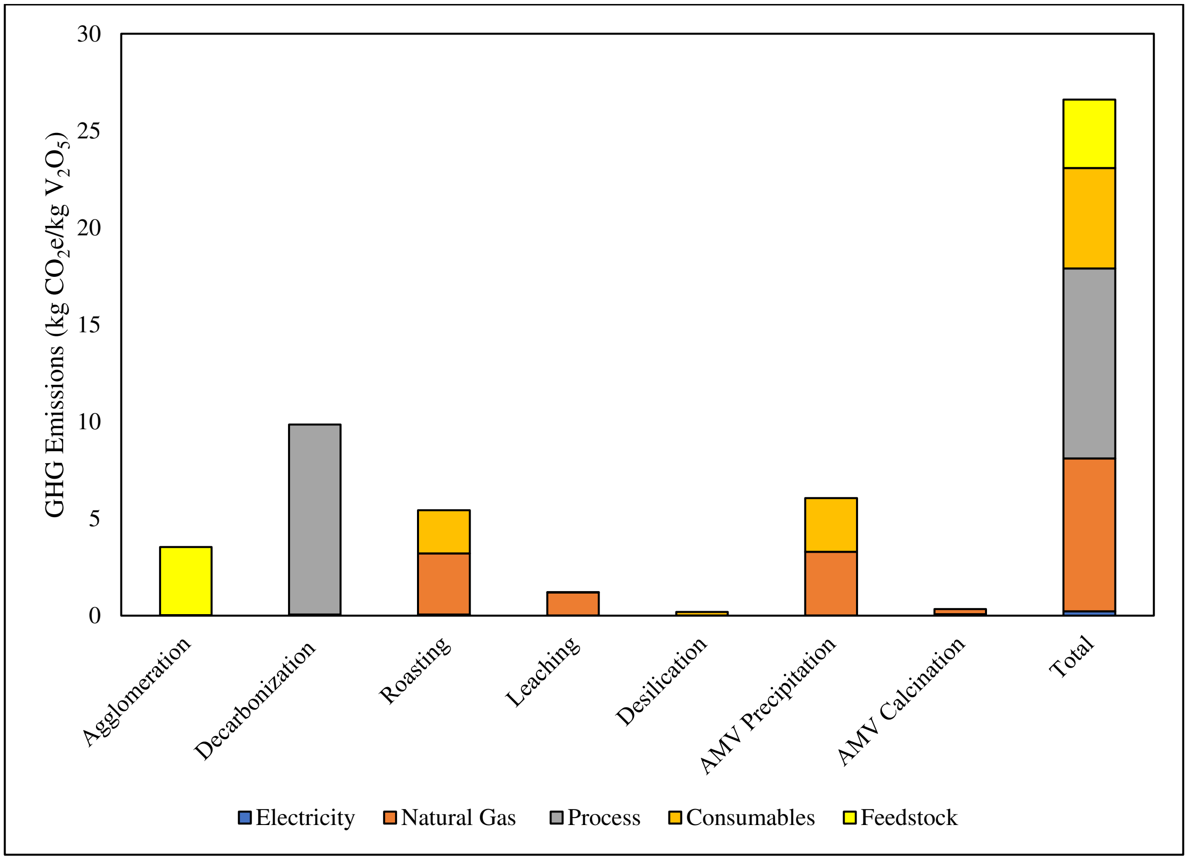

Figure 5-8. Contribution of each operation of the vanadium recovery process to the life cycle GHG emissions

The life cycle GHG emissions from the petcoke fly ash route were compared with other pathways to produce vanadium pentoxide. Vanadium pentoxide is usually produced from a pyrometallurgy treatment of the slag obtained as a by-product of steel production from a VTM ore. In this study, that route was considered as the primary production process of V_2O_5. Using energy consumption and direct emissions data from Chen et al. (Chen et al. 2015), the life cycle GHG emissions of that pathway were estimated. Also, it included the recovery of vanadium from spent catalyst generated in the upgrading of bitumen through a roasting and water leaching process. This process is compatible with hydroconversion upgraders, in contrast with delayed coking upgraders, which are compatible with the process considered in this study. The life cycle GHG emissions of this pathway were obtained in Chapter 3.

Compared with the other pathways, the petcoke fly ash route generates more than twice the life cycle GHG emissions. As seen in Figure 5-9., the petcoke fly ash pathway underperforms in both the indirect and direct emissions categories. The indirect emissions of the VTM pathway are allocated to steel and vanadium on a mass basis. According to Chen et al., only 2.4 kg of V_2O_5 is produced per metric ton of produced steel (Chen et al. 2015), hence the low emissions allocated to the vanadium product. The upstream operations to obtain the feedstock in the bitumen-upgrading spent catalyst pathway are similar to those in the petcoke fly ash pathway; however, the steam generation step is included in the latter but not needed in the former. Because the emissions from the combustion of petcoke constitute the bulk of the indirect emissions in the petcoke fly ash pathway, the life cycle emissions of that pathway are greater than in the bitumen-upgrading spent catalyst pathway.

Regarding the direct emissions, the reason for the big difference among the three pathways is the process emissions from the fly ash decarbonization. In the VTM pathway, the feedstock does not need to be decarbonized, while in the spent catalyst pathway, the amount of residual petcoke on the catalyst surface is very low and so are the emissions generated during the calcination step in the process.

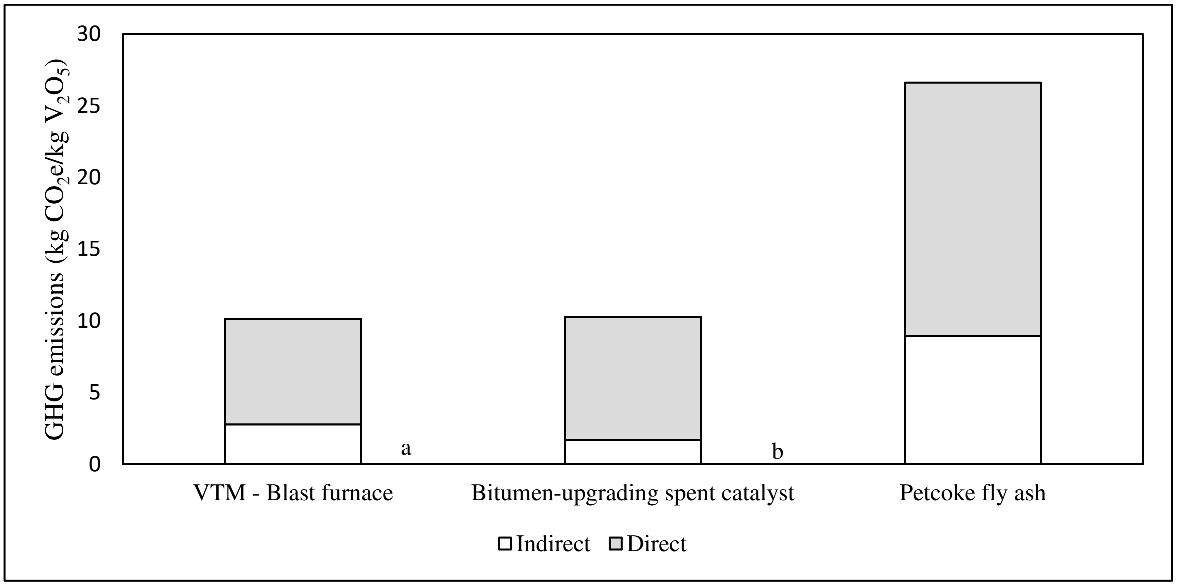

Figure 5-9. GHG emissions comparison among different vanadium sources

a. Data source: energy consumption and direct emissions from Chen et al. (Chen et al. 2015). System boundary: mining/dressing, sinter plant, blast furnace, basic oxygen furnace, coke plant, V_2O_5 plant, limestone production, quickstone production, electricity production. Main product: steel. By-products: ilmenite and vanadium pentoxide.
b. Data source: life cycle GHG emissions from an earlier study by the authors (Baritto et al. (Baritto et al. 2023a)). System boundary: bitumen production (mining), ADU, VDU, hydroconversion reactor. Main product: liquid hydrocarbon for synthetic crude oil production. By-products: vanadium pentoxide, molybdenum trioxide, and alumina.

5.3.3 Sensitivity and uncertainty analyses

The Morris method was used to perform the sensitivity analysis and a Monte Carlo simulation was used to address the uncertainty in the model inputs. An overview of both method is presented in Appendix B. Both analyses were conducted using the Regression, Uncertainty, and Sensitivity Tool (RUST) developed by our research colleagues Di Lullo et al. (Di Lullo et al. 2019), considering a uniform distribution of all the inputs within the assumed variation ranges.

The analysis aimed to identify those inputs to which the model outputs are sensitive. Thirty-nine inputs that govern the life cycle GHG emissions were considered, including energy consumption in upstream operations, equipment performance and process energy consumption, and emission factors for fuel combustion, electricity production, and consumable manufacturing. To discard insensitive inputs, the analysis was performed considering input variations of ±10%, ±30%, and ±50% relative to the values used as the base case. Then, the range of variation of the sensitive inputs was refined according to typical values, industry practices, and assumptions, as shown in Table 5-5.

Table 5-5. Input ranges considered in the sensitivity analysis

Input	Units	Base case	Min	Max	Comments
Boiler efficiency	-	0.88	0.85	0.92	Typical values (Ulrich and Vasudevan 2004).
Combustion efficiency – Rotary kiln for roasting	-	0.70	0.65	0.70	Typical values (Ulrich and Vasudevan 2004).
Heat loss – Rotary kiln for roasting	-	0.40	0.15	0.40	Fraction of energy input. Typical values (Ulrich and Vasudevan 2004; Engin and Ari 2005).
Air-to-fuel ratio – Roasting	kg air/kg natural gas	15.0	10.0	20.0	The stoichiometric ratio is 17.2. Lean and rich mixtures were considered.
CO_2 removal efficiency	-	0.90	0.80	0.95	Typical values for amine-based gas treatment systems

Input	Units	Base case	Min	Max	Comments
					(Fagerlund et al. 2021; International Energy Agency 2021a).
Gas treatment – Carbon intensity	kg CO_2e/kg CO_2 removed	0.20	0.173	0.23	Typical values. Lowest values from data from Rosental et al. (Rosental et al. 2020) and highest from Grant et al. (Grant et al. 2014).
NaCl production – Carbon intensity	kg CO_2e/kg NaCl	0.20	0.14	0.26	Widely varies depending on production process and plant location. A range of ±30% was assumed to discern the impact of these inputs on the model.
NH_4Cl production – Carbon intensity	kg CO_2e/kg NH_4Cl	1.18	0.83	1.53	
Petcoke combustion – Carbon intensity	kg CO_2e/kg petcoke	2.34	1.64	3.01	

Figure 5-10. presents the results of the sensitivity analysis. In the Morris plot, the horizontal axis represents the mean of the change in the model output as the inputs change from the lowest to the highest values. The vertical axis indicates the standard variation of these changes and represents the interaction of each input with other parameters in the model. The life cycle GHG emissions appear to be very sensitive to the air-to-fuel ratio used for the roasting operation, as well as to the emission factor of petcoke combustion and the emission factor of CO_2 removal. These inputs affect the emissions from the operations that contribute the most to the life cycle GHG emissions, thus it is expected that their variations significantly affect the model output. The emission factor of the production of NH_4Cl and NaCl, the heat loss in the kiln used for roasting, and the CO_2 removal efficiency are moderately sensitive inputs. The model output is less sensitive to boiler efficiency and combustion efficiency in the roasting operation. The air-to-fuel ratio and the heat loss in the roasting operation are inputs with higher interactions, and the interactions of the remaining inputs are low, which means that the response of the life cycle GHG emissions is nearly linear with respect to those variables.

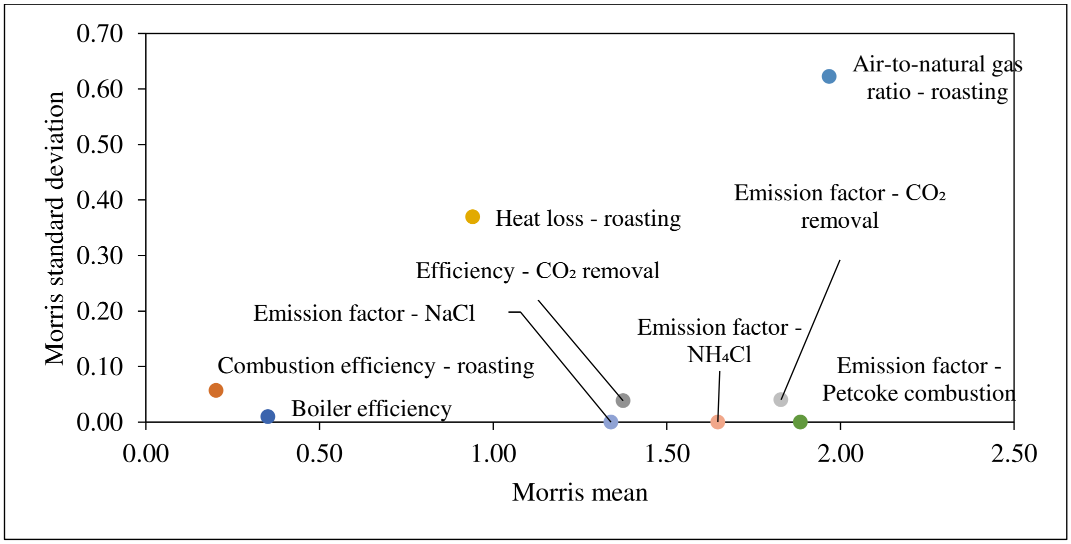

Figure 5-10. Sensitivity analysis results

The nine shortlisted inputs were used to perform the Monte Carlo simulation. Five thousand runs with the ranges shown in Table 5-5 were used to get the frequency distribution of the life cycle GHG emissions, presented in Figure 5-11.. The mean of the distribution is 25.5 kg CO_2e/kg V_2O_5 with a standard deviation of 1.20 kg CO_2e/kg V_2O_5. At a 90% confidence level, the life cycle GHG emissions would be between 22.7 and 27.5 kg CO_2e/kg V_2O_5. These expected values are greater than the life cycle GHG emissions of the other pathways considered in Section 5.3.2. Even the minimum value of the distribution (21.7 kg CO_2e/kg V_2O_5) is above the emissions from the VTM and spent catalyst pathways.

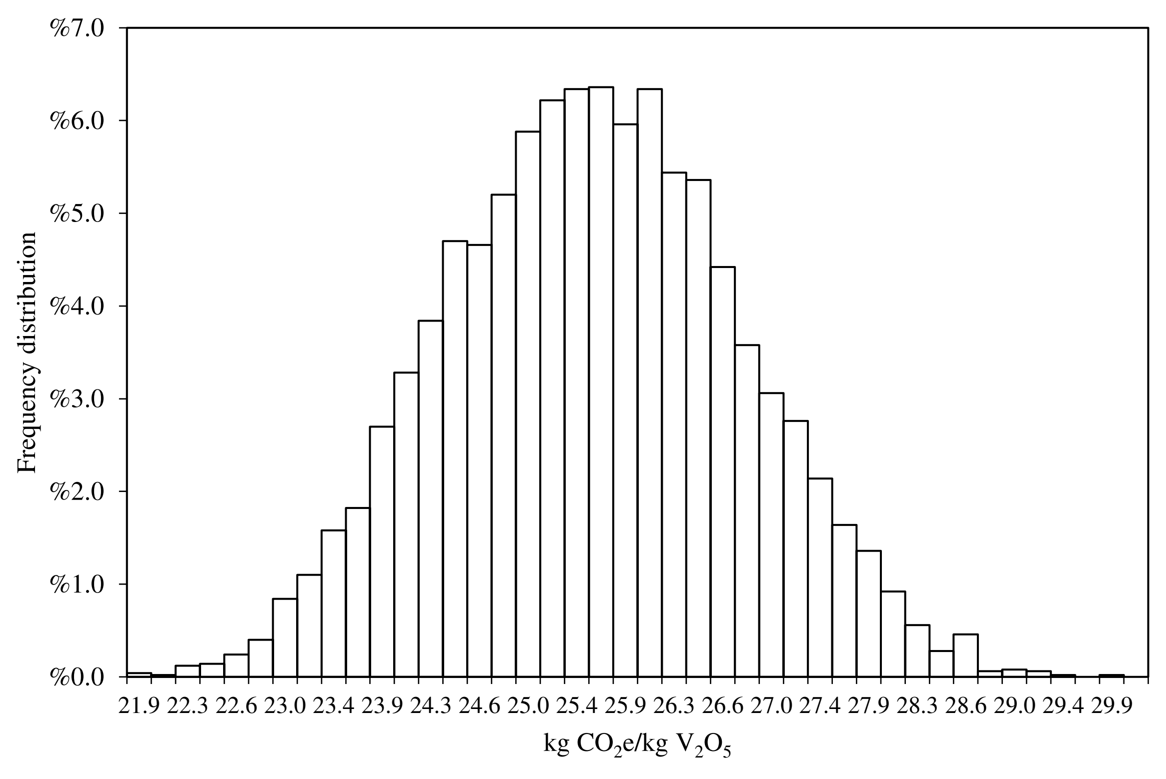

Figure 5-11. Frequency distribution of the life cycle GHG emissions obtained from the Monte Carlo simulation

5.4 Conclusions

In this study, the life cycle GHG emissions from the recovery of V_2O_5 from the fly ash obtained from the combustion of bitumen-derived petcoke were estimated. The system boundary was made up of the upstream operations (i.e., bitumen mining, ADU, VDU, delayed coking, petcoke combustion for steam generation, and the production of consumables) and the vanadium recovery process (i.e., salt roasting and water leaching).

The estimated life cycle GHG emissions are 26.6 kg CO_2eq/kg V_2O_5; 66% correspond to direct emissions and the balance to indirect (upstream) emissions. Most of the indirect emissions are due to the production of consumables, specifically NaCl and NH_4Cl, and the generation of steam by petcoke combustion. The direct emissions from fly ash decarbonization represent by far the main source of direct emissions, even if an amine-based gas treatment is implemented. Compared with other pathways to produce vanadium pentoxide, the studied route doubles the life cycle GHG emissions. Based on these results, some modifications could be implemented to reduce the emissions at least at the level of the VTM and spent catalyst pathways. Adding a salt recycling loop to the vanadium recovery process, using other means to obtain the feedstock to the process, and avoiding combustion for fly ash decarbonization are options worthy of consideration.

Sensitivity analysis shows that the life cycle GHG emissions are more sensitive to the air-to-fuel ratio in the roasting operation and to the emission factors from petcoke combustion and the gas treatment unit. Upstream operations have little effect on the life cycle GHG emissions, except in the emission factors associated with some consumables and the combustion of petcoke. Input uncertainties situate the expected life cycle GHG emissions between 22.7 and

27.5 kg CO_2e/kg V_2O_5, still greater than those from the other pathways used for comparison purposes.

This study lays the groundwork for further research on reducing the GHG emissions from the specific operations that most impact the life cycle GHG emissions of the recovery of vanadium from bitumen-derived petcoke fly ash. In this sense, alternative means of decarbonizing the fly ash or avoiding the combustion of petcoke to generate the feedstock for the recovery process are worthy of consideration. Should this goal be accomplished, Alberta's oil sands could emerge as a suitable source of vanadium pentoxide for the global market.

Chapter 6: The development of a techno-economic model for the assessment of heavy minerals recovery from bitumen extraction tailings

6.1 Introduction

Oil sands are a mixture of sand, clay, water, and a dense, highly viscous form of petroleum called bitumen. The oil sands deposits are found primarily in northern Alberta, Canada, one of the largest oil reserves in the world. Other major oil sands deposits are located in Venezuela and Russia, while small reserves are found in the United States, Nigeria, Madagascar, and Congo, and elsewhere. The means to produce bitumen from oil sands depend on the depth of the deposit and the characteristics of the oil sands, e.g., whether the sand is water wet or oil wet. In general, there are two ways to produce bitumen from oil sands: by injecting steam to the deep reservoir and then pumping the heated bitumen to the surface and by mining the oil sands and extracting the bitumen from the sands in a processing facility. Alberta produces about 490,000 cubic meters (3.0 million barrels) per day of crude bitumen. Surface mining accounts for 45% of the production and 55% is produced in situ (Alberta Energy Regulator 2023b). Mining operations are exclusively in the region of Athabasca, while in situ production is performed in Athabasca and Peace River counties and near Cold Lake (Figure 6-1.).

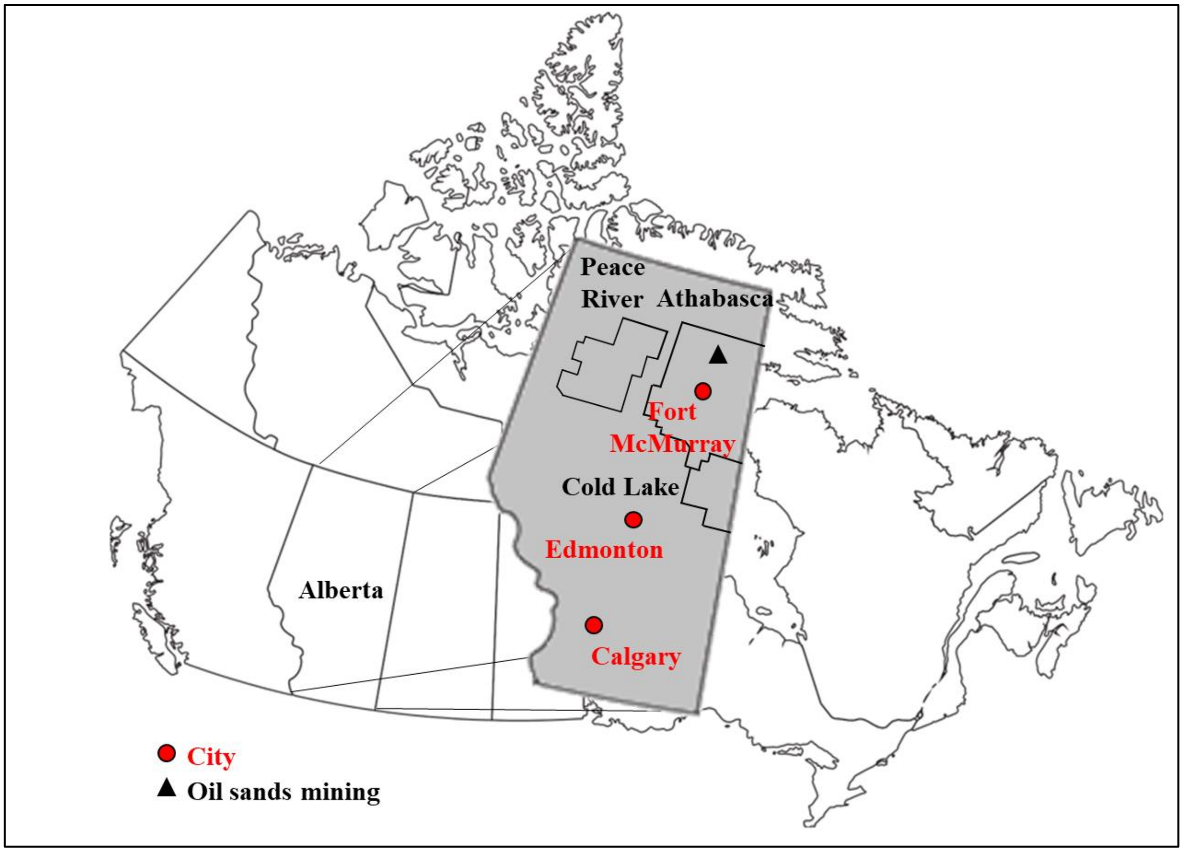

Figure 6-1. Location of oil sands operations in Alberta, Canada

The occurrence of zircon and titanium minerals in the solid constituent of Alberta's oil sands has long been known. These heavy minerals are traditionally produced from hard rock and mineral sands mining. Approximately 82% of the world's zirconium reserves are concentrated in Australia (63%) and South Africa (19%), and Australia (30%), China (24%), and India (10%) together contribute 63% of the titanium reserves (U.S. Geological Survey 2022). This uneven distribution of resources could significantly impact the titanium and zirconium market, affecting a wide range of industries, including steel production for construction, automotive, and aerospace, as well as refractories, ceramics, pigments, and the chemical industry. Emerging technologies in the energy sector may also be affected. The demand for titanium in geothermal energy and solar panels is expected to increase in the next three decades (International Energy Agency 2021a; Hund et al. 2023), while zirconium is considered a key component of electrolyzes for hydrogen production (International Energy Agency 2021b). Alberta's oil sands could serve as an alternative source of zircon and titanium minerals, helping to alleviate market pressure caused by an increase in demand or supply shortage. In feed-grade ore obtained through oil sands surface mining, the concentrations of titanium and zirconium minerals average 0.35 wt.% and 0.032 wt.%, respectively (Oxenford et al. 2001). In in situ production, most of the heavy mineral-rich sands are left in the reservoir by using sand control devices. For this reason, that bitumen production pathway is of little interest for this study.

The production of bitumen by surface mining is illustrated in Figure 6-2. The oil sands ore is extracted from an open pit mine using shovels and trucked to a slurry preparation plant to be crushed, mixed with hot water, and pumped to the extraction plant. There, the slurry is subjected to a series of flotation steps to separate bitumen as a froth. The underflow, often called main tailings, contains a mixture of clays and coarse sand, and is dewatered, thickened, and stockpiled in tailings ponds. The froth, containing bitumen, water, and mineral solids, is subjected to a naphthenic solvent froth treatment (NFT)[6] to produce a diluted bitumen, called dilbit, that is either sold or upgraded to produce synthetic crude oil. In NFT, the froth is mixed with naphtha and fed into a series of inclined plate separators and centrifuges to obtain a

---

[6] A paraffinic solvent froth treatment is used in some extraction plants. This type of treatment produces asphaltenes precipitation. Although asphaltenes precipitation is positive for the quality of dilbit, the presence of asphaltenes in the tailings could make the recovery of heavy minerals difficult. Therefore, we focused on tailings originating from the naphthenic solvent froth treatment.

dilbit stream and a water/solids/naphtha stream, which is directed to a naphtha recovery unit (NRU). The underflow of the NRU, known as froth treatment tailings (FTT), is a mixture of water, solids, and residual bitumen and solvent, and is disposed of in tailings ponds. About 12 to 15 m^3 of tailings are generated per cubic meter of bitumen produced. Of these, about 6% corresponds to FTT (Flint 2005). FTT typically contain 16-20 wt.% solids, 76-80 wt.% water, 2-5 wt.% bitumen, and traces of the diluent used in NFT (Erasmus et al. 2010). Approximately 15-30 wt.% of the solids in FTT is heavy minerals, and the balance is silica and fine clays. Zircon and titanium minerals, e.g., rutile, ilmenite, and leucoxene, are the predominant heavy minerals in the tailings, along with iron minerals and aluminosilicates. The grade of TiO_2 and ZrO_2 in FTT solids has been estimated to be 11.5% and 3.40%, respectively (H.A. Simons Ltd. 1996). However, titanium minerals and zircon grains predominantly occur in the size range of -154+45 μm (about 60-70% Ti and 65-80% Zr), while about 11-17% of titanium minerals and 12-20% of zircon are in the -38 μm range (Liu et al. 2006). The recovery of minerals from the latter range may be difficult using physical separation techniques. Thus, only grains larger than 38 μm are potentially recoverable.

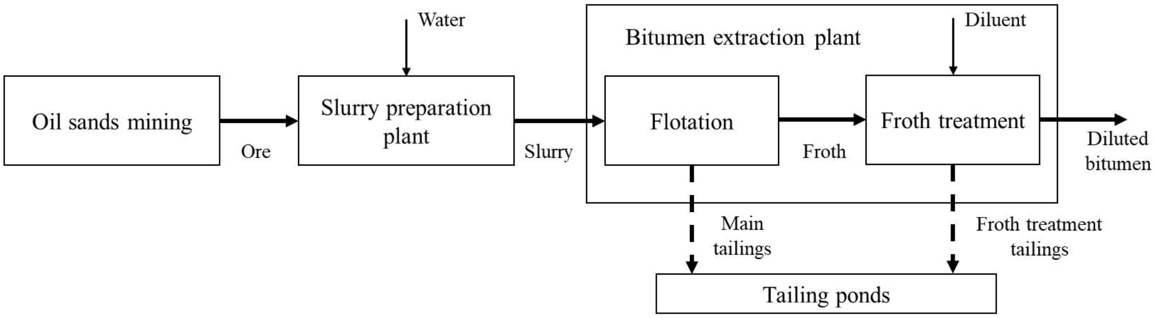

Figure 6-2. Simplified schematic of the bitumen production process by surface mining

Considering the current production of the extraction plants that implement NFT in Alberta and using typical tailings-to-bitumen volume ratios, it was estimated in this study that 560,000 tonnes of TiO_2 and 191,000 tonnes of ZrO_2 could be recovered from FTT (see Table 6-1). These figures represent about 6.5% and 16.0%, respectively, of the titanium and zirconium mined in the world in 2020 (U.S. Geological Survey 2022).

Because of the massive scale of the oil sands mining operations, and the high concentration of titanium minerals and zircon in the tailings, FTT are among the richest sources of those minerals worldwide. The grade of TiO_2 in FTT is greater than that in the mineral sands of South Africa and Australia (the biggest reserves in the world) and second to the hard rock ilmenite deposits in Quebec, Canada (H.A. Simons Ltd. 1996). The recovery of heavy minerals from FTT may be economically attractive not only because it creates value from bitumen extraction process waste, but because it diversifies Alberta’s and Canada’s economies. In fact, zircon from FTT has been identified as a potential non-combustion product of the oil sands industry (Meisen 2017). Diverse processes for the recovery of heavy minerals from FTT have been developed over the years, but only a few have been subjected to techno-economic analysis.

Table 6-1. Data of processed oil sands and bitumen production by plants in Alberta using NFT, and the estimated tailings generation and heavy minerals content in tailings

Plant/Operator	Processed oil sands[a] (x10^6 t)	Bitumen production[a] (x10^6 m^3)	FTT generated[b] (x10^6 m^3)	Solids in tailings[c] (x10^6 t)	Recoverable TiO_2[d] (x10^3 t)	Recoverable ZrO_2[d] (x10^3 t)
Base Plant/Suncor	150.4	14.9	13.8	2.62	211.0	71.3
Horizon/Canada Natural Resources	176.1	14.9	13.8	2.62	211.0	71.3
Mildred Lake/Syncrude	102.6	10.2	9.38	1.79	143.9	48.6
Total	429.1	40.1	36.9	7.03	565.9	191.2

a. Data from 2022 (Alberta Energy Regulator 2023a).

b. Based on a centrifuge tailings-to-bitumen volume ratio of 0.92 (Flint 2005).

c. Estimated assuming a tailings density of 1,120 kg/m^3 and a solids content of 17.0 wt.%.

d. Assuming 11.5% TiO_2 and 3.4% ZrO_2 in the solids fraction of FTT (H.A. Simons Ltd. 1996); only the particles in the size range -154+45 µm are recoverable (i.e., 70% TiO_2 and 80% ZrO_2) (Liu et al. 2006).

The cost-effective recovery of heavy minerals from FTT faces challenges that the mining of mineral sands or hard rock, the conventional sources of titanium and zirconium minerals, does not (Erasmus et al. 2010). The sand grains are coated by residual bitumen, which hampers the separation of the diverse minerals in the tailings; secondary mineralization increases the complexity of the process to separate minerals such as pyrite, calcite, and siderite, from titanium and zirconium minerals; the high proportion of aluminosilicates with similar physical properties to other minerals in the tailings hinders its separation by conventional means; and there is a high proportion of fines that should be handled but their value is very low. Several processes to tackle those obstacles have been proposed over the years, and despite the different technologies and unit operations, the main steps are common to most of them: deoiling for residual bitumen removal, concentration and separation of heavy minerals, zircon upgrading, and titanium minerals fractioning. The first step represents the major difference between these recovery processes and those used for processing traditional ores (e.g., mineral sands). Most of the valuable heavy minerals in centrifuge tailings are found in size fractions between 44 and 105 μm; therefore, some operations to reduce fines and coarse particles are usually included to concentrate heavy minerals. After concentration, titanium minerals and zircon can be separated from low-value minerals and gangue by taking advantage of differences in physical properties, e.g., specific gravity, electrostatic conductivity, magnetic susceptibility, and water affinity. After separation, the zircon grade is upgraded using magnetic separators and wet shaking tables, while different fractions of titanium minerals are obtained with high-tension and magnetic separators. Table 6-2 presents a summary of processes for heavy minerals recovery from FTT.

Table 6-2. Summary of processes for heavy minerals recovery from oil sands FFT

Process route	Mineral/oxide recovery	Metal/oxide grade of final products	Reference
Deoiling: solvent washing **Concentration:** water washing and settling + roasting			Baillie et al. (1976)
Deoiling: burning off **Concentration:** hydrocyclone + 3-spiral circuit **Separation:** two-stage high tension **Zr upgrading:** gravity circuit + high intensity magnetic and high-tension separators **Ti fractioning:** high-intensity magnetic separation		**Zircon:** 66.52 wt.% ZrO_2	Trevoy et al. (1978)
	Titanium minerals: 72-75%	**Ilmenite:** 28-30% TiO_2 **Leucoxene:** 30-38% TiO_2 **Rutile:** 45% TiO_2	
1st stage concentration: flotation **Deoiling:** burning off **2nd stage concentration:** water washing and settling + centrifugation		**Ilmenite:** 32-40 wt.% Ti **Rutile:** 38 wt.% Ti	Ityokumbul et al. (1987)
		Zircon: 29 wt.% Zr	
		Rare earth minerals: 6 wt.%	

Process route	Mineral/oxide recovery	Metal/oxide grade of final products	Reference
Separation: low intensity magnetic separation **Upgrading and fractioning:** high-intensity magnetic separation			
1st stage concentration: cyclones + flotation **Deoiling:** roasting **2nd stage concentration:** attritioning + vibrating screen + classify cyclones **Separation:** low intensity magnetic separation + spiral classifier **Zr upgrading:** high intensity magnetic separation **Ti fractioning:** high intensity magnetic separation + reverse flotation	Ilmenite: 10.5% Leucoxene: 16.8% Rutile: 5.7% Zircon: 8.6%	**Ilmenite:** 20 wt.% Ti* **Leucoxene:** 26.8 wt.% Ti* **Rutile:** 42.1 wt.% Ti* **Zircon:** 42.1 wt.% Zr*	H.A. Simons Ltd. (1996), Owen and Tipman (1999)

Process route	Mineral/oxide recovery	Metal/oxide grade of final products	Reference
1st stage concentration: agglomeration flotation **Deoiling:** calcination **Separation:** zircon flotation + titanium flotation **Zr upgrading:** gravity separation + high-gradient magnetic separation **Ti fractioning:** magnetic separation + reverse flotation	Zircon: 96%	**Rutile:** 87-89 wt.% TiO_2 **Zircon:** 65.1% wt.% ZrO_2	Bulatovic (2000); Chachula and Liu (2003)
Deoiling: gravity separation with pH control + attritioning + drying **Concentration:** wet spiral concentration **Separation:** multi-stage high-tension roll **Zr upgrading and Ti fractioning:** plate electrostatic separators + magnetic separators			Reeves (2008)
1st stage concentration: desliming by enhanced gravity separators **Deoiling:** attritioning		Concentrate: 68-70% TiO_2	Erasmus et al. (2010)

Process route	**Mineral/oxide recovery**	**Metal/oxide grade of final products**	**Reference**
2nd stage concentration: flotation + solvent washing + baking			
Concentration: enhanced gravity separation + two-stage flotation **Deoiling:** solvent extraction (attritionig + settling) + enhanced gravity separation **Separation:** Zr flotation **Zr upgrading:** gravity separation + high-tension separation + shaker tables	71.4% ZrO_2	**Concentrate:** 66.01% ZrO_2	Moran and Chachula (2014); Moran and Doiron (2015)

The main difference between the proposed recovery processes listed in Table 6-2 is the means for FTT deoiling. Earlier studies considered deoiling by burning off the residual bitumen from FTT, whether as received (Baillie et al. 1976; Trevoy et al. 1978) or after a first stage of concentration (H.A. Simons Ltd. 1996; Owen and Tipman 1999; Bulatovic 2000; Oxenford et al. 2001; Chachula and Liu 2003). The drawbacks of this deoiling method are twofold. First, the physical characteristics of the heavy minerals (e.g., magnetic susceptibility) may be altered during roasting, affecting the downstream separation processes and altering the grade of the concentrate (Ciu et al. 2013). Second, emissions are generated. Burning the residual bitumen produces greenhouse gases (GHGs), and the thermal decomposition of secondary minerals such as pyrite would generate SO_2 emissions. In a second generation of processes, a combination of gravity separation and solvent extraction (attritioning and settling) is implemented for deoiling (Reeves 2008; Erasmus et al. 2010; Moran and Chachula 2014). This deoiling method does not present the inconveniences of tailing roasting, but it does increase the complexity of the process because of the solvent handling.

Recently, the company Ucore Rare Metals Inc. partnered with a major Alberta oil sands operator to implement a proprietary process for the recovery of heavy minerals and rare earth elements (REE) from oil sands. More specifically, the process, based on molecular recognition technology (MRT), comprises the separation of metals and rare earth elements from a concentrate that any of the processes previously discussed can generate. The concentrate is subjected to a leaching operation to obtain a pregnant leach solution (PLS) that thereafter flows through a column filled with customized molecules (ligands) that attract specific elements. A weak acidic solution is then used to elute pure REE from the ligands in the column and finally precipitate it as high purity REE carbonate. Ucore has proved the concept in a pilot plant to process rare earth elements concentrates from mining operations in Southeast Alaska and expects to scale to a commercial system capable of accepting PLS from diverse feedstock sources, including heavy mineral concentrates from oil sands tailings. In 2017 Ucore announced that a suitable PLS from an oil sands concentrate was produced and initiated further separation testing via MRT (Ucore Rare Metals Inc. 2017).

Despite the number of recovery processes proposed in the literature, only a few studies deal with scaling-up laboratory results to commercial operation and report estimated costs of heavy minerals recovery from FTT.

Ityokumbul et al. (1987) estimated the annual recovery potential from tailings of a bitumen extraction plant producing 130,000 bbl/d (20,600 m^3/d), in 227,000 tonnes combined of rutile, TiO_2 slag, monazite, zircon, and iron oxide. According to Schutte (cited by Ityokumbul et al. (1987)), the capital cost of a recovery plant with recovery efficiencies of 70%, 80%, and 33% of Ti, Zr, and Fe minerals, respectively, would be around $20 million (1987 USD). The cost of recovering those minerals was estimated to be $35.24/t (1987 USD). However, the breakdown of this recovery cost was not reported.

Alberta’s 1996 Mineral Development Agreement (MDA) final report includes details, drawings, and flowsheets of a plant sized to recover heavy minerals from 2.6 M t/y of centrifuge tailings of Suncor and Syncrude 1994 operations (60 M and 120 M t/y of oil sands, respectively) (H.A. Simons Ltd. 1996). The proposed plant would produce 357,000 t/y combined of rutile, leucoxene, ilmenite, zircon, and rare earth elements. The capital cost was estimated at about $50 million (1996 USD), and the operating cost to produce titanium concentrate was estimated at $39.03/t (1996 USD). Besides producing concentrates, the report also considered the obtention of high-value products like synthetic rutile and pigments. These scenarios are summarized in Table 6-3.

Table 6-3. Capital and operating costs of titanium recovery from Athabasca oil sands for a plant capacity of 19.8 M tonnes FTT per year (H.A. Simons Ltd. 1996)

Scenario	Capital cost[a]	Operating cost[a]
TiO_2 concentrate	\$50 million	\$39.03/t of concentrate
Synthetic rutile	\$151.2 million	\$236/t of synthetic rutile
Pigment production	\$350 million	\$1,063/t of pigment

a. In 1996 USD.

To date, there are no commercial plants for heavy minerals recovery operating in Alberta. However, CVW Cleantech (formerly Titanium Corporation Ltd.) has developed a commercial-ready technology for the recovery of bitumen, solvent, water, titanium, zirconium, and REE from oil sands FTT and is planning to operate a concentrator plant and a mineral separation plant on the Horizon site operated by Canadian Natural Resources Ltd. The front-edge engineering design was completed in February 2019 and the commissioning and start-up was programmed by the first quarter of 2023 (Titanium Corporation Ltd. 2019). To the best of the author’s knowledge, the estimated recovery cost of this plant is not in the public domain; however, revenues of about \$100 million per year at each site are expected from the recovered minerals (Moran et al. 2016). Also, 6,000 bbl (950 m^3) of bitumen could be recovered per day at individual sites, at an operating cost well below \$10/bbl (Moran et al. 2016).

There is insufficient research on the cost of recovering heavy minerals from FTT to determine its feasibility. The few studies that conduct economic assessments use outdated costs and refer to processes using roasting or calcination of tailings for deoiling. This deoiling route is unlikely to be used at a commercial scale given the global efforts to reduce GHG emissions. To bridge the research gaps, the recovery of titanium minerals and zircon was investigated from FTT from a techno-economic perspective. The considered recovery process uses solvent extraction for deoiling. A data-intensive process model was developed that included mineral recovery and effluent treatment for the recovery of bitumen and solvent. The specific objectives of this research are to:

- Develop a techno-economic model to estimate the internal rate of return of recovering heavy minerals from froth treatment tailings;
- Evaluate the influence of plant capacity on the feasibility of the process;
- Conduct sensitivity and uncertainty analyses to assess whether input variations have an effect on the feasibility of the process;
- Study the effect of performing two separate phases (heavy minerals concentration and heavy mineral separation) on the economy of the whole process.

6.2 Methods

6.2.1 Feedstock description

The feedstock for the heavy mineral recovery process is FTT from extraction plants using a naphthenic froth treatment. In this study, a typical composition of centrifuge tailings (shown in Table 6-4) was used as a reference, as well as the chemical assay (Table 6-5), and the mineral quantity (Table 6-4) of centrifuge tailings generated in Suncor's bitumen extraction plant.

Table 6-4. Composition (wt.%) of the FTT considered as feedstock for this analysis (Moran and Chachula 2014)

Composition of FTT	wt.%
Water	80.9
Bitumen	2.00
Diluent	0.10
Solids	17.0

Table 6-5. Chemical assay (wt.%) of the FTT considered as feedstock for this analysis (H.A. Simons Ltd. 1996)

Element	Ti	Zr	Si	Fe	Al	Mg	K	Na
wt.%	5.51	1.34	34.02	4.20	1.01	0.15	0.29	0.07

Note: the weight percentage of each of the remaining elements is below 0.01 wt.%.

Table 6-6. Mineral quantities (wt.%) in the FTT considered as feedstock for this analysis (H.A. Simons Ltd. 1996)

Mineral	Rutile	Ilmenite	Leucoxene	Zircon	Monazite	Pyrite	Magnetite	Silicates
wt.%	5.57	0.09	11.09	2.58	0.30	1.46	0.22	78.6

Although the composition and mineral assemblage of FTT may vary with time and location, such variations should not be large, as shown by Owen and Tipman (Owen and Tipman 1999) and Oxenford et al. (Oxenford et al. 2001). The use of similar bitumen extraction processes by different oil sands operators and the consistent concentration of heavy minerals over most of the McMurray Formation in Athabasca (McCosh 1996) explain this comparable concentration of minerals in FTT.

6.2.2 Process description

The recovery process considered in this study is based on a series of patents (Reeves 2008; Erasmus et al. 2010; Moran and Chachula 2014; Moran and Doiron 2015). This reference process was selected because FTT deoiling is performed by solvent extraction rather than by burning. The process can be divided into two phases: concentration of heavy minerals (Figure 6-3) and separation of minerals into zircon and titanium fractions (Figure 6-4). Both phases are explained below.

The concentration of heavy minerals starts with the desliming of the as-received FTT. A hydrocyclone is used to separate the feed into a coarse mineral fraction and a fine mineral fraction. Most of the heavy minerals in the feed report to the coarse mineral fraction, while most of the particles that are smaller than 44 μm are concentrated in the fine mineral fraction (Moran and Chachula 2014). In addition, more than 90% of the water and free bitumen in FTT goes to the hydrocyclone tailings, which contain the fine mineral fraction (Moran and Chachula 2014). Such tailings could be treated for bitumen recovery. Moran et al. (2013) present a process to produce diluted bitumen from the hydrocyclone tailings. In this study, it was assumed that the hydrocyclone tailings are disposed of in tailings ponds as generated.

The coarse mineral fraction is subjected to froth flotation to concentrate the heavy minerals by discarding quartz and other minerals in the feed. A rougher stage followed by a scavenger stage were considered in this reference process. The heavy minerals concentrate (HMC) contains almost all the bitumen in the coarse mineral fraction. Bitumen may affect the subsequent operations that separate heavy minerals; therefore, the HMC is subjected to solvent extraction to reduce the content of bitumen in the concentrate. The HMC is mixed with naphtha in an attritioning cell to promote the liberation of bitumen from the heavy minerals. Heavy minerals are separated by gravity settling. Three solvent extraction stages were considered in the reference process as suggested by Moran and Chachula (2014). Naphtha is added to the third stage, and the overflow of the second and third stages are recycled back to the previous stages. The overflow of the first stage is fed into a diluent recovery unit to separate diluted bitumen and recover naphtha, through distillation. The underflow of the third stage is a slurry containing the heavy mineral concentrate and residual naphtha used in the solvent extraction operation. The slurry is dewatered in a hydrocyclone to obtain a debituminized HMC. The overflow of the hydrocyclone is sent to naphtha recovery in a DRU (Kan 2011).

In the second phase of the process, the debituminized HMC is subjected to froth flotation to concentrate zircon by rejecting coarse silicates and iron-bearing minerals. The flotation of ilmenite and leucoxene present in the HMC is suppressed by the addition of unmodified wheat starch. Sodium fluorosilicate, Flotigam, and C-007, are used as activator, collector, and frothing agent, respectively (Moran and Doiron 2015). The tails of this operation are dewatered and dried prior to the recovery of ilmenite and leucoxene using high tension rolls, plate electrostatic separators, and induced roll magnetic separators (Reeves 2008). The zircon-enriched slurry is fed into spiral separators to reject aluminosilicates (primary gravity separation), and then it is dewatered, dried, and subjected to primary electrostatic separation to remove residual ilmenite and leucoxene and to primary magnetic separation to discard iron-bearing magnetic minerals (Moran and Doiron 2015). High tension rolls and rare earth magnet rolls are used in these operations. The zircon concentrate is upgraded through a series of finishing gravity (shaking tables), electrostatic (high tension rolls), and magnetic (induced magnetic rolls) separations (Moran and Doiron 2015). Additional aluminosilicates and titanium bearing-minerals, likely rutile, are rejected in those operations. Rutile is recovered from the tails using plate electrostatic separators (Reeves 2008). Moran and Chachula (2014) show that the grade of the zircon concentrate is about 66% ZrO_2, with concentrations of TiO_2, Al_2O_3, and Fe_2O_3 lower than 0.3 wt.%, 0.2 wt.%, and 0.1 wt.%, respectively, while the MDA study estimated a grade of 60% ZrO_2 in the zircon concentrate (H.A. Simons Ltd. 1996). Zircon is relatively pure in oil sands but titanium minerals present extraneous elements (Kaminsly et al. 2008), therefore a high-purity rutile concentrate is not expected using this process. As a reference, the maximum grade of rutile obtained in the MDA study was 87.1 wt.% TiO_2. Ilmenite grade was 52.4 wt.%, and leucoxene's was 66.1 wt.% (H.A. Simons Ltd. 1996). The titanium dioxide content in the concentrates is too low to feed the sulphate or chloride processes for pigment production but these concentrates can be further upgraded to synthetic rutile (H.A. Simons Ltd. 1996).

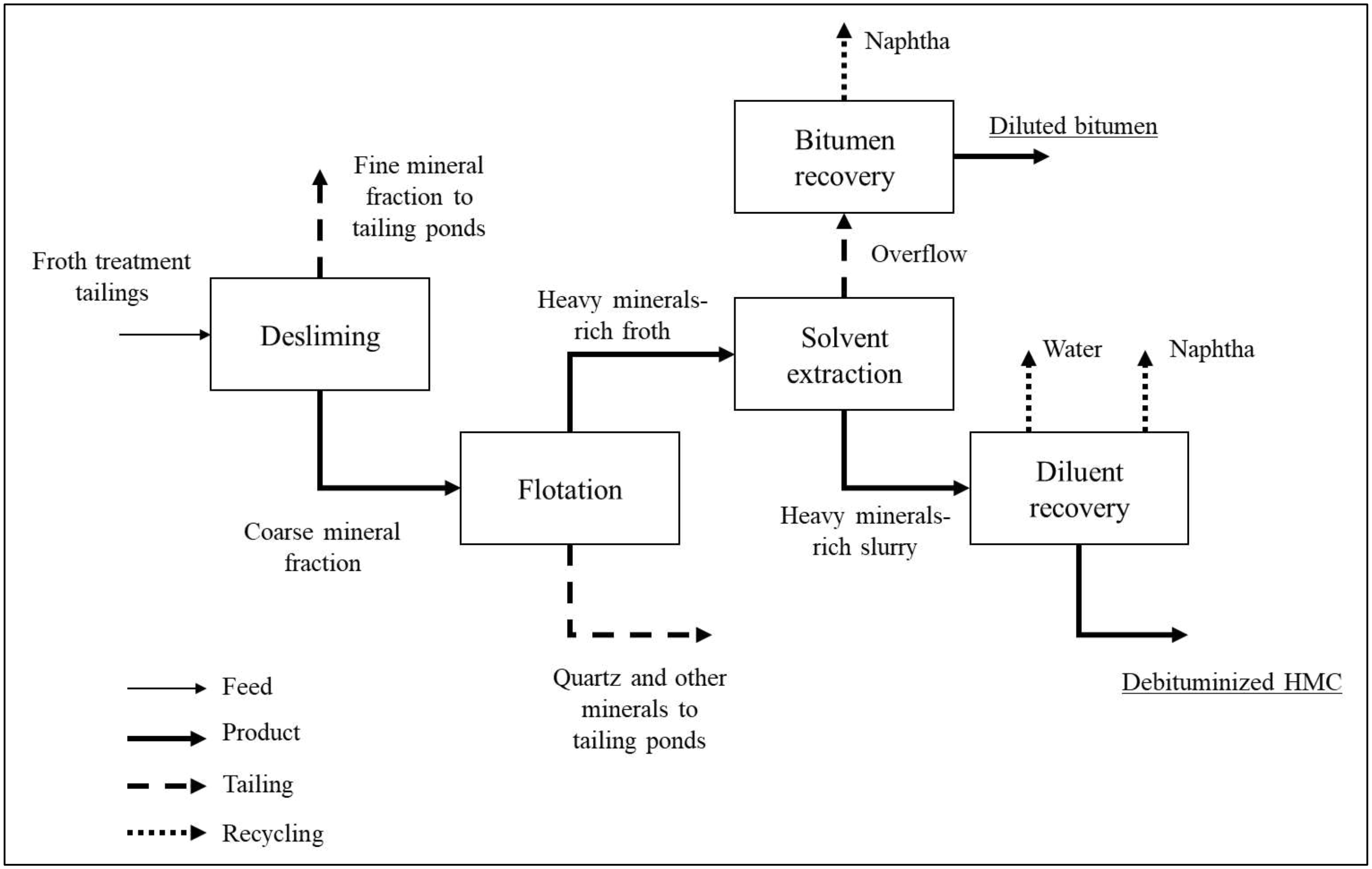

Figure 6-3. Schematic of the heavy mineral concentration phase

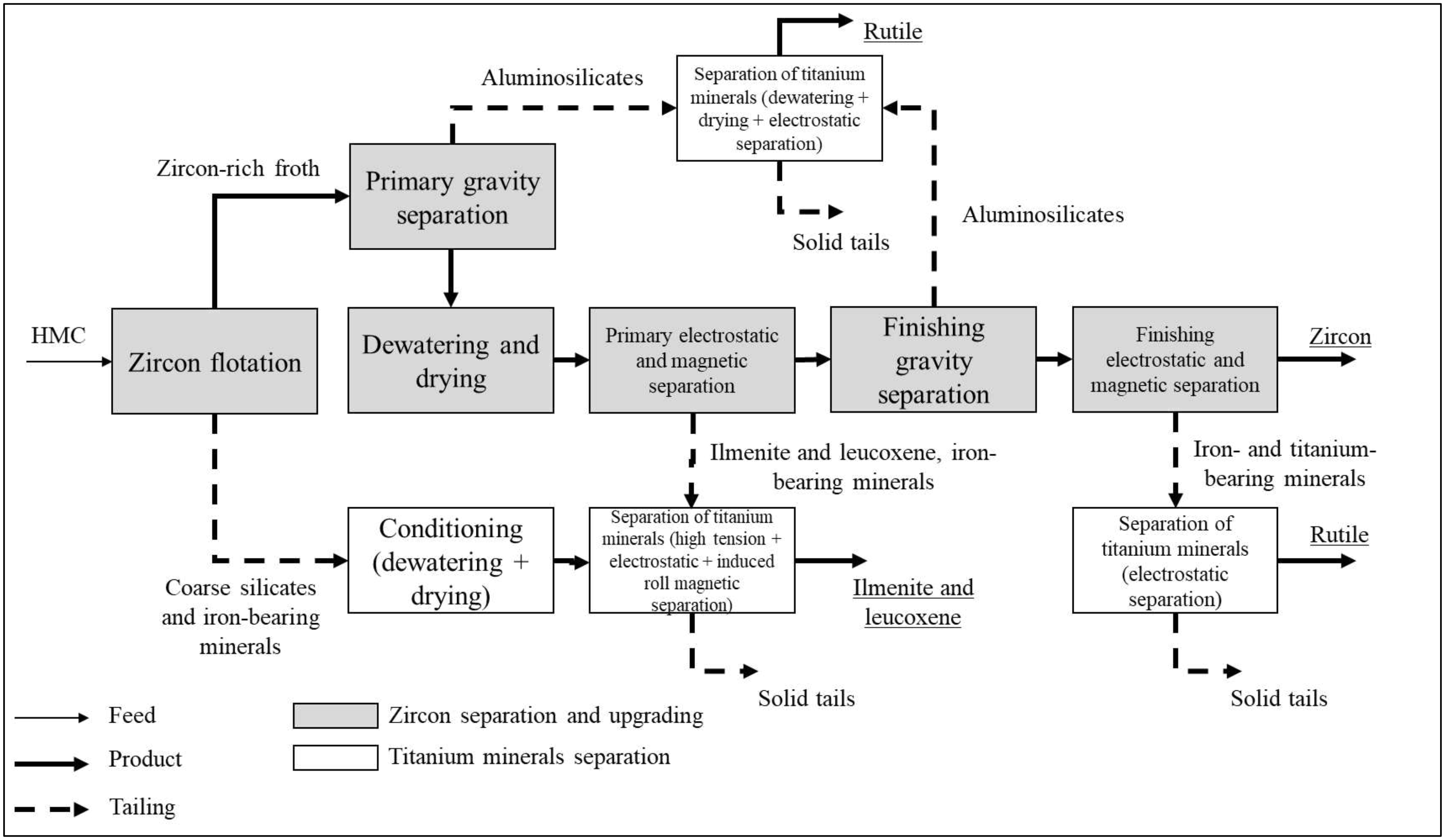

Figure 6-4. Schematic of the heavy mineral separation phase

The co-products of the entire process are a zircon concentrate, a rutile concentrate, an ilmenite-leucoxene concentrate, and diluted bitumen. The wastes are three solid streams (from the separation of titanium minerals), the desliming hydrocyclone tailings, and the flotation tailings.

6.2.3 Base case and scenarios

Two scenarios based on the plant configuration were considered in this study. In the first scenario, the whole process is performed next to the bitumen extraction plant where FTT are generated. In the second scenario, the heavy mineral concentrate is produced next to the bitumen extraction plant in a heavy mineral concentration plant (HMCP) and sent to a heavy mineral separation plant (HMSP) at a different location. Both scenarios are depicted in Figure 6-5. As mentioned above, Suncor's bitumen extraction plant was considered as a reference (15.5 million tonnes FTT per year, see Table 6-1) and designed a plant to process 100% of the generated FTT as the base case for both scenarios. However, by varying the feed rate we considered the effect of scale on the economics of the process. Also, scenario 2 can be used to approximate the operation of a centralized HMSP fed by multiple HMCPs, considering that the FTT composition is similar among the bitumen extraction plants operating in Alberta. Using separate plants offers the following advantages over a single plant:

- Each phase can be performed by expert parties on the required unit operations.
- The complexity of the operations at the bitumen extraction site is reduced.
- An HMSP with a higher capacity than a single plant could take advantage of economies of the scale. This scenario is possible if multiple HMCPs feed the HMSP.

6.2.4 Process modeling and equipment sizing

Material and energy balances were performed for each unit operation in the process using a spreadsheet-based model. Input and output data provided by Moran and Chachula (2014) and Moran and Doiron (2015) were used to complete the material balances. The consumables rates were estimated using typical values in mineral processing (Michaud 2016; Camachen N.d.), when needed. The main equipment was sized using correlations from the literature on process design (Peters et al. 2003; Ulrich and Vasudevan 2004; Towler and Sinnot 2013), and the number of units required was calculated based on the capacity of the commercial equipment. Process temperatures were used to estimate the heat consumption. Electricity consumption was calculated using the rated power of the equipment or correlations found in the literature. Process conditions and the main assumptions for the process model, as well as a list of main equipment and sizing approach, are presented in the Appendix C (Table C-1 and Table C-2, respectively).

6.2.5 Techno-economic assessment model

In scenario 1, the discounted cash flow (DCF) method was used to estimate the internal rate of return (IRR) of the entire process for a given set of co-products' selling prices. The calculated IRR can be compared with a reference hurdle rate to determine the profitability of producing heavy minerals from FTT. In scenario 2, separate plants were considered, i.e., one or more HMCPs and one HMSP. First, the DCF method was used to determine the production cost of HMC, including transportation to the HMSP, to obtain a certain return. In this way, the operator of the HMCP can estimate the minimum selling price of the HMC to break even. Then, the IRR for the HMSP was determined following the approach used for scenario 1, considering the calculated production cost as the feedstock cost. This metric enables decision-making on the feasibility of the plant and potential negotiation of the HMC price.

Appendix A presents an overview of the DCF method and how to determine both the IRR and the HMC production cost.

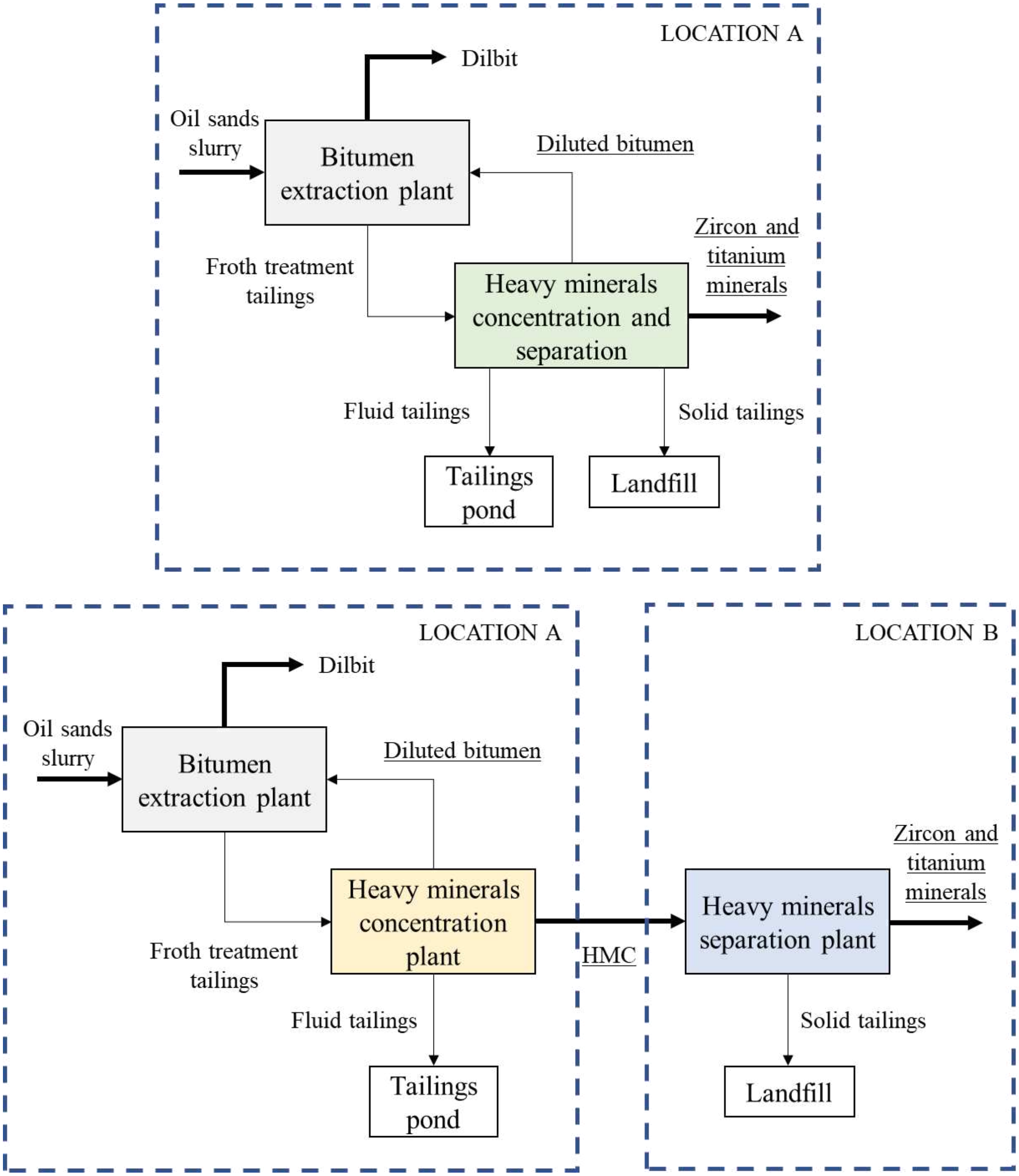

Figure 6-5. Illustration of plant configuration scenarios. Top: scenario 1; Bottom: scenario 2

For both scenarios, the material, energy, and equipment inventories resulting from the process model were used to calculate capital and operating costs, and revenues for selling zircon, titanium minerals, and recovered bitumen from the tailings. With this information, future cash flows were calculated and discounted at a rate such that the net present value (NPV) was equal to zero. General assumptions for the techno-economic assessment of the process are listed in Table 6-7.

Table 6-7. General assumptions for the discounted cash flow analysis

Item	Value	Comments
Plant lifetime	20 years	
On-stream factor	0.80	
Operating cost escalation	2%	
Zircon price	\$1,362/t	The 2018-2022 average price is about \$1,498/t for a 66% ZrO_2 grade concentrate (Zircomet 2023). A conservative grade of 60% ZrO_2 was assumed, and the price was scaled down.
Rutile price (as slag equivalent)	\$738/t	Sold as slag equivalent as suggested in the MDA study (H.A. Simons Ltd. 1996). The 2017-2020

Item	Value	Comments
		average price of titanium slag was used (U.S. Geological Survey 2022).
Ilmenite and leucoxene price	\$198/t	Sold as ilmenite. The 2017-2020 average price was used (U.S. Geological Survey 2022).
Diluted bitumen	\$60/bbl	The current dilbit price (Oil Sands Magazine 2024) was used.
IRR for HMCP in scenario 2	15%	
HMC transport cost in scenario 2	\$0.0018/t-km	Data from Marufuzzaman et al. (2015) and assuming a slurry density of 2,500 kg/m^3 calculated from model result.
HMC transport distance in scenario 2	30 km	Assumed, based on the location of bitumen extraction plants in Alberta.

Table 6-8 presents the assumptions to calculate the capital cost. The inside battery limit (ISBL) investment was calculated as the installed cost of main equipment. Published cost curves were used to obtain the purchased cost of common equipment, like hydrocyclones, vessels, agitators, distillation columns, filters, pumps, gravity settlers, thickeners, spiral separators, shaker tables, flotation cells and centrifuge decanters. The cost of specialized equipment, like electrostatic and magnetic separators, was provided by manufacturers. The equipment costs are based on a Chemical Engineering Plant Cost Index (CEPCI) of 776.9 or on a Marshal and Swift (M&S) Cost Index of 1,657, in 2021 USD, and were adjusted for the location of Fort McMurray, Alberta, Canada. The equipment delivery cost was estimated to be 10% of the purchased equipment cost. Installation and insulation, instrumentation, piping, electrical, and building costs were calculated as a fraction of the delivered equipment cost (Peters et al. 2003). The outside battery limit (OSBL) investment includes the cost of ancillary equipment and auxiliary facilities, and yard improvement. For a process with high solid handling, the OSBL investment is comparable to the ISBL investment (Towler and Sinnot 2013). Engineering, contingency, and working capital were estimated as factors of the sum of the ISBL and OSBL investments, while indirect construction costs and contractor's fees were calculated as a percentage of the total capital cost.

Table 6-10 presents the data and assumptions for the estimation of the operating cost. The feedstock, i.e., FTT, is assumed to be free of charge because it is considered a waste with no value and is owned by the bitumen extraction facility operator. For the consumable cost, bulk prices provided by vendors were used, and for the utility cost, the price of natural gas and electricity for industrial customers in Alberta was considered. Labor cost was calculated based on the number of operators, required shifts, and labor rate. The remaining cost components were estimated through factors given in published sources.

Table 6-8. Assumptions for the estimation of capital cost

Item	Value	Comments/remarks
CEPCI	776.9	Used for hydrocyclones, attritioning and flotation cells, filters, dryers, and columns
M&S	1,657	Used for spiral concentrators, shake tables, and electrostatic and magnetic separation equipment
Location factor	1.43[a]	For Fort McMurray, Alberta
Purchased-equipment cost	Depends on the equipment	From cost curves and manufacturers
Purchased-equipment delivery cost	10% purchased-equipment cost	For predesign estimate (Peters et al. 2003)
Purchased-equipment installation cost	67% delivered purchased-equipment cost	55% corresponds to installation and 9% to insulation (Peters et al. 2003)
Instrumentation	50% delivered purchased-equipment cost	(Peters et al. 2003)
Piping	80% delivered purchased-equipment cost	(Peters et al. 2003)

Item	Value	Comments/remarks
Electrical systems	30% delivered purchased-equipment cost	(Peters et al. 2003)
Building	47% delivered purchased-equipment cost	Assuming new plant in new site (Peters et al. 2003)
Inside battery limit investment (ISBL)	Installed purchased-equipment + Instrumentation + Piping +Electrical systems + Building	(Towler and Sinnot 2013)
Outside battery limit investment (OSBL)	100% ISBL	New site and high solid handling (Towler and Sinnot 2013)
Engineering	30% (ISBL + OSBL)	(Towler and Sinnot 2013)
Contingency	30% (ISBL + OSBL)	Typical value for uncertain technology (Towler and Sinnot 2013)
Indirect construction cost	10% total capital cost	(Peters et al. 2003)
Contractor’s fee	6% total capital cost	(Peters et al. 2003)
Working capital	15% (ISBL + OSBL)	Typical value for general plants (Towler and Sinnot 2013)

Item	Value	Comments/remarks
Total capital cost	ISBL + OSBL + engineering + contingency + indirect + construction + contractor's fee + working capital	

a. Based on the 2003 location factor (1.60) (Towler and Sinnot 2013) and exchange rate (1.40 CAD/USD) and updated with 2021 exchange rate (1.25 CAD/USD).

Table 6-9. Data for operating cost estimation

Category	Item	Cost	Comments
Feedstock	Froth treatment tailings	-	FTT are residue of bitumen extraction with no commercial application and no value.
Consumable	DSP 007	\$1,410/t	(Camachen N.d.)
	Flotigam	\$3,000/t	Provided by vendors
	Glycol-based frother	\$4,680/t	Provided by vendors
	Naphtha	\$113/m^3	(Government of Canada 2023a)
	Process water	\$0.53/t	(Peters et al. 2003)
	Sodium fluorosilicate	\$580/t	Provided by vendors
	Sulfuric acid	\$200/t	Provided by vendors
	Unmodified wheat starch	\$790/t	Provided by vendors
Utility	Electricity	\$0.042/kWh	(Canada Energy Regulator 2017)
	Natural gas	\$1.62/GJ	
Waste disposal	Disposal of solid waste	\$55/t	(Peters et al. 2003)

Labor	Labor	Based on salary, number of workers per shift per operation, three 8 h/shifts, 5 days/week, and 48 weeks/year.	(Ulrich and Vasudevan 2004; Chemistry Industry Association of Canada 2021)
Other costs	Maintenance	5% ISBL	(Towler and Sinnot 2013)
	Insurance	1% ISBL	
	Plant overhead	1% revenue (R&D) + 65% labor (G&A)	

6.2.6 Sensitivity and uncertainty analyses

In this study, the Regression, Uncertainty, and Sensitivity Tool (RUST) (Di Lullo et al. 2019) was used for sensitivity and uncertainty analysis. The Morris method was implemented to study the sensitivity of the model output, i.e., the IRR, on 54 inputs. The inputs considered were process conditions and yield, equipment performance, consumables rates and prices, energy consumption and price of electricity and natural gas, operational conditions, selling price of co-products, and economic assumptions (Table C-3 in the Appendix C). Ten approaches and four levels, for a total of 550 samples, were used in the study. The sensitivity analysis facilitates the identification of the inputs with greater influence on the model output and then to narrow the number of variables included in the Monte Carlo simulation to study the effect of the uncertainties on the estimated IRR. Appendix B shows an overview of both methods.

6.3 Results and discussion

6.3.1 Scenario 1: a single plant

The base case corresponds to a plant processing 15.5 million tonnes of FTT per year. Both phases, heavy mineral concentration and separation, are performed next to the bitumen extraction plant where FTT are generated. Considering an on-stream factor of 0.80, the required processing capacity is 2,205 t/h. It was estimated that 87% of the heavy minerals in feed were recovered, specifically 97% of the zircon and 85% of the titanium minerals. In addition, 9% of the bitumen in FTT can be recovered as diluted bitumen. Table 6-10 shows the results of the developed model that were used for the techno-economic analysis of the base case.

Table 6-10. Summary of the material and energy inventories for the base case obtained from the developed model

Category	Item	Value
Feedstock	Froth treatment tailings	15.5 M t/y
Co-products	Zircon concentrate	34.0 k t/y
	Rutile concentrate	25.5 k t/y
	Leucoxene-ilmenite concentrate	97.2 k t/y
	Diluted bitumen	259 k bbl/y
Wastes	Liquid tailings	13.9 M m^3/y
	Gauge	345 k t/y
Energy consumption	Electricity	35,053 MWh/y
	Natural gas	1.39 M GJ/y

The results of the techno-economic analysis for scenario 1 are presented in Table 6-11. The capital cost is estimated at \$419.1 M. The breakdown of the capital cost into cost components is shown in Figure 6-6. The required ISBL investment is \$100.6 M, distributed among the different operations, as shown in Figure 6-7. Solvent extraction demands 10.3% of the ISBL investment because of the large size of the attrition cells and agitators, and the settling tanks used in that operation. Cells of about 35.5 m^3 and settling tanks of about 25 m^3 are needed for each of the three solvent extraction stages used in the process. Primary gravity separation and the separation of titanium minerals from gravity separation tails contribute 11.1% and 13.9% to the ISBL investment, respectively. The former requires 553 spiral concentrators to handle the flow of the zircon flotation overflow, while the latter includes filtration and drying of the tails and electrostatic separation of titanium minerals. Tailing desliming requires 12.2% of the ISBL, including four 2.96 m-diameter hydrocyclones, and intake, underflow, and overflow pipes with diameters of 0.457 m, 0.203 m, and 0.406 m, respectively.

Table 6-11. Summary of the techno-economic assessment of scenario 1, base case

Item	Value
Capital cost	\$419.1 M
Operating cost at year one	\$44.6 M/y
Revenue	\$99.9 M/y
IRR	9.8%

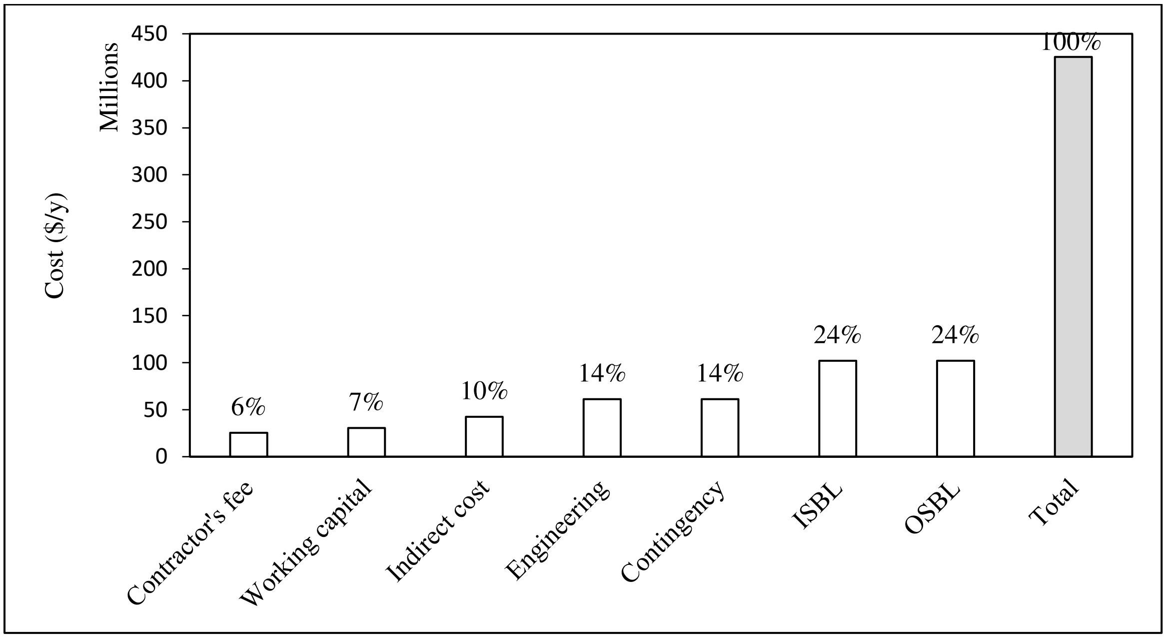

Figure 6-6. Capital cost breakdown. Scenario 1, base case

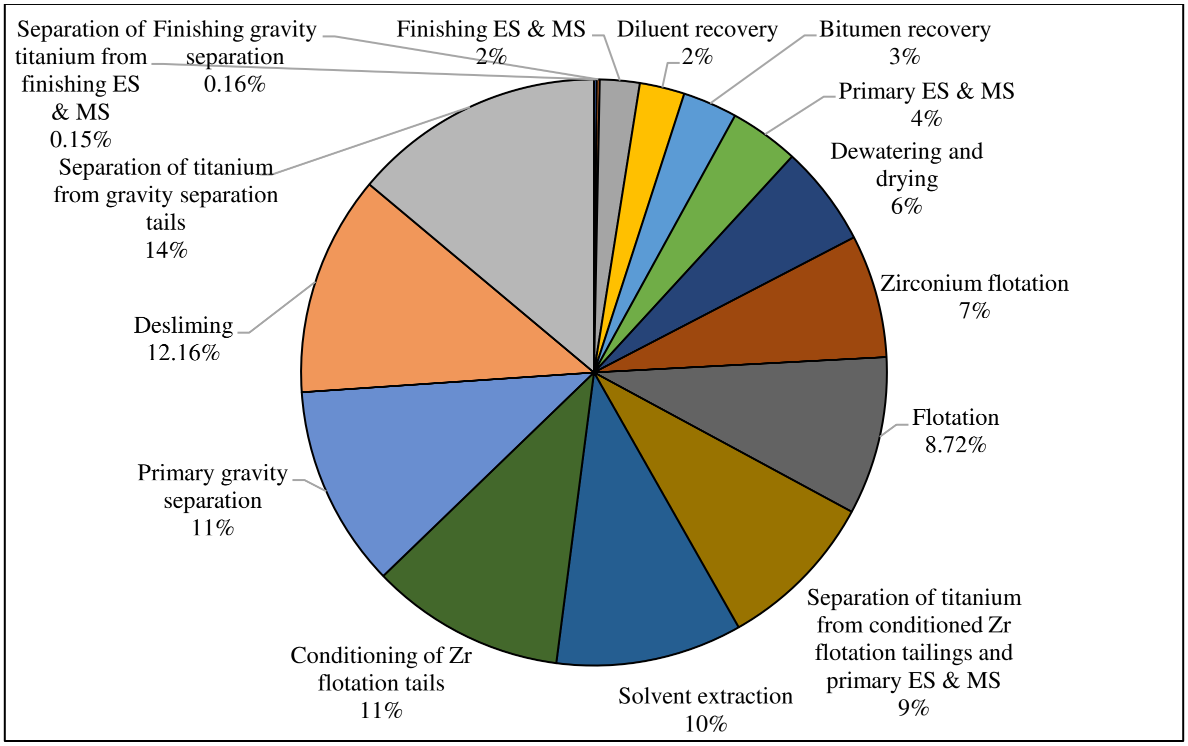

Figure 6-7. ISBL investment per unit operation. Scenario 1, base case

The operating cost at year one is estimated to be $44.6 M, distributed as shown in Figure 6-8. The disposal of the solid residue from the heavy mineral separation operations represents 42.6% of the operating cost. This residue contains mainly aluminosilicates and other minerals like garnet and tourmaline. Recovering additional materials from the solid waste would not only represent an additional revenue stream but reduce the amount of waste to be disposed of, increasing the profitability of the overall process. Consumables is the second greatest contributor to the operating cost at 13.6% of the total. Although naphtha is partially recovered from the overflow and underflow of solvent extraction, this material represents 46.7% of the cost of consumables. Glycol-based frother (16.0%), unmodified wheat starch (15.3%), and the collector used in the zircon flotation operation (14.5%) are other consumables with an important share in the consumables cost. The process is labor-intensive, requiring about 18 operators per shift. About 67% of the operators are dedicated to primary gravity separation, as well as magnetic and electrostatic separation, 11% to flotation and solvent extraction, and the balance to the remaining operations and ancillary equipment. Utilities contribute 8.2% to the operating cost. Of this, 61.7% corresponds to natural gas and the balance to electricity. The drying of concentrates prior to magnetic and electrostatic separation, heating water up to the required temperature in flotation operations, and the separation of bitumen from diluent are the greatest natural consumers. Regarding electricity, agitators in attrition cells and disk filters consume the most.

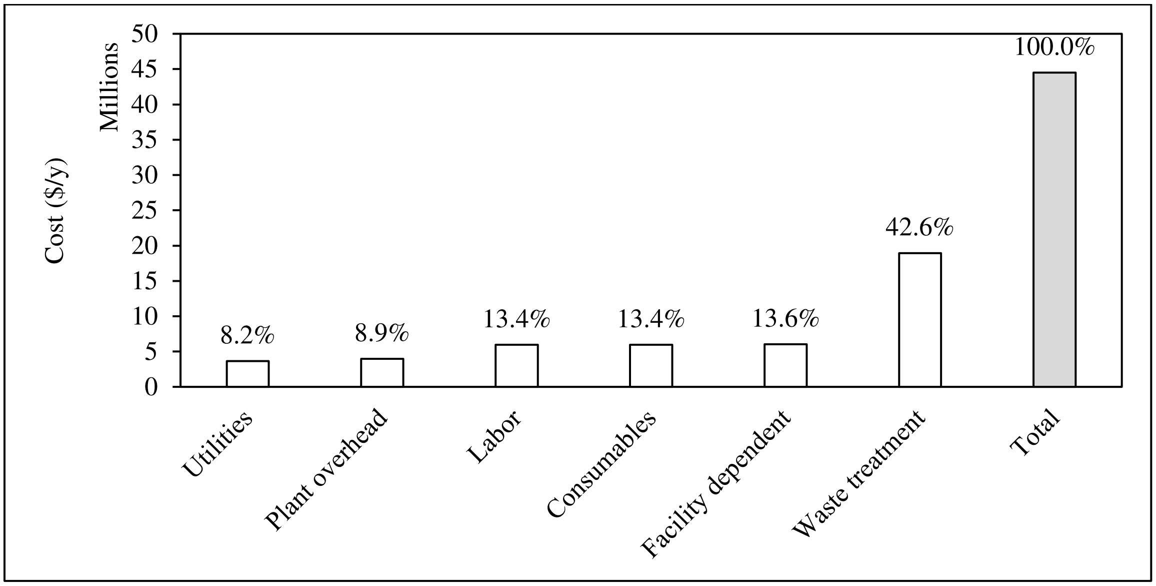

Figure 6-8. Breakdown of operating cost. Scenario 1, base case

The revenue from selling the co-products of the process increases to $99.9 M per year. About 46.4% of the revenue comes from zircon, currently the most valuable of the recovered heavy minerals. Rutile and the leucoxene-ilmenite concentrate contribute about 18.8% and 19.3% to the revenue, respectively. The amount of recovered leucoxene-ilmenite is around 4 times the amount of recovered rutile; however, the latter is more valuable, hence the similar share. Diluted bitumen makes up the balance of the revenue.

As shown in Table 6-11, the IRR of the project was estimated to be 9.8%. The project would be attractive depending on the hurdle rate of the company running the process. To the best of the author's knowledge, there are no techno-economic assessments in the public domain that estimate the IRR of recovering heavy minerals from FTT. Thus, as a reference for the reader, the IRR from traditional sources of zircon and titanium are provided, as well as for the recovery of different minerals from mining tailings. The IRR of mineral sands mining projects in Australia is between 23% and 30% for annual zircon and titanium mineral production similar to or slightly higher than the production of these minerals in the base case in scenario 1 (Australian Trade and Investment Commission 2022). For underground mining, the IRR reported by one company was around 23% (Iluka 2023). The return of rare earth elements recovery from copper mine tailings in Chile was estimated to be 10% while the recovery of vanadium pentoxide produces a return of 21% (Araya et al. 2020). Regardless of the IRR of the project, recovering heavy minerals from FTT represents a great opportunity for Alberta and the oil sands industry. It not only creates value from waste and a revenue stream other than fuel-related products but also could position Alberta as a key player in the energy transition to a low-carbon economy. Zirconium is currently used for nuclear fuel cladding, but it is expected that the manufacturing of electrolyzes used to produce hydrogen will drive the demand for zirconium for energy production (International Energy Agency 2021b). Simultaneously, geothermal energy is likely to become the primary consumer of titanium among the existing and emerging low-carbon energy technologies (International Energy Agency 2021b). While the demand for zirconium and titanium in energy systems is relatively low compared to traditional applications (e.g., steel production and the chemical industry) (Hund et al. 2023), future technological changes combined with disruptions in the already constrained supply chain could hamper the deployment of such systems. In this context, Alberta's oil sands have the potential to diversify the supply of zircon and titanium minerals, currently dominated by a handful of countries (U.S. Geological Survey 2022), reducing the risk of future shortage through a profitable process, as demonstrated in this study.

Figure 6-9 shows the results of the sensitivity analysis of scenario 1. The Morris mean indicates the average change in the IRR as the input moves from its minimum to maximum value. The Morris standard deviation is a measure of the non-linearity of the IRR with respect to the input. The results are normalized to the average output value of all the samples. The output is more sensitive to the inputs located on the far right, while the effect of the inputs located near to the origin is negligible. Nine out of fifty-four inputs considered in the analysis exhibit a Morris mean greater than 10%. Of those, the IRR is most sensitive to the zircon selling price. Zircon has the highest revenue stream of the process; thus, this result was expected. The nominal capacity of the spiral separators also has a great impact on the IRR, not only because it modifies the ISBL investment but because the labor requirement is also affected. This interaction may be the reason for the relatively high Morris standard deviation of this input. The IRR is also sensitive to the waste disposal cost (the greater contributor to the operating cost), the factor used to estimate the OSBL investment (it directly impacts the capital cost), the on-stream factor (it affects the annual production of heavy minerals), the bitumen selling price, and the annual labor rate (the process is labor-intensive). The IRR is moderately sensitive to the selling price of the other co-products. The analysis shows that the IRR is most sensitive to economic parameters rather than process conditions. A heavy mineral concentration and separation plant could be a risky venture given the high volatility of the zircon price. A prospective market study is needed to determine the profitability of the project.

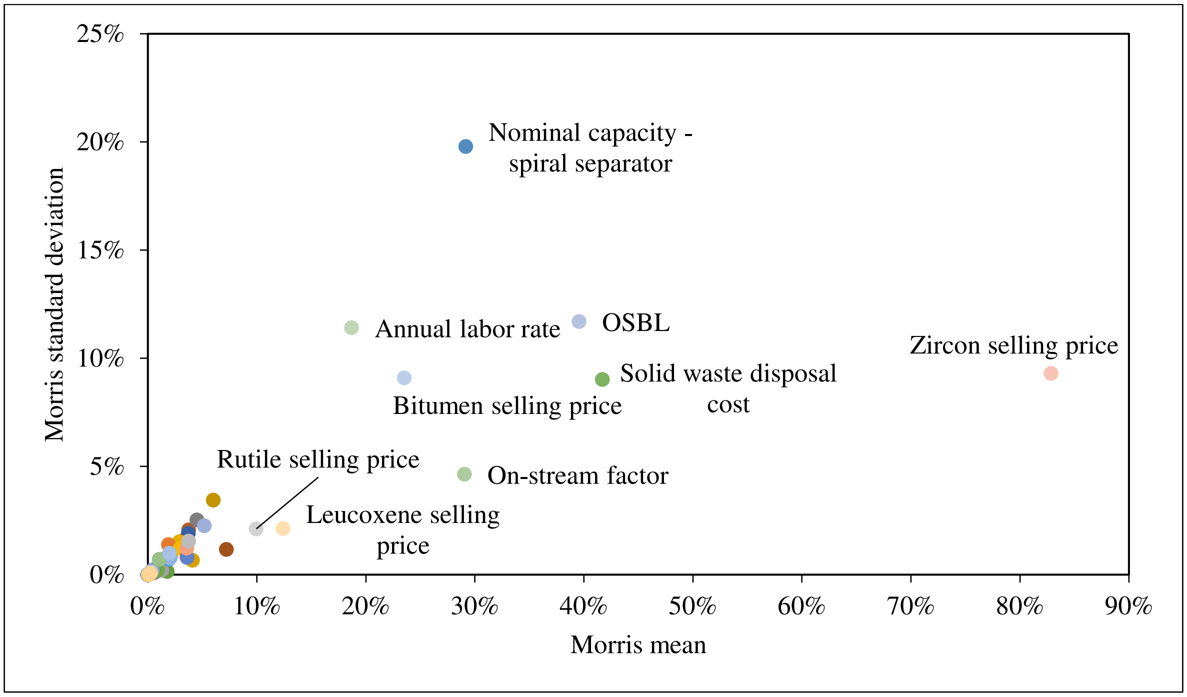

Figure 6-9. Results of the sensitivity analysis – scenario 1

The nine inputs identified as sensitive were considered for the uncertainty analysis. The mean value of the IRR obtained from the Monte Carlo simulation was 8.9% with a standard deviation of 3.8%. The maximum return obtained was 20.4%, while 1% of the samples resulted in zero return. Figure 6-10 presents the frequency distribution of the IRR obtained from the Monte Carlo simulation. For 44% of the samples, the IRR was between 6.9% and 11.5%. These results confirm the high risk of such a project, given the spread of the expected IRR over a wide range of values, including very low returns that could be unattractive to investors. Adding additional revenue streams would improve the economics of the process. For example, CVW Cleantech explored the integration of the mineral concentration process into the bitumen separation process that produce the tailing. Besides adding revenue streams through the recovery of bitumen and naphtha from desliming tailings, such an integration would reduce operating costs from tailings rehandling and heat recovery (CVW Cleantech Inc. 2023).

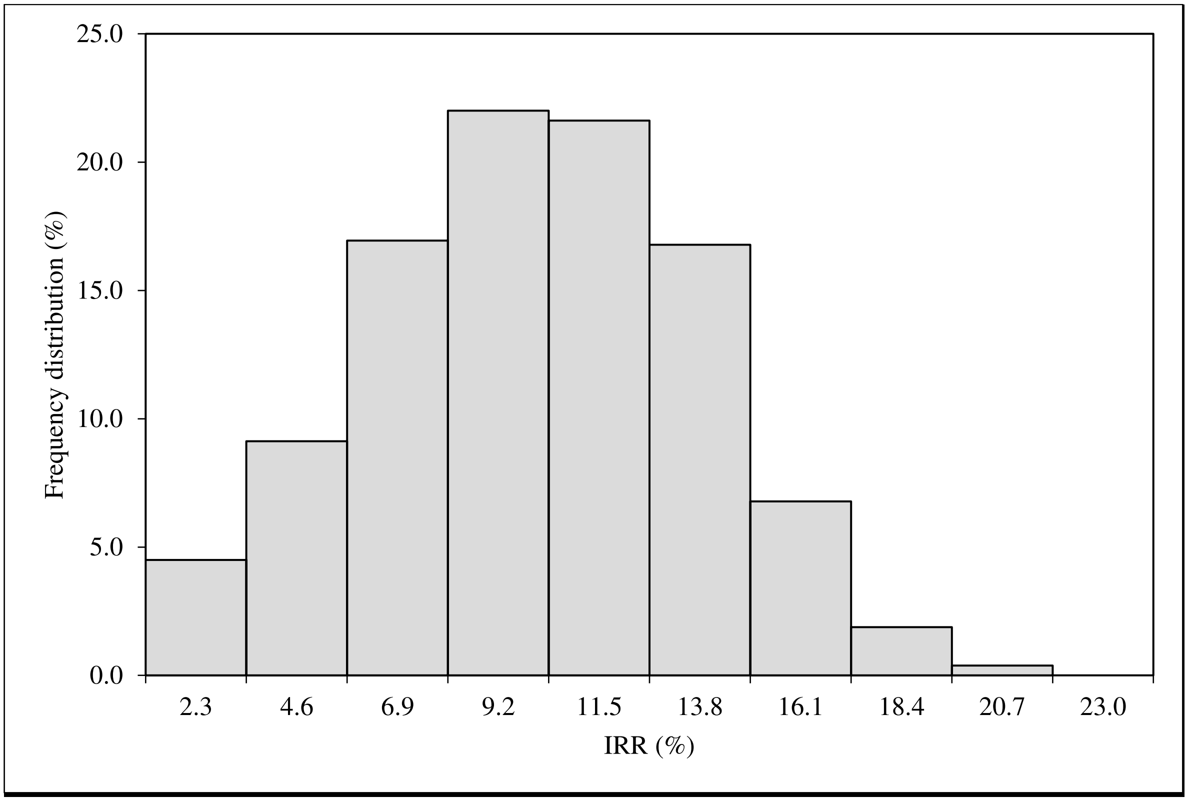

Figure 6-10. Frequency distribution of the IRR obtained from the Monte Carlo simulation

The effect of scale on the internal rate of return was also examined. Figure 6-11 shows the IRR as a function of the plant capacity, expressed as a fraction of the capacity in the base case. The IRR increases with the scale to 14.6% when the capacity is doubled. This is equivalent to processing the tailings generated in the two largest bitumen extraction plants in Alberta. Although such a return seems appealing for investors, a 200% capacity plant is a capital-intensive project ($668 M; see Table C-4 in the Appendix C), and thus the motivation for scenario 2.

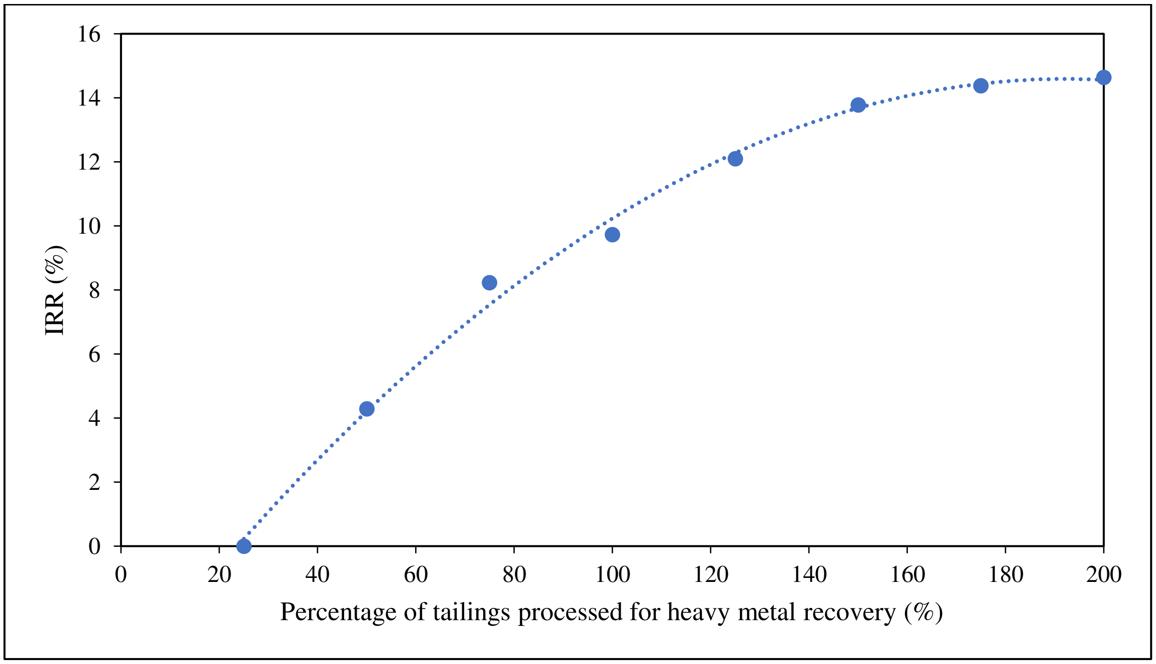

Figure 6-11. Internal rate of return vs. plant capacity expressed as a percentage of the capacity in the base case

6.3.2 Scenario 2: heavy mineral concentration plant(s) and one heavy mineral separation plant

The base case for this scenario consisted of one HMCP with a processing capacity of 15.5 million tonnes of FTT per year and one HMSP with a capacity of 574,000 tonnes of HMC, enough to process the heavy mineral concentrate obtained from the HMCP. To obtain a 10% IRR, for example, the HMCP, with a capital cost of $147.4 M, should provide the HMC to the HMSP at a cost of $21.52/t, including truck transportation. These figures are consistent with the estimate provided by H.A. Simons Ltd. (H.A. Simons Ltd. 1996). For that HMC cost, the IRR of the HMSP is 7.6%. The main reason for this difference in the plants' IRR may be the charge for feedstock and the disposal of solid waste generated after titanium minerals fractioning in the HMSP. The capital cost, operating cost, and revenue of the HMCP and HMSP are presented in Table C-4, in the Appendix C.

The greater the return in the HMCP, the lower the return in the HMSP, as shown in Figure 6-12 There should be a balance between the IRR expected by each plant to obtain a sustainable activity. For example, should the HMCP agree to reduce its IRR to 8.64%, the HMC cost would drop to $18.81/t, and the IRR of each plant would be the same.

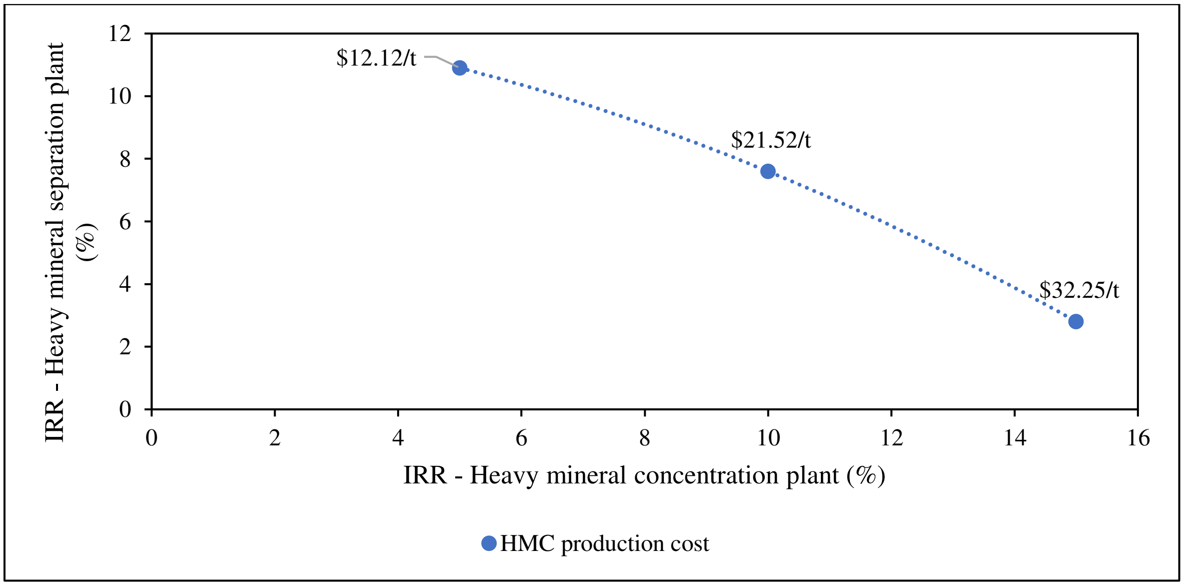

Figure 6-12. Relationship between the IRR of the HMCP (15.5 M tonnes FTT per year) and the IRR of the HMSP (574,000 tonnes HMC per year)

A way to increase the IRR of the HMSP without sacrificing the return of the HMCP is to involve more concentration plants in the industrial coalition. In this way, the separation plant would take advantage of economies of the scale to improve its return. For instance, operating an HMSP fed by concentration plants located at the three bitumen extraction plants based on naphthenic froth treatment in Alberta would generate an IRR of 11.6%, and the concentration plants would get a 10% return. The IRR of the separation plant fed by different numbers of concentration plants is shown in Table 6-12. The scale of the projected HMSP is technically feasible, considering existing commercial plants with processing capacities between 0.4 million and 1.2 million tonnes of HMC per year (Mining Technology 2021; RZ Resources 2023).

Table 6-12. IRR of the HMSP at different capacities and a 10% IRR for each HMCP

Capacity – separation plant (M tonnes HMC/y)	IRR (%)	No. of concentration plants[a,b]
0.57	7.6	One (15.5 M tonnes FTT/y)
0.96	9.8	Two (15.5 + 10.5) M tonnes FTT/y
1.15	11.1	Two (15.5 + 15.5) M tonnes FTT/y
1.54	11.6	Three (15.5 + 15.5 + 10.5) M tonnes FTT/y

a. Capacities were selected based on the current FTT generation rate in naphthenic froth treatment plants in Alberta.
b. The HMC production cost, for a 10% IRR, was estimated at \$21.52/t in the 15.5 M t/y HMCP and \$28.21/t in the 15.5 M t/y HMCP.

6.4 Conclusions

A data-intensive techno-economic model of a process for recovering heavy minerals from froth treatment tailings of bitumen extraction was developed. A heavy mineral concentrate, containing zircon and titanium minerals, is obtained after tailings desliming, flotation, and solvent extraction. Zircon is separated from the concentrate by flotation and upgraded – along with the fractioning of the remaining titanium minerals into rutile, and ilmenite/leucoxene – by a series of gravity, electrostatic, and magnetic separation. The model provides information to complete the material and energy balances and to estimate equipment sizes and capital and operating costs. Two scenarios were considered: a single plant for the whole process and one or more heavy minerals concentration plants that feed a centralized mineral separation plant.

In scenario 1, it was found that for a capacity of 15.5 M tonnes of FTT per year, the internal rate of return is 9.8%, obtained from selling the recovered heavy minerals and residual bitumen separated from the concentrate in the process. The estimated IRR is sensitive to the zircon selling price, the nominal capacity of spiral separators used in the primary gravity separation operation, the cost of disposing the rejected non-valuable mineral material, the annual labor rate, the on-stream factor, the outside boundary limit investment, and the selling price of the recovered titanium minerals and bitumen. The uncertainty analysis shows that the IRR is likely to be between 6.9% and 11.5% with variations in those parameters. The IRR increases with plant capacity due to economies of scale; however, a larger plant is capital-intensive.

In scenario 2, for a capacity of 15.5 M tonnes of FTT, the heavy minerals concentration plant would obtain an estimated 10% IRR when the heavy mineral concentrate is sold at \$21.52/t, and the return of the heavy mineral separation plant would be 7.6%. The economics of the separation plant are improved by increasing its capacity to process the heavy mineral concentrates obtained from several concentration plants. The economic potential of recovering heavy minerals from FTT increases under this cooperative scenario. The return generated for every actor in the industrial coalition, i.e., operators of the bitumen extraction plants, concentration plants, and centralized separation plant, would depend on the terms and conditions of such cooperation.

Chapter 7: Life cycle GHG emissions assessment of heavy minerals recovery from bitumen extraction tailings

7.1 Introduction

Titanium and zirconium are widely used in several industries, from construction to military, chemical, and energy. Titanium metal is a strong lightweight structural material used in the aerospace, automotive, military and construction industries, as well as for medical and dental prostheses and implants, manufacturing of sport implements and jewelry, and electronic devices. Also, titanium is widely used as a catalyst in several chemical and industrial processes and is a common white pigment in paints, printing inks, soaps, plastics, cosmetics, and even food. Titanium is obtained from minerals such as rutile, ilmenite, anatase, sphene, and altered ilmenite (commonly called leucoxene). These minerals, especially rutile and ilmenite, are processed to obtain titanium dioxide (TiO_2), which is used as feedstock for manufacturing pigments or to produce titanium metal and welding rods flux wire cords. Zirconium is used mainly as an opacifier in surface glazers and pigments, refractories, and metallurgical furnaces. It is also used in paper coatings, paint driers and catalysts, in the structure of nuclear reactor cores, and in steel production and jewelry. The most important source of zirconium is the mineral zircon ($ZrSiO_4$), which can be used directly to produce ceramics or processed to obtain zirconium dioxide or zirconia (ZrO_2). In general, titanium and zirconium minerals are co-produced by mining hard-rock deposits or processing mineral sands. Titanium is an abundant material in nature; however, about 64% of the world reserves are concentrated in Australia, China, and India. South Africa and Australia produce the most titanium minerals, closely followed by China (U.S. Geological Survey 2022). Unlike titanium, zirconium is rather scarce. Australia (70%) and South Africa (21%) control the world reserves (U.S. Geological Survey 2022). Demand for zirconium is increasing, motived by a growing use of zircon in foundries and refractories (Mordor Intelligence 2018; Perks and Mudd 2019) as well as in the telecommunication and energy sectors (Zhu et al. 2023). New sources of titanium minerals and zircon are needed to reduce future supply risks driven by the increasing demand for traditional and emerging applications, and reserves dominated by a handful of countries. The oil sands[7] deposits in Alberta, Canada, have the potential to become one of the main sources of such materials (Meisen 2017).

The occurrence of heavy minerals in the solid constituent of Alberta's oil sands has long been known. In feed grade ores obtained through surface mining[8], the concentrations of titanium and zirconium minerals average 0.35 wt.% and 0.032 wt.%, respectively (Oxenford et al. 2001). The oil sands ore is mined using shovels and trucked to a slurry preparation plant to be crushed, mixed with hot water, and pumped to the extraction plant. There, a series of flotation steps is used to obtain bitumen as froth. The underflow, a mixture of clays and coarse sand, is stockpiled in tailings ponds. The froth, containing bitumen, water, and mineral solids, undergoes naphthenic solvent froth treatment (NFT)[9] to produce a diluted bitumen, called

---

[7] A mixture of sand, clay, water, and a dense, highly viscous form of petroleum called bitumen.

[8] There are two ways to produce bitumen from oil sands, depending on the depth of the deposit: through in situ extraction, that is, by injecting steam to the deep reservoir and then pumping the bitumen to the surface, or by mining the oil sands and extracting the bitumen from the sands in a processing facility. In in situ production, most of the heavy mineral-rich sands are left below (in the reservoir) using sand control devices.

[9] A paraffinic froth treatment is used in some extraction plants. This type of treatment produces asphaltenes precipitation. Although asphaltenes precipitation is positive for the quality of dilbit, the presence of asphaltenes in the tailings could make the recovery of heavy minerals difficult. Therefore, we focused on tailings originating from naphthenic froth treatment.

dilbit, that is either sold or upgraded to produce synthetic crude oil (SCO). In NFT, the froth is mixed with naphtha and fed into a series of inclined plate separators and centrifuges to obtain a dilbit stream and a water/solids/naphtha stream that is directed to a naphtha recovery unit (NRU). The underflow of the NRU, known as froth treatment tailings (FTT), is a mixture of water (76-80 wt.%), solids (16-20 wt.%), residual bitumen (2-5 wt.%) and traces of solvent (Erasmus et al. 2010), and is disposed of in tailings ponds. Zircon (3.4 wt.%) and titanium minerals (11.5 wt.%), e.g., rutile, ilmenite, and leucoxene, are the predominant heavy minerals in the tailings, along with iron minerals and aluminosilicates (H.A. Simons Ltd. 1996). About 60-70% titanium minerals and 65-80% zircon are found in the recoverable size range (-154+45 μm) (Liu et al. 2006). With 430 million tonnes per year of mined oil sands fed into NFT-based bitumen extraction plants (Alberta Energy Regulator 2023a), the potential production of heavy minerals is equivalent to 6.5% and 16% of the titanium and zirconium mined worldwide (U.S. Geological Survey 2022). The recovery of heavy minerals from FTT may be economically attractive not only because of the creation of value from a waste of the bitumen extraction process, but because of the diversification of the economy of Alberta and Canada. Bitumen production, upgrading, and refining are greenhouse gas (GHG)-intensive activities already (Bergerson et al. 2012; Nimana et al. 2015c; Nimana et al. 2015a), contributing to about 11% of Canada’s carbon footprint (Government of Canada 2023a). An environmental assessment is required, therefore, to understand how the production of heavy minerals from FFT would affect the environmental impact of oil sands operations in Alberta.

Several processes to recover heavy minerals from FTT have been proposed over the years, and, despite the use of different technologies and unit operations, the main steps are common to most of them: *deoiling* for residual bitumen removing, *concentration* and *separation* of heavy minerals, zircon *upgrading* and titanium minerals *fractioning*. Tailings deoiling is unique to FTT processing and can be done either by burning off or solvent washing the residual bitumen coating the sand grains. A desliming operation could be included before or after deoiling to remove fines and improve subsequent separation operations. The remaining steps can be performed using the same technology for processing traditional ores, e.g., mineral sands, such as flotation, hydrocyclones, and gravity, electrostatic, and magnetic separation. Table 6-2 presents a summary of processes for recovering heavy minerals from oil sands FTT. Ciu et al. (2013) reviewed processes for the recovery of zirconium and titanium minerals from oil sands tailings. Earlier studies considered deoiling by burning off the residual bitumen from FTT, whether as-received (Baillie et al. 1976; Trevoy et al. 1978) or after a first stage of concentration (H.A. Simons Ltd. 1996; Owen and Tipman 1999; Bulatovic 2000; Oxenford et al. 2001; Chachula and Liu 2003). The drawbacks of this deoiling method are twofold. First, the physical characteristics of the heavy minerals (e.g., magnetic susceptibility) may be altered during roasting, affecting the downstream separation processes and altering the grade of the concentrate (Ciu et al. 2013). Second, the generation of emissions: burning the residual bitumen produces GHGs, but also the thermal decomposition of secondary minerals such as pyrite would generate SO_2 emissions. In other processes, a combination of gravity separation and solvent extraction (attritioning and settling) is implemented for deoiling (Reeves 2008; Erasmus et al. 2010; Moran and Chachula 2014)). This deoiling method does not present the inconveniences of tailings roasting, but it does increase the complexity of the process because of the solvent handling.

Understanding the net carbon footprint of recovering heavy minerals from FTT is critical for stakeholders to make informed decisions on the development of such activity, given the already high environmental burden of oil sands operations in Alberta. It is known that tailing ponds are a significant source of GHG emissions, mainly methane via microbial methanogenesis (Holowenko et al. 2000). Carbon dioxide is also found in the gas bubbling up from tailing ponds. Mechanisms like aerobic biodegradation and the catabolic process occurring in the bitumen film on the pond's surface are the reasons for the CO_2 emissions (Burkus 2014a; Small et al. 2015). Therefore, the emissions can be reduced by removing part of the residual diluent and bitumen in the tailings before they enter the tailing ponds, which can be achieved as a side benefit of recovering titanium and zirconium minerals from FTT (Moran et al. 2016). However, tailings processing would generate additional emissions that could offset said reduction by diverting tailings from tailing ponds. The net GHG emissions, from a life cycle perspective, should be addressed.

Despite efforts to develop a suitable heavy mineral recovery process, information on GHG emissions is very limited in the public domain. CVW Cleantech Inc. (2023) (formerly Titanium Corporation Ltd.) has developed a commercial-ready technology for the recovery of bitumen, solvent, water, titanium, zirconium, and rare earth elements from oil sands FTT and is planning to operate a concentrator plant and a mineral separation plant on the Horizon site operated by Canadian Natural Resources Ltd. (Titanium Corporation Ltd. 2019). The company estimated an emission abatement of 380,000 tonnes CO_2eq per year for a plant processing the tailings corresponding to a production of 250,000 bbl/day SCO. The estimation considered heat integration between the heavy mineral recovery plant and the oil sands operator facilities, avoided emissions by diverting tailings from tailing ponds, the displacement of heavy minerals production from traditional sources, and the reduction in emissions by the incremental hydrocarbon production after bitumen and diluent recovery. From the aggregated data presented in CVW Cleantech's report, it is not possible to identify the main GHG sources, which is critical to optimize/modify the process and reduce the emissions at a commercial scale. In addition, an assessment of the GHG emissions from a life cycle perspective is needed to compare the production of titanium and zirconium minerals from oil sands to incumbent pathways and understand the potential tradeoffs and benefits. Other than this corporate report, there are no studies on the GHG emissions from recovering heavy minerals from FTT.

Considering the identified research gap, the recovery of heavy minerals from FTT was investigated from a GHG emissions perspective. The results will support informed decision-making on the development of this economic activity integrated with bitumen extraction plants. The specific objectives of this research are to:

- Develop a process model of the recovery of heavy minerals from FTT;
- Conduct a life cycle GHG emissions assessment of the heavy mineral recovery process;
- Conduct sensitivity and uncertainty analyses to assess the influence of input variations on GHG emissions.

7.2 Methods

7.2.1 Case study

There are three bitumen extraction plants based on NFT currently operating in Alberta (Table 6-1). The composition and mineral assemblage of the FTT generated in those plants may vary with time and location; however, given the similar bitumen extraction processes used by oil sands operators and the consistent concentration of heavy minerals over most of the McMurray Formation in Athabasca (McCosh 1996), comparable heavy mineral grades in the FTT from the different bitumen extraction plants are expected (Owen and Tipman 1999; Oxenford et al. 2001). For this study, the centrifuge tailings generated in Suncor's Base Plant were considered as a reference feedstock.

The typical composition of FTT is shown in Table 6-4. The chemical assay and mineral quantity of FTT are presented in Table 6-5 and Table 6-6, respectively. About 15 m^3 of tailings are generated per cubic meter of bitumen produced. Of these, about 6% is FTT (Flint 2005). In 2022, Suncor's Base Plant produced 14.9 M m^3 (Alberta Energy Regulator 2023a); therefore, the generated FFT is estimated to be 13.7 M m^3, equivalent to about 15.5 M t of tailings if a density of 1,120 kg/m^3 is considered. In this analysis, it is assumed that all of the generated FTT feeds the heavy minerals recovery plant.

7.2.2 Scope and objectives, functional units, and system boundary

This study concerns the recovery of zircon and titanium minerals from tailings generated in the naphthenic froth treatment in the extraction of bitumen from Alberta's oil sands. The objective of the study is twofold: first, to estimate the cradle-to-gate carbon footprint of the recovered minerals (from oil sands mining up to the point they leave the plant, without considering their use or disposal), and second, to quantify potential benefits for the oil sands industry after the implementation of the recovery process. The functional unit (FU) was defined as one tonne of heavy minerals recovered from FTT. The results can be expressed per tonne of zircon, rutile, or leucoxene/ilmenite following an allocation procedure, if needed, for comparison with primary production systems. Also, the GHG emissions can be expressed per cubic meter of produced bitumen in the bitumen extraction plant. Equivalence to the FU is 0.016 t of heavy minerals per cubic meter of bitumen produced, which is given by the FTT generation rate (0.92 m^3/m^3 bitumen), tailings density (1,120 kg/m^3), and the recovery process yield obtained from the results of the model developed in this study (0.020 t/t FTT).

Figure 7-1. presents the study's system boundary. The foreground system corresponds to FTT processing for heavy mineral concentration and subsequent separation of the concentrate into zircon and titanium minerals. GHG emissions from the foreground system are considered direct or process emissions and are generated during the combustion of natural gas to provide heat to the process. The background system comprises all the operations required to generate the FTT feeding the foreground system, i.e., from oil sands mining to froth treatment. Fugitive emissions from tailing ponds are also included in the background system. Those emissions are a consequence of methanogenesis due to the bacterial decomposition of residual diluent found in the tailings. The production of the consumables, electricity, and natural gas required by the foreground system are also considered the background system. GHG emissions from the background system are considered upstream emissions.

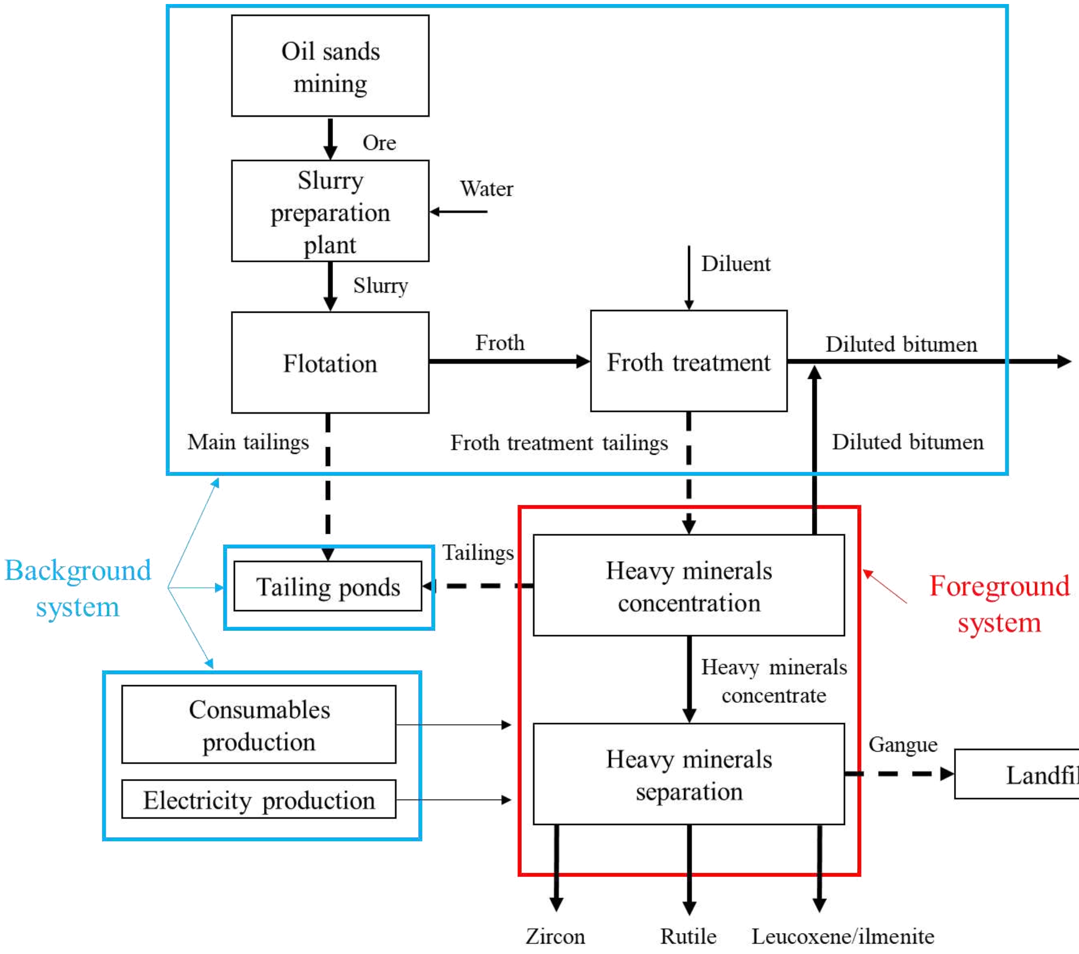

Figure 7-1. System boundary considered in this study

7.2.3 Inventory analysis

7.2.3.1 Process emissions

The recovery process used as the reference in this study is based on the process patented by CVW Cleantech (former Titanium Corporation) (Erasmus et al. 2010; Moran et al. 2013; Moran and Chachula 2014; Moran and Doiron 2015). In this process, the deoiling of FTT is done through solvent extraction rather than by combustion. The process has two phases: the concentration of heavy minerals and the separation of minerals into zircon and titanium fractions, as explained in Section 6.2.2.

Process emissions are generated by the combustion of natural gas to provide heat to the different operations. The specific operations in the HMC stage that require heat are froth flotation of hydrocyclone underflow, solvent extraction, naphtha recovery, and bitumen separation. In the heavy mineral separation phase, drying the primary gravity separation product and the conditioning of tails from gravity separation and zircon flotation use natural gas as a source of heat. A spreadsheet-based process model was developed to quantify the heat demand and, therefore, the natural gas consumption. The general framework of the model development is depicted in Figure **7-2**. Details of the process modeling are in Section 6.2.4). A summary of the data used for process modeling is in Appendix C (Table C-1 and Table C-2). Once the natural gas consumption is estimated, the process emissions are calculated using the emission factor for natural gas consumption (Table 7-2).

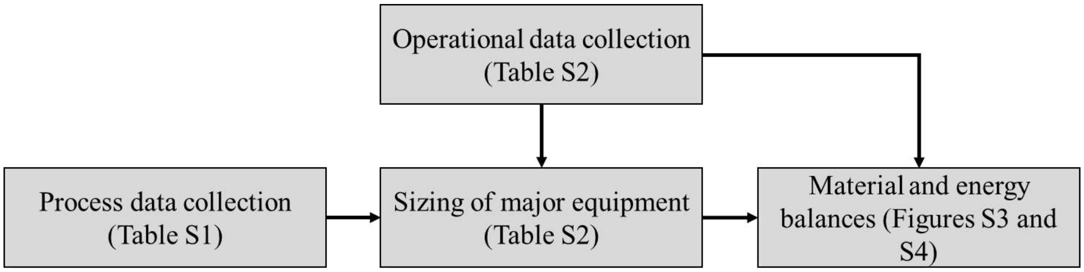

Figure 7-2. General framework for process modeling

7.2.3.2 Upstream emissions

In the current bitumen value chain, diluted bitumen is the product of oil sands mining and bitumen extraction, and FTT are considered a waste. Therefore, 100% of the GHG emissions associated with those operations are usually allocated to the dilbit stream. Nimana et al. (2015a) estimated the emissions from oil sands mining and bitumen extraction to be in the range of 180-302 kg CO_2eq/m^3 bitumen, depending on whether cogeneration is used or not.

Sleep et al. (2018) used the model developed by Bergerson et al. (2012) and estimated the emissions from those operations to be between 3.5 and 12.7 gCO_2eq/MJ dilbit. Those authors used a high heat value of dilbit of 40.6 GJ/m^3 dilbit and 75 vol.% bitumen in dilbit, therefore the mentioned range is equivalent to 189-687 kg CO_2eq/m^3 bitumen. An intermediate value of 460 kg CO_2eq/m^3 bitumen was considered in this study.

In this analysis, however, FFT are treated as a by-product of the bitumen extraction process, from which some value can be generated. A fraction of the GHG emissions from the bitumen value chain is allocated to the FTT. A mass-based allocation was used in this study. About 0.92 m^3 of FTT is generated per cubic meter of bitumen produced (BGC Engineering Inc. 2010), and the FTT density is around 1,120 kg/m^3. About 17 wt.% of FTT is solid matter. It is estimated that 1.3 wt.% of the solids is zircon, while 5.5 wt.% is titanium-bearing minerals. Of the latter, 33 wt.% is rutile and 67% is ilmenite and leucoxene. This information was used to calculate the mass fraction of all the co-products of the bitumen extraction process, i.e., produced bitumen and heavy minerals in FTT. Table 7-1 presents the production of co-products for a reference production of 1,000 m^3 bitumen, which is equivalent to 1,429 m^3 dilbit. About 98.8 wt.% of the co-products corresponds to bitumen and 1.20 wt.% to heavy minerals in the tailings. Those proportions were used as weight factors to allocate GHG emissions to the dilbit stream and the FTT, respectively.

Table 7-1. Mass of co-products obtained for a production of 1,000 m^3 bitumen

Product	Production	Mass fraction
Bitumen	1,013 t	0.988
Zircon	2.35 t	0.002
Rutile	3.19 t	0.003
Leucoxene-ilmenite	6.47 t	0.006

A fraction of the GHG emissions by the methanogenesis of naphtha in the tailing ponds was also allocated to the FTT, following the allocation method described above. However, with the implementation of the reference process, a fraction of the residual diluent in the FTT is diverted from the tailing ponds, while the balance is carried along with the desliming hydrocyclone tailings and the flotation tailings. This diversion represents a reduction of the GHG emissions by the methanogenesis of naphtha in the tailing ponds, which was considered in the allocation of GHG emissions to the FTT. Burkus (2014b) developed a model to estimate the GHG emissions from oil sands tailing ponds based on fermentable substrates. In that study, methane emissions were calculated from the diluent entering ponds, different successive aerobic and anaerobic fermentation losses, and methanogenic mass balance, while carbon dioxide emissions were calculated from the difference in the mass of carbon that entered the pond and the mass of carbon that was fermented into methane. In the model, the emissions are proportional to the diluent volume lost per volume of bitumen produced (DVL); therefore, the GHG emissions reduced by diverting diluent from the tailing ponds after implementing the process can be calculated from the current GHG emissions by:

$$GHG_{TP.r} = \frac{DVL_p}{DVL_c} GHG_{TP,c} \tag{7-1}$$

$GHG_{TP,r}$: reduced GHG emissions from tailing ponds after implementing the process, kg CO_2eq/m^3 bitumen produced

DVL_p: diluent volume lost per volume of bitumen produced after implementation of the process, m^3 diluent/1,000 m^3 bitumen produced

DVL_c: current diluent volume lost per volume of bitumen produced, m^3 diluent/1,000 m^3 bitumen produced

GHG_c: current GHG emissions from tailing ponds, kg CO_2eq/m^3 bitumen produced

Using the fermentable substrate model, Burkus (2014b) estimated the current GHG emissions from tailing ponds in the order of 376 kg CO_2eq/m^3 bitumen produced, for a DVL_c of 4.0 m^3 naphtha per 1,000 m^3 bitumen produced. The value of DVL_p is determined from the material balance of the recovery process. According to the weight factor described above, 1.20% of the reduced GHG emissions given by Equation (7-1) are allocated to the FTT.

The upstream emissions also include those associated with the production of consumables and electricity. The emission factors used in this study are shown in Table 7-2. Naphtha accounts for 87 wt.% of the consumables and unmodified wheat starch 5 wt.%. The production of those materials was considered in the upstream emissions estimation. The rest of the materials were excluded from the GHG emissions calculations because they contribute less than 2 wt.% each to the share. Electricity consumption was estimated through the process model developed in this study.

Table 7-2. Emission factors used to calculate process and upstream emissions

Emission source	Emission factor	Comments/References
Naphtha production	52.3 kg CO_2eq/bbl	Average value of data provided by Sleep et al. (2018)
Unmodified wheat starch production	0.56 kg CO_2eq/kg	Food grade wheat starch's cradle-to-gate carbon footprint (CarbonCloud 2023)
Electricity generation (grid)	0.53 kg CO_2eq/kWh	(Government of Alberta 2019b)
Natural gas combustion	52.4 kg CO_2eq/GJ	(Government of Canada 2015)

7.2.4 Treatment of co-products

The co-products of the entire process are a zircon concentrate, a rutile concentrate, an ilmenite-leucoxene concentrate, and diluted bitumen from the underflow of the solvent extraction operation in the heavy mineral concentration stage. The wastes are: three solid streams (from the separation of titanium minerals), the desliming hydrocyclone tailings, and the flotation tailings.

As mentioned before, the results of this study are expressed in terms of one tonne of recovered heavy minerals, and so the zircon, rutile, and ilmenite-concentrate are treated as a single product. To avoid allocating GHG emissions among heavy minerals and bitumen, and following the guidelines provided by the International Organization for Standardization (ISO) in ISO 14040, the system boundary was expanded to include displaced processes and further processing of the co-products (International Organization for Standardization 2006). Oil sands mining and bitumen extraction (subsystem B) were included in the original system (subsystem A) because the recovered bitumen displaces the production of dilbit. The GHG emissions from subsystem B are then subtracted from the those from subsystem A to obtain the GHG emissions associated with the recovery of heavy minerals through the process considered in this study. A carbon intensity of 460 kg CO_2eq/m^3 bitumen was considered for the subsystem B, as discussed in Section 7.2.3.2.

7.2.5 Sensitivity and uncertainty analyses

In this study, the Regression, Uncertainty, and Sensitivity Tool (RUST) (Di Lullo et al. 2019) was used for sensitivity and uncertainty analysis. The Morris method was implemented to study the sensitivity of life cycle GHG emissions to 37 inputs, including process conditions, equipment performance and energy consumption, consumables rates, and emission factors. Appendix B presents an overview of the Morris method. The model used in this study was developed based on several assumptions, which introduce uncertainty in the results. To deal with the uncertainties, a Monte Carlo simulation was performed considering the same inputs used for the sensitivity analysis. The range of variation in the inputs was based on typical values found in the literature (see Appendix D), and a uniform distribution was considered to populate the sample.

7.3 Results and discussion

7.3.1 Material and energy balances – base case

For a 15.5 Mt FFT-heavy mineral recovery plant, the production of heavy minerals was estimated to be 22.4 tonnes per year, representing a recovery of 87.1 wt.% of the heavy minerals found in the feed. Additionally, 41.4 km^3 of diluted bitumen is recovered from the tailings, 9.20 vol.% of the residual bitumen content in the FTT. Table 7-3 presents a summary of the material balance obtained from the developed process model.

Table 7-3. Co-products and wastes from a 15.5 M t/y heavy mineral recovery plant

Co-products/wastes	Annual production/generation rate
Zircon	34.0 kt
Rutile	25.5 kt
Ilmenite-leucoxene	97.3 kt
Diluted bitumen	41.4 km^3
Hydrocyclones overflow	11.7 Mm^3
Gangue	344.6 kt

The electricity and natural consumption of the whole process were estimated to be 223.6 kWh/t heavy minerals and 9.28 GJ/t heavy minerals, respectively. About 39.3% of the electricity is required by the concentration phase and 60.7% by the separation phase. In the concentration phase, solvent extraction is the operation that consumes the most electricity (21.1%). In total, six units (attrition cell plus settling chamber) are required for the three solvent extraction stages. In addition, attrition cells are power-demanding equipment, thus the obtained result. Desliming (8.3%) and flotation (7.2%) also contribute significantly to electricity consumption. The desliming operation handles all of the FTT; therefore, the pumping power required to overcome the pressure drop in the intake pipe and through the hydrocyclones is high. The energy required to pump the overflow to the tailing ponds for storage is also included in the inventory. This overflow represents 90% of the FTT fed to the process and demands a significant amount of power as well. The separation phase demands the most electricity because of the many electrostatic and magnetic separation steps as well as the dewatering and drying of different streams. The operations that consume the most electricity in the separation phase are the separation of rutile from the gravity separation tails (24.5%) and of ilmenite-leucoxene from the zircon flotation and primary electrostatic and magnetic (E&M) separation (23.6% including the conditioning of zircon flotation tailings). In both operations, a slurry is dewatered by filtration prior to the E&M separation of titanium minerals. The disk filters assumed for the required filtration are the equipment with the most electricity consumption in the whole process.

Regarding natural gas, 15.5% of the demand is consumed in the concentration stage and 82.9% in the separation stage. The heat required for naphtha and bitumen recovery, which together make up 9.44% of the total natural gas consumption, is accounted in the concentration stage. Zircon flotation is the operation with the greatest natural gas consumption in the separation stage and the whole process (54.7%). This operation is the first step in the separation stage; therefore, it handles a great flow of materials, especially of water, which is heated from room temperature to about 90°C, thus the great consumption of natural gas to supply the required sensible heat. The remaining natural gas is consumed by drying the different mineral-rich streams obtained throughout the separation stage. Specifically, drying the product stream of the primary gravity separation prior to primary E&M separation requires 10.6% of the total natural gas, and drying the tailings from the primary gravity separation and zircon flotation consumes 15.7%. In these operations, filtration cakes with about 25 wt.% moisture content are dried.

Electricity and natural gas consumption by operation are shown in Table 7-4. These figures were used along with the corresponding emission factors to calculate process and upstream emissions due to the production of the electricity consumed in the process.

Table 7-4. Electricity and natural gas consumption per unit operation in the heavy mineral concentration and separation phases

Operation	**Electricity (kWh/t heavy mineral)**	**Natural gas (GJ/t heavy mineral)**
Heavy minerals concentration		
Desliming	18.6	-
Flotation	16.1	0.19
Solvent extraction	47.1	-
Diluent recovery	0.25	0.28
Bitumen recovery	4.86	0.60
Heavy minerals separation		
Zircon flotation	8.89	4.86
Primary gravity separation	0.07	-
Dewatering and drying	0.04	0.98
Primary ES & MS	10.3	-

Operation	Electricity (kWh/t heavy mineral)	Natural gas (GJ/t heavy mineral)
Finishing gravity separation	0.16	-
Finishing ES & MS	5.81	-
Separation of titanium from gravity separation tails	54.7	0.53
Conditioning of Zr flotation tails	27.9	1.45
Separation of titanium from conditioned Zr flotation tailings and primary ES & MS	24.9	-
Separation of titanium from finishing ES & MS	1.24	-
Ancillary equipment	2.68	-
Total	**223.6**	**8.89**

7.3.2 Life cycle GHG emissions

Considering upstream and process GHG emissions, life cycle GHG emissions total 1,540 kg CO_2eq/t heavy minerals. The calculated upstream emissions are 1,055 kg CO_2eq/t heavy mineral. Those associated with the generation of the FTT to feed the heavy mineral recovery process were estimated to be 530.9 kg CO_2eq/t heavy mineral. As mentioned in Section 7.2.3.2, 1.20% of the 460 kg CO_2eq emitted to produce 1 m^3 of bitumen are allocated to the FTT. The emissions per cubic meter of bitumen produced are expressed in terms of the FU using the rate of FTT generation (0.92 m^3 FTT/m^3 bitumen), the tailings density (1,120 kg/m^3), and the process yield obtained from the developed model (10.1 kg heavy minerals per tonne of FTT processed).

According to the material balance of the process, 5.43% of the residual diluent content in the FTT is diverted from the tailing ponds (Figure 7-3.). Considering that the current DVL of Suncor's bitumen extraction plant is about 3.39 m^3 naphtha per 1,000 m^3 bitumen produced, the DVL after the implementation of the heavy mineral recovery process would be 3.21 m^3 naphtha per 1,000 m^3 bitumen produced. According to Equation (7-1 the reduced GHG emissions after implementing the process are an estimated 301.7 kg CO_2eq/m^3 bitumen produced, of which 3.77 kg CO_2eq/m^3 bitumen produced, equivalent to 372.1 kg CO_2eq/t heavy minerals, are allocated to the FTT.

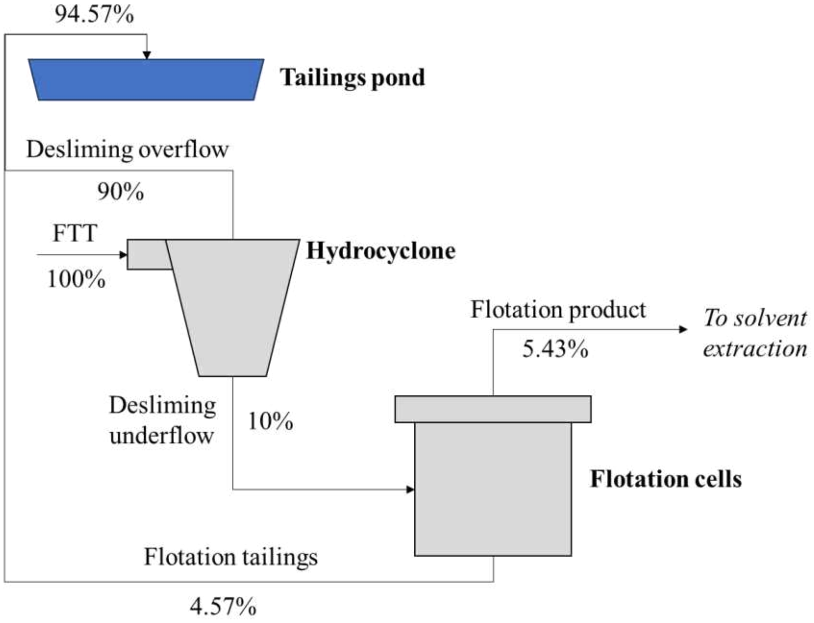

Figure 7-3. Percent distribution of residual diluent in FTT through different unit operations of the HMC stage

The production of consumables emits 56.9 kg CO_2eq/t heavy minerals (92.7% from the production of naphtha), while electricity production contributes 118.5 kg CO_2eq/t heavy minerals. Process emissions, i.e., from the combustion of natural gas to provide heat to the process, are estimated to be 484.9 kg CO_2eq/t heavy minerals. Process emissions could be reduced if the process is integrated into the bitumen extraction plant, for instance, heat recovery from the main tailings to reduce natural gas consumption. This approach was explored by CVW Cleantech (2023).

Figure 7-4. presents the percent contribution of process and upstream emissions to the life cycle GHG emissions. Upstream emissions make up 70% of the total emissions, with the generation of FTT generating the greater share (36%), even surpassing process emissions (30%). Allocating emissions associated with bitumen production to FTT represents a huge penalty to the carbon footprint of the recovered heavy minerals (59% from mining and bitumen extraction, as well as fugitive emissions from tailings ponds). Because of the low concentration of minerals in the tailings, a considerable amount of FTT needs to be processed to obtain one tonne of HMC, thus the great contribution to the life cycle GHG emissions of the recovered materials. On the other hand, emissions from oil sands mining and bitumen extraction represent about 32% of the SCO life cycle GHG emissions[10]; therefore, reducing the former by 1.20% by allocating emissions to FTT barely affects the latter (0.38%). The decision on whether to allocate GHG emissions generated in oil sands mining and bitumen extraction to FTT would depend on how the parties have settled their emissions reporting. For example, unless the benefits to the oil sands operator are considerable (for example in a carbon tax scenario), GHG emissions associated with oil sands mining and bitumen

---

[10] This value includes mining and bitumen extraction (460 kg CO_2eq/m^3 bitumen), transport and upgrading (16.6 gCO_2eq/MJ SCO, and fugitive emissions from tailings ponds (376 kg CO_2eq/m^3 bitumen). The conversion between gCO_2eq/MJ SCO and kg CO_2eq/m^3 bitumen is done using the factor 1.15 (gCO_2eq/MJ SCO)/(gCO_2eq/MJ bitumen) and a bitumen heat value of 40.8 MJ/m^3 bitumen.

extraction should be totally allocated to diluted bitumen to avoid an excessive burden on the HMC.

Finally, considering the avoided GHG emissions by recovering diluted bitumen from FTT, life cycle GHG emissions would be reduced in 90.6 kg CO_2eq/t heavy minerals, decreasing to 1,449 kg CO_2eq/t heavy minerals. Such a reduction is achieved after recovering 9.20 wt.% of the residual bitumen in the FTT. The balance is lost to tailings ponds. Should the desliming hydrocyclone's overflow be processed to recover additional bitumen from the FTT, the benefit could be greater. Moran et al. (2013) developed a process to do that, based on flotation and solvent extraction. However, the net effect of the additional operations could increase life cycle GHG emissions because emissions from the consumption of additional energy and naphtha could surpass the increase in the avoided GHG emissions.

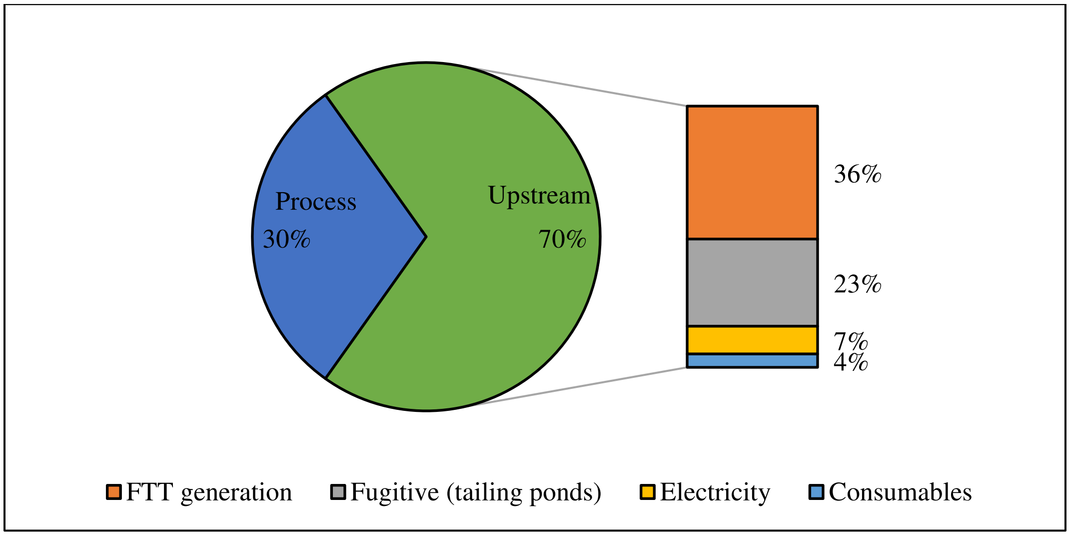

Figure 7-4. Contribution of process and upstream emissions to life cycle GHG emissions

Figure 7-5. presents the results of the sensitivity analysis. The Morris plot ranks the influence of the parameters on the model output, i.e., the life cycle GHG emissions, based on the position of the absolute Morris mean and the standard deviation in the plot (Di Lullo et al. 2019). The high sensitivity and high non-linear parameters are located at the top right of the plot. It is observed that life cycle GHG emissions are more sensitive to the emission factor associated with mining and bitumen extraction, on which the emissions allocated to the FTT directly depend. The generation of FTT contributes the most to life cycle GHG emissions; therefore, this result was expected. Life cycle GHG emissions are also sensitive to the emission factor of natural gas combustion, i.e., to the process emissions, and to the emission factor of electricity generation. The DVL is another input whose variation greatly impacts the model output because the fugitive emissions avoided by diverting diluent from tailings ponds are estimated based on the current DVL. The emission factors associated with the production of consumables, as well as the inputs related to process conditions and equipment performance and energy consumption, impact the Morris mean by less than 5%.

The mean value of the life cycle GHG emissions obtained from the Monte Carlo simulation was 1,406 kg CO_2eq/t heavy minerals with a standard deviation of 184.6 kg CO_2eq/t heavy minerals. Figure 7-6. presents the frequency distribution of the life cycle GHG emissions resulting from the simulation. For about 80% of the samples, the life cycle GHG emissions are in the range 1,230-1,670 kg CO_2eq/t heavy minerals. The minimum value obtained was 913 kg CO_2eq/t heavy minerals. These results show that recovering heavy minerals from FTT is potentially more carbon-intensive than producing the minerals from primary sources. For example, the production of one tonne of heavy minerals from mineral sands emits around 804 kg CO_2eq (Lundberg 2011). Such a conclusion, however, depends on whether emissions associated with oil sands mining and bitumen extraction, and fugitive emissions from tailings ponds, are allocated to the FTT. Those emissions represent 59% of the life cycle GHG emissions, as mentioned above.

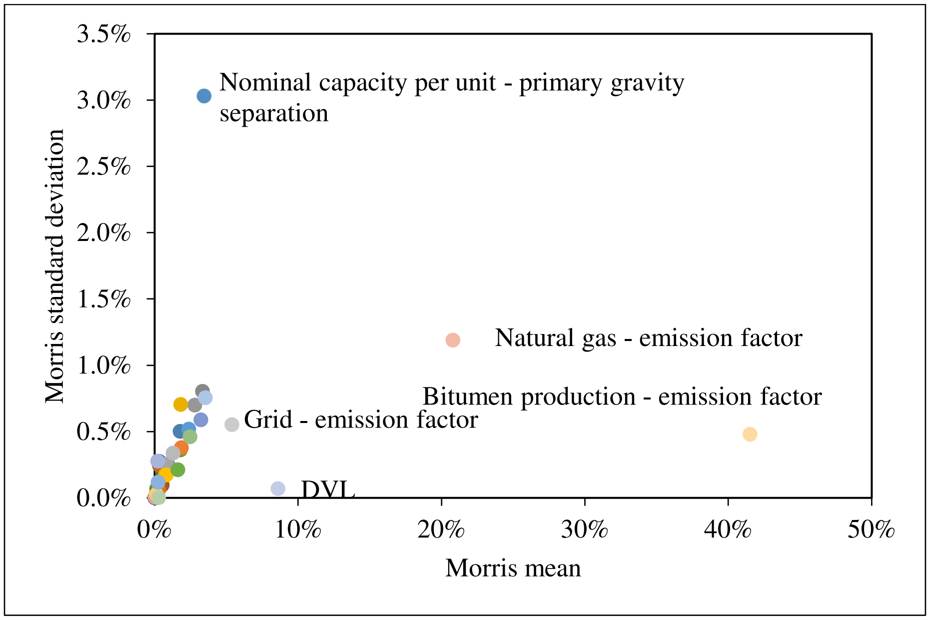

Figure 7-5. Morris plot showing the results of sensitivity analysis

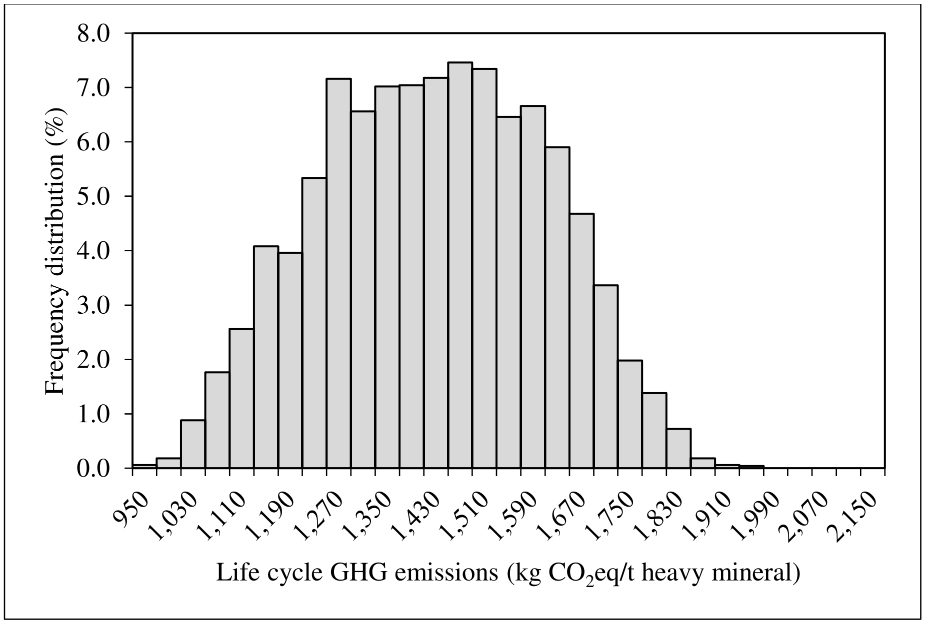

Figure 7-6. Frequency distribution of the life cycle GHG emissions obtained through a Monte Carlo simulation

7.4 Conclusions

In this study, the life cycle GHG emissions of heavy minerals obtained from the froth treatment tailings of the bitumen extraction process were estimated. Besides considering the emissions generated during the two stages of the process, i.e., mineral concentration and separation, a fraction of the emissions associated with oil sands mining and bitumen extraction, as well as fugitive emissions from tailings ponds, was allocated to the FTT. The GHG emissions due the production of electricity and consumables were also considered.

estimated that 1,540 kg CO_2eq/t heavy minerals would be produced. Of these, 70% are upstream emissions, with oil sands mining and bitumen extraction contributing 36%. Considering the avoided upstream emissions by recovering residual bitumen from the FTT, life cycle GHG emissions would be reduced to 1,499 kg CO_2eq/t heavy minerals.

The results show that the life cycle GHG emissions of heavy minerals from FTT are driven by the upstream emissions associated with the generation of the tailings that feed the mineral concentration process, i.e., oil sands mining and bitumen extraction. Whether those emissions are partially allocated to the FTT or fully attributed to bitumen production would depend on how the parties agree to report their emissions. If the latter, process emissions from the combustion of natural gas and upstream emissions from the production of electricity would be the main contributors to the life cycle GHG emissions. In that case, the produced emissions would be 660.3 kg CO_2eq/t heavy minerals, which is comparable to the emissions from primary sources of zircon and titanium minerals.

Chapter 8: The development of a techno-economic model for the assessment of asphaltene-based carbon fiber production[11]

8.1 Introduction

Carbon fibers (CFs) are fibers with at least 92 wt.% carbon, with mechanical properties superior to steel and aluminum (Morgan 2005) and a fraction of their densities. For these reasons, it can be used as a structural material in the aerospace (Lowe 2005; Tang and Hu 2017; Barile and Casavola 2019), automobile (Ahmad et al. 2020; Wan and Takahashi 2021), and renewable energy industries (Ennis et al. 2019), as well as in the manufacturing of medical (Chua et al. 2021) and sports equipment (Tang 2013). However, its high production cost limits the use of carbon fibers to market niches (Zhang et al. 2023).

Carbon fibers can be obtained from diverse precursors, from polymers to biomass. Currently, about 90% of the carbon fibers produced commercially worldwide are made from polyacrylonitrile (PAN) and the rest from petroleum pitch or rayon. In general, the production of PAN comprises the polymerization of acrylonitrile and the formation of a dope, spinning the dope into fibers, and a series of washing, stretching, coating, and drying operations. The PAN fibers are stabilized by heating at 200-300°C using air. The objective of the stabilization is to transform the precursor into a form that can be thermally treated at temperatures above the melting point. The stabilized fibers are carbonized in the absence of oxygen by heating, first at about 1,000°C and then at 1,800°C (Morgan 2005). Non-carbon molecules are

---

[11] A version of this chapter has been published as M. Baritto, A.O. Oni, A. Kumar. The development of a techno-economic model for the assessment of asphaltene-based carbon fiber production. Journal of Cleaner Production 2023. 428:139489.

removed, producing fiber with high carbon content. Surface treatment is required to increase the adhesion between the matrix resin and the carbon fibers for manufacturing composite materials. Usually, an electrolytic surface treatment process is used. Finally, the carbon fibers are sized by coating them with an epoxy to ease handling, then wound in spools and packaged for transportation. Because of the formation of hydrogen cyanide (HCN) during thermal operations, a gas abatement system should be included to clean the off-gases. The PAN-based carbon fiber (PAN-CF) process has a yield of around 50%, that is, about 2 kg of PAN is required to produce one kg of carbon fiber (Morgan 2005; Park and Heo 2015).

PAN production accounts for about half the production cost, and the conversion from PAN to carbon fiber makes up the rest. The U.S. Department of Energy (DOE) through the Oak Ridge National Laboratory (ORNL) developed cost models for PAN-CF production and estimates a production cost of \$22.67/kg CF for a capacity of 2,500 t/y (Warren N.d.). This number is similar to that reported by Harper International (2013) (\$21.00/kg CF for a plant capacity of 2,750 t/y), a manufacturer of carbon fiber production lines. According to data in Harper International, the production cost benefits from economies of scale, with a scale factor of about 0.23 (the production cost goes from \$35.00/kg CF at 300 t/y to \$21.00/kg CF at 2,750t/y) (Harper International 2013). Omnia LLC. (2012) assessed PAN-CF produced in Iceland and compared it with that produced in the U.S. and Europe. They estimated a production cost of \$20.49-21.86 per kg of CF for a capacity of 4,000 t/y. Ellringmann et al. (2016) estimated PAN-CF production costs through process modeling of both PAN and carbon fiber. For a plant capacity of 3,000 t/y and a tow size of 24,000 filaments (24k), the estimated production cost is EUR 19.64/kg (\$20.52/kg at a rate of 1.04 \$/EUR). Precursor manufacturing accounts for 54% of the total, with 19% corresponding to raw material (acrylonitrile) and 16% to energy costs, mainly from the washing of PAN fibers and the recovery of the solvent used to form the dope. In fact, solvent recovery is an energy-intensive operation based on simple evaporation and fractional distillation. In terms of the cost of carbon fiber production alone, the energy cost makes up 18% of the total cost. Of this, about 10% and 4% are from electricity consumption in carbonization and stabilization operations, respectively. The equipment cost represents 11% of the total cost, with carbonization and stabilization making up most of this. Nunna et al. (2019) developed a cost model for PAN-CF production, including the manufacturing of PAN and carbon fibers. The main innovation of their model is to consider the tow size as a parameter for the production cost. The authors concluded that heavy tows are much cheaper to produce than small tows ($10.5/kg CF for 100k versus $34.7/kg for 3k). However, for tow sizes greater than 48k, the cost difference is negligible. As expected, precursor manufacturing accounts for 53% of the total cost. Electricity makes up 7%, but this cost is surpassed by the natural gas required for gas abatement (11%) and labor (15%) (Nunna et al. 2019).

The development of low-cost precursors is key to achieving the cost reduction required to increase the use of carbon fiber. For example, the automobile industry targets a carbon fiber cost below $11-$15.40/kg CF (Baker and Rials 2013). The use of textile-grade PAN, melt-spun PAN, lignin, polyolefin, asphaltenes, and other materials as carbon fiber precursors is undergoing research. Projections of the production cost using some of those precursors are available in the literature. Lignin and polyolefin are promising precursors, with production costs estimated at $7.79/kg CF (Chien-Wei Chen 2014) and $5.04/kg CF (Warren 2010), respectively. Coal tar pitch is also a low-cost option, with a projected cost of $10.29/kg CF (Das and Nagapurkar 2021). The use of asphaltenes as a carbon fiber precursor is attractive because of the opportunity of creating value from a by-product of crude oil processing with limited commercial interest. Particularly for the oil sands industry in Alberta, Canada, such activity would contribute to diversifying the economy of the region; increasing the profitability of upgraded bitumen, which is currently sold at a price differential respecting similar crude oils; and maintaining the competitiveness of the industry should the market for fossil fuels shrink due to the decarbonization of the economy.

Asphaltene is the heavy fraction of bitumen[12] and crude oil that is not soluble in n-heptane (Redelius 2011). It consists of polar components from condensed aromatic and naphthenic rings. High-molecular-weight molecules in asphaltenes tend to associate and form clusters, which can lead to increased viscosity and thickness of bitumen and crude oil. Therefore, asphaltenes are removed from bitumen or crude oil during upgrading or refining to improve the quality of the final product. Currently, asphaltene has very limited use, therefore it is seen as a low-value by-product or even as waste. Because of its high carbon concentration (>80 wt.%) and relatively low cost, asphaltene is considered a potential raw material for carbon fiber production. The main drawback of using asphaltene as a carbon precursor is its low softening point; additional pre-treatment is therefore needed to produce a material that can be processed at the temperature required for stabilization. The technology to produce asphaltene-based carbon fiber (ACF) is in the early stages of research, but some efforts have been made to get a suitable process. Regardless of the origin of the asphaltene, the general process is essentially the same: asphaltene modification (thermal or chemical treatment), melt

---

[12] A highly viscous extra heavy oil that hardly flows at room temperature. Bitumen is found naturally in deposits like oil sands and pitch lakes.

spinning, stabilization, and carbonization (Leal and Penaloza 2002; Ni et al. 2019; Qin et al. 2019; Leistenschneider et al. 2021; Zuo et al. 2021a; Zuo et al. 2021b; Baritto et al. 2023c). The process resembles that of producing pitch-based carbon fiber, which is currently at a commercial scale. Table 8-1 summarizes the process conditions found in the literature. For bitumen-derived asphaltenes, other spinning methods have been used at laboratory scale with different degrees of success. Yadav et al. (2021) were able to produce ACF from bitumen-derived asphaltenes using wet spinning instead of melt spinning; however, the mechanical properties of the fiber were too low to match automotive targets. Chacón-Patiño et al. (2023) found that sulfur removal by treatment with molten sodium in a stirred autoclave under hydrogen atmosphere improves the spinnability of bitumen-derived asphaltenes compared with thermal treatment. However, the green fibers (GFs) obtained through such method are unsuitable for carbon fiber production because they melt at the stabilization temperature. De Crisci et al. (2022) determined the ideal electrospinning parameters for producing asphaltene green fibers. The behavior of such fibers during stabilization and carbonization was not reported in that study.

Table 8-1. Summary of the literature review on the ACF production process

Feedstock	Thermal/chemical modification	Melt spinning	Stabilization	Carbonization	Results	Reference
Deasphalting bottoms, 63.5% asphaltenes, 105ºC SP	320-400ºC for 2 hr 265ºC SP	40-60ºC above SP, 100 m/min	1st stage: 140ºC, 1ºC/min, 10 min 2nd stage: 327ºC, 2ºC/min, 2 h	Nitrogen, 800-1,000 ºC, 5ºC/min, 30-60 min	90.1 wt.% carbon; smooth surface and free of bumps	Leal and Penaloza (2002)
Asphaltenes extracted from solid residues of coal and heavy oil co-refining, 70-75ºC SP	Air blowing at 300ºC, ºC/min, 2-4 hr Nitrogen blowing at 350ºC for 2-4 hr 217-225ºC SP	40-50ºC above SP 100 m/min 0.5-2.0 MPa	1st stage: 220ºC, 3ºC/min 2nd stage: 280ºC, 0.5ºC/min, 2 h	Argon, 1,000 ºC, 5ºC/min, 15 min	Yield: 70 wt.% Average diameter: 12 µm Smooth surface Tensile strength: 600-1,100 MPa	Qin et al. (2019)

Feedstock	Thermal/chemical modification	Melt spinning	Stabilization	Carbonization	Results	Reference
Asphaltene from coal tar, 70ºC SP	Mixed with SEBS (5 wt.%) Air blowing at 340ºC for 3 hr 221ºC SP	40-50ºC above SP 300 m/min	400ºC, 0.5ºC/min	1,000 ºC, 5ºC/min, 10 min	Tensile strength: 600-1,100 MPa	Ni et al. (2019)
Bitumen-derived asphaltenes separated by solvent deasphalting	Heating in a nitrogen atmosphere at 300-350ºC for 2 hr	220ºC	Pre-stabilization in HNO_3 at 25ºC for 10 min. Stabilization at 300ºC for 6 h	Nitrogen, at 1,500ºC 2 h	Tensile strength 1,000 MPa, Modulus 55 GPa	Zuo et al. (2021b); (Zuo et al. 2021a)
Bitumen-derived asphaltenes: powder (76%	The gel feedstock was subjected to solvent extraction	230-240ºC	1st stage: 260ºC, 1ºC/min, 4 h	Nitrogen,	Tensile strength 400 MPa, Modulus 70 GPa	Saad et al. (2022)

Feedstock	Thermal/chemical modification	Melt spinning	Stabilization	Carbonization	Results	Reference
asphaltenes) and gel (22% asphaltenes)	with n-pentane to increase the asphaltene content		2nd stage: 350ºC, 5ºC/min, 2 h	1st stage at 500ºC for 30 min 2nd stage at 800ºC 30 min		
Bitumen-derived asphaltenes separated by solvent deasphalting	Pre-treatment with organic solvent (toluene)	240-260ºC	Pre-stabilization in HNO_3 for 5-10 min. Stabilization at 250-350ºC for 2-3 h	Nitrogen, 1st stage at 500ºC 2nd stage at 1500ºC for 1.5 h	Yield: 49.69% Tensile strength: 1,130 MPa, Modulus 71 GPa	Al Bari et al. (2023)

With an asphaltene content between 14 and 17 wt.% (Gray 2015; Gray 2019), and a production of 2.6 million barrels per day, Alberta oil sands bitumen has the potential to become the principal supplier of ACF. It is estimated that between 4.12 and 6.86 million barrels of bitumen per year would be enough to supply the asphaltenes required to meet the world's demand for carbon fiber (Meisen 2017; Baritto et al. 2023c). Currently, asphaltenes from bitumen oil sands are stockpiled or used as a low-value fuel, therefore it is difficult to assign a commercial value. Some reports assumed the cost of asphaltenes to be between \$44/t (sold as carbon) (Stantec Consulting Ltd. 2018) and \$650/t (sold as asphalt binder) (Zhou et al. 2021). In any case, the low cost of asphaltenes represents a competitive advantage over the expensive PAN (\$3,300-\$5,000/t) (Gill et al. 2016) as a carbon fiber precursor. Besides the economic potential, producing ACF generates environmental benefits. The cradle-to-gate greenhouse gas (GHG) emissions from the production of ACF were estimated by the authors to be 16.2 kg CO_2eq/kg CF, which is equivalent to 8.91 kg CO_2 eq-per kg of asphaltene used as precursor (for a 55% process yield) and 68.7% fewer GHGs than those from the production of PAN-CF (Baritto et al. 2023c). In addition, using asphaltenes to produce carbon fiber diverts such material away from combustion uses. Carbon in asphaltenes remains sequestered within the carbon fibers and is not released (Zhou et al. 2021).

Because of the low technology readiness level of the ACF production process, there is limited data available on the production cost of ACF. This information is critical to assess the advantages of using asphaltene as a low-cost precursor over PAN or non-petroleum raw materials. Based on the price of asphaltene sold at a market coal price, and on a very rough estimation of capital and operation costs, Stantec Consulting Ltd. (2018) presented a business case for the production of bitumen-derived ACF in Alberta. Arya (2020) estimated a production cost of \$5.03/kg CF using capital and operation costs available for PAN-CF production and an asphaltene-carbon fiber conversion efficiency of 45%. These studies make the idea of bitumen-derived ACF production compelling; however, they were based on generic assumptions and are not process-specific. In a recent study, Al Bari et al. (2023) presented an economic and environmental assessment of ACF, based on their own laboratory-scale data. They estimated a production cost of $6.64/kg for a 2,000 tonnes per year line. However, the capital cost estimate was based on PAN-CF lines rather than more suitable equipment for ACF. Also, the effect of the plant size on the production cost was not assessed in that study. Bisheh and Abdin (2023) discussed the market potential of bitumen-derived ACF as an alternative to other fiber-reinforced composites. In the analysis, the authors assumed an ACF production cost lower than PAN-CF and Kevlar fiber, and comparable to glass fiber, however, no details were provided. More detailed cost estimation is required to determine the potential profitability of this activity.

To bridge the gap in the economics of the production of ACF, in this study, a techno-economic assessment of the production process was performed. The specific objectives of the research were to:

- Develop a process model for production of asphaltene-based CF;
- Conduct techno-economic assessment using the process model to estimate the cost of asphaltene-based CF;
- Estimate the production cost of asphaltene-based carbon fiber, using Alberta’s oil sands bitumen as a case study;
- Perform sensitivity and uncertainty analyses to identify key parameters and provide a probable range of production costs;
- Compare the estimated production cost with that of carbon fibers made of different precursors.

8.2 Method

Figure 8-1. presents the framework for this study. The process modeling step includes the description of the reference process to produce ACF. For each unit operation in the process, the material and energy inputs and outputs were identified, and a process model was developed to complete the material and energy balances. The outputs of this stage are material flows, consumable requirements, and electricity and natural gas consumption. With that information, the equipment for the production plant were sized and the batch size and the number of units required to satisfy a given capacity were calculated. The next step was to calculate the capital and operations costs and then the production cost through a discounted cash flow (DCF) analysis. Finally, the relevant inputs and the probable range of production costs after considering uncertainties in the model were identified.

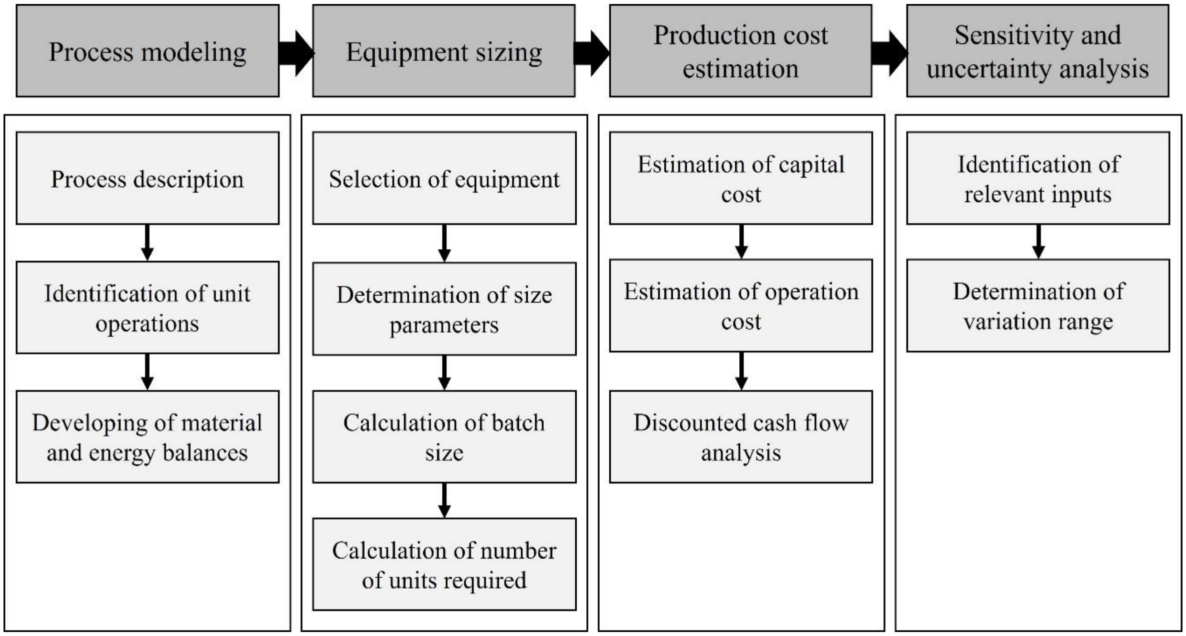

Figure 8-1. Framework for the techno-economic assessment of ACF production

8.2.1 Process modeling

The feedstock to produce carbon fiber is bitumen-derived solid asphaltene. The asphaltene separated from bitumen through standard industrial processes, such as solvent deasphalting, is suitable for the reference process (Chen 2021), but to produce powder-like asphaltene, a higher solvent-to-feed ratio than that currently used in commercial operations is needed (Montoya Sánchez and de Klerl 2016; Turunga 2017). Solid asphaltene can be produced using partial upgrading technologies like selective extraction of asphaltenes (SELEX-Asp), Hi-Q®, and BituMax™ (Keeson and Gieseman 2018). Bohnert and Bowen (2014) presented a method to produce carbon fiber from solid asphaltene obtained through heavy-oil upgrading, thus this type of feedstock does not present a technical constraint.

The reference process considered in this study is based on published laboratory-scale studies and on comparisons with pitch-CF and PAN-CF production processes. The process to produce ACF is shown in Figure 8-2. and comprises the following: thermal pre-treatment of asphaltene, melt spinning, pre-stabilization, stabilization, carbonization, surface treatment, sizing, and winding. The green fibers, i.e., fibers pre-stabilization, are not able to support their weight and therefore cannot be extended and transported through the entire process using drive rollers. Thus, a semi-batch process is required to produce ACF. The operations from thermal pretreatment to carbonization are performed in batches, while those from surface treatment to winding are performed in a continuous process. The process conditions assumed in this study are presented in Table 8-2.

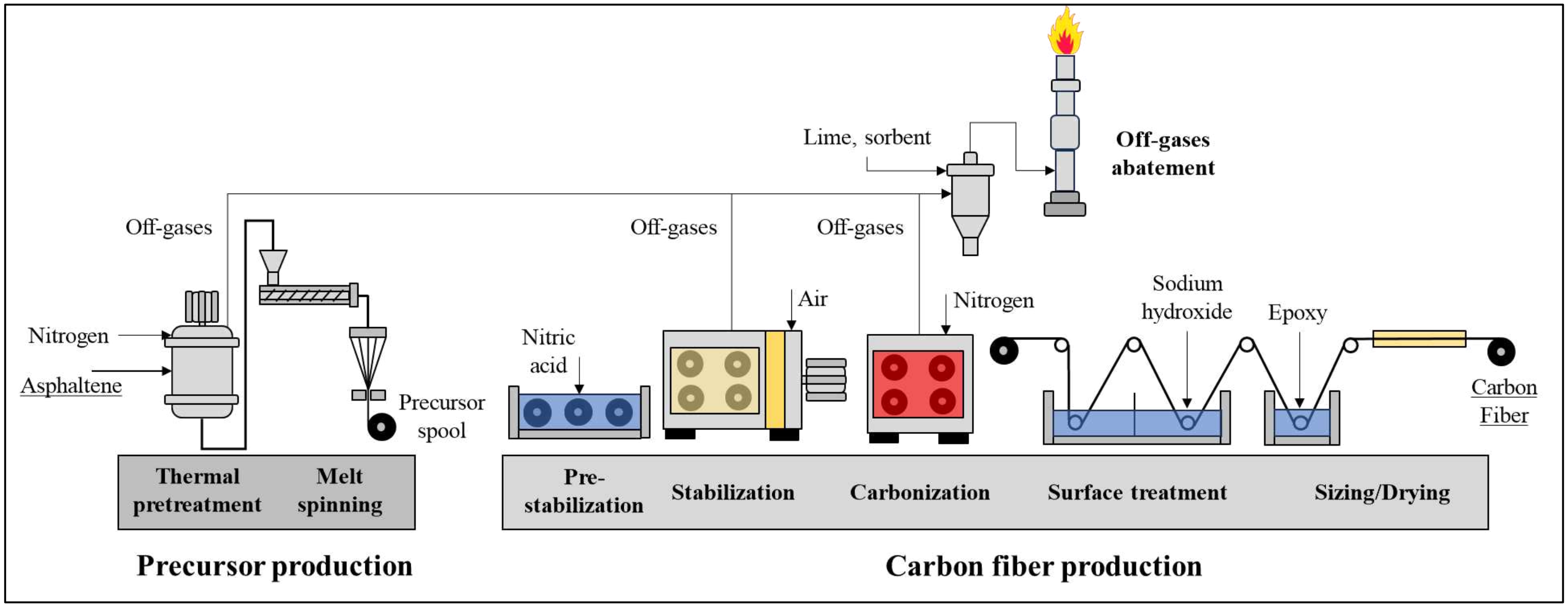

Figure 8-2. Reference ACF production process used in this study

The objective of thermal pretreatment is to remove volatile materials and increase the softening point of asphaltene (Leal and Penaloza 2002; Ni et al. 2019; Qin et al. 2019; Zuo et al. 2021b). The solid asphaltene is melted under pressure in a nitrogen atmosphere. The process conditions of the downstream operations, as well as the mechanical properties of the resulting ACF, depend on the temperature and time of the thermal pretreatment. The optimal combination of temperature and duration, as presented by Zuo et al. (2021a), was considered. Also, agitation of the asphaltene during thermal pretreatment was included. In pitch-CF production, agitation ensures uniform heating and avoids the formation of a two-phase melted pitch (isotropic and mesophase) that makes fiber spinning difficult (Aldosari et al. 2020). It was assumed that agitation would be also required in the production of ACF.

The melted asphaltene is spun into green fibers at a temperature according to the pretreatment conditions. The melt spinning was considered because it is the preferred method for spinning pitch (Morgan 2005), and it is used in asphaltene-based processes as well (Leal and Penaloza 2002; Ni et al. 2019; Qin et al. 2019).

The green fibers tend to fuse during heating for stabilization. To avoid this issue, a pre-stabilization step is included (Zuo et al. 2021b). Soaking the fibers in HNO_3 at room temperature for about 10 minutes promotes the addition of oxygen and the release of hydrogen, increasing the softening point of the fibers and thus circumventing fusing during stabilization (Leistenschneider et al. 2021; Zuo et al. 2021a). This approach has been proven in the production of pitch-CF (Vilaplana-Ortego et al. 2003).

The pre-stabilized fibers are stabilized in an air atmosphere and then carbonized in a nitrogen atmosphere. In the experimental studies of Chen (2021) and (2021a); Zuo et al. (2021b), different combinations of temperature (150 to 350°C) and time (0.25 to 24 h) were used in the stabilization operation. Low temperatures and long times produced highly brittle carbon fibers that were hard to manipulate without fracturing. Conversely, flexible fibers were obtained at high temperatures and short times. For the reference process used in this study, a combination of 250°C and 6 h was selected because after thermal pretreatment at 300°C, the mechanical properties of the ACF were the highest among those obtained by Zuo et al. (2021a). Variations in those parameters was considered through sensitivity and uncertainty analysis. According to Chen (2021), the higher tensile strength of the resulting ACF is obtained with one carbonization stage at a high temperature. It was assumed that the surface treatment, sizing, and winding operations performed at a commercial scale for the production of PAN-CF are valid for ACF. Details of these operations are provided by Morgan (2005) and Ellringmann et al. (2016).

In the experiments done by Zuo et al. (2021a), the cumulative weight losses after thermal pretreatment, stabilization, and carbonization were 10.7 wt.%, 14.5 wt.%, and 60.2 wt.%, respectively. This means 0.398 kg of carbon fiber is produced per kilogram of raw asphaltene fed to the process. In the experimental studies by Leistenschneider et al. (2021) and Zuo et al. (2021b), the process yield improves to about 0.50 kg CF/kg asphaltene and is expected to reach 0.60 CF/kg asphaltene after optimizing the process. In this study, it was assumed a process yield of 0.55 kg CF/kg asphaltene as the base case. This yield value was used to scale cumulative weight losses reported by (Zuo et al. 2021b).

The tensile strength of ACF obtained through this process is between 500 and 2,500 MPa, while the elastic modulus is between 25 and 125 GPa (Leistenschneider et al. 2021; Zuo et al. 2021a; Zuo et al. 2021b). The lower and upper bounds of the ranges correspond to fibers with diameters of 5 and 3μm, respectively. These mechanical properties are comparable to those obtained using similar feedstocks and production processes, as observed in Table 8-1. It can be said, thus, that the process and product considered in this study are representative of the current development state of ACF.

The mechanical properties of ACF obtained so far are lower than PAN-CF's (tensile strength between 3,000 and 7,000 MPa and elastic modulus between 200 and 500 GPa for commercial grade (Mirdehghan 2021)) but greater than aluminum's. The tensile strength of ACF is greater than steel's, but with about half the elastic modulus. ACF can still be used in structural applications, especially as a filler material for which low modulus and strength carbon fibers are suitable materials (Mirdehghan 2021). Besides as a structural material, ACF could be used to make functional composites such as thermal insulation and electrodes for supercapacitors (Bisheh and Abdin 2023). In addition, the elastic modulus of ACF could be increased by implementing a graphitization step at temperatures about 3,000°C (Chen 2021). Further research in this field is required.

Table 8-2. Process operating conditions to produce ACF

Operation	Process condition	Value	Reference
Thermal pretreatment	Temperature	350°C	Zuo et al. (2021b)
	Residence time	2 h	
	Cumulative weight lost	8%	
Spinning	Temperature	220°C	Zuo et al. (2021b)
Pre-stabilization	Temperature	25°C	Chen (2021), Leistenschneider et al. (2021)
	Time	10 min	
	Acid concentration	17%	

Operation	Process condition	Value	Reference
Stabilization	Temperature	250ºC	Zuo et al. (2021b)
	Residence time	6 h	
	Cumulative weight lost	10.8 wt.%	
Carbonization	Temperature	1,500ºC	Chen (2021)
	Residence time	2 h	
	Cumulative weight lost	45.0 wt.%	

The process conditions shown in Table 8-2 were used to develop a spreadsheet-based model to generate the material and energy balances of each operation in the process. The feedstock requirement was calculated from the overall yield of the process, and the consumable consumption was estimated based on assumptions and analogies with the PAN-CF and pitch-CF production processes. The energy balance of the thermal pretreatment, stabilization, and carbonization considered the latent heat of the feed and the operation atmosphere, the energy of reaction, the energy carried by the off-gases, and heat losses. The composition of the off-gases was estimated from experimental studies of similar operations using bitumen-derived asphaltene as the feed. Heat for thermal pretreatment is provided by the combustion of natural gas, while heat for carbonization is provided by electric heaters. Usually, heat for carbonization is also provided by electricity; however, natural gas is preferred in locations where its price is competitive (Witting et al. n.d.), like Alberta.

The energy required to heat the feed to the operating temperatures for melt spinning and pre-stabilization was calculated. The specific energy consumption in surface treatment and sizing was retrieved from published sources. The electricity consumption of the main equipment was also considered. The main assumptions for developing the process model are presented in Appendix E (Table E-1).

8.2.2 Equipment sizing and scaling

It was assumed that commercial heat treatment walk-in ovens and pyrolysis furnaces are suitable for stabilization and carbonization operations, respectively. For surface treatment and sizing, standard equipment similar to that used to produce pitch-CF and PAN-carbon fiber were considered. Regarding gas abatement, a flare system is deemed suitable. Unlike PAN-CF production, hydrogen cyanide is not expected in the off-gases, but sulfur compounds, i.e., sulfur dioxide and hydrogen sulfide, are found in the gases that evolve during the thermal treatment of bitumen asphaltenes (Moschopedis et al. 1978). For this reason, a means of removing those compounds from the off-gases is required. Wet scrubbing with lime and adsorption by iron oxides for the removal of SO_2 and H_2S, respectively, were considered in this study. Table E-2 in Appendix E lists the equipment and sizing approach. For a given plant capacity, and assuming the weight of each carbon fiber spool, the rate of spool production was calculated. Then the number of spools required by each batch operation based on the duration of the operation was calculated. This information, along with the size of a single piece of equipment, was used to calculate the number of pieces of equipment for stabilization and carbonization.

8.2.3 Production cost estimation

The production cost of ACF was calculated through the DCF method. Appendix A presents an overview of the method. Future cash flows were calculated based on capital and operation costs, which were estimated from the results of the process model. Additional economic assumptions are presented in Table 8-3.

Table 8-3. Economic assumptions for the techno-economic assessment

Item	**Value**
Plant lifetime	20 years
On-stream factor	0.80
Operating cost escalation	2%
Internal rate of return	10%

Table E-3 in Appendix E presents the assumptions for the estimation of the capital cost. The inside battery limit (ISBL) was assumed to be the cost of the installed equipment, while the rest of the cost components were calculated as factors of the ISBL. For a given plant capacity, the published cost curves were used to get the cost of common equipment, like vessels and agitators. For specialized equipment, such as spinning machines, ovens, and furnaces, manufacturers were consulted. If not provided by the reference, a free-on-board (FOB) factor of 10% was used to estimate the delivered cost and a 40% delivered cost factor to estimate the installed cost (Peters et al. 2003). When necessary, the equipment cost was updated to the Chemical Engineering Plant Cost Index (CEPCI) of 776.9 (2021 USD) (Maxwell 2022). A location factor was included to consider the freight and installation cost in Fort McMurray, Canada. Table E-4 in Appendix E presents a summary of the data used for the estimation of the ISBL investment.

Table E-5 in Appendix E shows the input data and assumptions for the estimation of the operation cost. As mentioned above, asphaltene has limited commercial applications so it is difficult to appraise. The projected price of asphaltene considered in the Stantec report (Stantec Consulting Ltd. 2018) was used as the feedstock cost in this study. For the consumable cost, bulk prices were used provided by vendors, and for the utility cost, the price of natural gas and electricity for industrial customers in Alberta was considered. Labor cost was calculated based on the number of operators, required shifts, and labor rate. The remaining cost components were estimated through factors suggested in published sources.

8.2.4 Sensitivity and uncertainty analysis

In this study, the Regression, Uncertainty, and Sensitivity Tool (RUST) (Di Lullo et al. 2019) was used for sensitivity and uncertainty analysis. The Morris method was implemented to study the sensitivity of the model output, i.e., the ACF production cost, to 37 inputs. The inputs considered were process conditions and yield, equipment performance, consumables and energy consumption, prices, raw material cost, material properties, operational conditions, product characteristics, and economic assumptions (Table E-6 to Table E-9 in Appendix E). Among the considered inputs, some modifications were included to the reference model envisioned by researchers to improve the mechanical properties of the produced ACF. The sensitivity analysis allows us to identify the inputs with greater influence on the model output and then to narrow the number of variables included in the Monte Carlo simulation conducted to study the effect of the uncertainties on the estimated production cost. Appendix B presents an overview of both the Morris method and Monte Carlo simulation.

8.2.5 Base case and scenarios

For the base case, a plant capacity of 3,000 tonnes of ACF per year was considered. Other authors used a similar capacity in economic assessments of PAN-CF and pitch-CF production (Ellringmann et al. 2016; Nunna et al. 2019; Das and Nagapurkar 2021). For the current state of the technology, producing a tow with a high number of filaments represents a technical challenge. For purpose of this study, a tow size of 12,000 filaments (12k) was assumed, which is a typical size for both PAN-CF and pitch-CF (Compositesword.com 2016). Finally, a spool weight of 6 kg was assumed, because it is found in the market (Toray N.d.) and can be safely handled by one operator.

Several different scenarios were considered to study how the production cost departs from the base case. The production cost for different plant capacities, tow sizes, and spool weights were calculated. Table 8-4 presents the definition of scenarios.

Table 8-4. Scenario description

Scenario	**Plant capacity (t/y)**	**Tow size**	**Comments**
Base case	3,000	12k	Typical capacity; medium tow; the weight of commercial spools.
Scenario 1	500 – 4,000	12k	Capacity range includes the capacity of existing pitch- and PAN-CF plants.
Scenario 2	3,000	1k-100k	Tow size range includes small and large tows.

8.3 Results and discussion

8.3.1 Results for the base case

8.3.1.1 Material and energy balances

For a 3,000 t/y ACF plant, a feed of 5,455 t/y asphaltene is required. For a 6 kg-carbon fiber spool, about 71 spools should be produced per hour to satisfy the plant capacity. The raw asphaltene is fed to the thermal pretreatment unit for a batch process with a cycle time of 2 hours. For 7,000 hours of operation per year, the annual number of batches is 3,500. To satisfy the required production flow, the pretreated asphaltene must be spun at a rate of 717 kg/h. The green fibers are pre-stabilized in nitric acid and fed into the stabilization oven. The cycle time of the stabilization operation is 6 hours; therefore, 1,000 batches are run per year considering a setup time of one hour. The batch size is 500 spools. The stabilized fibers are then carbonized. For a cycle time of 2 hours plus one hour of setup time, 2,330 batches per year, with a size of 214 spools, are run. Finally, the carbon fibers undergo a surface treatment and sizing. After those operations, about 2 wt.% is gained thanks to the epoxy coating incorporated into the fibers. Table 8-5 presents the material balance of each operation, in terms of kg of produced ACF. This table includes the consumable requirement.

Table 8-5. Material balance for the base case

Operation	Stream	Input (kg/kg CF)	Output (kg/kg CF)
Thermal pre-treatment and melt spinning	Raw asphaltene	1.82	
	Nitrogen	0.29	
	Green fiber		1.67
	Off-gases:		
	Hydrogen		7.7×10^{-5}
	Carbon dioxide		0.05
	Carbon monoxide		0.01
	Hydrogen sulfide		6.4×10^{-3}
	Methane		0.04
	Ethane		0.03
	Propane + Butane		1.0×10^{-3}
	Ethylene + Propylene		2.6×10^{-4}
	Nitrogen		0.29

Operation	**Stream**	**Input** **(kg/kg CF)**	**Output** **(kg/kg CF)**
Pre-stabilization and stabilization	Green fiber	1.69	
	Nitric acid	0.02	
	Air	133	
	Stabilized fiber		1.62
	Off-gases:		
	Water		0.94
	Carbon dioxide		0.68
	Carbon monoxide		0.43
	Sulfur dioxide		0.08
	Oxygen		28.8
	Nitrogen		102
Carbonization	Stabilized fiber	1.62	
	Nitrogen	6.00	
	Carbon fiber[a]		1.00

Operation	Stream	Input (kg/kg CF)	Output (kg/kg CF)
	Off-gases[b]		
	Carbon		0.07
	Nitrogen		6.03
	Hydrogen		0.03
	Sulfur		0.08
	Oxygen		0.41
Surface treatment and sizing	Carbon fiber	1.00	
	Electrolyte (NaOH) make up	0.05	
	Epoxy	0.02	
	Sized carbon fiber		1.02
	Electrolyte (NaOH) lost		0.05
Off-gases abatement	SO_2 in off-gases	0.0002	
	Lime	0.04	
	Sorbent	0.03	

Operation	**Stream**	**Input** **(kg/kg CF)**	**Output** **(kg/kg CF)**
	Process water	0.02	
	Gypsum		0.092

a. Plant capacity is based on the throughput of the carbonization operation.

b. Elemental composition.

Some assumptions made to complete the material balance could affect the cost estimate and should be revisited once more information is available as the technology advances towards a high technology readiness level (TRL). The process yield used in this study is supported by published experimental studies; however, the consumables' rates were assumed from the standard PAN-CF production process and other proxy data because they depend on the operation of equipment that is not yet available for ACF production. Specifically, the flow of air and nitrogen used to set the atmosphere in the stabilization and carbonization operations significantly affect the energy consumption, and therefore the operation cost. The influence of those inputs on the production cost was investigated through sensitivity and uncertainty analysis (presented in Section 8.3.1.3). The composition of the off-gases from thermal-pretreatment, stabilization, and carbonization was also assumed using proxy processes as references because it has not been included in the studies on ACF production. Such information is critical for the estimation of GHG emissions from the process , but also to size the off-gases abatement system and quantify the natural gas requirement to incinerate the off-gases, if needed. Finally, the batch size and number of required units were defined based on the rated capacity of existing equipment that were deemed suitable for ACF stabilization and carbonization. Those parameters affect the capital investment, energy consumption, and labor; therefore, they should be taken into consideration to design tailored equipment and a process flowsheet for ACF production.

About 24.8 kWh per kg of ACF is required. Of this, 53.3% corresponds to electricity and 46.7% to natural gas. These values were obtained by completing the energy balance of the operations. Stabilization dominates energy consumption, mainly because of the elevated flow of air required. Most of the energy consumption in the stabilization operation is in the form of natural gas to provide heat to the process. The consumption of electricity is for the air blowers (fans).

Carbonization is the operation with the second highest energy consumption, in this case in the form of electricity. Besides the energy required for the process, heating the purge nitrogen contributes significantly to the amount of energy needed for carbonization. Melt spinning is third in energy consumption, thanks to the high demand for electricity to spin the fibers. Because the nominal power requirement per position was used, further research considering the specific case of melted asphaltene should be done. The heat required for the thermal pretreatment and melt spinning is low compared with stabilization and carbonization because of the relatively low temperature of those operations. The electricity required for surface treatment and sizing accounts for 28.3% of the total consumption. It was assumed that the same operations used for PAN-CF are valid for ACF and retrieved the energy consumption from a manufacturer. Given the important contribution of those operations to the total energy consumption, further research on the conditions tailored to ACF is required. Table 8-6 presents the energy consumption by each operation in the ACF production process per kg of produced carbon fiber.

Table 8-6. Energy consumption for the base case

Operation	**Electricity (kWh/kg CF)**	**Natural gas (kWh/kg CF)**
Thermal pre-treatment	0.262	0.427
Melt spinning	1.46	0.202
Pre-stabilization and Stabilization	0.059	11.0
Carbonization	4.41	-
Surface treatment	3.44	-
Sizing	3.60	-

8.3.1.2 Production cost

The summary of cost and revenue for the base case (30,000 t/y capacity, 12k) is presented in Table 8-7. The capital cost for this plant capacity was estimated at $110.6 M. Of this, 43.3% corresponds to the ISBL. Melt spinning is the most capital-intensive operation, with 64.8% of the ISBL. This is a consequence of the number of spinning positions required to meet the production flow. The number of positions depends on the number of spools produced per hour, the spool mass, and the spinning rate. For the conditions considered in this study, thirty-one positions are required, hence the high equipment cost. Surface treatment (14.2%) and sizing (12.6%) are the operations with the second and third highest equipment costs. Similar equipment to that used to produce PAN-CF was assumed. Given the important contribution of these operations to the ISBL, more suitable and less expensive equipment should be considered.

The equipment cost of the carbonization operation represents 5.9% of the ISBL. That said, the relatively low cost of furnaces, large cycle time, and limited capacity of the equipment require six units to fulfill the plant capacity. Thermal pretreatment requires 1.7% of the ISBL. Because of the high viscosity of the melted asphaltene, the power consumption of the agitator is elevated, increasing the equipment cost. The contribution of each of the remaining operations is less than 1% of the ISBL. Stabilization is worthy of further comment. Assuming that commercial heat treatment walk-in ovens are suitable for the oxidation of the green fibers, only one unit is needed to accommodate the required batch size, resulting in a low-capital operation. Additional costs for the manufacturing and installation of special spools were not considered. Special spools may be required for uniform oxidation, as suggested by Morgan (2005), Barnett (1959), and Redick (1986).

Table 8-7. Summary of costs and revenue at a capacity of 3,000 tonnes of ACF per year

Cost/revenue	**Value**
Capital cost (Million dollars)	110.6
ISBL	47.9
OSBL	19.1
Engineering	13.4
Contingency	20.1
Working capital	10.1
Operation cost[a] (Million dollars per year)	14.9
Feedstock	0.24
Consumable cost	3.54
Electricity	2.12
Natural gas	1.12
Labor	2.09
Facility dependent	4.21
Plant overhead	1.66
Revenue[b] (Million dollars per year)	30.4

a. In year one of operations.

b. To break even.

The operation cost in year one is $14.9 M. The consumable cost is 23.7% of the operation cost and is driven by the high requirement of nitrogen in the carbonization furnaces. The combined contribution of the most expensive materials (NaOH, HNO_3, epoxy, sorbent, and lime) is about

6.4% of the consumable cost. The utility cost represents 21.6% of the operation cost, with 14.1% corresponding to electricity and 7.47% to natural gas. Labor contributes 13.9% to the operation cost. Because of the highly manual nature of the production process, specifically to load and unload the spools in and out of the ovens and furnaces, the labor requirement is considerably high compared with a continuous operation. Facility-dependent costs represent 28.1% of the operation cost and plant overhead 11.1%. These cost components are high because they were estimated as factors of the ISBL, labor, and revenue, resulting in relatively elevated costs. Finally, the cost of the asphaltene fed to the process is roughly 1.6% of the operating cost. The low feedstock cost is one of the advantages of this precursor over PAN.

The ACF production cost calculated through the techno-economic analysis is \$10.16/kg CF; this is the selling price to break even in the plant life span. Figure 8-3. presents the breakdown of the production cost. Capital cost, at 42.6%, is the cost component with the highest contribution to the production cost. As discussed above, labor cost has an important contribution because of the type of production process implemented. Its share is 8.0% of the production cost. Facility-dependent costs represent 16.1% of the total cost. Because these costs depend on the ISBL, their share is relatively high. Utilities represent 12.4% of the production cost, with 8.1% corresponding to electricity and 4.3% to natural gas. The share of the consumable cost is 13.5%. The overhead cost mainly depends on the labor cost, hence its share of 6.3%, surpassing feedstock (1.1%) costs, whose shares are low because of asphaltene's relative zero value.

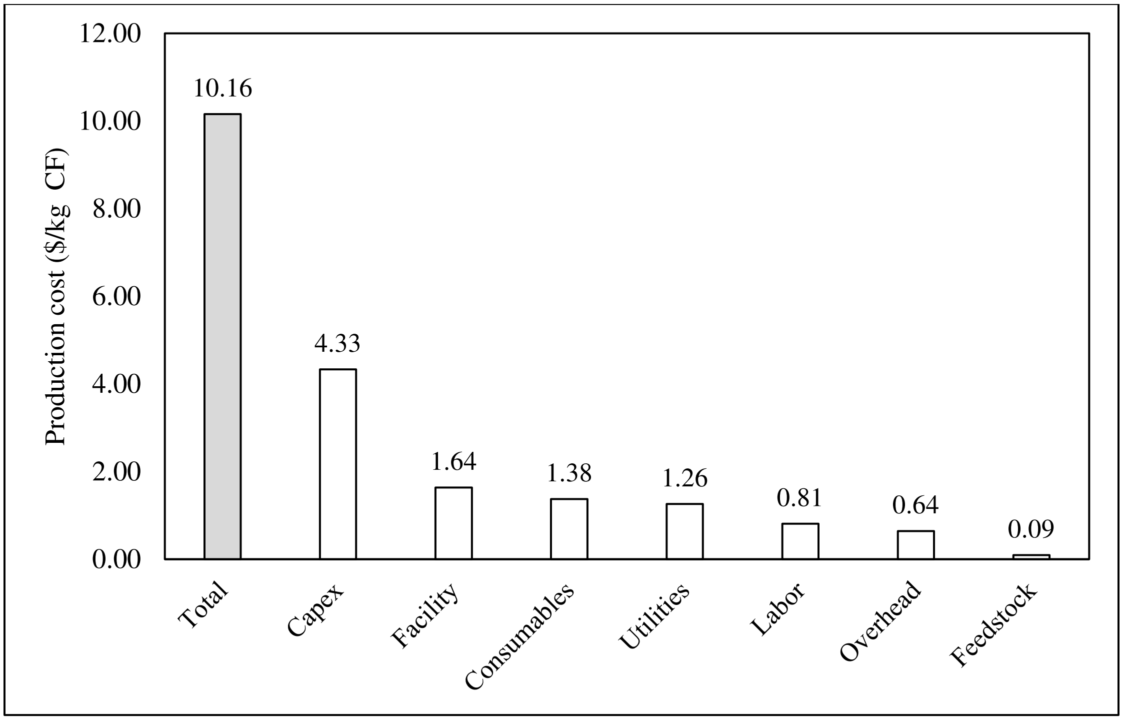

Figure 8-3. Production cost breakdown

8.3.1.3 Influence of uncertainties on the production cost

Figure 8-4. shows the sensitivity analysis results from the Morris method. The horizontal axis represents the range of the calculated production cost as the input changes from the low bound value to the high bound value, while the vertical axis shows the standard deviation of this variation. The model output, i.e., ACF production cost, is highly sensitive and exhibits non-linear behavior with respect to those parameters located at the upper right of the plot. According to the results, the output model is more sensitive to the stabilization time. This input is used to calculate the batch size required to match the production flow; therefore, it modifies the number of units, required labor, energy consumption and air requirement for stabilization, and the spinning positions that define the cost of that equipment. Because of these multiple interactions, along with a stepwise change in the number of units with the batch size, the production cost exhibits a high non-linearity with respect to the stabilization time. The same can be said about the setup time of stabilization, which affects the batch size of that operation. Reducing stabilization time has been a subject of interest in many studies because that operation is generally the most time-consuming, irrespective of the carbon precursor (Morgan 2005). Some of the techniques that have been successfully implemented to reduce the stabilization time of carbon fiber from different precursors, and that could be investigated for the production of ACF, include using pressurized air flow for stabilization of pitch-based carbon fiber (<1 h; mechanical properties are maintained) (Shimanoe et al. 2019), a combination of electron beam and thermal oxidation for the stabilization of PAN- and pitch-based carbon fiber (Park et al. 2016) (2 h; improved tensile strength), and continuous stabilization at high heating rates and under tension of lignin-based carbon fiber (1 h; improved tensile strength) (Bengtsson et al. 2022). Also, the available data on ACF production has been developed at laboratory scale. After process optimization, the stabilization time should be reduced. Zuo et al. (2021a) investigated the effect of stabilization conditions on the mechanical properties of ACF with and without thermal pretreatment. They concluded that the best mechanical properties are obtained in fibers pretreated at 300°C and oxidated at 300°C for 1 h. After incorporating these conditions into the model developed in this study, the production cost for the base case was estimated to be \$7.35/t.

As expected, the carbon yield also has a great influence on the production cost, because the throughput of the plant is directly related to that input. The nitrogen required to set the atmosphere of the carbonization operations defines the energy consumption in the furnaces, and as mentioned earlier, the nitrogen consumption in this operation strongly drives the consumable cost. For these reasons, the nitrogen consumption in carbonization and the nitrogen price are among the inputs for which the model's output is more sensitive.

Besides the mentioned inputs, it was found that the model output is moderately sensitive to the energy cost (electricity and natural gas prices and efficiency of the electric heater in furnaces), inputs affecting the energy balance of the stabilization operation (air requirement and off-gases temperature), economic inputs that modify the ISLB (purchased-delivered and installation costs), and parameters used for sizing equipment (spool diameter and spinning speed).

The sensitivity analysis provides stakeholders with a prioritized list of parameters that should be optimized to obtain a competitive ACF production cost. Also, the identified sensitive inputs drive decision-making processes at different stages throughout the development of the technology and scaling the process up to commercial operation. In terms of practical implications of the sensitivity analysis, the minimization of the stabilization time should be a top priority for researchers working on process development at low TRL; optimizing the air flow through the stabilization ovens is a concern for engineers designing tailored equipment for ACF production; since the setup time is a sensitive input in the considered batch process, planning the plant layout should include lean manufacturing principles to reduce idle time and work in progress; the consumption rate and price of nitrogen would drive the decision on purchasing this consumable from suppliers or producing it in situ; and the natural gas price would determine whether natural gas or electricity is used as a heat source for stabilization, and, even at a high management level, the location of the plant.

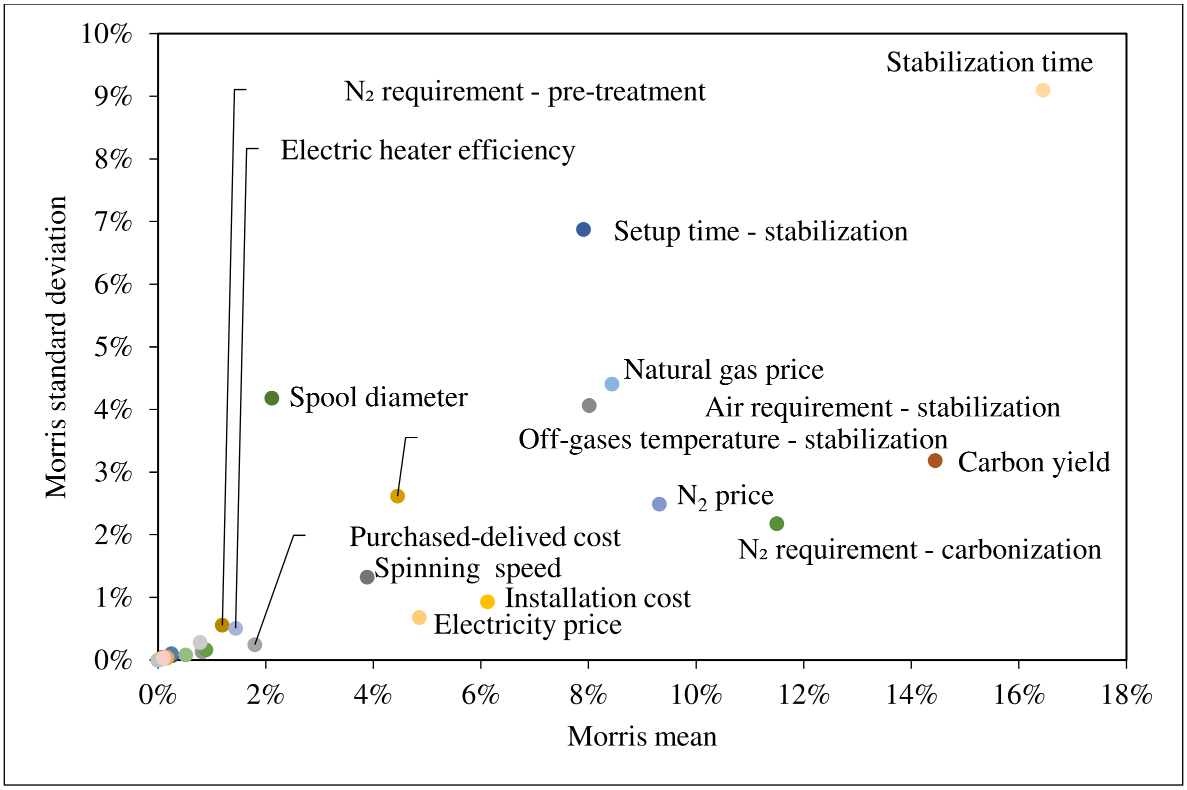

Figure 8-4. Morris plot for the sensitivity analysis of ACF production cost on selected inputs

The results of the sensitivity analysis were used to narrow the number of inputs used for the uncertainty analysis. Monte Carlo simulations were carried out using the inputs identified as relevant according to the Morris plot. The mean value of the production cost is $12.92/kg CF with a standard deviation of $1.31/kg CF.

Figure 8-5. presents the frequency histogram and the percentile distribution of the results. Considering the uncertainties in the inputs, the production cost ranges between $9.31 and $19.08 per kg of ACF, with a median of $12.92/kg CF. However, about 90% of the results lies in the intervals with class marks between 11.50 and 14.80 $/kg CF, while 60% of the results are located between 12.60 and 13.70 $/kg CF. The base case result is near the low end of the range because modifications were considered that increase the cost of the process (e.g., higher carbonization temperature, lower spinning speed, lower overall yield, larger stabilization time) among the uncertainties. Despite the increase in the expected production cost, it is still lower than PAN-CF and slightly higher than the target cost for automobile applications.

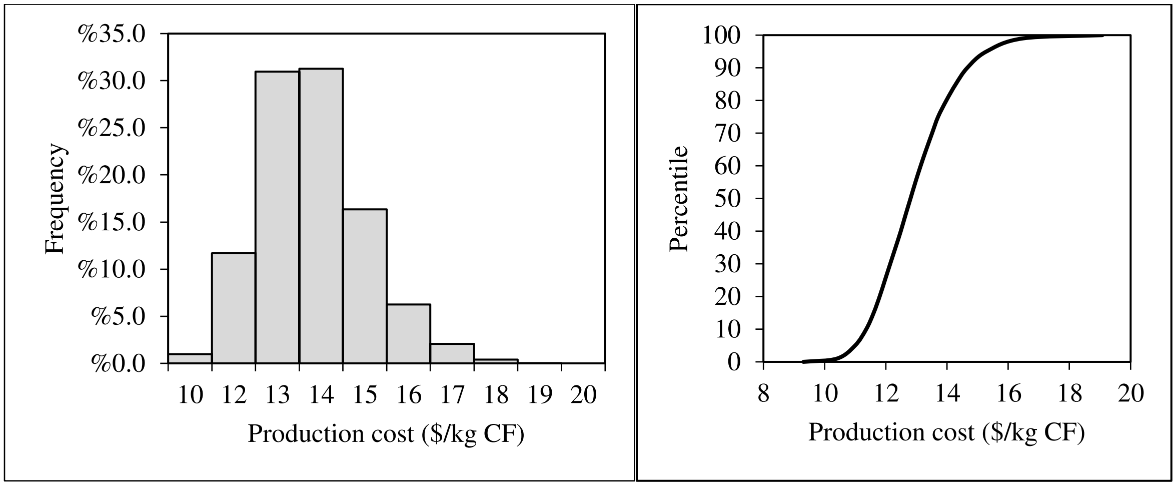

Figure 8-5. Results of the Monte Carlo simulation: Left: frequency histogram. Right: percentile distribution

8.3.2 Scenarios

Figure 8-6. presents the breakdown of the production cost for different plant capacities. A reduction in production cost with increases in the plant capacity was observed. The cost varied significantly for capacities below 1,000 t/y; negligible change was seen above 2,500 t/y. For any capacity, the capital cost is the greatest contributor with about 41-46% of the production cost, exhibiting economies of scale with a scale factor of 0.605. The facility-related cost, which directly depends on the capital cost, is second highest. The utility cost tends to decrease with capacity increases; however, specific energy consumption increases after the incorporation of any additional unit for stabilization or carbonization. As capacity increases, and more spools are loaded into the additional units, the specific energy consumption decreases until an additional unit is required to satisfy a greater capacity. The labor cost varies significantly because the number of operators is not proportional to the number of units. The additional units for greater capacities does not require additional laborers, and so costs are lower. The overhead depends on the labor cost; thus, they follow the same trend.

Considering the current market price of PAN-CF as a reference ($20/kg CF), the production of ACF is potentially profitable for plant capacities greater than 890 t/y. However, for the target considered by automotive applications, i.e., $10/kg CF, the lower profitable plant capacity would be around 3,060 t/y.

Increasing the plant capacity produces an economic benefit but carries some operational complexity that could increase the production cost; this was not reflected in the developed model. For example, the batch size in the stabilization operation increases from 95 spools for a 2,000 t/y plant to 167 spools for a 3,500 t/y, while in the carbonization operation it goes from 143 spools to 250 spools. Such an increase of spool handling in a highly manual batch process could lead to a longer setup time in both stabilization and carbonization operations. In the scenario analysis, a constant setup time was considered for all plant capacities because labor increased accordingly. However, should the setup time increase by ten minutes, the production cost increment would be $0.80/t for a 3,500 t/y plant. A half-hour delay would represent an extra cost of $2.31/t for the same plant capacity.

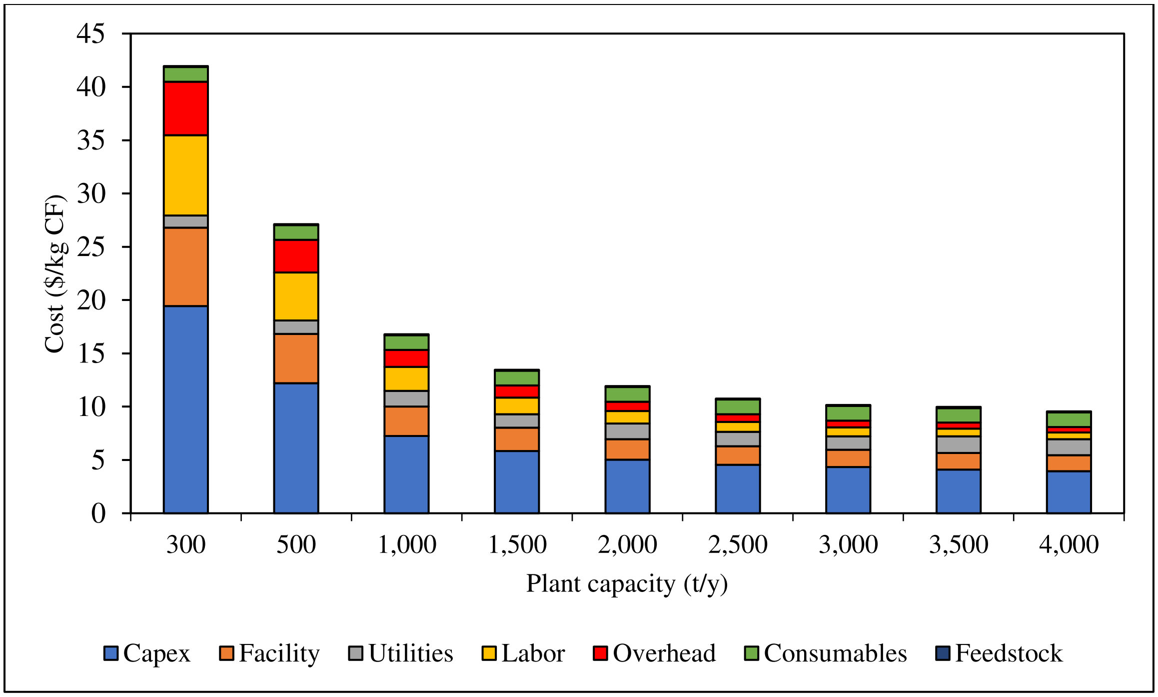

Figure 8-6. Production cost vs. plant capacity. Scenario 1: tow size: 12k

Production cost decreases as tow size increases, as depicted in Figure 8-7.. The cost reduction is mainly because fewer spinning positions are required to match the production flow as tow size increases. For a fixed spool weight, a larger tow size means a shorter filament and thus a shorter spinning time per spool. The results suggest that typical tow sizes for PAN- and pitch-CF (e.g., 12k, 50k, 100k) are feasible for ACF, with production costs below the current PAN-CF market price.

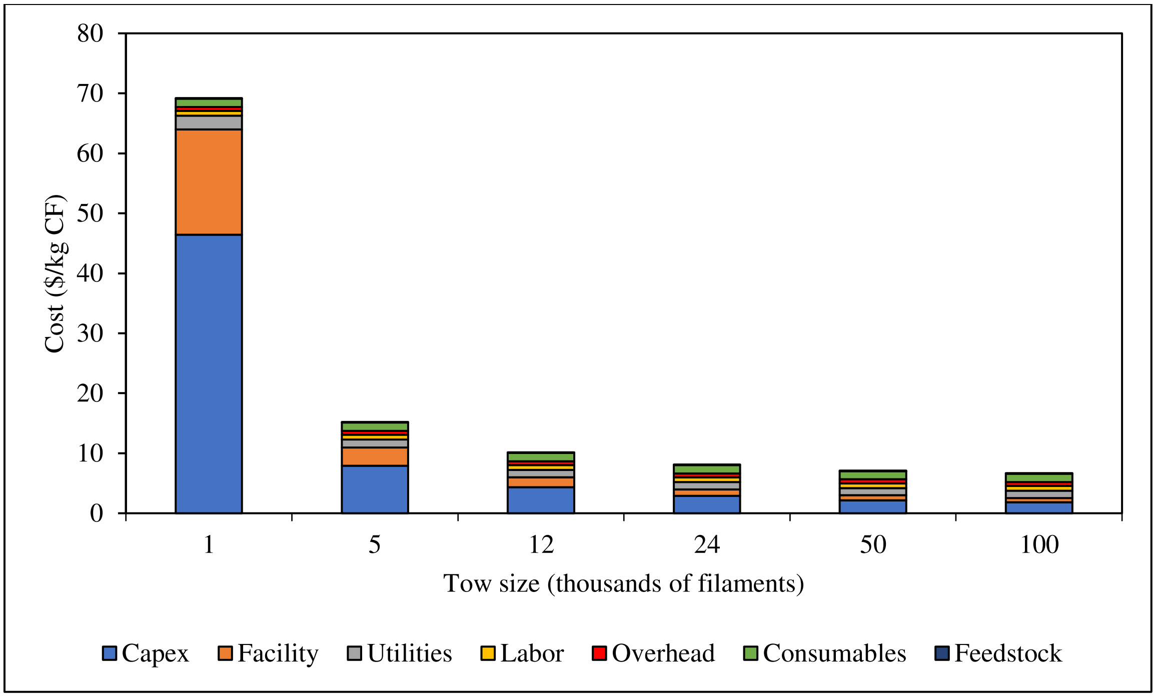

Figure 8-7. Production cost vs. tow size. Scenario 2: plant capacity: 3,000 t/y

8.3.3 Comparison with other studies

One of the biggest challenges of techno-economic assessments of low TRL technologies is the lack of operational data for cost model validation (van der Spek et al. 2017). With the aim of validating the developed model, the output can be compared with the results of independent studies on similar technologies (Kobos et al. 2020). Given the very early stage of development of bitumen-derived ACF, cost data of the production process is limited. The study by Al Bari et al. (2023) was selected for comparison because it is the only study published to date that includes a detailed production cost estimation. In addition, the reference process conditions used by those authors, as well as the final product, are like those considered in this study, therefore the comparison is pertinent. For a 2,000 tonnes per year plant Al Bari et al. estimated a production cost between \$5.00/kg CF and \$8.90/kg CF, with a base value of \$6.64/kg CF. For the same conditions (2,000 t/y, 25 years of operation) the model developed in this study estimates a production cost of $11.85/kg CF for a 12k tow and $8.92/kg CF for a 48k tow. Given the similarities in process conditions and yield, the difference in the cost estimation is likely due to different approaches to modeling the production process at a commercial scale. The main discrepancy between the studies is Al Bari et al.'s assumption of a continuous process. Capital and labor costs tend to be higher in batch processes. Other differences between the studies that could affect the production cost are the estimation of air and nitrogen flow to set the atmosphere in the stabilization and carbonization operations, the exclusion of an off-gases abatement system in Al Bari et al. (2023) study, and the calculation of miscellaneous costs like labor, maintenance, and plant overhead. Figure 8-8. presents a comparison of the cost estimate by Al Bari et al. (2023) and the cost estimate obtained with the developed model in this study. The plant capacity is 2,000 t/y and the plant life was assumed in 25 years. For their base case, Al Bari et al. (2023) obtained a production cost of $6.64/t, which is lower than the $11.85/t for a 12k tow and $8.95/t for a 48k tow, estimated in this study. Table 8-8 shows the differences between the assumptions made in both studies, which could explain the divergence in the cost estimates. Despite the differences, the cost estimates are relatively close to each other when compared with PAN-CF cost and even overlap under certain conditions. The progressive elaboration of the cost estimate will lead to a more accurate figure as more information about the process is known and pilot-scale data is available.

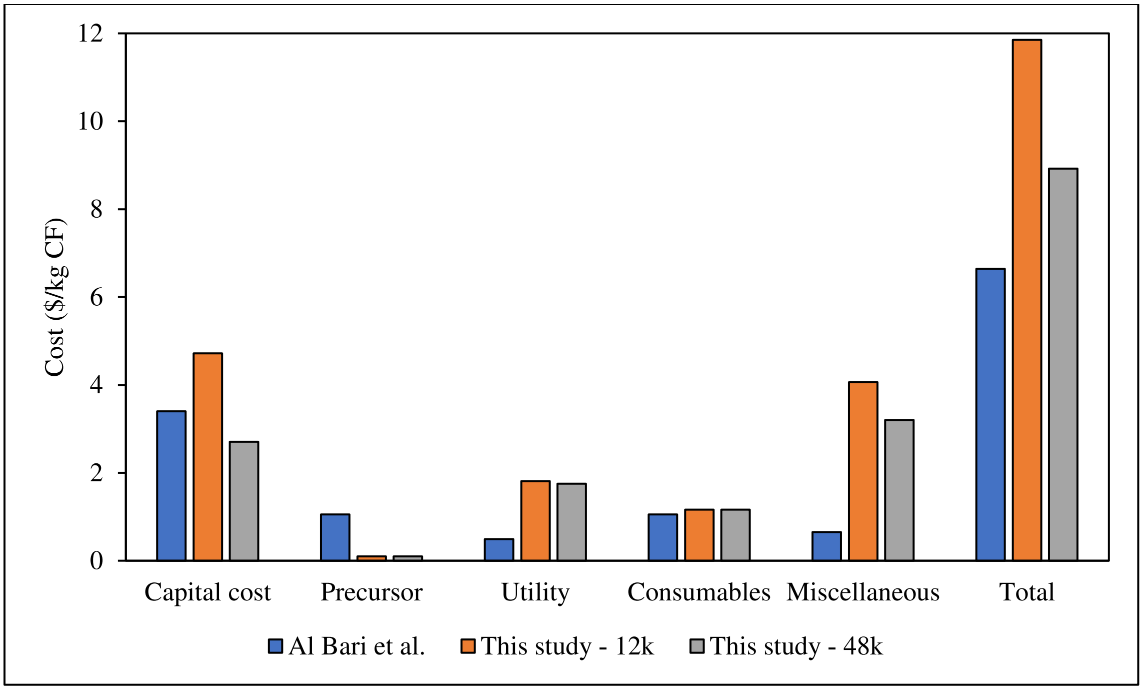

Figure 8-8. Cost estimate comparison between the study by Al Bari et al. (2023) and this study

Table 8-8. Comparison of the main assumptions for cost estimation

Cost component	**Al Bari et al.**	**This study**
Capital cost	Considered a continuous process and equipment similar to those used for PAN-CF production. Continuous stabilization ovens and carbonization	In the batch process considered in this study, stabilization and carbonization equipment do not require moving parts to drive the fiber or gas seals to

Cost component	Al Bari et al.	This study
	furnaces are highly specialized equipment, thus their high cost. That equipment, along with the drivers and rollers required to transport the fiber throughout the production line, accounts for 43.4% of the capital cost estimated.	preserve the inner atmosphere, as the continuous equipment do (Morgan 2005), therefore the expected lower cost. The elevated capital cost for a 12k tow is because the number of spinning positions required, as explained in Section 8.3.1.2
Precursor cost	Used a conservative approach and assigned to raw asphaltene the value of asphalt binder, a finished product with high demand.	Raw asphaltene is considered a residue of bitumen deasphalting, with no commercial application and a near-zero value (Stantec Consulting Ltd. 2018).
Utility	Air flow in stabilization oven and nitrogen flow in carbonization furnaces at laboratory scale were used	The air flow in commercial heat treatment ovens was used to estimate the energy consumption to heat the

Cost component	Al Bari et al.	This study
	to calculate the energy to heat up the process atmospheres at industrial scale. For continuous equipment, such energy consumptions are significant (55% in stabilization ovens and 13% in carbonization furnaces , therefore the utility cost could have been underestimated (Harper International 2013). Electricity required to drive the recirculation fans in stabilization ovens was not included in the inventory. Fans consume about 34% of the total energy input to the ovens (Fakhrhoseini 2018)	oxidating atmosphere of the operation. In the case of nitrogen flow to set the carbonization atmosphere, typical nitrogen-to-carbon fiber mass ratio in commercial furnaces were used (see Table E-1 in Appendix E). Rated power of fans in commercial heat treatment ovens was used to estimate electricity consumption by fans in stabilization ovens.

Cost component	Al Bari et al.	This study
Consumables	Besides nitrogen for carbonization, this study included solvent for asphaltene dilution and acid for pre-stabilization.	Included nitrogen for pre-treatment and carbonization, acid for pre-treatment, epoxy for sizing, sorbent for H_2S cleaning, $Ca(OH)_2$ for SO_2.
Miscellaneous	Included labor, overhead, maintenance, and ancillary costs. It was assumed 20% of total cost.	Included labor, overhead, insurance, and building rent. Each component was estimated as indicated in Appendix E (Table E-5).

8.3.4 Comparison with other precursors

To compare the estimated production cost with that of carbon fiber based on other precursors, the total cost was split into precursor cost (i.e., thermal pretreatment and melt spinning) and carbon fiber cost (i.e., pre-stabilization, stabilization, carbonization, surface treatment, and sizing). The raw material cost (asphaltene) was allocated to the precursor cost. The comparison is shown in Figure 8-9..

It was observed that the production cost of ACF is potentially lower than that of PAN-CF. As expected, there is a reduction of the cost component corresponding to precursor manufacturing, but also the manufacturing of the carbon fiber is projected to be cheaper in the case of the asphaltene precursor. This reduction is a combination of the following:

- Lower energy consumption as well as the use of natural gas to provide heat in the stabilization operation.
- The use of a flare system to clean the off-gases. The generation of HCN is not expected, according to the composition of the evolved gases from thermal processing of bitumen asphaltenes; therefore, a thermal oxidizer is not required. This equipment is responsible for the great contribution of the gas abatement to the PAN-CF production cost.
- The cost of the equipment assumed for stabilization and carbonization is very low compared with that used for PAN-CF. Although different equipment costs through a contingency budget and in sensitivity and uncertainty analyses were considered, a progressive elaboration of the present cost estimation is recommended, as dedicated equipment becomes available for the process.

Coal pitch and lignin represent low-cost alternatives to PAN as a precursor. Asphaltene is potentially a cheaper option than coal pitch, mainly because of the lower precursor cost. The overall yield (40% coal pitch vs. 55% asphaltene) and raw material cost ($700/tonne coal-pitch vs. $44/tonne asphaltene) drive the difference in the production cost of those precursors. Compared with lignin, the precursor cost of ACF is considerably higher. Both processes have similar overall yields, but a cheaper raw material is an advantage for lignin as a precursor. Polyolefin has been included as a reference since the development of this material as a precursor is in the very early stage and no estimates of production cost at a large scale are available.

Should the mechanical properties of ACF be improved with no significant additional cost, asphaltenes would have a competitive advantage over other precursors, not only in the automotive industry but in building and construction, and medical protheses and implants industries, as stated by Bisheh and Abdin (2023).

8.4 Conclusions

The production cost of asphaltene-based carbon fiber was estimated through the development of a data-intensive techno-economic model. Oil sands bitumen was considered as the source of asphaltene, and a process based on thermal pretreatment, melt spinning, stabilization, and carbonization was considered. The capital and operation cost were determined from the material and energy balances of each operation in the process. The ACF production cost was estimated using the developed techno-economic model.

At a plant capacity of 3,000 tonnes of carbon fiber, a tow size of 12,000 filaments, and a spool weight of 6 kilograms, the production cost is \$10.16 per kg of carbon fiber. This estimate is lower than the current production cost of PAN-based carbon fiber and is close to the target cost for massive adoption in the automobile industry. Production costs decrease with plant capacity and tow size. A combination of these parameters would be selected based on market specifications.

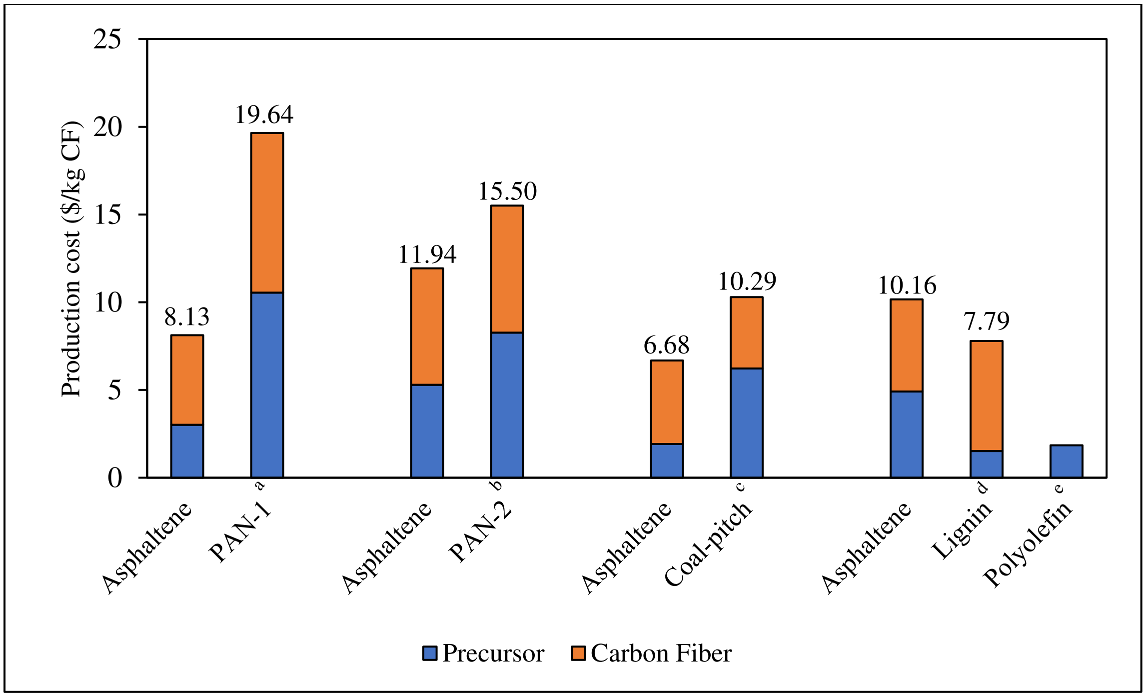

a. Capacity: 3,000 t/y; tow size: 24k; PAN data from Ellringmann et al. (2016).

b. Capacity: 2,000 t/y; tow size: 12k; PAN data from Nunna et al. (2019).

c. Capacity: 3,750 t/y; tow size: 50k; Coal-pitch data from Das and Nagapurkar (2021).

d. Asphaltene data corresponds to the base case of this study. Lignin data is from Chien-Wei Chen (2014).

e. Polyolefin data is an average of costs provided by (Chien-Wei Chen 2014) and Warren (2010).

Figure 8-9. Comparison of ACF production costs with those of carbon fiber based on other precursors

The production cost estimated through the developed model is more sensitive than the other inputs to the stabilization time, therefore optimization of this process variable to obtain a low-cost carbon fiber at large-scale production is recommended. Other inputs with great influence on the model output are the carbon yield, nitrogen consumption in the carbonization furnace, and the air requirement in the stabilization ovens. According to these findings, designing tailored equipment to optimize the flows of air and nitrogen should impact the production cost of ACF, therefore it should be a subject of interest even at an early stage of technology development. The raw material cost, e.g., asphaltene price, has negligible influence on the ACF production cost, which keeps the economy of the process separate from the price of crude oil.

The results of this study are not definitive because the technology to produce ACF is in a very early stage of development. The mechanical properties of ACF should be improved before the market scenario for this product and its potential advantage over other precursors are evaluated. However, the results can be used by researchers, oil sands operators, and policymakers to drive decision-making process throughout the different phases of technology development, from optimization of process conditions to equipment design and shaping projects on asphaltene-based carbon fiber production. The techno-economic assessment of ACF production should be revisited to improve accuracy as the technology progresses and more information becomes available.

Chapter 9: Estimation of life cycle GHG emissions of asphaltene-based carbon fibers derived from oil sands bitumen[13]

9.1 Introduction

Alberta's oil sands are among the world's largest oil deposits. Bitumen, the type of oil found in oil sands, is primarily used to produce liquid fuels such as gasoline and diesel. Bitumen production is increasing; about 2.6 million barrels per day were produced in 2016, and production is projected to reach 4.5 MMb/day by 2040 (Canada Energy Regulator 2018). Despite the increase in production, strict regulations shrink sales margins and hinder the survival of the oil sands industry. In addition, the plan to decarbonize the economy is expected to lower the market demand for combustion products in favor of renewable and low-carbon energy sources. These challenges pose the need to diversify the use of bitumen beyond fuel combustion by producing valuable non-combustible products while maintaining other oil sands products' qualities and competitiveness.

Asphaltene-based carbon fiber (ACF) is a non-combustible product that could have major mid- to long-term market potential and has been the focus of studies on technical suitability and large-scale production (Meisen 2017; Stantec Consulting Ltd. 2018). Asphaltenes are a heavy fraction of bitumen and crude oil not soluble in n-heptane (Redelius 2011). They consist of polar components from condensed aromatic and naphthenic rings. Processed asphaltene can produce a carbon fiber with high modulus and strength. The produced carbon fiber is a plausible raw material for manufacturing lightweight structural materials and other reinforced products. Furthermore,

---

[13] A version of this chapter has been published as M. Baritto, A.O. Oni, A. Kumar. Estimation of life cycle greenhouse gas emissions of asphaltene-based carbon fibers derived from oil sands bitumen. Sustainable Materials and Technologies 2023. 36:e00627.

asphaltenes are cheaper than conventional phenolic and resin-based carbon products, and they have higher carbon concentrations than pitch because they contain no naphthenic acids. Currently, about 90% of carbon fiber manufactured worldwide is from polyacrylonitrile (PAN) and the rest is from petroleum pitch. PAN is produced through a chain of processes that depends on conventional crude oil or natural gas-based processes using either propylene or propane as a raw material. Processing these raw materials with ammonia and air produces acrylonitrile (ACN), a feedstock for PAN production. PAN-based carbon fiber (PAN-CF) supports reinforced composites using carbon fiber. Its carbon fiber is superior to steel and aluminum. The tensile strength and weight are five times and one-fourth of steel's, respectively. However, PAN-CF is made from expensive raw materials. As mentioned earlier, asphaltene is cheap, and its raw material is readily available in Alberta. Asphaltene-based carbon fiber could be a promising alternative to PAN-based carbon fiber.

The technology for the production of bitumen-derived ACF fiber is in the early stages of research and development (Alberta Innovates 2021). Because of its low technology readiness level (TRL), there is limited data available on the life cycle GHG emissions from its production. A few studies on carbon fiber based on asphaltenes derived from different sources bring insight into the production process (Leal and Penaloza 2002; Ni et al. 2019; Qin et al. 2019) and show that the general process is essentially the same, regardless of the origin of the asphaltene: asphaltene modification, melt spinning, stabilization, and carbonization. Moreover, the process resembles that of producing pitch-based carbon fiber, which is currently at a commercial scale. Recently, a series of studies on the production at laboratory scale of carbon fiber using asphaltene derived from Alberta bitumen was published (Chen 2021; Leistenschneider et al. 2021; Zuo et al. 2021a; Zuo et al. 2021b). For this type of ACF, the main difference with the pitch-based carbon fiber process is the pre-stabilization step through acid soaking. This step is not included as a standard operation for commercial pitch-based carbon fiber but is a proven method (Vilaplana-Ortego et al. 2003). Here, processes covered in previous works are summarized. Chen patented a process to produce ACF (Chen 2021). The process steps include melting asphaltene solids in a sealed vessel, spinning melted asphaltenes to fabricate green fibers, stabilizing the green fibers, carbonizing the stabilized green fibers, and optionally graphitizing carbonized fibers. Leistenschneider et al. studied the acid pre-stabilization of precursor fibers and found that an oxidizing acid is required to retain the fiber structure during stabilization. They concluded that the higher the acid concentration, the smaller the fiber diameter, which leads to better mechanical properties of the carbon fiber (Leistenschneider et al. 2021). Zuo et al. demonstrated that the thermal pretreatment of asphaltenes improves the melt spinnability of green fibers and established a relation between the temperature of the thermal pretreatment and the diameter and mechanical properties of the carbon fiber (Zuo et al. 2021b); they also optimized the oxidation conditions for the stabilization of asphaltene precursor (Zuo et al. 2021a). The literature review is summarized in Table 8-1.

Scaling the process to commercial scale and estimating the GHG emissions from it were not the focus of those studies. Regarding the environmental impact of bitumen-derived ACF, Arya developed a high-level life cycle assessment to estimate the GHG emissions of a carbon fiber plant (Arya 2020). Arya's results showed an ACF GHG emissions value of 29.1 kg CO2/kg CF. However, this result can be misleading because Arya used the emission factors of PAN-based carbon fiber as proxy data to estimate the GHG emissions of ACF production. Furthermore, Arya reported upstream emissions associated with bitumen production and asphaltene separation but did not define the system boundary nor enumerate the unit operations involved in the processes. The accuracy of the reported GHG emissions can be improved by considering the actual process conditions of ACF production. To the best of the authors' knowledge, no other studies on the life cycle GHG emissions of ACF are available in the public domain.

The main purpose of this study is to estimate the life cycle energy consumption and GHG emissions footprint of the production of ACF derived from oil sands bitumen. The specific objectives of this study are to:

- Estimate the GHG emissions from the production of asphaltene-based carbon fiber and perform sensitivity and uncertainty analyses to identify key parameters and provide a probable range of values;
- Estimate the life cycle GHG emissions from a pathway to produce bitumen-derived ACF in Alberta, Canada;
- Compare the life cycle GHG emissions from the asphaltene-pathway with those from a PAN pathway.

9.2 Methods

9.2.1 Pathway description

This section presents a general description of the pathways for carbon fiber production considered in this study. Figure 9-1 shows the stages within each pathway. Details of the stages in the asphaltene pathway are presented below; the PAN pathway process details are in Appendix D.

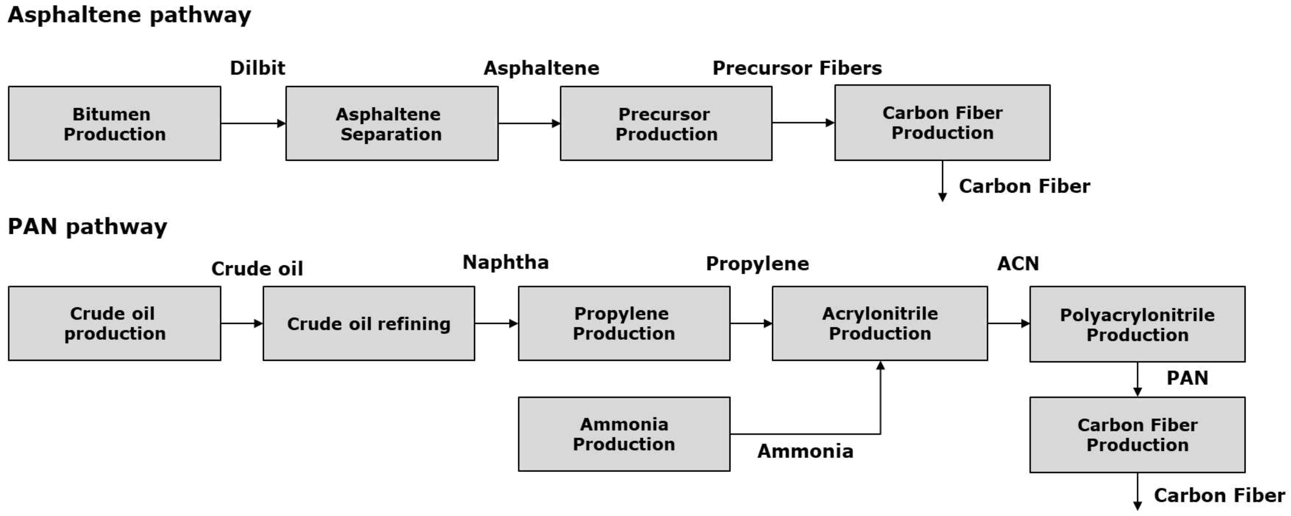

Figure 9-1. Pathways for carbon fiber production

9.2.1.1 Asphaltene pathway

The asphaltene pathway comprises four main processes: the production of bitumen, the separation of asphaltenes from the bitumen, the production of the precursor, and the production of carbon fibers. The technological method adopted, the feedstock used, and the product from each process are summarized in Table 9-1. Precursor and carbon fiber production are considered the foreground processes because they are important for asphaltene conversion into carbon fiber. Bitumen production and asphaltene separation are background processes because their function is to provide the raw material for the foreground processes. All the processes are performed in Alberta, Canada, at a plant capacity of 1,650 t/y, a typical value for a PAN-CF plant (James 2016).

Table 9-1. Processes within the asphaltene pathway

Process	Technology	Feedstock	Product
Bitumen production	SAGD	-	Dilbit
Asphaltene separation	HI-Q	Dilbit	Solid asphaltene
Precursor production	Thermal pretreatment, melt spinning,	Solid asphaltene	Precursor fiber
Asphaltene-based carbon fiber production	Pre-stabilization, stabilization, carbonization	Precursor fiber	Carbon fiber

9.2.1.1.1 Bitumen production

Bitumen is produced by mining or in situ. In both cases, the product is a diluted bitumen (mixed with solvent) called dilbit. Most of the dilbit produced in Alberta is sold to high-conversion refineries and the rest is upgraded into a synthetic light crude oil before being sent to refineries. Most of the dilbit sold directly is produced in situ, while most of the upgraded bitumen comes from mining operations. About 76% of in situ production in Alberta is via steam-assisted gravity drainage (SAGD) (Alberta Energy Regulator 2021). In this study, the production of ACF untied to bitumen upgrading was explored. Therefore, in situ production was considered, specifically by SAGD, as the bitumen production method. In SAGD, one wellbore is used to continuously inject steam into the reservoir and a second to produce bitumen. The hot mixture of water and bitumen is pumped to the surface where it is separated. A suitable diluent, for instance naphtha or natural gas condensate, is added to the mixture to facilitate gravity separation and ease the transportation of the produced bitumen. The separated water is treated and recycled for steam generation. Fuel is required to generate steam for the process, and electricity is used to run pumps, compressors, evaporators, and other equipment. Usually, natural gas is used as fuel for a steam generation; however, part of the produced gas is used to reduce the natural gas requirement. The remaining produced gas is flared.

9.2.1.1.2 Asphaltene separation

Asphaltenes can be separated from bitumen before their transportation to refineries. This practice is called partial upgrading, and its objective is to improve the quality of the bitumen to match the pipeline requirements, reducing, or even avoiding, the use of diluent. Asphaltene is a low-value by-product of the partial upgrading process, and it is usually stockpiled. Using asphaltenes to produce carbon fiber adds value to the bitumen value chain, and it is a solution to stockpiling the by-product. Among the various partial upgrading schemes, one combining visbreaking (Vis) and solvent deasphalting (SDA) was considered for this study. This scheme allows one to produce a transportable deasphalted bitumen while asphaltene is produced. Specifically, the HI-Q Technology developed by MEG Energy was considered because it produces solid asphaltenes that are easier to transport and process than an asphaltene-rich slurry. Dilbit is processed in a diluent recovery unit (DRU). The separated diluent is returned to the production facility, while the bottoms from the DRU are fed to the mild visbreaking unit. Naphtha and light fractions from this unit are sent to an olefin saturation unit. The bottoms are fed to the SDA unit to generate deasphalted oil (DAO) and a solid asphaltene powder, which is the product of interest in this study. BituMax is another technology worth considering for asphaltene separation; it also produces solid asphaltenes.

The main difference between the two technologies is the process sequence. In HI-Q, visbreaking is performed before SDA, while in BituMax the sequence is reversed. Zachariah and de Klerk determined that the yield of solids from the processes is similar, 16.6 wt.% for SDA-Vis and 17.0 wt.% for Vis-SDA based on the fed bitumen mass (Zachariah and De Klerl 2017). The solid asphaltene is used to produce the carbon precursor for ACF production.

9.2.1.1.3 Precursor production

The precursor production process comprises two operations, asphaltene thermal pretreatment in a nitrogen atmosphere and spinning, as explained by Zuo et al. (Zuo et al. 2021b) and Chen (Chen 2021). Carbon fiber production involves pre-stabilization by soaking the spun asphaltene in nitric acid, stabilizing it in air, and carbonizing it in nitrogen. The finishing operations – surface treatment, sizing, drying, and handling – were assumed to be the same as those performed in PAN-based carbon fiber production (Huson 2017). Figure 9-2 shows the reference process for precursor and carbon fiber production.

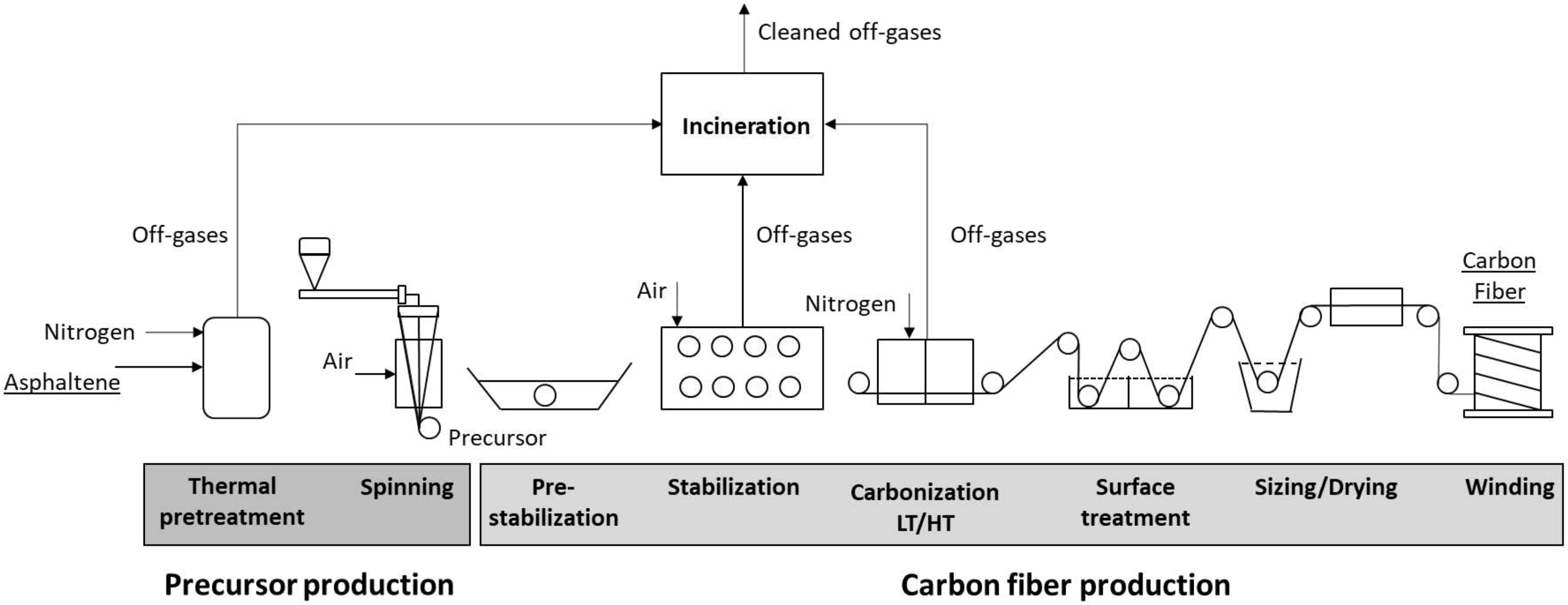

Figure 9-2. Schematic of the asphaltene precursor and carbon fiber production process

9.2.1.2 PAN pathway

The PAN production pathway has seven processes: the production of crude oil, the refining of crude oil to produce naphtha, the production of ammonia, the production of propylene, the production of acrylonitrile (ACN), the production of polyacrylonitrile (PAN), and the production of carbon fiber (CF). The GHG emissions of ammonia production include upstream emissions from producing the natural gas used as feedstock in the process. The technology, feedstock, and product of each process are shown in Table 9-2. The production of PAN and CF was defined as the foreground processes. The other processes in the pathway are considered background processes. All the stages in the PAN pathway are explained in Appendix D.

Table 9-2. The PAN pathway processes

Process	Technology	Feedstock	Product
Crude oil production		-	Crude oil
Crude oil distillation	Atmospheric distillation	Crude oil	Light naphtha
Propylene production	Steam cracking	Light naphtha	Propylene
Ammonia production	Methane steam reforming, Haber-Bosch process	Natural gas, air	Ammonia
Acrylonitrile production	Ammoxidation of propylene	Ammonia, propylene, air	Acrylonitrile

Process	Technology	Feedstock	Product
Polyacrylonitrile production	Suspension polymerization, wet spinning	Acrylonitrile	Polyacrylonitrile
PAN-CF production	Stabilization, carbonization	Polyacrylonitrile	Carbon fiber

9.2.2 Evaluation of life cycle GHG emissions

In this study, the goal of the life cycle assessment is to quantify and compare the GHG emissions from the PAN and asphaltene pathways. The PAN pathway is a mature technology currently used to produce carbon fiber for automotive applications. For this reason, that pathway was set as the baseline for comparison. The scope of this study is a cradle-to-gate analysis, i.e., from raw material production to carbon fiber production before transportation to final use. The functional unit for this study is one kilogram of produced carbon fiber. The purpose is to produce carbon fibers for the manufacturing of vehicle parts. The goal of the analysis is to determine the impact of the resources used by each process on the GHG emissions throughout their life cycles.

For the energy inventory, only the external energy used for the transformation of the feedstock into final products, e.g., electricity and fuel combustion, was considered. The energy contents of the feedstock and by-products were excluded. As far as possible, energy consumption was segregated into electricity and heat. Unless stated otherwise, it was assumed that the grid provides electricity, and the primary heat energy is natural gas. GHG emissions were then estimated using energy consumption data and local emission factors. Process emissions from off-gases were also considered. Emissions associated with process plant construction, equipment maintenance, the production of consumables, additives, and catalysts, and the disposing of wastes and by-products were excluded. For those processes involving co-products and by-products, e.g., crude oil production, refining, and propylene production in the PAN pathway, and bitumen production and asphaltene separation in the asphaltene pathway, the GHG emissions were allocated to the product of interest. Finally, the GHG emissions were reported based on the functional unit (per kg of carbon fiber) using the yield of each process.

Figure 9-3 presents the framework for the estimation of life cycle GHG emissions from both the asphaltene and the PAN pathway. For the asphaltene pathway, the feedstock requirement and energy consumption data for each background process were collected from published studies; for the foreground processes, a spreadsheet process model was developed to quantify energy consumption (Section 9.2.3.1). For the PAN pathway, the feedstock requirement and energy consumption data for all the processes were collected from the existing literature.

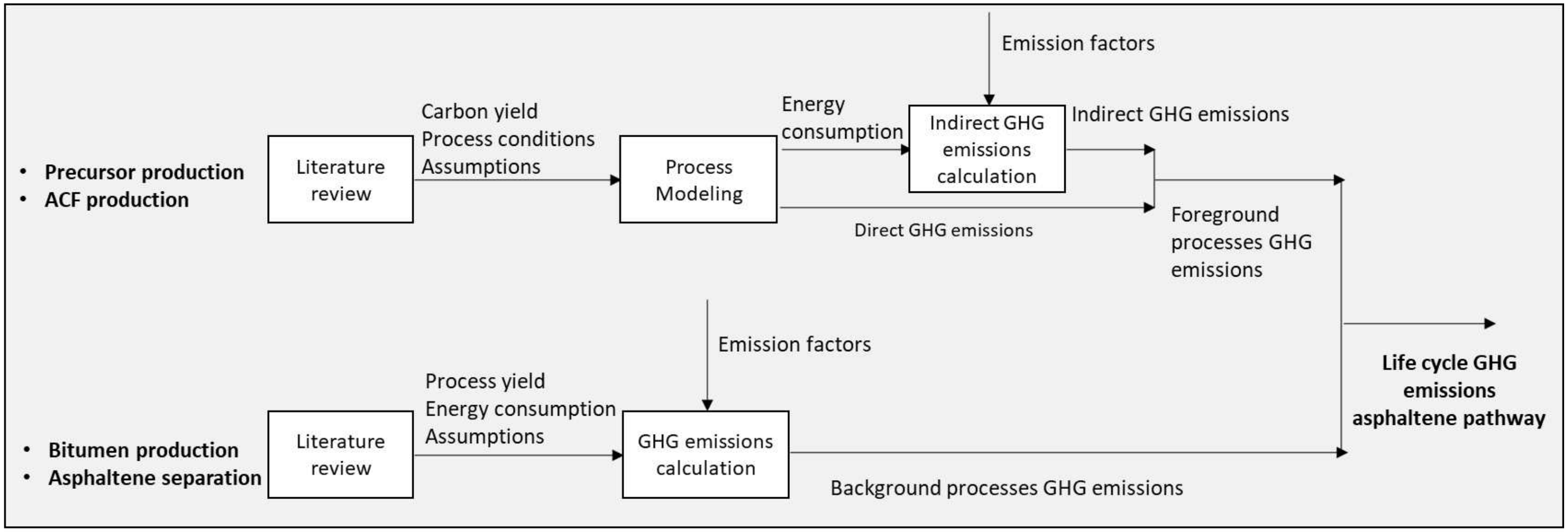

PAN Pathway

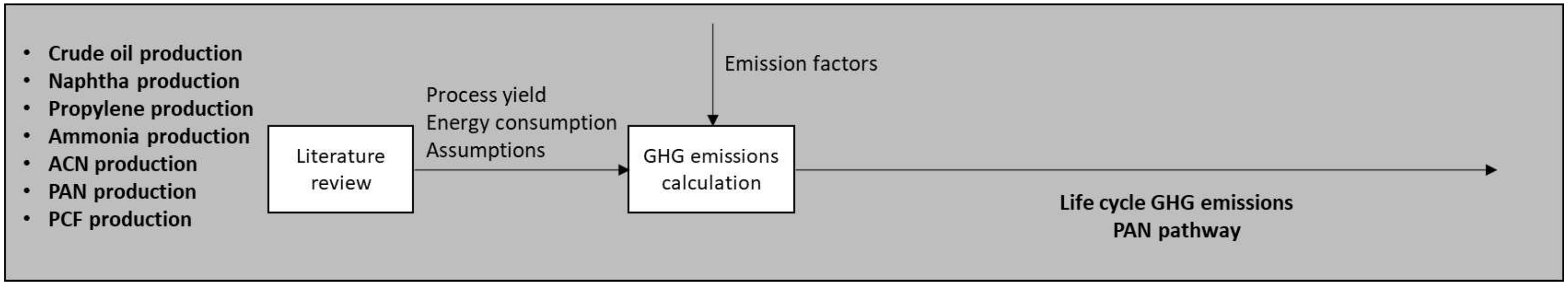

Figure 9-3. Framework for the estimation of life cycle GHG emissions from the asphaltene and the PAN pathways

9.2.2.1 Life cycle GHG emissions of the asphaltene pathway

Figure 9-4 shows the system boundary diagram used to estimate the life cycle GHG emissions from the asphaltene pathway. The emission factors used to estimate the GHG emissions are presented in Table 9-3.

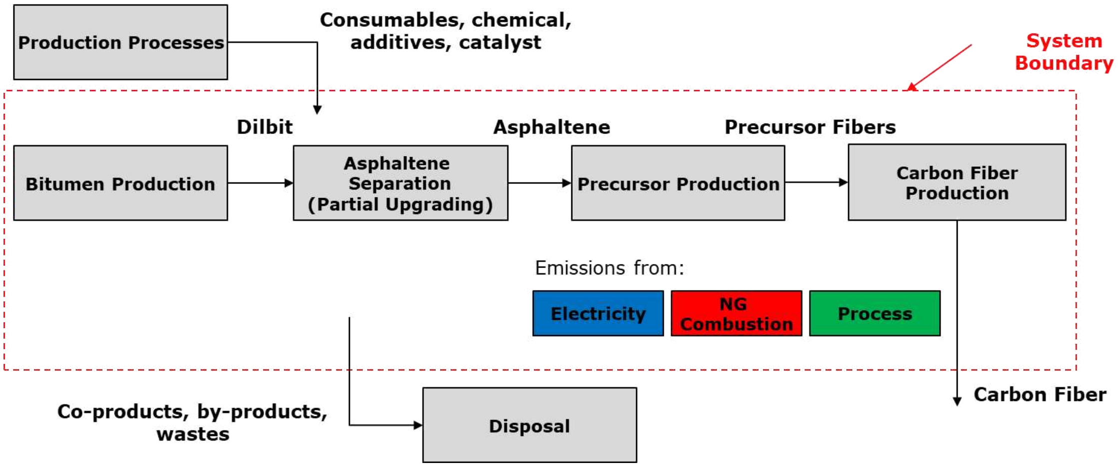

Figure 9-4. System boundary diagram, asphaltene pathway

Table 9-3. Emission factors for electricity production from the grid and the combustion of natural gas, Alberta, Canada

Energy type	Emission factor
Electricity production (grid)	530 kg CO_2eq/MWh
Natural gas combustion	188 kg CO_2eq/MWh[a]

a. Based on 1.954 kg CO_2eq/m^3 (Government of Alberta 2019b) and 10.37 kWh/m^3 (Government of Canada 2015).

Greenhouse gases are emitted from three sources in the in situ bitumen production process: combustion of natural and produced gas to produce steam, electricity production to run equipment, and flaring of produced gas. Figure 9-5 shows the system boundary for bitumen production through SAGD. Our research group colleagues Nimana et al. estimated the energy consumption in the production of bitumen (Nimana et al. 2015a). The produced gas includes the fraction used for steam generation and for flaring. According to Nimana et al., about 40% of the produced gas is flared. The emission factor for the combustion of produced gas was assumed to be the same as that for the combustion of natural gas.

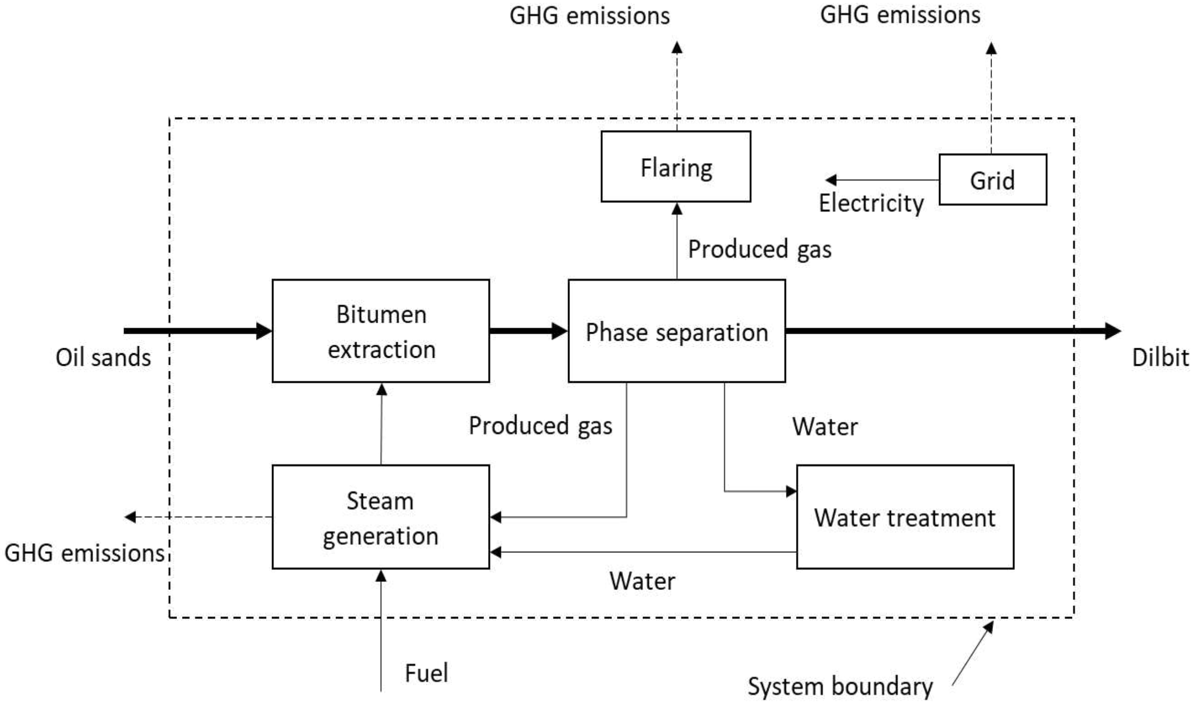

Figure 9-5. System boundary for the bitumen production stage

Figure 9-6 shows the system boundary for the asphaltene separation process. Pacheco et al. estimated the energy consumption of each operation of an HI-Q-like process (Pacheco et al. 2020). Because energy consumption was allocated to the asphaltene-containing streams, the diluent recovery unit (DRU), the visbreaking unit, and the solvent deasphalting (SDA) unit were the focus of the study. Specifically, energy consumption was allocated to the bitumen, bottoms, and asphaltene streams shown in Figure 9-6. The HI-Q process avoids the production of steam by using natural gas as a stripping agent. This natural gas is recovered and used as fuel. Because that energy can be used by any unit operation, including those outside the system boundary of the study, it was allocated to the asphaltene stream using an overall yield. The allocation of energy consumption was made on a mass basis following the method proposed by Wang et al. (Wang et al. 2004) and explained in Appendix D. The allocation weights are shown in Table 9-4. The collected data for the bitumen production and asphaltene separation stage are summarized in Table 9-5.

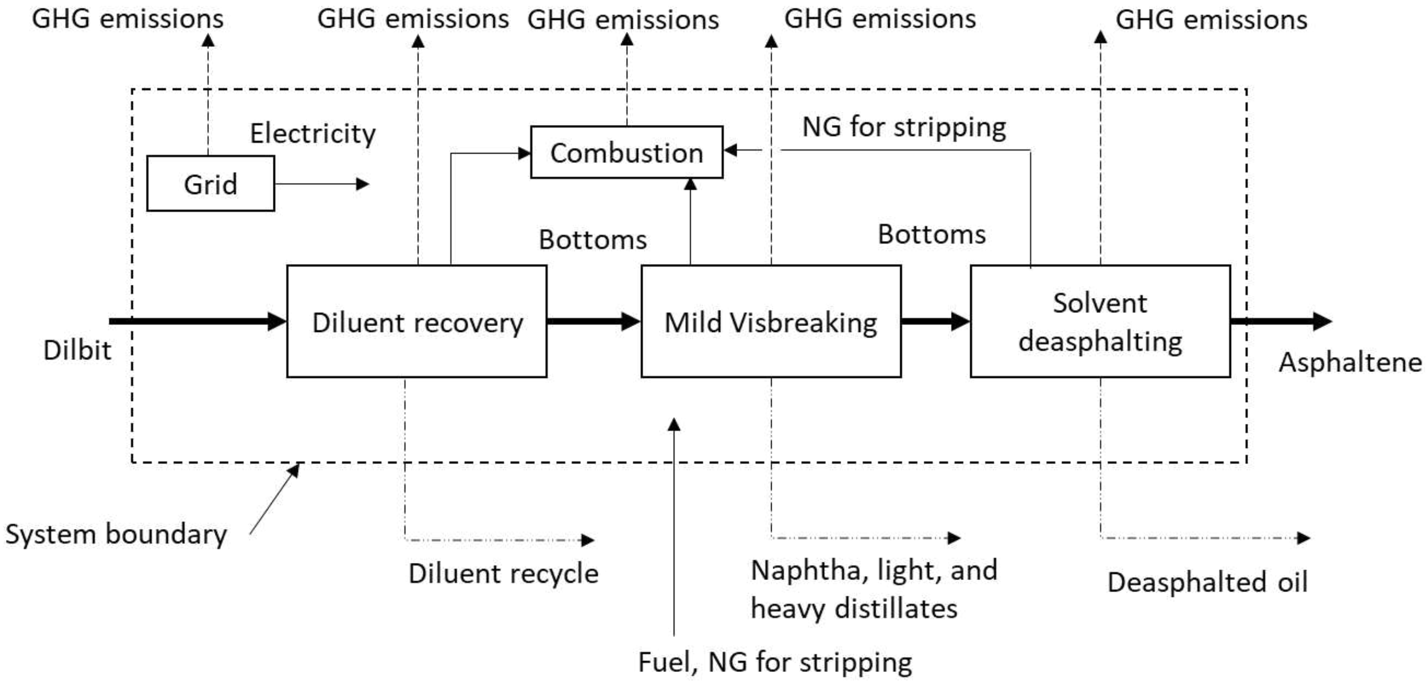

Figure 9-6. System boundary for the asphaltene separation stage

Table 9-4. Weight factors for the allocation of energy consumption to asphaltene-related streams in the asphaltene separation stage

Operation	Weight	Comments
Diluent recovery	0.769	Based on a 70:30 bitumen-to-diluent volume ratio
Visbreaking	0.962	Based on bottom yield (Zachariah and De Klerl 2017)
Solvent deasphalting	0.177	Based on asphaltene yield (Zachariah and De Klerl 2017)
Combustion of natural gas used as stripping agent	0.163	Based on the overall yield of the process (Zachariah and De Klerl 2017)

Table 9-5. Summary of collected data for the background processes in the asphaltene pathway

Product	Electricity	Natural gas
Bitumen production	62.8 kWh/m^3 bitumen (Nimana et al. 2015a)[a]	200.5 m^3/m^3 bitumen (Nimana et al. 2015a)[b]

Asphaltene separation	0.5 kWh/bbl dilbit for diluent recovery (Pacheco et al. 2020) 4.4 kWh/bbl bitumen for visbreaking (Pacheco et al. 2020) 2.0 kWh/t feed for solvent deasphalting (Pacheco et al. 2020)	53.9 scf/bbl dilbit for diluent recovery (Pacheco et al. 2020) 1,082 scf/t bitumen for visbreaking (Pacheco et al. 2020) 552.3 scf/t feed for solvent deasphalting (Pacheco et al. 2020) 150 scf/bbl feed for stripping (Pacheco et al. 2020)[c]

a. No-cogeneration scenario.

b. This consumption includes 180 m^3/m^3 bitumen of natural gas and 20.5 m^3/m^3 bitumen of produced gas. About 12.3 m^3/m^3 bitumen of the produced gas is also used as fuel, and the emission factor is assumed to be the same as for natural gas. The balance of the produced gas is flared and the GHG emissions are accounted for as direct emissions. This data was retrieved from a study by our research group.

c. Stripping agent in the solvent recovery, visbreaking, and SDA operations. This gas is recovered and used as fuel to supply heat to the whole process.

Figure **9-7** presents the system boundary used to estimate the GHG emissions from the precursor and carbon fiber production processes. Energy consumption and process emissions were estimated through process modeling, and then the GHG emissions from electricity production and natural gas combustion were calculated using emission factors. Details of the process model and GHG emissions estimation are presented in Section 9.2.3.

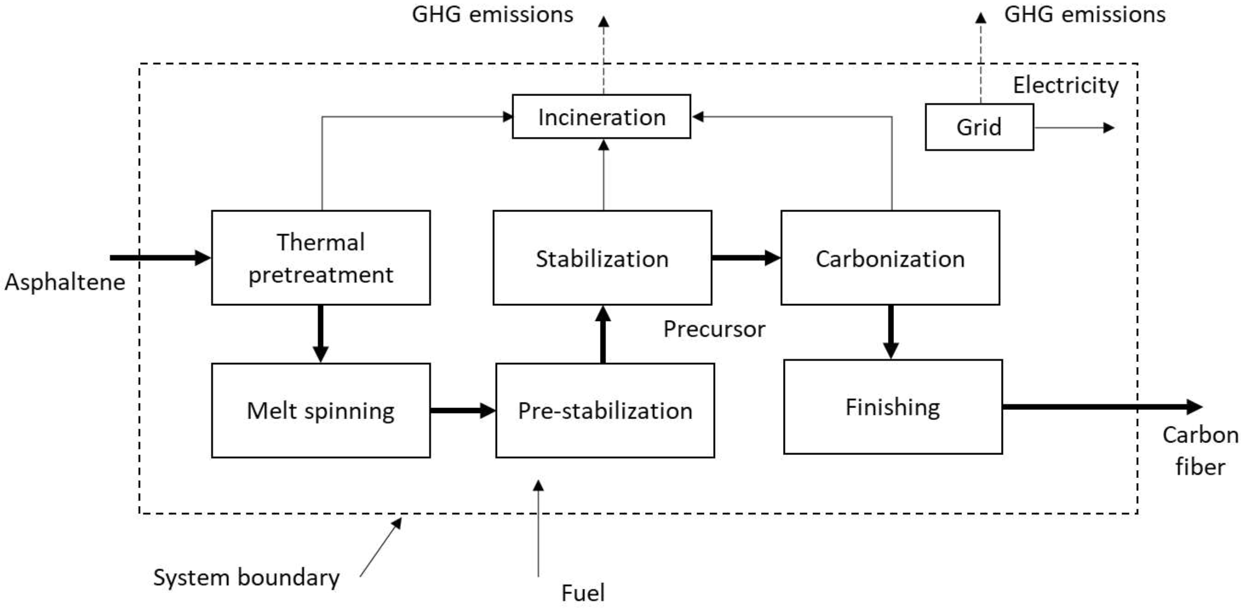

Figure 9-7**. System boundary for the precursor and carbon fiber production process**

9.2.2.2 Life cycle GHG emissions of the PAN pathway

Figure 9-8 presents the system boundary used in the estimation of the PAN pathway GHG emissions. A supply chain around an existing carbon fiber plant in the USA was defined because the market for PAN-CF is well established in that country. Conventional crude oil is produced in the Gulf of Mexico and transported to Houston, TX for refining. Light naphtha obtained in the refining process is transported to stream crackers in Port Arthur, TX, where propylene is produced.

Ammonia and acrylonitrile are also produced there. Acrylonitrile is transported to Decatur, AL, to produce PAN and, ultimately, carbon fiber.

For crude oil production, GHG emissions were obtained directly from published studies. For naphtha production, electricity consumption data was retrieved from published studies and heat consumption estimated from process simulation using Aspen HYSYS V10. Details on system boundary and main assumptions for each stage, as well as the emission factors used in the PAN pathway, are presented in Appendix D, and the data collected are summarized in Table 9-6.

9.2.3 Modeling and GHG emission estimation of the precursor and carbon fiber production processes in the asphaltene pathway

9.2.3.1 Model development

The feedstock to produce carbon fiber is bitumen-derived solid asphaltene. The asphaltene separated from bitumen through standard industrial processes, such as solvent deasphalting, is suitable for the reference process (Chen 2021; Leistenschneider et al. 2021; Zuo et al. 2021a; Zuo et al. 2021b). However, the asphaltene produced is likely a slurry because of the low solvent-to-bitumen ratio and the short residence time at a commercial scale (Turunga 2017). Industrial asphaltene is about 70 wt.% asphaltene, and the balance is lighter components (Montoya Sánchez and de Klerl 2016). The production of powder-like asphaltene requires precipitation using a solvent-to-feed ratio of about 40:1. Solid asphaltene was assumed as the feedstock to the process. Solid asphaltene can be produced using partial upgrading technologies like SELEX-Asp, Hi-Q, and BituMax (Keeson and Gieseman 2018), thus this type of feedstock does not present a technical constraint.

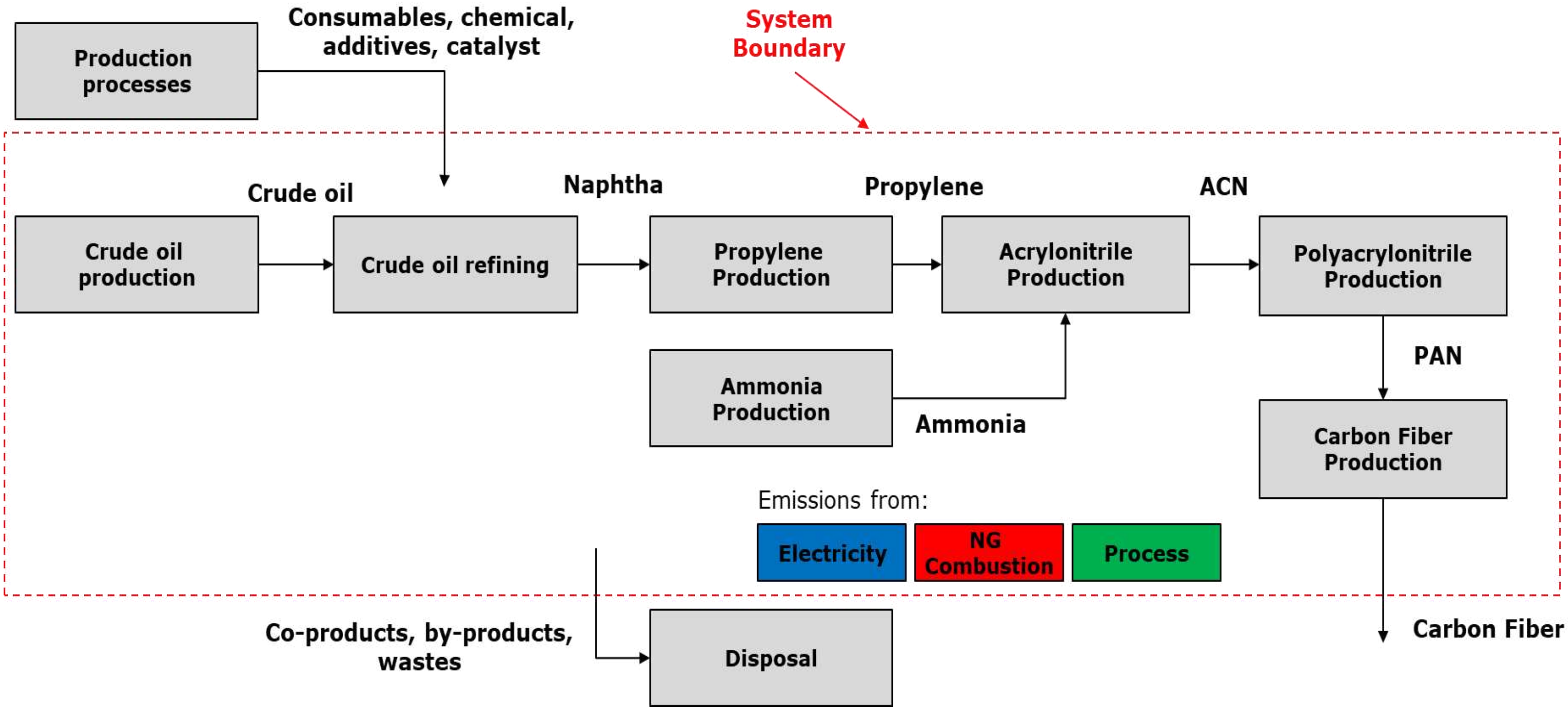

Figure 9-8. System boundary diagram, PAN pathway

Table 9-6. Summary of data collected for the background process of the PAN pathway

Product	Electricity	Natural gas
Crude oil	-	43.30 kWh/bbl crude oil[a]
Naphtha	0.04 kWh/bbl crude oil for oil pumping (Haynes 1974) 0.01 kWh/bbl crude oil for water pumping (Haynes 1974) 0.015 kWh/bbl crude oil for high-potential electrical field (Haynes 1974; Integrated Pollution and Prevention Control 2002) 0.06 kWh/bbl crude oil for pumping crude oil, products, and reflux, and for running air-cooled heat exchangers (Haynes 1974) 0.043 kWh/bbl crude oil for pumping products and for running air-cooled heat exchangers (Haynes 1974)	31.0 MJ/bbl crude oil for desalting 92.1 MJ/bbl crude for preheating in the furnace 2.4 MJ/bbl crude oil for production of main steam 0.8 MJ/bbl crude oil for production of gasoil steam 0.9 MJ/bbl crude oil for production of diesel steam 13.4 MJ/bbl crude oil for feed heating 0.6 MJ/bbl crude oil for production of stripping steam 11.2 MJ/bbl for reboiler heat duty

Product	Electricity	Natural gas
Ammonia	0.5 MJ/kg NH_3 (Boulamanti and Moya 2017)	14.2 MJ/kg NH_3 (2008)[b]
Propylene	0.83 MJ/kg propylene[c]	69.7 MJ/kg propylene[d]
Acrylonitrile	0.90 MJ/kg ACN[e]	0.456 kg/kg ACN[f]
PAN	0.35 kWh/lb PAN (Das 2011)	0.10 mmBtu/lb PAN (Das 2011)
PAN-CF	9.1 kWh/lb CF (Das 2011)	0.042 mmBtu/lb CF (Das 2011)

a. Based on 18.66 kJ/MJ crude oil and 11.77 kJ/MJ crude oil required for extraction and processing (Rahman et al. 2014), 36.7 MJ/kg crude oil (Speight 2014), and 879 kg/m3 crude oil. Electricity is produced on-site using simple gas turbines with 32.6% efficiency.

b. Primary and secondary reformers. Supplied by the combustion of natural gas.

c. Based on 1.0 MJ/kg ethylene primary energy, 40% conversion efficiency, and a propylene-to-ethylene mass ratio of 0.48 (Ren et al. 2006).

d. Heat is supplied by the combustion of fuel-grade by-products. Based on 10.1 MJ/kg naphtha and a propylene yield of 14.5 wt.% (Ren et al. 2006).

e. Boulamanti et al. estimated electricity consumption of 1.0 MJ/kg CAN (Boulamanti and Moya 2017); Deloitte's figure is 0.8 GJ/t ACN (Deloitte 2013).

f. For the incineration of by-products (Morales-Mora et al. 2012).

Unlike the continuous process to produce PAN-CF, ACF requires a semi-batch process. This is because the green fibers, the spun asphaltene before stabilization, are not able to support their weight. Therefore, the fibers cannot be extended and transported through the entire process using driven rollers. The yield and duration of each operation and the annual operation hours were used to calculate the number of batches per year and the kg of output per batch. The material balance of the batch operations is expressed in kg per batch and in kg per hour for continuous operations. Results on energy consumption are expressed per kg of produced carbon fiber.

The fed asphaltene loses weight in the form of gaseous products that evolve through the different operations in the precursor and carbon fiber production processes. Understanding the weight loss and the composition of the evolved gases permits the estimation of direct GHG emissions. The overall weight loss, from raw asphaltene to carbonized fibers, was quantified by Zuo et al. (Zuo et al. 2021b) for different pretreatment temperatures. At 350ºC, the cumulative weight losses after thermal pretreatment, stabilization, and carbonization were 10.7 wt.%, 14.5 wt.%, and 60.2 wt.%, respectively. This means 0.398 kg of carbon fiber is produced per kilogram of raw asphaltene fed to the process. In the experimental studies by Leistenschneider et al. and Zuo et al., the process yield improves to about 0.50 kg CF/kg asphaltene (Leistenschneider et al. 2021; Zuo et al. 2021a), and it is expected to reach 0.60 CF/kg asphaltene after optimizing the process. In this study, a process yield of 0.55 kg CF/kg asphaltene was assumed as the base case. This yield value was used to scale cumulative weight losses reported by Zuo et al. (Zuo et al. 2021b). The cumulative weight losses after thermal pretreatment, stabilization, and carbonization used in this study were 8.0 wt.%, 10.8 wt.%, and 45.0 wt.%, respectively. The effect of the process yield on GHG emissions was investigated using sensitivity and uncertainty analyses.

The objective of the thermal pretreatment is to remove volatile materials and increase the softening point of asphaltene. Once this is done, the fiber can be stabilized at the required temperature in the subsequent operations. In this study, the pretreatment time and temperature were 2 hr and 350ºC, as suggested by Zuo et al. (Zuo et al. 2021b). The gas that evolved during the thermal pretreatment was estimated from Moschopedis et al.'s data on the pyrolysis of asphaltenes from Athabasca bitumen, in a nitrogen atmosphere (Moschopedis et al. 1978), shown in Table 9-7. The calculated weight loss using this data is 11.41 wt.%. These numbers were scaled to match the weight loss after the thermal pretreatment used in this study, 8.0 wt.% (see Table 9-7).

Table 9-7. The accumulated amount of gas product from the pyrolysis of Athabasca asphaltene. Heating range: 200-350°C (Moschopedis et al. 1978).

Gas product	Amount (mmol/100 g Asp.)	Amount (g/100 g Asp.)	Amount (g/100 g Asp.) scaled to 8.0 wt.% weight loss
Hydrogen	3.0	0.006	0.004
Carbon dioxide	81.5	3.6	2.5
Carbon monoxide	39.5	1.1	0.8
Hydrogen sulfide	14.5	0.5	0.4
Methane	211.9	3.4	2.4
Ethane	91.5	2.7	1.9
C_3H_8+C_4H_{10}	1.5	0.08	0.1
C_2H_4+C_3H_6	0.5	0.02	0.01
Weight loss		11.41	8.0

Melt spinning was considered because it is the preferred method for spinning pitch, and it is used in asphaltene-based processes (Leal and Penaloza 2002; Ni et al. 2019; Qin et al. 2019). The assumed spinning temperature was 220ºC based on data presented by Zuo et al. (Zuo et al. 2021b).

The spun asphaltene fibers tend to fuse during heating for stabilization. To avoid this issue a pre-stabilization step is included (Zuo et al. 2021b). Soaking the fiber in HNO_3 at room temperature for about 10 minutes promotes the addition of oxygen and the release of hydrogen, increasing the softening point of the fibers, and circumvents fusing during stabilization (Chen 2021; Leistenschneider et al. 2021). After the acid prestabilization, the fibers are stabilized at 250 ºC for 6 hours.

As mentioned before, the spun asphaltene is not able to support their weight; therefore, using the same type of oven as for PAN-CF is not possible. The same issue exists in the production of pitch-based carbon fiber. Two methods for the air oxidation of pitch fibers can be used and are described by Morgan (Morgan 2005). In this study, it was considered that those methods are valid for ACF, and the use of walk-in type oxidation ovens was assumed. The spun asphaltene fibers are wound directly onto special heat-resistant spools set in the oven. The design of the spools and oven should allow the oxidizing air to reach the center of the fiber package to ensure uniform oxidation and at an adequate rate to avoid the build-up of heat due to the exothermic reaction. Details of this equipment are presented by Barnett (Barnett 1959) and Redick (Redick 1986).

Lavin provides data of gas evolution during the stabilization of mesophase pitch at 240ºC for 90 minutes (Lavin 1992). Only CO, CO_2, and H_2O were found in the off-gas. In the case of asphaltenes, Chen reported the elemental composition of green fibers and stabilized fibers, which were used to estimate the elemental weight loss (Chen 2021). Then, to calculate the off-gas composition, we assumed that the evolved gas consists of CO, CO_2, and H_2O, as suggested by Lavin, as well as SO_2.

The carbonization of stabilized fibers is performed in two stages: first, a low-temperature (LT) carbonization stage at 1,000ºC and then high temperature (HT) carbonization at 1,500ºC. It was assumed that after stabilization the fibers are strong enough to support their weight; therefore, existing equipment for PAN-CF carbonization could be suitable for ACF production.

The composition of the off-gas from the carbonization operation is hard to estimate because the original asphaltene undergoes many transformations through the entire process. The elemental composition of the stabilized fiber and carbonized fiber reported by Chen (Chen 2021) were used to estimate the carbon loss, which was assumed to be released as CO_2. This assumption is valid because the off-gas is treated in a thermal oxidizer before being released into the atmosphere.

After carbonization, the mass of the fiber is considered constant, while the energy consumption in surface treatment, sizing, and handling was considered equal to that in the PAN-CF production process; these values were retrieved from a carbon fiber manufacturer's presentation (Harper International).

The process conditions and main assumptions for modeling the ACF production process are summarized in Table 9-8. Such conditions were used to develop a spreadsheet-based process model to generate the material and energy balances of each unit operation in the process.

Table 9-8. Process conditions assumed for the ACF production model

Operation	Process condition	Value	Reference	Comments
General	Annual operation hours	7,000 hr	-	
	Overall yield	0.55 kg CF/kg asphaltene	(Leistenschneider et al. 2021; Zuo et al. 2021a)	
Thermal pretreatment	Temperature	350ºC	(Zuo et al. 2021b)	
	Time	2 hr	(Zuo et al. 2021b)	
	Cumulative weight lost	8.0 wt.%	-	Scaled to keep the proportions reported by Zuo et al. (Zuo et al. 2021b)
	Purge nitrogen per batch	137.5 kg/batch	-	Assumed twice the amount of evolved gas per batch

Operation	Process condition	Value	Reference	Comments
Spinning	Temperature	220ºC	(Zuo et al. 2021b)	
Pre-stabilization	Temperature	25ºC	(Zuo et al. 2021b)	
	Time	10 min	(Zuo et al. 2021b)	
Stabilization	Temperature	300ºC	(Zuo et al. 2021a)	
	Time	6 hr	(Zuo et al. 2021b)	
	Mass load per oven	567 kg green fiber	(Despatch N.d.)	Commercial wall-in oven capacity
	Spool diameter	0.19 m	-	To estimate oven dimensions
	Spool length	0.25 m	-	To estimate oven dimensions
	Indirect fired heater efficiency	80%	-	

Operation	Process condition	Value	Reference	Comments
Carbonization	Low temperature	1,000ºC	(Chen 2021)	
	High temperature	1,500ºC	(Zuo et al. 2021b)	
	Time	2 hr	(Zuo et al. 2021b)	
	Mass per spool	6.0 kg/spool		
	Electrical heater efficiency	75%		
Finishing operations	Specific energy consumption	9.08 kWh/kg CF	(Harper International)	Same as PAN-CF process

9.2.3.2 Estimation of GHG emissions of the precursor and carbon fiber production

Once the material and energy balances of the precursor and carbon fiber production processes were calculated, the GHG emissions associated with the production of electricity and fuel combustion were estimated using the emission factors shown in Table 9-3. It was assumed that the heat required for precursor production is provided by steam generated by the combustion of natural gas. The heat for stabilization is also provided by the combustion of natural gas in indirect fired heaters (IFHs). This option is preferred over electric heaters when the cost of natural gas is low (Witting et al. n.d.), which is the case in Alberta. Heat for carbonization is provided by electrical heaters. The type of heating element in LT furnaces is generally a wire-resistance heating element, while in an HT furnace, it is a rod heating element, for example, the $MoSi_2$-based super alloy rod provided by Kanthal. For rod heating elements, connections tend to get hot, therefore water cooling on the end of the elements is used to keep the temperature below the operation limit. Finally, electricity was considered as the energy source for surface treatment, sizing, and handling.

Regarding the direct emissions, the abatement of the off-gases from thermal pretreatment, stabilization, and the carbonization process from combustion with natural gas were considered. The CO_2 generated in this reaction was treated as a direct emission from the thermal pretreatment operation. It was assumed that the carbon that evolved into gaseous products during stabilization and carbonization was released as CO_2, after thermal oxidation.

9.2.3.3 Sensitivity and uncertainty analysis

Because of the sparsity of data on the ACF production process, the model was based on assumptions that introduce uncertainties in the results. The inputs assumed include the properties of intermediate and final products, process conditions, process yield, and capacities and performance of equipment. The sensitivity of the calculated GHG to the model inputs was assessed through the Morris method implemented through the RUST tool (Di Lullo et al. 2019). See Appendix B for an overview of the method. The GHG emissions from bitumen extraction and asphaltene separation were included among the inputs to evaluate the effect of the background processes on the ACF life cycle GHG emissions. The list of the inputs and their corresponding lower and upper bounds, as well as the base case values, are shown in Table 9-9. Once we narrowed the number of sensitive inputs, uncertainty analysis was conducted through Monte Carlo simulations using RUST (Di Lullo et al. 2019). For a sampling error lower than 5%, 18,000 runs were performed.

Table 9-9. List of inputs for the sensitivity analysis

Input	Lower bound	Base case	Upper bound
Overall yield, kg CF/kg asphaltene	0.40	0.55	0.60
Pretreatment time, hr	1	2	3
Mass of CF per spool, kg	6	4	8
Multiplier of theoretical N_2 flow in pretreatment, dimensionless	2	2	10
Heat transfer resistance of reactor for pretreatment, m^2K/W	1.35	1.93	2.51
Stabilization time, hr	6	6	16
Mass load per stabilization oven, kg	386	567	600
Spool diameter, m	0.13	0.19	0.25

Input	Lower bound	Base case	Upper bound
Spool length, m	0.18	0.25	0.33
C_p of stabilized fiber, kJ/kgK	1.47	2.10	2.73
Off-gas temperature - stabilization, ^oC	282	300	300
The heat of oxidation, kJ/kg	-1585	-1219	-366
Heat transfer resistance of stabilization ovens, m^2K/W	1.35	1.93	2.51
High temperature of carbonization, ^oC	1,500	1,500	2,000
Heat of carbonization, kJ/kg	353	504	655
N_2/stabilized fiber mass ratio, kg/kg	6	12.5	12.5
C_p of carbon fiber, kJ/kgK	0.71	0.8	0.8
Boiler efficiency, dimensionless	0.70	0.80	0.90
Indirect fired heater efficiency, dimensionless	0.70	0.80	0.90
Electric heater efficiency, dimensionless	0.70	0.75	0.80
Energy consumption in finishing operations kWh/kg CF	6.36	9.08	11.80
GHG emissions of bitumen extraction stage[a]	0.39	0.56	0.72
GHG emissions of asphaltene separation stage[a]	0.23	0.33	0.43

a. Base case value is from this study. The lower and upper bounds were considered -30% and +30% of the base case.

9.3 Results and discussion

9.3.1 Asphaltene-based precursor and carbon fiber production processes

9.3.1.1 Material and energy balance

Table 9-10 shows the material balance of precursor and ACF production. For an overall yield of 0.55 kg CF/kg asphaltene, a production of 1,650 t CF/y (236 kg/hr) requires a feed of 3,000 t/y asphaltene (429 kg/hr). The raw asphaltene is fed to the thermal pretreatment along with flowing nitrogen. Thermal pretreatment is a batch process with a cycle time of 2 hours. For 7,000 hours of operation per year, the number of annual batches is 3,500. The mass of asphaltene fed to the operation is 857 kg/batch. Because of the evolution of gas products, asphaltene loses 8.0 wt.% during thermal pretreatment, resulting in 788 kg/batch pretreated asphaltene.

The pretreated asphaltene is melt spun into green fibers, which are pre-stabilized by soaking in nitric acid. The weight change after this operation is considered negligible. The pre-stabilized green fibers are fed into walk-in ovens for stabilization in air. This operation is performed in batches with a cycle time of 6 hours, becoming the bottleneck of the entire process. According to the mass load per oven assumed in this study, 567 kg/batch pre-stabilized fiber is fed. The net weight loss, after oxygen uptake and the evolution of gas products, is 3.0 wt.%. Therefore, the throughput of one cycle is 550 kg/batch. Considering that one cycle of stabilization corresponds to three cycles of thermal pretreatment, 2,364 kg of pretreated asphaltene will be available at the beginning of each stabilization cycle. With a mass load per oven of 567 kg, 5 stabilization ovens are needed to avoid waiting time, which represents an average rate of 382 kg/hr stabilized fiber. Table 9-10 shows the inputs and outputs per batch.

Carbonization and the subsequent finishing operations are continuous processes. The material balance of the carbonization operation was calculated for the mass flow required to satisfy the plant capacity, e.g., 236 kg/hr carbon fiber. This process has a yield of 61.7 wt.% based on the mass of the stabilized fiber fed into the operation; therefore, 382 kg/hr stabilized fiber is required. As previously discussed, the set formed by one thermal pretreatment unit and five stabilization ovens can supply stabilized fiber to the carbonization operation at the needed rate. Table 9-10 presents the material balance for the carbonization operation. As for the PAN-CF process, the weight loss during the finishing operations was considered to be negligible.

Table 9-11 presents the energy consumption by each operation in the ACF production process per kg of produced carbon fiber. These values were obtained by completing the energy balance of the operations. Carbonization dominates the energy consumption, mainly because of the high temperature and the elevated demand for nitrogen, which for the case base was assumed to be 12.5 kg N_2/kg stabilized fiber fed into the furnaces (Harper International). About 54.5% of the energy consumption in the carbonization operation corresponds to the LT stage and the balance to the HT stage. This is because the nitrogen flow required for purging the furnace atmosphere is higher in the LT stage. Also, the energy for heating up the feed to the furnace is higher in the LT step due to a higher mass flow and required temperature difference. The heat required for thermal pretreatment, melt spinning, and stabilization is low compared with carbonization because of the relatively low temperature of those operations. The electricity required for the finishing operations accounts for 37.7% of the total consumption. It was assumed that the same operations used for PAN-CF are valid for ACF and retrieved the energy consumption from a manufacturer. Given the important contribution of those operations to the total energy consumption, further research on the conditions tailored to ACF is required.

Table 9-10. Material balance of the ACF production process. Plant capacity: 1,650 t CF/y

Batch operation	Stream	Input (kg/batch)	Output (kg/batch)
Thermal pretreatment	Raw asphaltene	857	
	Nitrogen	138	
	Pretreated asphaltene		788
	Off-gases:		
	Hydrogen		0.04
	Carbon dioxide		21.7
	Carbon monoxide		6.63
	Hydrogen sulfide		3.01
	Methane		20.5
	Ethane		16.3
	Propane + Butane		0.48
	Ethylene + Propylene		0.12
	Nitrogen		138

Batch operation	Stream	Input (kg/batch)	Output (kg/batch)
Stabilization	Pre-stabilized green fibers[a]	567	
	Air	6,125	
	Stabilized fibers		550
	Off-gases:		
	Water		319
	Carbon dioxide		231
	Carbon monoxide		147
	Sulfur dioxide		25.7
	Oxygen		712
	Nitrogen		4,707
Continuous operation	**Stream**	**Input (kg/h)**	**Output (kg/h)**
Carbonization	Stabilized fiber	382	
	Nitrogen	4,776	
	Carbon fiber[b]		236

Batch operation	Stream	Input (kg/batch)	Output (kg/batch)
	Off-gases:		
	Carbon dioxide[c]		444
	Nitrogen[d]		4,776

a. Green fiber mass does not change during pre-stabilization.

b. Carbon fiber mass does not change during subsequent finishing operations.

c. After the incineration of hydrocarbons in off-gases.

d. d. 3,152 kg/h from the LT furnace and 1,624 kg/h from the HT furnace.

Table 9-11. Energy consumption by operation resulting from energy balance

Operation	Energy consumption (kWh/kg CF)	Comments
Thermal pretreatment	0.43[a]	Heat supplied by steam. This heat includes heating raw asphaltene, wall losses, and energy carried by the off-gases.
Melt spinning	0.20[a]	Heat supplied by steam for heating the treated asphaltene to the spinning temperature.
Stabilization	1.76[b]	Heat supplied by natural gas combustion. This heat includes heating spun asphaltene and air atmosphere, the heat of reaction, wall losses, the energy carried by the off-gases, and energy carried by the stabilized fibers.
Carbonization	11.9[c]	Heat supplied by electricity. This heat includes heating stabilized fibers fed to the furnaces and nitrogen atmosphere, the heat of reaction, wall losses, the energy carried by the off-gases, and energy carried by the carbonized fibers.
Finishing operations	9.08	Electricity for electrolytic surface treatment, drying fibers, and driving rollers.

a. Considers a boiler efficiency of 80%.
b. Considers an IFH efficiency of 80%.
c. Considers an electric heater efficiency of 75%.

9.3.1.2 GHG emissions

The estimated GHG emissions from precursor and ACF production are 15.2 kg CO_2eq/kg CF. Table 9-12 shows the breakdown of the GHG emissions. Precursor production contributes only 8.0% of the total GHG emissions, and carbon fiber production accounts for the remaining 92.0% from precursor and asphaltene-based carbon fiber production. It is important to note that for precursor production, direct emissions make up 90.4% of the emissions from this stage, corresponding to the emissions from the thermal pretreatment unit. For the carbon fiber process, electricity accounts for 79.2% of GHG emissions. About 59.6% is from electricity consumption in the carbonization furnaces. Direct emissions are also significant, making up 16.7% of the total value. Direct emissions from the carbonization furnaces contribute 12.4%, and the other 4.4% come from the stabilization ovens. Given the high influence of direct emissions on the total GHG emissions, the process yield has a key role in the carbon footprint of the process. The greater the yield, the lower the evolution of gas products during thermal operations and therefore the lower the direct emissions. Conversely, a low yield implies a high conversion of carbon atoms into gas products. This carbon will inevitably end in the form of CO_2 because the off-gases are incinerated before being released into the atmosphere.

Table 9-12. Breakdown of GHG emissions from precursor and asphaltene-based carbon fiber production (kg CO_2eq/kg CF)

Process	Operation	Electricity	Natural gas combustion	Direct	Total
Precursor	Thermal pretreatment	-	0.08	1.13	1.21
	Melt spinning	-	0.04	-	0.04
	Total operation	-	0.12	1.13	1.25
Carbon fiber	Stabilization	-	0.33	0.68	1.01
	Carbonization	6.32	-	1.89	8.21
	Finishing operations	4.81	-	-	4.81
	Total operation	11.1	0.33	2.57	15.3
	Total process	**11.1**	**0.45**	**3.70**	**15.2**

9.3.2 ACF life cycle GHG emissions

Data on feedstock requirements for each stage of the ACF life cycle were developed and are expressed in terms of the output of the process and functional unit of this study. The results are shown in Table 9-13.

The results on feedstock requirements facilitate the estimation of potential production of asphaltene-based carbon fiber given the current bitumen production in Alberta. The current world demand for carbon fiber is about 98,000 tonnes per year. To supply this demand, 6.86 million bbl per year of bitumen would be required. According to data provided by Alberta

Energy Regulator, 412.2 million barrels of bitumen were produced in Alberta by SAGD in 2020 (Alberta Energy Regulator 2021), thus there exists the potential to supply the world demand of carbon fiber even if current SAGD production were cut down by 98.3%. This estimate is higher than that made by Meisen, who estimated that 4.12 million barrels of bitumen per year are enough to supply the world's demand for carbon fiber (Meisen 2017).

Table 9-13. Input-to-output ratio and feedstock requirement per kg CF for each stage of the ACF life cycle

Process	Input/output	Requirement per functional unit
Bitumen production	-	0.07 bbl bitumen/kg CF
Asphaltene separation	0.04 bbl bitumen/kg asphaltene[a]	1.82 kg asphaltene/kg CF
Precursor production	1.09 kg asphaltene/kg precursor[b]	1.67 kg precursor/kg CF
Carbon fiber production	1.67 kg precursor/kg CF[b]	1.00 kg CF/kg CF

a. Based on 16.3 wt.% asphaltene yield (Zachariah and De Klerl 2017) and 1,013 kg/m^3 bitumen density.

b. Based on cumulative yield (Zuo et al. 2021b).

That author considered a carbon fiber yield of 80 wt.% asphaltene, which is higher than 55 wt.% used in this work and supported by experimental results (Leistenschneider et al. 2021; Zuo et al. 2021a).

Figure 9-9 shows the energy consumption values in the ACF life cycle. The life cycle energy consumption to produce asphaltene-based carbon fiber is 26.8 kWh/kg CF. Note that this number only considers the electricity and combusted fuel (natural gas and produced gas) to supply heat and not the energy content of the feedstocks. The production of carbon fiber accounts for 85% of the life cycle energy consumption, while the production of the precursor and the background operations contribute 2% and 13% of the emissions, respectively. The energy consumption in the bitumen production and asphaltene separation process were allocated on a mass basis to the asphaltene stream separated from the produced bitumen, hence the low contribution of these processes to the total energy consumption. The energy consumed in the precursor production process corresponds to the heat required for thermal stabilization and spinning.

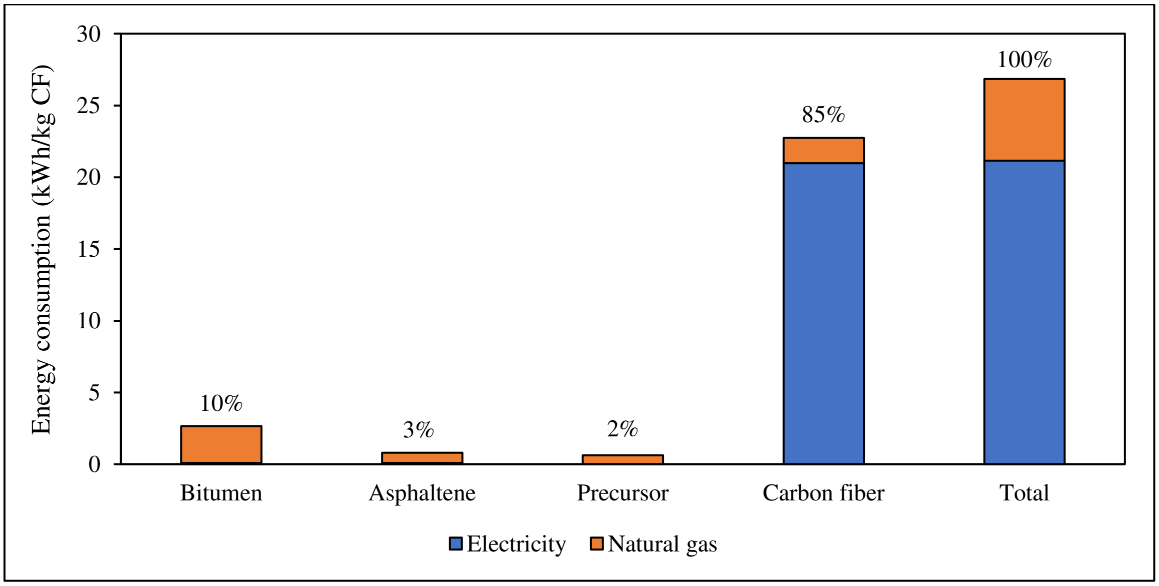

Figure 9-9. Breakdown of life cycle energy consumption of the ACF life cycle

Figure 9-10 presents the breakdown of the ACF life cycle GHG emissions, which total 16.2 kg CO_2eq/kg CF. The contribution of the background processes, i.e., bitumen production and asphaltene separation, is 5%. This contribution is low because of the relatively low energy consumption allocated to the asphaltene streams in those processes. As expected, carbon fiber production contributes most of the life cycle GHG emissions, about 87%, while the production of the precursor contributes 8%, most of this corresponding to direct emissions from the thermal pretreatment operation. As life cycle GHG emissions are dominated by the electricity used in the carbon fiber production stage, the carbon intensity of the pathway would be significantly reduced not only by reducing electricity consumption, e.g., implementing energy-efficient furnaces for carbonization, but also by reducing the emission factor of the grid, that is, incorporating renewables to the energy mix.

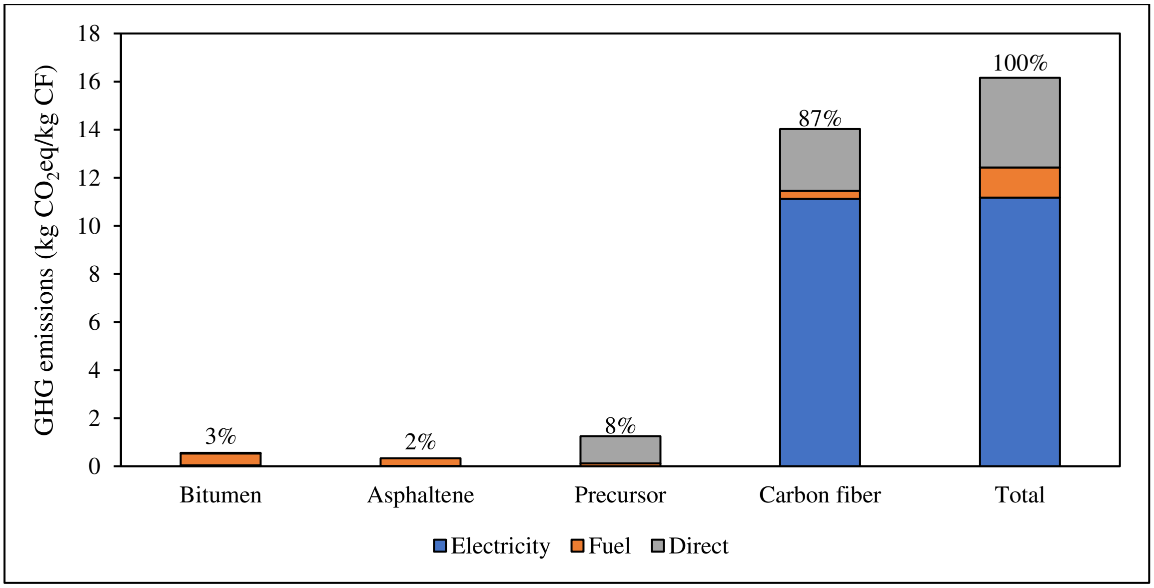

Figure 9-10. Breakdown of the life cycle GHG emissions of the asphaltene pathway

Four categories of GHG emission results from the PAN and asphaltene pathways were compared: life cycle, background processes, precursor production, and carbon fiber production. As shown in Table 9-15, the GHG emissions from the asphaltene pathway are lower than those from the PAN pathway at all levels. The life cycle GHG emissions from the asphaltene pathway are 68.7% lower than those from the PAN pathway. This difference shows the potential of ACF as a raw material for carbon fiber-based products with a low carbon footprint. The breakdown of the PAN pathway life cycle energy consumption and GHG emissions is presented in Table 9-14. In the PAN pathway, the total energy consumed and life cycle GHG emissions are 197.6 kWh/kg CF and 51.6 kgCO_2eq/kg CF. Details of the energy and emissions breakdown are provided in Appendix F (Figure F-12 and Figure F-13).

Table 9-14. Breakdown of the PAN pathway life cycle energy consumption and GHG emissions

Stage	**Energy consumption (kWh/kg CF)**	**GHG emissions (kg CO_2eq/kg CF)**
Crude oil	1.27	0.57
Naphtha	2.86	0.51
Propylene	0.14	2.18
Ammonia	4.88	4.80
Acrylonitrile	15.1	3.78
PAN	125.8	12.53
Carbon fiber	47.6	15.44

The percentage reduction in emissions from background processes is high. This is because the asphaltene pathway requires two relatively low energy-intensive background processes (bitumen production and asphaltene separation), while the PAN pathway requires much higher energy-intensive processes (in the production of crude oil, naphtha, ammonia, propylene, and ACN). The total energy consumed by the background processes is estimated to be 24.2 kWh/kg CF, which is 6.9 times higher than the asphaltene-based carbon fiber. Moreover, in the background processes of the asphaltene pathway, a major part of energy consumption and direct emissions is allocated to the bitumen stream rather than the asphaltene stream. In the PAN pathway, the energy consumption and direct emissions in two background processes, ammonia and ACN production, are fully allocated to the life cycle of carbon fiber, drastically increasing the life cycle emissions of this pathway. Furthermore, a greater percentage reduction in the emissions from precursor production was estimated, mostly because of the high consumption of natural gas in the PAN production process. The PAN process requires the recovery of solvent used for dope preparation, and this is an energy-intensive operation. The production of an asphaltene-based precursor does not include solvent recovery operations. The GHG emissions come from the heat supply to thermal pretreatment and heating the pretreated asphaltene before spinning. In addition, the PAN process includes many other energy consumer operations that are not part of the asphaltene-based precursor process, for instance, coagulation of spun fibers, washing, and drying. The PAN and PAN-CF production consume 173.4 kWh/kg CF, which is 7.4 times high than the precursor and carbon fiber production in the asphaltene pathway.

Regarding the emissions from carbon fiber production, ACF generates 9.09% fewer emissions than PAN-CF. A direct comparison is not possible because the breakdown of GHG emissions from PAN-CF production is not available. However, it is speculated that this difference is because the use of natural gas as energy input for stabilization in the ACF process. Also, because the requirement of additional natural gas to incinerate the off-gases from stabilization in the PAN-CF process, while in the ACF process, hydrocarbon in the off-gases supply heat for incineration.

Table 9-15. GHG emissions comparison between the PAN and asphaltene pathways

Category	PAN pathway, kg CO_2eq/kg CF	Asphaltene pathway, kg CO_2eq/kg CF	Difference kg CO_2eq/kg CF	Reduction, %
Life cycle	51.6	16.2	35.4	68.7
Background processes	11.8	0.89	10.9	92.5
Precursor	24.3	1.25	23.1	94.9
Carbon fiber	15.4	14.0	1.4	9.09

9.3.2.1 Sensitivity and uncertainty analyses

Figure 9-11 shows the sensitivity analysis results from the Morris method. The horizontal axis represents the range of the calculated GHG emissions as the input changes from the low bound value to the high bound value, while the vertical axis shows the standard deviation of this variation. This Morris plot ranks the influence of the parameters on the model output, ACF life cycle GHG emissions, based on the position of the absolute mean value and standard deviation in the plot. The high sensitivity and high non-linear parameters are located at the top right of the plot. Of the input parameters, the nitrogen-to-stabilized fiber mass ratio and the overall yield have the greatest influence on GHG emissions. The results are moderately sensitive to energy consumption in the finishing operations, mass load per oven, airflow for stabilization, and the temperature of HT carbonization. The efficiency of the electric heater, the specific heat of the stabilized fiber, the efficiency of indirect fired heaters, and the GHG emissions of the bitumen extraction stage have little influence on the GHG emissions. The remaining inputs have almost no influence on the model output.

The nitrogen-to-stabilized fiber mass ratio, carbonization HT, and efficiency of electrical heating are inputs corresponding to the carbonization operation. Among these inputs, the first has the most influence but also high uncertainty. It was assumed that furnaces used for PAN-CF production are suitable for ACF production and therefore the required nitrogen mass flow per kg of stabilized fiber fed to the furnace is the same in both processes. However, the nitrogen flow depends on the evolved gas that should be evacuated from the furnace. In the PAN-CF carbonization process, about 45 wt.% of the furnace feed is lost as off-gases (Morgan 2005), and for ACF the weight loss is about 53 wt.% (Zuo et al. 2021b). These numbers suggest that the required nitrogen flow should be greater for the latter.

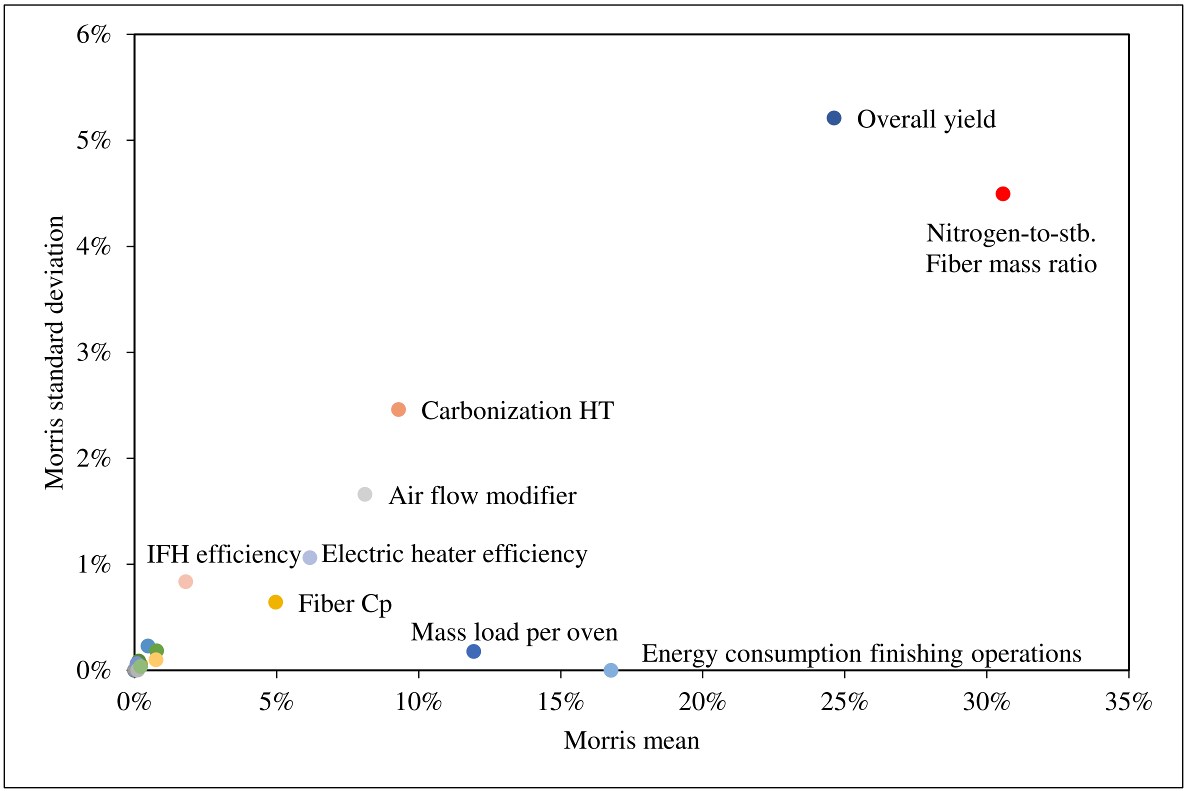

Figure 9-11. Morris method results for the sensitivity of inputs to the output model

As expected, the overall yield of the process influences the output results. The greater the yield, the lower the GHG emissions per kg of carbon fiber produced. Also, this input modifies the intermediate yield of the operations, which affects the energy consumption and direct emissions from thermal pretreatment, stabilization, and carbonization. Because the process is in the early development stage, there is uncertainty in this input. Further research is required to narrow the range of variation and improve the accuracy of the output results. For the lower bound, the overall yield reported by Zuo et al. (Zuo et al. 2021b) was assumed, and for the upper bound the expected target yield after optimizing the process was assumed. This information was retrieved from Leistenschneider et al. (Leistenschneider et al. 2021) and Zuo et al. (Zuo et al. 2021a).

The energy consumption in finishing operations is also subject to high uncertainty. As mentioned before, the same operations performed for PAN-CF production, that is, electrolytic surface treatment, sizing, drying, and handling, were assumed. However, no such information was found in the literature, and a suitable surface treatment method for ACF has not been established yet. For pitch-based carbon fiber, for example, surface treatment in a near-boiling H_2O_2 solution has been reported to increase the transverse tensile strength of the fiber (Morgan 2005). This approach is different from the electrolytic surface treatment used for PAN-CF, and it might be suitable for ACF. Further research is required.

Finally, the mass load of green fiber into the stabilization ovens, airflow for stabilization, and efficiency of the IFH are parameters of the stabilization operation. The mass load per oven is a technology constraint. The typical load per oven for commercial walk-in ovens, based on Despatch's data (Despatch N.d.) was used; however, for the ACF production process, a tailored stabilization oven may be required, as discussed in Section 9.2.3.1. The same can be said of the airflow required for stabilization. The required oxygen supply for the oxidation reaction and the evolved gases was estimated, after which the theoretical airflow was calculated. However, the actual airflow is expected to be higher because sufficient fresh air intake is needed to avoid heat build-up due to the exothermic reaction. The actual airflow highly depends on the oven design, and it is difficult to quantify given the sparsity of operation data, hence the high uncertainty in this input. The efficiency of the IFH is among the sensitive inputs because it directly affects the natural gas requirement in the stabilization operation, which is in turn affected by the airflow and the mass load per oven.

Figure 9-12 summarizes the results of the uncertainty analysis. The output model ranges from 10.4 to 21.8 kg CO_2eq/kg CF after the outliers are removed. The mean value is 15.5 kg CO_2eq

/kg CF, and the standard deviation is 1.82 kg CO_2eq /kg CF. Despite the wide range, the ACF life cycle GHG emissions are far below those of the PAN-CF life cycle (51.6 kg CO_2eq /kg CF). As more information on the ACF production process becomes available, the model can be updated to narrow the uncertainty.

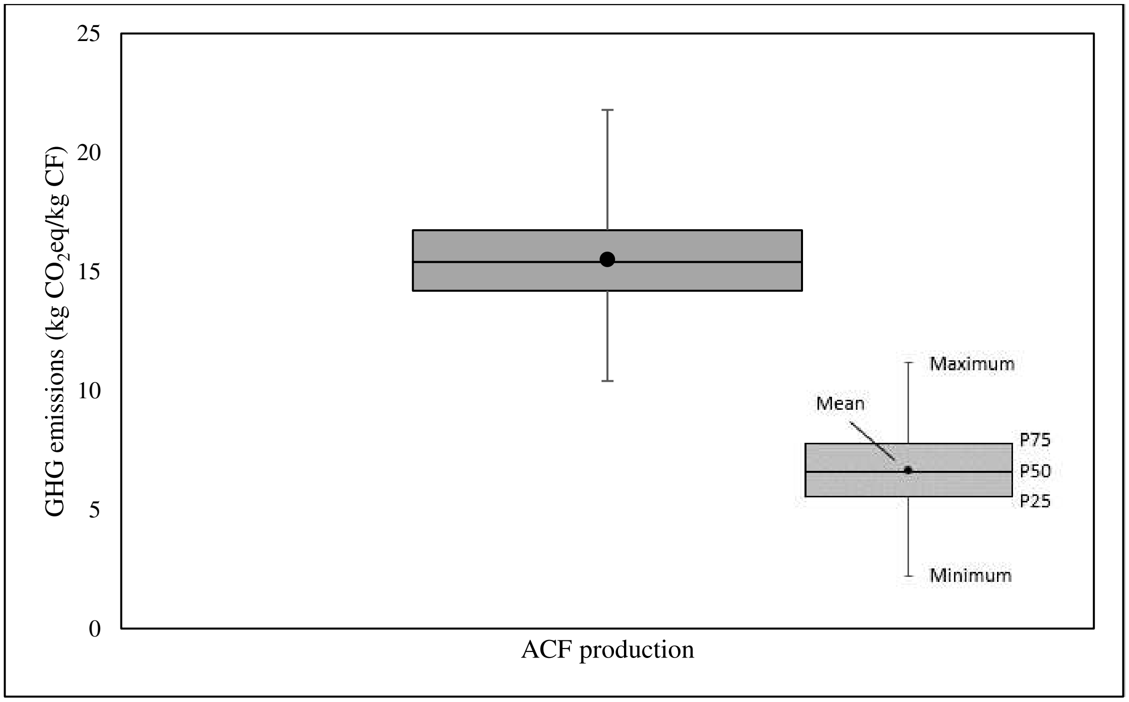

Figure 9-12. Monte Carlo simulation results

9.4 Conclusions

In this study, the life cycle GHG emissions of asphaltene-based carbon fibers were estimated. Data-intensive models to account for the GHG emissions of bitumen production, asphaltene separation, precursor manufacturing, and carbon fiber production were developed. The results were compared with a polyacrylonitrile (PAN) pathway whose energy consumption data were obtained from previous studies.

The calculated ACF life cycle GHG emissions is 16.2 kg CO_2eq/kg CF. Of these, 14.0 kg CO_2eq/kg CF corresponds to the production of the carbon fibers (stabilization, carbonization, and finishing operations). The greater contributor to the life cycle GHG emissions is the production of electricity to supply the heat input to the carbonization operation, accounting for 39.0% of the total value. Direct emissions from precursor and carbon fiber stages contribute significantly, with 22.8% of the share, because of the relatively low overall yield of the process, 0.55 kg carbon fiber per kg fed asphaltene. Compared with the PAN-CF life cycle, ACF's life cycle GHG emissions are 68.7% lower. The asphaltene pathway has lower GHG emissions for two reasons: fewer raw material conversion processes and a simple precursor production process that requires no solvent recovery. Using the Morris method, sensitive inputs impacting the estimated ACF life cycle GHG emissions were identified. The results indicate that the model is highly sensitive to the overall yield (precursor and carbon fiber production) and the nitrogen-to-stabilized mass ratio in the carbonization operation. The model is moderately sensitive to energy consumption in the finishing operations, mass load per oven, airflow for stabilization, and the temperature of HT carbonization. The efficiency of the electric heater, the specific heat of stabilized fiber, the efficiency of indirect fired heaters, and GHG emissions of the bitumen extraction stage have a low influence on the model output. Monte Carlo simulations were performed to assess the uncertainty in the ACF life cycle GHG emissions. The variability of the sensitive inputs leads to uncertainties in the results in the range of 10.4-21.8 kg CO_2eq /kg CF, with a mean of 15.5 kg CO_2eq/kg CF, which is still lower than the 51.6 kg CO_2eq /kg CF estimated for the PAN-CF life cycle.

An estimated 0.07 bbl bitumen is required to produce one kg of carbon fiber. Therefore, the current production of bitumen in Alberta is enough to supply the world's demand for carbon fiber. This, along with the low GHG emissions from the asphaltene pathway, makes this activity worthy of consideration in Alberta.

Chapter 10:Conclusions and recommendations for future research

10.1 Conclusions

Non-combustion products appear to be a solution for some of the present and future challenges for oil sands industry, which relies on the conversion of bitumen into different types of fuels. Product diversification would help overcome the price differential at which bitumen products are sold and strengthen the industry before the imminent decarbonization of the global economy. Developing such products, however, depends on the economic feasibility and environmental impact of the production processes.

In this study, data-intensive techno-economic and life cycle GHG emissions assessments of commercial-scale production of selected non-combustion products from oil sands were developed. The production of vanadium from bitumen upgrading spent catalysts and bitumen-derived petcoke fly ash, the recovery of zircon and titanium minerals from bitumen extraction froth treatment tailings, and the production of bitumen-derived asphaltene-based carbon fiber were considered. These products would create value from wastes and by-products of the oil sands industry that have near-zero commercial interest.

Using process data, material and energy balances were scaled to a commercial operation through process modeling. The main equipment was sized, and capital and operation costs were calculated. A techno-economic model was used to estimate production cost or internal rate of return, thus enabling the derivation of conclusions on the expected profitability of the processes. The assessment of GHG emissions included the definition of the functional unit and system boundary, derivation or collection of appropriate emission factors, and quantification of the cradle-to-gate GHG emissions. Emissions were allocated among the main products of the bitumen value chain and waste streams that feed the production processes of the non-combustion products. Sensitivity and uncertainty analyses were conducted to identify the most influential inputs and the most probable range of results. The main findings of this research are summarized in the following sections.

10.1.1 Techno-economic and life cycle GHG emissions assessments of vanadium recovery from bitumen upgrading spent catalysts

Data-intensive techno-economic and life cycle GHG emissions models of vanadium recovery from bitumen upgrading spent catalyst were developed. The reference process corresponds to a hydrometallurgy route based on roasting followed by water leaching and selective precipitation. A plant with the capacity of processing 30,000 tonnes of spent catalyst per year was considered for the base case scenario. The capacity was defined based on the typical generation rate of hydroprocessing spent catalyst in Alberta's upgraders. The functional unit for the life cycle GHG assessment is one tonne of recovered V_2O_5. Indirect emissions include those from the upstream operations (from bitumen production to hydroprocessing), the consumption of electricity, and the production of consumables. Direct GHG emissions are those generated on site and include emissions from the combustion of fuels to provide heat to the process as well as those generated during the transformation of the feedstock to obtain the final product.

Recovering vanadium from bitumen upgrading spent catalysts is potentially profitable in all the considered scenarios; however, the dependence on the MoO_3 market is a risk. In terms of GHG emissions, recovering vanadium from a waste apparently does not represent a practical advantage since life cycle GHG emissions are comparable to those from other vanadium sources; that said, the emissions are offset by the avoided emissions from the displacement of the co-produced MoO_3 and Al_2O_3 from their primary production processes.

The findings of the study supporting these conclusions are summarized below.

- Through the developed techno-economic model, a vanadium recovery cost of $9.89 per kg of V_2O_5 was estimated, considering the revenue from selling the co-products of the process, e.g., MoO_3, Al_2O_3, and a nickel alloy. The process is potentially profitable since the estimated recovery cost is lower than the reference market price. However, an uncertainty analysis shows that variations in the transport cost, the wash ratio implemented in filtration operations, the percentage of vanadium and molybdenum leached out from the catalyst support, and the selling price of MoO_3 could affect the economic feasibility of the process.
- Negotiating the feedstock cost is key to the profitability of the process. The metal recovery plant operator should not buy spent catalyst for the upgrader at a cost higher than $300/t. On the other hand, if a fee for managing and processing hazardous materials is charged by the metal processing plant to the upgrader, the vanadium recovery cost could be as low as $3.23 per kg of V_2O_5.
- If the leaching cake is disposed of instead of further processed to recover alumina and nickel, the vanadium recovery cost would be $9.23 per kg of V_2O_5. From a cost perspective, only MoO_3 is worth co-producing.
- Standalone plants for processing spent catalyst are not economically feasible. The spent catalyst generation rate of individual hydroprocessing upgraders in Alberta is below the minimum profitable plant capacity when economies of the scale and the effect of the plant capacity on the vanadium recovery cost are considered.

- Life cycle GHG emissions are 10.3 kg CO_2eq/kg V_2O_5. Of these, 35% are direct emissions and 65% indirect (upstream) emissions. Roasting spent catalyst is by far the greatest source of GHG, at 52% of the total.
- The grid emission factor and the specific energy consumption in the EAF are the inputs with the greatest effect on life cycle GHG emissions. The carbon intensity of Na_2CO_3 production and the salt-to-spent catalyst ratio have a moderate influence on the model output.
- The estimated values of the life cycle GHG emissions, including uncertainties in the sensitive inputs, are lower than the emissions from the production of vanadium pentoxide from VTM ore.
- Considering only the process emissions, recovering vanadium from spent catalysts in the form of V_2O_5 generates fewer emissions than doing so in the form of FeV, in terms of kg CO_2eq per kg of vanadium in the product.
- The displacement of the co-produced alumina and molybdenum trioxide from their primary production would generate a credit of 0.94 kg CO_2eq/kg V_2O_5.

10.1.2 Techno-economic and life cycle GHG emissions assessments of vanadium recovery from bitumen-derived petcoke fly ash

Petcoke generated during bitumen upgrading has the potential to become an important source of vanadium. This metal can be recovered from the fly ash remaining after the combustion of petcoke. Techno-economic and life cycle GHG emissions assessments were performed to evaluate the feasibility of the process in the context of Alberta's oil sands industry. The reference process considered in the study is based on salt-roasting the fly ash, followed by water leaching and selective precipitation to recover vanadium pentoxide. The base case consisted of a plant with a capacity of 16,000 tonnes of fly ash per year, which corresponds to the generation rate of fly ash in an upgrader where petcoke is used as fuel to generate steam. The boundary system for the GHG emissions life cycle assessment includes the production of bitumen, atmospheric and vacuum distillation, delayed coking, and steam generation, i.e., all the operations required to get petcoke fly ash from oil sands. The emissions associated with the production of consumables and electricity were considered as well.

Recovering vanadium from bitumen-derived petcoke fly ash is unlikely to be profitable under the conditions considered in this study. For the base case scenario, the recovery cost is greater than the current market price, and the plant capacity would need to be almost tripled to reduce the cost to profitable levels. Some process modifications and negotiating the feedstock price could reduce the recovery cost. Compared with other pathways to produce vanadium pentoxide, the studied route doubles the life cycle GHG emissions, mainly because of the substantial emissions generated during roasting for fly ash decarbonization. Contrary to recovering vanadium from spent catalyst, the fly ash pathway considered in this study does not benefit from the co-products of the recovery process (vanadium pentoxide is the only product considered in the analysis), neither by adding revenues nor avoiding emissions by primary production displacement. The key findings of the study are presented below.

- For the base case, the recovery cost was estimated to be \$18.77/kg V_2O_5. This cost is higher than the reference market price of vanadium pentoxide. Some modifications to the process are required for vanadium recovery to compete with other primary production processes. The highest contributors to the vanadium recovery cost are the cleaning of the off-gases from fly ash decarbonization and the sodium chloride and ammonium chloride used for roasting and AMV precipitation, respectively. Such costs were also identified among the inputs whose variation most affects the recovery cost, along with the feedstock cost and the solid disposal cost.

- The minimum profitable capacity was estimated to be 45,100 tonnes of fly ash per year. To achieve such a capacity, all the generated petcoke needs to be burned. However, the current steam demand in the upgrader is supplied by burning only 11% of the generated petcoke. Ash ponds are alternative sources of fly ash to feed the process at the required capacity to generate profit. Further study in this area is required.
- About 26.6 kg CO_2eq/kg V_2O_5 would be generated through the life cycle of the recovered vanadium. Of this, 34% corresponds to indirect (upstream) emissions and 66% to direct emissions. The production of sodium chloride and ammonium chloride, and the generation of steam by petcoke combustion, are the primary contributors to the indirect emissions, while emissions from fly ash decarbonization are by far the main source of direct emissions.
- Sensitivity analysis shows that the life cycle GHG emissions are more sensitive to the air-to-fuel ratio in the roasting operation and to the emission factors from petcoke combustion and the gas treatment unit. Upstream operations have little effect on the life cycle GHG emissions, except in the emission factors associated with some consumables and the combustion of petcoke.
- Adding a salt recycling loop to the vanadium recovery process, using other means to obtain the feedstock for the process, and avoiding combustion for fly ash

decarbonization are options worthy of consideration to reduce both the vanadium recovery cost and the life cycle GHG emissions.

10.1.3 Techno-economic and life cycle GHG emissions assessments of heavy minerals recovery from bitumen extraction tailings

Data-intensive techno-economic and life cycle GHG emissions models of a process for recovering heavy minerals from froth treatment tailings of bitumen extraction were developed. The tailings from naphthenic froth treatment were considered in this study. The reference recovery process has two phases: tailings processing to obtain a heavy mineral concentrate and the separation of zircon and titanium mineral fractions from the concentrate. A fraction of the residual bitumen contained in the tailings is also recovered during the concentration phase. A capacity of 15.5 million tonnes of froth treatment tailings was considered. This capacity was selected based on the current tailing generation rates of the bitumen extraction plants operating in Alberta. For the TEA, two scenarios were considered. In the first, the whole process is performed in a single plant. In the second, one or more individual concentration plants feed a centralized separation plant. For the life cycle GHG emissions assessment, the system boundary includes oil sands mining and bitumen extraction, both phases of the recovery process (performed in a single plant), fugitive emissions from tailings ponds, and the production of electricity and consumables. The functional unit is one tonne of recovered heavy minerals.

Considering the current market price of zircon and titanium minerals and including the revenue stream from recovering bitumen from the tailings, the process is profitable in both scenarios. Scenario 2 offers the opportunity of cooperation between operators of bitumen extraction plants, concentration plants, and a centralized separation plant. Adjusting the internal rate of return expected by each actor would improve the economy of the whole process. The project would be appealing depending on the hurdle rate of the company running the process; however, its opportunity cost is zero since heavy minerals in tailings are currently stockpiled in tailings ponds. Regarding GHG emissions, the FTT pathway to produce heavy minerals is potentially more carbon-intensive than primary production processes if the upstream emissions, i.e., those from oil sands mining and bitumen extraction, are partially allocated to the FTT. The conclusions from this study are supported by the findings summarized below:

- The IRR under scenario 1 was 9.8%, obtained from selling the recovered heavy minerals and residual bitumen separated from the concentrate in the process. The estimated IRR is more sensitive to the zircon selling price, the nominal capacity of the spiral separators used in the primary gravity separation operation, the cost of disposing the rejected non-valuable mineral material, the annual labor rate, the on-stream factor, the outside battery limit investment, and the selling price of the recovered titanium minerals and bitumen.
- In scenario 2, a single heavy minerals concentration plant would get a 10% IRR by selling the heavy mineral concentrate at \$21.52/t, while the return of the heavy mineral separation plant would be 7.6%. The IRR of the separation plant increases to 11.6% if its capacity increases to process the heavy mineral concentrates obtained from concentrations plants in each of the three naphthenic froth treatment plants operating in Alberta.
- Considering indirect (upstream) and direct emissions, the life cycle GHG emissions of the recovered heavy minerals were estimated to be 1,540 kg CO_2eq per tonne.

Considering the avoided upstream emissions by recovering the residual bitumen from the FTT, the life cycle GHG emissions would be reduced to 1,499 kg CO_2eq/t heavy minerals.

- Life cycle GHG emissions of heavy minerals from FTT are driven by the upstream emissions associated with the generation of the tailings that feed the mineral concentration process, i.e., oil sands mining and bitumen extraction, and by fugitive emissions from tailings ponds. Those emissions represent 59% of the total.
- The bitumen production (mining and extraction), grid, and natural gas emission factors, along with the DVL are the inputs with the most effect on the life cycle GHG emissions.

10.1.4 Techno-economic and life cycle GHG emissions assessments of bitumen-derived asphaltene-based carbon fibers

Some studies have demonstrated the suitability of bitumen-derived asphaltenes as a precursor for carbon fiber production, at least at laboratory scale. Although the technology is still at an early stage of development, projections of the economic and environmental performances of the production process at a commercial scale would help researchers to optimize in advance the process, with the aim of a low-cost and low carbon-intensive operation, compared with the use of PAN as precursor. Also, these projections would bring insights into the value chain of asphaltene to feed ACF production and inform decision-making toward reducing the cost and carbon footprint of the produced carbon fiber. To that end, techno-economic and life cycle GHG emissions assessments of the production of carbon fiber from asphaltenes derived from oil sands bitumen were performed in this study. The reference process considered in the study consists of asphaltene thermal modification, melt spinning, fiber stabilization and carbonization, and finishing operations. The process feedstock is asphaltene obtained from solvent deasphalting of in situ-produced bitumen as part of a partial upgrading scheme. For the TEA, a plant with capacity of 3,000 tonnes of carbon fiber (12k tow size) was considered as the base case. This capacity is typical of existing PAN-CF commercial plants. The effect of scale and tow size on production cost were also studied. For the life cycle GHG emissions assessment, direct emissions from the production process of precursor and carbon fiber, upstream emissions from bitumen production and deasphalting, and the production of electricity and consumables, were accounted for.

Using bitumen-derived asphaltenes as a precursor would significantly reduce the production cost of carbon fiber compared with PAN-CF. The process is profitable, and the production cost is within the range considered by the automotive industry for mass adoption. Asphaltene-based carbon fiber is potentially less carbon-intensive than PAN-CF. Life cycle GHG emissions are less than two-thirds of those from the PAN pathway, mainly because fewer raw material conversion processes and a simple precursor production process are required in the asphaltene pathway. Both the production cost and GHG emissions are sensitive to the carbon yield of the process, stabilization time, nitrogen consumption in the carbonization furnace, and the air requirement in the stabilization ovens. The conclusions from this study are supported by the findings summarized below:

- For the base case, the production cost was estimated at $10.16 per kg of carbon fiber. This cost is about half of the current market price of PAN-CF, which makes the process profitable. The low cost of precursor manufacturing is the main reason for the overall low production cost. Even after considering uncertainties in the model, the production cost is below the market price. Because the technology is at an early stage of development, progressive elaboration is required to improve the accuracy of the estimate; however, there is a high chance that the process will be profitable at a commercial scale.

- The process benefits from economies of the scale. The minimum profitable capacity is relatively low (890 tonnes CF per year) compared with typical capacities of existing PAN-CF plants. Increasing the capacity (above 3,060 tonnes CF per year) would reduce the production cost to levels that are appealing to the automotive industry (less than \$10/kg CF). The plant capacity is not a constraint because the current production of bitumen in Alberta is more than enough to supply the asphaltenes required to meet the world's demand for carbon fiber.
- Production cost also decreases with the tow size, mainly because fewer spinning positions are required to match the production flow as tow size increases. Typical commercial tow sizes (e.g., 12k, 50k, 100k) are feasible for asphaltene-based carbon fiber production, with profitable production costs. A combination of plant capacity and tow size would be selected based on market specifications.
- The life cycle GHG emissions were estimated at 16.2 kg CO_2eq/kg CF, 68.7% less than those from the production of PAN-CF. About 87% corresponds to the production of carbon fiber. The contribution of precursor manufacturing (asphaltene modification and melt spinning) is 8%, while upstream operations are responsible for 5% of the share.
- The production of electricity to supply heat to the carbonization operation generates most of the life cycle GHG emissions. Off-gas GHG emissions from the precursor

and carbon fiber stages also contribute significantly because of the relatively low overall yield of the process.

10.2 Recommendations for future work

The following suggestions provide direction to further advance the research and pave the way for developing an industry based on non-combustion products of oil sands in Alberta.

10.2.1 Consider the effect of additional supply on the market price of non-combustion products

Alberta's oil sands have the potential to become a significant source of zircon, titanium minerals, vanadium, and carbon fiber. At their current market price, their production is profitable above certain capacities. Yet once these non-combustion products are produced at a commercial scale, there is a risk of flooding the market with a surge in supply, which could significantly reduce prices and render the processes unfeasible. The balance between the production capacity of these materials and their impact on market price should be addressed to determine their actual economic potential. The developed techno-economic models can be coupled with a market model to assess the effect of the additional supply on the market price and, consequently, on the revenue from the processes. Then, the profit can be optimized as a function of the plant capacity.

10.2.2 Consider other sources of non-combustion products in the oil sands value chain

Besides those considered in this study, other wastes and by-products of the oils sands industry are potential sources of the targeted non-combustion products. The tailings from paraffinic froth treatment could be processed to recover heavy minerals, and precipitated asphaltenes could be used to produce carbon fiber. Xu et al. (2013) developed a process to recover asphaltenes from bitumen extraction tailings by means of solvent extraction or agglomeration. At the back end of the bitumen value chain, asphaltenes could be separated from asphalt. The process developed by Sun (2022) could be used as a reference to explore this alternative source of asphaltenes from oil sands bitumen. Instead of being combusted, petcoke can be gasified to produce steam, electricity, chemicals, or liquid fuels. The concentrations of vanadium and nickel in the resulting slag are expected to be high. Nakano and Nakano (Nakano and Nakano 2017) have proven the technical feasibility of recovering such metals from gasification slag.

10.2.3 Explore other non-combustion products

Beside the non-combustion products considered in this study, other products that could be derived from oil sands can be explored from a techno-economic and environmental perspective. Meisen (2017) identified the following potential products: asphalt, graphene, controlled-release fertilizers, and nickel, among others. The production process of some of these products has been proven at laboratory scale and the available data can be used to develop techno-economic and GHG emissions estimates at a commercial scale. AlHumaidan et al. (2023) developed a process to synthetize graphene from asphaltenes through high temperature carbonization, while Saadi et al. (2022) used a flash joule heating process to convert asphaltenes into graphene. Vishnyakov (2023) reviewed processes to recover vanadium and nickel from crude oil, petcoke, and ashes of crude oil, petcoke, and asphalt. Chauhan and de Klerk (2020) studied the extraction of vanadium and nickel from bitumen using ionic liquids. Feng (2017) developed a process flowsheet to recover vanadium by producing activated carbon from fluid petcoke.

References

[1] Canadian Ammonia Producers. Benchmarking energy efficiency and carbon dioxide emissions. Prepared for the Canadian Fertilizer Institute and Natural Resources Canada, 2008. Available from: https://www.nrcan.gc.ca/sites/www.nrcan.gc.ca/files/oee/files/pdf/industrial/ammonia-study.pdf. Access date: November 20, 2021.

[2] Abella, J. and J. Bergerson. Model to investigate energy and greenhouse gas implications of refining petroleum: Impacts of crude quality and refining configuration. Environmetal Science & Technology. **46**(24): 13037-13047.

[3] Adroit Market Research. Global vanadium redox batteries market size 2017 by type, by application, by region and forecast 2018-2025, 2019. Available from: https://www.adroitmarketresearch.com/industry-reports/vanadium-redox-batteries-market. Access date: July 15th, 2020.

[4] Ahmad, H., A.A. Markina, M.V. Porotnikov, and F. Ahmad. A review of carbon fiber materials in automotive industry. IOP Conference Series: Materials Science and Engineering, 2020. **971**(3): 032011 DOI: 10.1088/1757-899x/971/3/032011.

[5] Akcil, A., F. Veglio, F. Ferella, M.D. Okudan, and A. Tuncuk. A review of metal recovery from spent petroleum catalysts and ash. Waste Management, 2015. **45**: 420-33 DOI: 10.1016/j.wasman.2015.07.007.

[6] Al-Sheeha, H., M. Marafi, V. Raghavan, and M.S. Rana. Recycling and Recovery Routes for Spent Hydroprocessing Catalyst Waste. Industrial & Engineering Chemistry Research, 2013. **52**(36): 12794-12801 DOI: 10.1021/ie4019148.

[7] Al Bari, M.A., S.K. Nabil, S. Saad, R. Sarkar, S. Sabiha, M.M. Rahman, and M.G. Kibria. Economic and environmental assessment of asphaltene-derived carbon fiber production. Green Chemistry, 2023. **25**: 6446-6458.

[8] Alberta Energy Regulator. 2018 [cited 2020 November 21st]; Available from: https://www.aer.ca.

[9] Alberta Energy Regulator. Alberta mineable oil sands plant statistics. Monthly supplement. August 2020, 2020. Statistical Series 39. Available from: https://static.aer.ca/prd/documents/sts/ST39.pdf.

[10] Alberta Energy Regulator. Alberta mineable oil sands plant statistics. Monthly supplement. December 2019, 2019. Statistical Series 39. Available from: https://static.aer.ca/prd/documents/sts/ST39-2019.pdf.

[11] Alberta Energy Regulator. ST39: Alberta mineable oil sands plant statistics monthly supplement, 2023a. Available from: https://www.aer.ca/providing-information/data-and-reports/statistical-reports/st39. Access date: April 21st, 2023.

[12] Alberta Energy Regulator. ST53: Alberta in situ oil sands production summary. 2021 [cited 2021 October 10]; Available from: https://www.aer.ca/providing-information/data-and-reports/statistical-reports/st53.

[13] Alberta Energy Regulator. Statistic and data. 2023b [cited 2023 April 22nd]; Available from: https://www.aer.ca/providing-information/data-and-reports/statistical-reports/st98/statistics-and-data.

[14] Alberta Innovates. Carbon Fibre Grand Challenge. 2021 [cited 2021 September 1]; Available from: https://albertainnovates.ca/programs/carbon-fibre-grand-challenge/.

[15] Aldosari, S.M., M. Khan, and S. Rahatekar. Manufacturing carbon fibres from pitch and polyethylene blend precursors: a review. Journal of Materials Research and Technology, 2020. **9**(4): 7786-7806.

[16] AlHumaidan, F.S., M.S. Rana, M. Vinoba, H.M. AlSheeha, A.A. Ali, and R. Navvamani. Synthesis of graphene derivatives from asphaltenes and effect of carbonization temperature on their structural parameters. RSC Advances, 2023. **13**(12): 7766-7779 DOI: 10.1039/D2RA07481H.

[17] alibaba.com. Fly ash price per ton. 2022a [cited 2022 October 10]; Available from: https://www.alibaba.com/showroom/fly-ash-price-per-ton.html.

[18] alibaba.com. Price of NaCl. 2022b [cited 2022 October 10]; Available from: https://www.alibaba.com/showroom/price-of-nacl.html.

[19] Allam, N.E., B.S. Zakaria, P.V. Kuznetsov, B.R. Dhar, and A.C. Ulrich. Mitigating methane emission from oil sands tailings using enzymatic and lime treatments. Chemosphere, 2023. **313**: 137455.

[20] Alonso-Fariñas, B., M. Rodríguez-Galán, C. Arenas, F. Arroyo, and C. Leiva. Sustainable management of spent fluid catalytic cracking catalyst from a circular economy approach. Waste Management, 2020. **110**: 10-19.

[21] AMG Vanadium. Sustainability. [cited 2022 January 8]; Available from: https://amg-v.com/sustainability/.

[22] Ancheyta, J. and J.G. Speight. Hydroprocessing of Heavy Oils and Residua. Chemical Industries. 2007: CRC Press.

[23] Araya, N., Kraslawaki, Andrzej, and L.A. Cisternas. Towards mine tailings valorization: Recovery of critical materials from Chilean mine tailings. Journal of Cleaner Production, 2020. **263**: 121555.

[24] Argonne National Laboratory. GREET model 2020. 2020 [cited 2021 December 15]; Available from: https://greet.es.anl.gov/index.php.

[25] Arroyo, F., C. Fernandez-Pereira, and P. Bermejo. Demonstration plant equipment design and scale-up from pilot plant of a leaching and solvent extraction process. Minerals 2015. **5**: 298-313.

[26] Arya, T.A. Economic and environmental analysis of carbon fibres from bitumen, 2020. Capstone project. MSc. in Sustainable Energy Development. University of Calgary.

[27] Aterburn, R.A. The sizing and selection of hydrocyclones. N.d. [cited 2023 March 14th]; Available from: https://www.911metallurgist.com/blog/wp-content/uploads/2015/10/SIZING-AND-SELECTION-OF-HYDROCYCLONES.pdf.

[28] Australian Trade and Investment Commission. Australian critical minerals prospectus 2022. 2022 [cited 2023 May 28]; Available from: https://www.globalaustralia.gov.au/sites/default/files/2022-12/australian-critical-minerals-prospectus-dec-2022.pdf.

[29] Baddour, F. and L.J. Snowden-Swan. Catalyst cost model development (CatCost), 2019. U.S. Department of Energy, Bioenergy Technologies Office. Available from: https://www.energy.gov/sites/prod/files/2019/03/f61/Catalyst%20Cost%20Model%20Development%20%28CatCost%29_NL0030154.pdf. Access date: November 20, 2020.

[30] Baillie, R.A., L.F. Schmoyer, and T.E. Skarada. Process for recovering hydrocarbons and heavy minerals from a tar sand hot water process waste stream. US 3,990,885. United States Patent and Trademark Office. 1976.

[31] Bajpai, P. Chapter 2 - Raw materials and processes for the production of carbon fiber, in Carbon Fiber. 2021a. Elsevier. pp. 13-50.

[32] Bajpai, P. Chapter 9 - The carbon fiber/carbon fiber reinforced plastic/recycled carbon fiber-reinforced polymer market, in Carbon Fiber. 2021b. Elsevier. pp. 157-170.

[33] Baker, D.A. and T.G. Rials. Recent advances in low-cost carbon fiber manufacture from lignin. Journal of Applied Polymer Science, 2013. **130**: 713-728 DOI: 10.1002/APP.39273.

[34] Barile, C. and C. Casavola. Mechanical characterization of carbon-fiber-reinforced plastic specimens for aerospace applications, in Mechanical and Physical Testing of Biocompositrs, Fibre-Reinforced Composites and Hybrid Composites, M. Jawaid, M. Thariq, and N. Saba, Editors. 2019. Woodhead Publishing.DOI: https://doi.org/10.1016/B978-0-08-102292-4.01001-8.

[35] Baritto, M., A. Oni, and A. Kumar. Life cycle GHG emissions assessment of vanadium recovery from spent catalysts from bitumen upgrading. Fuel, 2023a. **(Submitted)**.

[36] Baritto, M., A. Oni, and A. Kumar. Vanadium recovery from oil sands petcoke fly ash: a comprehensive techno-economic assessment. Waste Management, 2023b. **(Submitted)**.

[37] Baritto, M., A.O. Oni, and A. Kumar. The development of a techno-economic model for the assessment of vanadium recovery from bitumen upgrading spent catalyst. Journal of Cleaner Production, 2022. **363**(20): 132376.

[38] Baritto, M., A.O. Oni, and A. Kumar. Estimation of life cycle GHG emissions of asphaltene-based carbon fibers derived from oil sands bitumen. Sustainable Materials and Technologies, 2023c. **36**: e00627.

[39] Barnett, I. Thermal modification of acrylonitrile yarns. US 2,913,802. United States Patent and Trademark Office. 1959. Available from: https://patentimages.storage.googleapis.com/1d/af/51/e1a1ec85f30831/US2913802.pdf. Access date: March 2, 2022.

[40] Bazyleva, A., M. Fulem, M. Becerra, B. Zhao, and J.M. Shaw. Phase behaviour of Athabasca bitumen. Journal of Chemical & Engineering Data, 2011. **56**: 3242-3253.

[41] Benchaita, T. Greehouse gas emissions from new petrochemical plants, 2013. Inter-American Development Bank. IDB-TN-562. Available from: https://publications.iadb.org/publications/english/document/Greenhouse-Gas-Emissions-from-New-Petrochemical-Plants-Background-Information-Paper-for-the-Elaboration-of-Technical-Notes-and-Guidelines-for-IDB-Projects.pdf.

[42] Bengtsson, A., J. Bengtsson, K. Jedvert, M. Kakkonen, O. Tanhuanpää, E. Brännvall, and M. Sedin. Continuos stabilization and carbonization of a lignin-cellulose precursor to carbon fiber. ACS Omega, 2022. **7**(19): 16793-16802.

[43] Bergerson, J.A., O. Kofoworola, A. Charpentier, S. Sleep, and H.L. MacLean. Life cycle greenhouse gas emissions of current oil sands technologies: Surface mining and In Situ applications. Environmental Science & Technology, 2012. **46**: 7865-7874.

[44] Berrebi, G., P. Dufresne, and Y. Jacquier. Recycling of spent hydroprocessing catalysts: EURECAT technology. Environmental Progress, 1993. **12**(2): 97-100.

[45] BGC Engineering Inc. Oil sands tailings technology review, 2010. Oil Sands Research and Information Network, University of Alberta, School of Energy and the Environment. OSRIN Report No. TR-1. Available from: https://era.library.ualberta.ca/items/d54a3e22-cf15-4c3b-baeb-2ee10578a259/view/ad8166dd-861d-4162-afac-949a5ac82582/Tailings-20Technology-20Review-20--202010-2007-2019.pdf. Access date: November 13, 2023.

[46] Bisheh, H. and Y. Abdin. Carbon fibers: from PAN to asphaltene precursors; a state-of-art review. C - Journal of Carbon Research, 2023. **9**(1): 19 DOI: https://doi.org/10.3390/c9010019.

[47] Biswas, R.K. Recovery of vanadium and molybdenum from heavy oil desulphurization waste catalyst. Hydrometallurgy, 1985. **14**: 219-230.

[48] Bjerknes, V., E.R. Iversen, T. Bakke, A. Helland, B. Sivertsen, and T. Bekkestad. Preliminary environmental impact assessment for a plant for the recovery of vanadium and nickel from flexicoke (VNRP) at Refineria de Amuay, Venezuela (2nd edition). 1995 [cited 2022 December 4]; Available from: https://niva.brage.unit.no/niva-xmlui/handle/11250/208308.

[49] Bohnert, G. and D. Bowen. Methods of making carbon fiber from asphaltenes. US2014/0175688A1. United States Patent and Trademark Office. 2014. Available from: https://patents.google.com/patent/US20140175688A1/en. Access date: December 14, 2021.

[50] Bond, F.C. Crushing and grinding calculations. British Chemical Engineering, 1961. **6**: 378-385.

[51] Boulamanti, A. and J.A. Moya. Energy efficiency and GHG emissions: Prospective scenarios for the chemical and petrochemical industry, 2017. Joint Research Centre. Science for Policy Report. EUR 28471 EN. doi:10.2760/20486

[52] BP. Crude assays. 2021 [cited 2021 June 3]; Available from: https://www.bp.com/en/global/bp-global-energy-trading/features-and-updates/technical-downloads/crudes-assays.html.

[53] Brown, H.L., B.B. Hamel, B.A. Hedman, M. Koluch, B.C. Gajanana, and P. Troy. Energy Analysis of 108 Industrial Processes. 1996: The Fairmont Press, Inc.

[54] Bulatovic, S. An investigation of the recovery of zircon and titanium from Athabasca oil sand samples, 2000. Lakefield Research Final report LR5569.

[55] Burkus, Z. GHG emissions from oil sands tailings ponds: Overview and modelling based on fermentable substrates. Part II: Modeling of GHG emissions from tailing ponds based on fermentable substrates, 2014a. Alberta Environment and Sustainable Resources Development. Available from: https://open.alberta.ca/publications/ghg-emissions-from-oil-sands-tailing-ponds-overview-and-modelling-based-on-fermentable-substrates. Access date: Septembre 10 2023.

[56] Burkus, Z. GHG emissions from oil sands tailings ponds: overview and modelling based on fermentable substrates. Part II: modelling of GHG emissions from tailing ponds based on fermentable substrates, 2014b. Alberta Environment and Sustainable Resource Development. Available from: https://era.library.ualberta.ca/items/411947ce-1a33-42d5-a2cf-172fba9a2553. Access date: November 18, 2023.

[57] Bushveld Minerals. The vertically integrated primary vanadium producer. February 2020 corporate presentation, 2020. Available from: http://www.bushveldminerals.com/wp-content/uploads/2020/02/Corporate-presentation-Feb-2020-Final-20022020-website.pdf.

[58] Camachen. Sodium diisobutyl dithiophosphate/dithiophosphate IBS 49% - 51%. N.d. [cited 2023 May 1]; Available from: https://camachem.com/en/sodium-diisobutyl-dithiophosphate-dithiophosphate-ibs-49-51.html.

[59] Canada Energy Regulator. Canada's Energy Future 2019: Energy Supply and Demand Projections to 2040. 2017 [cited 2020 January 14th]; Available from: https://apps.cer-rec.gc.ca/ftrppndc/dflt.aspx?GoCTemplateCulture=en-CA%3f%2f.

[60] Canada Energy Regulator. Canada's Energy Future 2020: Energy Supply and Demand Projections to 2050. 2020 [cited 2020 December 09, 2020]; Available from: https://apps.cer-rec.gc.ca/ftrppndc/dflt.aspx?GoCTemplateCulture=en-CA.

[61] Canada Energy Regulator. Market snapshot: oil sands bitumen production will continue to grow to 2040. 2018 [cited 2021 September 19]; Available from: https://www.cer-rec.gc.ca/en/data-analysis/energy-markets/market-snapshots/2018/market-snapshot-oil-sands-bitumen-production-will-continue-grow-2040.html.

[62] CarbonCloud. Wheat starch BE. 2023 [cited 2023 November 15]; Available from: https://apps.carboncloud.com/climatehub/product-reports/id/159429329442#:~:text=%E2%80%9DWheat%20starch%E2%80%9D%20currently%20has%20a,of%20this%20product's%20climate%20footprint.

[63] Cec Mining Systems. Power comparison study - Tailings filtration options. 2017 [cited 2023 March 14]; Available from: https://cecminingsystems.com/wp-content/uploads/2017/06/Power-Comparison-Study-Filtration-Equipment-Options.pdf.

[64] Cengel, Y.A. and M.A. Boles. Thermodynamics. An Engineering Approach. Eighth ed. 2015. New York: McGraw Hill.

[65] Cespi, D., F. Passarini, E. Neri, I. Vassura, L. Ciacci, and F. Cavani. Life cycle assessment comparison of two ways for acrylonitrile production: the SOHIO process and an alternative route using propane. Journal of Cleaner Production, 2014. **69**: 17-25.

[66] Chachula, F. and Q. Liu. Upgrading a rutile concentrate produced from Athabasca oil sands tailings. Fuel, 2003. **82**: 929-942.

[67] Chacón-Patiño, M., A. Neumann, C. Rüger, P. Bomben, L. Friederici, R. Zimmermann, E. Frank, P. Kreis, M. Buchmeiser, and M. Gray. Chemistry and properties of carbon fiber feedstocks from bitumen asphaltenes. Energy Fuels, 2023. **37**(7): 5341-5360.

[68] Chauhan, G. and A. de Klerk. Extraction of vanadium and nickel from diluted bitumen and partially deasphalted oil using ionic liquids. Energy & Fuels, 2020. **34**(9): 10849-10857 DOI: 10.1021/acs.energyfuels.0c02004.

[69] ChemAnalyst. Track real-time price movement of 300+ chemical and petrochemical products for informed purchase decisions. 2022 [cited 2022 May 25]; Available from: https://www.chemanalyst.com/Pricing/Pricingoverview.

[70] Chemistry Industry Association of Canada. Economic review of chemistry, 2021. Available from: https://canadianchemistry.ca/wp-content/uploads/2021/10/2021-Economic-Review-of-Chemistry-CIAC.pdf. Access date: September 20, 2022.

[71] Chen, S., X. Fu, M. Chu, Z. Liu, and J. Tang. Life cycle assessment of the comprehensive utilisation of vanadium titano-magnetite. Journal of Cleaner Production, 2015. **101**: 122-128.

[72] Chen, W. Fabrication of carbon fibers with high mechanical properties. W0/2021/072559. W.I.P. Organization. 2021. Available from: https://patentscope.wipo.int/search/en/detail.jsf?docId=WO2021072559&tab=PCTDESCRIPTION&_cid=P20-KS101F-83760-1. Access date: January 16th 2022.

[73] Chen, X.-l., L.-s. Xiao, J. Xu, and J.-s. Wang. A study on recovering vanadium and molybdenum from spent catalyst. Mining and Metallurgical Engineering, 2004. **2004-3**.

[74] Chen, Y., Q. Feng, Y. Shao, G. Zhang, L. Ou, and Y. Lu. Investigations on the extraction of molybdenum and vanadium from ammonia leaching residue of spent catalyst. International Journal of Mineral Processing, 2006. **79**(1): 42-48 DOI: 10.1016/j.minpro.2005.11.009.

[75] Chen, Y., Q. Feng, G. Zhang, L. Ou, and Y. Lu. Study on the recycling of valuable metals in spent Al2O3-based catalyst. Mineral and Metallurgical Processing, 2007. **24**(1): 30-34.

[76] Chichanowicz, J.E. Current capital cost and cost-effectiveness of power plant emissions control technologies, 2010. Utility Air Regulatory Group. Available from: https://downloads.regulations.gov/EPA-R08-OAR-2012-0026-0241/attachment_43.pdf. Access date: September 15, 2022.

[77] Chien-Wei Chen, M. Commercial viability analysis of lignin based carbon fibre, 2014. Master of Business Administration. Simon Fraser University.

[78] Chua, C.Y.X., H.-C. Liu, N. Di Trani, A. Susnjar, J. Ho, G. Scorrano, J. Rhudy, A. Sizovs, G. Lolli, N. Hernandez, M.C. Nucci, R. Cicalo, M. Ferrari, and A. Grattoni. Carbon fiber reinforced polymers for implantable medical devices. Biomaterials, 2021. **271**: 120719 DOI: 10.1016/j.biomaterials.2021.120719.

[79] Cibati, A., F. Pagnanelli, and L. Toro. Metal recovery from end-of life hydrotreating catalysts by selective precipitation: Laboratory tests and preliminary process analysis. Environmental Progress and Sustainable Energy, 2015. **34**(703-712).

[80] Ciotola, A., M. Fuss, S. Colombo, and W.-R. Poganietz. The potential supply risk of vanadium for the renewable energy transition in Germany. Journal of Energy Storage, 2021. **33**: 102094.

[81] City of Winnipeg. Emission factors in kg CO2-equivalent per unit. [cited 2022 January 28]; Available from: https://www.winnipeg.ca/finance/findata/matmgt/documents/2012/682-2012/682-2012_Appendix_H-WSTP_South_End_Plant_Process_Selection_Report/Appendix%207.pdf.

[82] Ciu, Z., Q. Liu, T.H. Etsell, J. Oxenford, and J. Coward. Heavy minerals in the athabasca oil sands tailings - potential and recovery processes. Canadian Metallurgical Quarterly, 2013. **42**(4): 383-392 DOI: 10.1179/cmq.2003.42.4.383.

[83] Compositesword.com. Materials & processes: fiber formats for composites. 2016 [cited 2022 Jan 2]; Available from: https://www.compositesworld.com/articles/fiber-reinforcement-forms.

[84] Cousins, A., R.W. Hughes, D.J. McCalden, D.Y. Lu, and E.J. Anthony. Waste classification of slag generated in a pilot-scale entrained-flow gasifier. Coal Combustion and Gasification Products, 2018. **4**: 37-44.

[85] CVW Cleantech. Process and technology overview, 2023. Available from: https://cvwcleantech.com/technology/process-and-technology-overview/.

[86] CVW Cleantech Inc. Process and technology overview, 2023. Available from: https://cvwcleantech.com/technology/process-and-technology-overview/. Access date: September 10, 2023.

[87] Das, S. Life cycle assessment of carbon fiber-reinforced polymer composites. Internation Journal of Life Cycle Assessment, 2011. **16**: 268-282.

[88] Das, S. and P. Nagapurkar. Sustainable coal tar pitch carbon fiber manufacturing, 2021. Oak Ridge National Laboratory. ORNL/TM-2021/1889. Available from: https://www.osti.gov/servlets/purl/1784125.

[89] Das, S., J. Warren, D. West, and S.M. Schexnayder. Global carbon fiber composites supply chain competitiveness analysis, 2016. Oak Ridge National Laboratory. ORNL/SR-2016/100.

[90] Davila Armas, C.E. The extraction of vanadium and nickel from petroleum cokes, 1988. Department of Mineral Resources Engineering. PhD. University of London. London.

[91] De Crisci, A., R. Gieleciak, M.H. Mobarok, M. Ali, T.D. Ngo, K. Goswani, A. Khan, and J. Chen. Producing asphaltene fibres from bitumen-derived asphaltenes for carbon fibre development: Part one-electrospinning. The Canadian Journal of Chemical Engineering, 2022. **101**(5): 2341-3008.

[92] Deloitte. Report on developing baseline specific energy consumption in petrochemicals industry in India, 2013. Shakti Sustainable Energy Foundation. Available from:

https://shaktifoundation.in/wp-content/uploads/2017/06/Petrochemicals.pdf. Access date: May 29, 2021.

[93] Despatch. Industrial walk in ovens and truck in ovens. N.d. [cited 2021 July 29]; Available from: https://www.despatch.com/walkin-ovens-and-truck-in-ovens.html.

[94] Di Lullo, G., E. Gemechu, A. Oni, and A. Kumar. Extending sensitivity analysis using regression to effectively disseminate life cycle assessment results The International Journal of Life Cycle Assessment, 2019. **25**: 222-229 DOI: 10.1007/s11367-019-01674-y.

[95] Di Lullo, G., E. Gemechu, A.O. Oni, and A. Kumar. Extending sensitivity analysis using regression to effectively disseminate life cycle assessment results. The International Journal of Life Cycle Assessment, 2020(2).

[96] Duchesne, M. Slagging in entrained-flow gasifiers, 2012. Deprtment of Chemical and Biological Engineering. PhD in Chemical Engineering. University of Ottawa.

[97] Duchesne, M., S. Champagne, and R. Hughes. Dry petroleum coke gasification in a pilot-scale entrained-flow gasifier and inorganic element partitioning model. Energy Fuels, 2017. **31**: 6658-6669.

[98] Duchesne, M., J. Nakano, Y. Hu, A. MacLennan, R. Hughes, J. Bennett, and A. Nakano. Vanadium oxidation state determination by X-Ray absorption spectroscopy. Presented at the The 10th International Conference on Molten Slags, Fluxes and Salts (MOLTEN16). 2016. Seattle, Washington, USA. pp. 1405-1412.

[99] Dufresne, P. Hydroprocessing catalysts regeneration and recycling. Applied Catalysis A: General, 2007. **322**: 67-75 DOI: 10.1016/j.apcata.2007.01.013.

[100] Edwards, L. The history and future challenges of calcined petroleum coke production and use in aluminum smelting. The Journal of The Minerals, Metals & Materials Society, 2015. **67**(2): 308-321.

[101] El-Nadi, Y.A., N.S. Awwad, and A.A. Nayl. A comparative study of vanadium extraction by Aliquat-336 from acidic and alkaline media with application to spent catalyst. International Journal of Mineral Processing, 2009. **92**(3-4): 115-120 DOI: 10.1016/j.minpro.2009.03.005.

[102] Ellringmann, T., C. Wilms, M. Warnecke, G. Seide, and T. Gries. Carbon fiber production costing: a modular approach. Textile Research Journal, 2016. **86**(2): 178-190.

[103] Engin, T. and V. Ari. Energy auditing and recovery for dry type cement rotary kiln systems - A case study. Energy Conversion and Management, 2005. **46**: 551-562.

[104] Engineering Toolbox. Electrical motors efficiency ratings. 2009 [cited 2022 November 20]; Available from: https://www.engineeringtoolbox.com/nema-electrical-motors-efficiency-ratings-d_1501.html.

[105] Engineering Toolbox. Fans - Efficiency and power consumption. 2003 [cited 2022 July 14]; Available from: https://www.engineeringtoolbox.com/fans-efficiency-power-consumption-d_197.html.

[106] Engineering toolbox. Fossil and alternative fuels - Energy content. 2008 [cited 2022 October 14]; Available from: https://www.engineeringtoolbox.com/fossil-fuels-energy-content-d_1298.html.

[107] Ennis, B.L., C.L. Kelley, B.T. Naughton, R.E. Norris, S. Das, D. Lee, and D. Miller. Optimized carbon fiber composites in wind turbine blade design, 2019. U.S. Department of Energy. Available from: https://www.osti.gov/biblio/1592956. Access date: June 10, 2022. 10.2172/1592956

[108] Environmental Protection Agency. EPA_Flares_costcalculations_sheet_august2019. 2019 [cited 2022 May 26]; Available from: https://www.epa.gov/sites/production/files/2019-08/epa_flares_costcalculations_sheet_august2019vf.xlsm.

[109] Erasmus, D., N. Dawson, and F. Chachula. Process for recovering heavy minerals from oil sand tailings. US 7,695,612 B2. United States Patent and Trademark Office. 2010.

[110] Fagerlund, J., R. Zevenhoven, J. Thomassen, M. Tednes, F. Abdollahi, L. Thomas, C.J. Nielsen, T. Mikoviny, A. Wisthaler, L. Zhu, C. Biliyok, and A. Zhurkin. Performance of an amine-based CO_2 capture pilot plant at the Fortum Oslo Varme Waste to Energy plant in Oslo, Norway. International Journal of Grennhouse Gas Control, 2021. **106**: 103242.

[111] Fakhrhoseini, S.M. Pathways to reduce energy consumption in thermal stabilisation process of polyacrylonitrile fibre, 2018. Institute of Frontier Materials. PhD. Deakin University.

[112] Feng, J. Feasibility of utilizing oil-sands fluid coke as a secondary source of vanadium, 2017. Department of Chemical Engineering and Applied Chemistry. MASc. University of Toronto.

[113] Ferella, F., I. D'Adamo, S. Leone, V. Innocenzi, I. De Michelis, and F. Veglio. Spent FCC E-Cat: towards a circular approach in the oil refining industry. Sustainability, 2019. **11**(113) DOI: 10.3390/su11010113.

[114] Ferella, F., A. Ognyanova, I. De Michelis, G. Taglieri, and F. Veglio. Extraction of metals from spent hydrotreating catalysts: physico-mechanical pre-treatments and leaching stage. J Hazard Mater, 2011. **192**(1): 176-85 DOI: 10.1016/j.jhazmat.2011.05.005.

[115] Flint, L. Bitumen recovery technology: a review of long term R&D opportunities, 2005. LENEF Consulting. Available from: https://collections.lib.utah.edu/details?id=213965. Access date: March 1st, 2023.

[116] Focus Economics. Alumina Price Outlook. 2019 [cited 2020 January 15th]; Available from: https://www.focus-economics.com/commodities/base-metals/alumina.

[117] Furimsky, E. Gasification of oil sand coke: Review. Fuel Processing Technology, 1998. **56**: 263-290.

[118] Furimsky, E. Spent refinery catalysts: Environment, safety and utilization. Catalyst Today, 1996. **30**(4): 223-286.

[119] Gao, W., Z. Sun, H. Cao, H. Ding, Y. Zeng, P. Ning, G. Xu, and Y. Zhang. Economic evaluation of typical metal production process: A case study of vanadium oxide production

in China. Journal of Cleaner Production, 2020. **256**: 120217 DOI: 10.1016/j.jclepro.2020.120217.

[120] Gardner, H. Recovery of vanadium and nickel from petroleum residues. US Patent 4,816,236. US Patent and Trademark Office. 1987.

[121] Gary, J.H. and G.E. Handwerk. Petroleum refining, technology and economics. 4th ed. 2001. New York: Marcel Dekker.

[122] Ghosh, T., H. Chul Kim, R. De Kleine, T.J. Wallington, and B.R. Bakshi. Life cycle energy and greenhouse gas emissions implications of using carbon fiber reinforced polymers in automotive components: front subframe case study. Sustainable Materials and Technologies, 2021. **28**: e00263.

[123] Gill, A.S., D. Visotsky, L. Mears, and J.D. Summer. Cost estimation model for PAN based carbon fiber manufacturing process. Presented at the ASME 2016 11th International Manufacturing Science and Engineering Conference. 2016. Blacksburg, Virginia, USA. https://doi.org/10.1115/MSEC2016-8724.

[124] Gomez-Bueno, C.O., D.R. Spink, and G.L. Rempel. Extraction of vanadium from Athabasca tar sands fly ash. Metallurgical Transactions B, 1981. **12B**: 341-352.

[125] Gorain, B., J.-P. Franzidis, and E. Manlapig. Flotation Cell Design: Application of Fundamental Principles, in Flotation. 2000. Academic Press. pp. 1502-1512.

[126] Goss, I. Production functions and cost models for fibers in advanced composite materials, 1986. Materials Science and Engineering Master of Science. Massachusetts Institute of Technology.

[127] Government of Alberta. Carbon Offset Emission Factors Handbook. 2019a [cited 2021 February 3]; 2:[Available from: https://open.alberta.ca/publications/9781460146064.

[128] Government of Alberta. Carbon offset emission factors handbook, 2019b. Available from: https://open.alberta.ca/publications/9781460146064. Access date: February 3, 2021.

[129] Government of Alberta. Oil sands facts and statistics. 2017 October 31, 2020]; Available from: https://www.alberta.ca/oil-sands-facts-and-statistics.aspx#:~:text=Reserves%20and%20production,bbl%2Fd)%20in%202017.

[130] Government of Alberta. WCS oil price. 2023 [cited 2023 June 2]; Available from: https://economicdashboard.alberta.ca/dashboard/wcs-oil-price/.

[131] Government of Canada. Emission factors and reference values. 2022 [cited 2022 November 19]; Available from: https://www.canada.ca/en/environment-climate-change/services/climate-change/pricing-pollution-how-it-will-work/output-based-pricing-system/federal-greenhouse-gas-offset-system/emission-factors-reference-values.html#toc10.

[132] Government of Canada. Fuel charge rates. 2023a [cited 2023 June 1]; Available from: https://www.canada.ca/en/revenue-agency/services/forms-publications/publications/fcrates/fuel-charge-rates.html.

[133] Government of Canada. Greenhouse gas emissions. Canadian environmental sustainability indicators, 2023b. August 2. Available from: https://www.canada.ca/content/dam/eccc/documents/pdf/cesindicators/ghg-emissions/2023/greenhouse-gas-emissions-en.pdf.

[134] Government of Canada. Natural gas: a primer. 2015 [cited 2021 February, 2]; Available from: https://www.nrcan.gc.ca/energy/energy-sources-distribution/natural-gas/natural-gas-primer/5641.

[135] Grant, T., C. Anderson, and B. Hooper. Comparative life cycle assessment of potassium carbonate and monoethanolamine solvents for CO_2 capture from post combustion flue gases. International Journal of Grennhouse Gas Control, 2014. **28**: 35-44.

[136] Gray, M. Fundamentals of partial upgrading of bitumen. Energy & Fuels, 2019. **33**: 6843-6856.

[137] Gray, M. Upgrading oilsands bitumen and heavy oil. 2015. Edmonton, Alberta: The Univesity of Alberta Press.

[138] Gray, M.R., Y. Zhao, and C.M. McKnight. Coke and minerals removal from bitumen hydroconversion catalyst. Fuel, 2000. **79**: 285-294.

[139] Griffin, P.J. and T.H. Etsell. Extraction of vanadium and nickel from Athabasca oil sands fly ash, in The Future of Heavy Crude and Tar Sands, R.F. Meyer, J.C. Wynn, and J.C. Olson, Editors. 1984. McGraw-Hill: New York.

[140] Griffing, E. and M. Overcash. Carbon fiber from PAN. Contents of factory gate to factory gate life cycle inventory summary. 2009 [cited 2021 January 30]; Available from: http://www.environmentalclarity.com/.

[141] Gupta, A. and D.S. Yan. Mineral processing design and operation. An introduction. 2006: Elsevier Science. pp. 718.

[142] H.A. Simons Ltd. Mineral development agreement. Co-products study. Final report, 1996. Alberta Chamber of Resources. Y248C.

[143] Haas, F. and W. Hesse. Method for recovering vanadium from petroleum coke. US Patent 4,243,639 A. United States Patent and Trademark Office. January 06, 1981.

[144] Hansora, D. Industrial manufacturing process of acrylonitrile. 2013. Germany: Lambert Academic Publishing.

[145] Harper International. Energy efficiency in the carbon fiber conversion process. Presented at the JEC 2012. N.d. Paris, France. Available from: http://www.harperintl.com/wp-content/uploads/2011/09/energy-efficiency-carbon-fiber-conversion.pdf. Access date: July 27, 2021.

[146] Harper International. Energy efficiency in the carbon fiber conversion process. Presented at the JEC 2012. Paris, France. Available from: http://www.harperintl.com/wp-content/uploads/2011/09/energy-efficiency-carbon-fiber-conversion.pdf. Access date: July 27, 2021.

[147] Harper International. Processing advancements within reach for achieving significant reductions in carbon fiber cost of manufacturing, 2013. Available from: https://www.harperintl.com/wp-content/uploads/2011/09/processing-advancements-within-reach.pdf. Access date: January 14, 2021.

[148] Hashim, H., M.H. Raselan, I.M. Yazid, S.S. Shariffudin, and P.S.M. Saad. Influence of film thickness on electrical and optical properties of vanadium dioxide thin films for smart window coating application. Presented at the 6th International Conference on Electrical and Electronics Engineering (ICEEE). 2019. Instanbul, Turkey. Available from: https://ieeexplore.ieee.org/abstract/document/8792498. Access date: June 14, 2022.

[149] Haug, G. Aspects of rotary vacuum filter design and performance. Fluid/Particle Separation Journal, 2000. **13**(1).

[150] Haynes, V.O. Energy use in petroleum refineries, 1974. Oak Ridge National Laboratory. ORNL/TM-5433. Available from: https://www.osti.gov/servlets/purl/7261027. Access date: February 4, 2021.

[151] Hill, J., A. Karimi, and M. Malekshahian. Characterization, gasification, activation, and potential uses for the millions of tonnes of petroleum coke produced in Canada each year. The Canadian Journal of Chemical Engineering, 2014a. **92**: 1618-1626.

[152] Hill, J.M., A. Karimi, and M. Malekshahian. Characterization, gasification, activation, and potential uses for the millions of tonnes of petroleum coke produced in Canada each year. The Canadian Journal of Chemical Engineering, 2014b. **92**: 1618-1626.

[153] Holcombe, T. and D.P. Malone. Recovering vanadium oxides from petroleum coke by melting. US 6,235,253 B1. US Patent and Trademark Office. May 22, 2001.

[154] Holloway, P.C. Vanadium recovery from oil sands fly ash, 2003. Department of Chemical and Materials Engineering. MSc, Materials Engineering. University of Alberta. Edmonton, Alberta.

[155] Holloway, P.C. and T.H. Etsell. Alternative reagents for roasting Suncor oil sands fly ash. Mineral Processing and Extractive Metallurgy, 2004. **113**(3): 153-160.

[156] Holloway, P.C. and T.H. Etsell. Process for the complete utilization of oil sands fly ash. Canadian Metallurgical Quarterly, 2005. **45**(1): 25-32.

[157] Holloway, P.C., T.H. Etsell, and C.F. Bunnell. Atmospheric leaching of oil sands fly ash from Syncrude and Suncor. Minerals & Metallurgical Processing, 2005. **22**(3): 145-152.

[158] Holowenko, F.M., M. M.D., and P.M. Fedorak. Methanogens and sulfate-reducing bacteria in oil sands fine tailings waste. Canadian Journal of Microbiology, 2000. **46**: 927-937.

[159] Hund, K., D. La Porta, T.P. Fabregas, T. Laing, and J. Drexhage. Minerals for climate action: The mineral intensity of the clean energy transition, 2023. World Bank. Available from: https://openknowledge.worldbank.org/entities/publication/4dd08d0c-ab51-4955-a464-35a95201a5eb. Access date: December 12, 2023.

[160] Huson, M.G. High-performance pitch-based carbon fibers, in Structure and properties of high-performance fibers, G. Bhat, Editor. 2017.DOI: 10.1016/B978-0-08-100550-7.00003-6.

[161] Iluka. BMO global metals, minig and critical minerals conference. 2023 [cited 2023 May 28]; Available from: https://iluka.com/media/yraf3sau/presentation-bmo-global-metals-mining-critical-mnrls-conf.pdf.

[162] Inokawa, H., S.F. Zaman, M.A. Daous, A. Al-Zahrani, and L. Petrov. Vanadium oxide catalyst supported on CeO2—ZrO2 for formaldehyde production via partial oxidation of methanol. US10207253B1. United States Patent and Trademark Office. February 19th, 2019, 2017.

[163] Integrated Pollution and Prevention Control. Reference document on best available techniques for mineral oil and gas refineries, 2002. Joint Research Centre, European Commission. Available from: https://eippcb.jrc.ec.europa.eu/sites/default/files/2020-03/superseded_ref_bref-0203.pdf. Access date: March 15, 2021.

[164] International Energy Agency. Is carbon capture too expensive? 2021a [cited 2022 September 20]; Available from: https://www.iea.org/commentaries/is-carbon-capture-too-expensive.

[165] International Energy Agency. The role of critical minerals in clean energy transitions, 2021b. Available from: https://www.iea.org/reports/the-role-of-critical-minerals-in-clean-energy-transitions. Access date: December 13, 2023.

[166] International Organization for Standardization. Life cycle assessment. Principles and framework. Standard number: 14040, in Environmental Management. 2006.

[167] IPCC. 2006 IPCC Guidelines for national greenhouse gas inventories, 2006. National Greenhouse Gas Inventories Programme. Available from: https://www.ipcc-nggip.iges.or.jp/public/2006gl/index.html. Access date: July 14, 2021.

[168] iScrap App. Current scrap metal prices. 2020 [cited 2020 July 7th]; Available from: https://iscrapapp.com/prices/.

[169] Ityokumbul, M.T., W. Bulani, and N. Kosaric. Economic and environmental benefits from froth flotation recovery of titanium, zirconium, iron and rare earth minerals from oilsand tailings. Water Science and Technology, 1987. **19**(323-331).

[170] Jack, T.R., E. Sullivan, A., and J.E. Zajic. Leaching of vanadium and other metals from Athabasca oil sands coke and coke ash. Fuel, 1979. **58**: 589-594.

[171] Jack, T.R., E. Sullivan, A., and J.E. Zajic. The release of vanadium from Athabasca oil sands cokes by leaching techniques. CIM Bulletin, 1980. **73**(817).

[172] Jafarinejad, S. Solid-waste management in the petroleum industry, in Petroleum Waste Treatment and Pollution Control. 2017. Elsevier. pp. 269-345.

[173] James, F. The future of high capacity carbon fiber production. Presented at the Jecworld. Composites Show & Conferences. 2016. Paris. **2021**(February, 17). Available from: http://harperbeacon.com/wp-content/uploads/2016/04/The-Future-of-High-Capacity-Carbon-Fiber-Production-Lines-Harper-International.pdf. Access date: December 14, 2021.

[174] Kaminsly, H.A., T.H. Etsell, D.G. Ivey, and O. Omotoso. Characterization of heavy minerals in the Athabasca oil sands. Minerals Engineering, 2008. **21**: 264-271.

[175] Kan, J. Tailings solvent recovery unit. US20120043178A1. United States Patent and Trademark Office. 2011.

[176] Keeson, B. and J. Gieseman. Bitumen partial upgrading 2018 whitepaper, 2018. Jacobs Consultancy. AM0401A. Available from: https://albertainnovates.ca/wp-content/uploads/2018/05/Bitumen-Partial-Upgrading-2018-Whitepaper-2433-Jacobs-Consultancy-rev7.pdf. Access date: June 4, 2021.

[177] Kelley, K.D., C.T. Scott, D.E. Polyak, and B.E. Kimball. Vanadium, in Critical Mineral Resources of the United States - Economic and environmental Geology and Prospects for Future Supply, K.J. Schulz, J.H. DeYoung, R.R. Jr. Seal, and D.C. Bradley, Editors. 2017. U.S. Geological Survey. pp. U1-U36.DOI: https://doi.org/10.3133/pp1802U.

[178] Kim, H.-I., K.-W. Lee, D. Mishra, K.-M. Yi, J.-H. Hong, M.-K. Jun, and H.-K. Park. Separation and recovery of vanadium from leached solution of spent residue hydrodesulfurization (RHDS) catalyst using solvent extraction. Journal of Industrial and Engineering Chemistry, 2014. **20**(6): 4457-4462 DOI: 10.1016/j.jiec.2014.02.017.

[179] Kinidi, L., I.A.W. Tan, N.B. Abdul Wahab, K.F.B. Tamrin, C.N. Hipolito, and S.F. Salleh. Recent development in ammonia stripping process for industrial wastewater treatment. International Journal of Chemical Engineering, 2018. **2018**: 1-14 DOI: 10.1155/2018/3181087.

[180] Kobos, P.H., T.E. Drennen, A. Outkin, E.K. Well, S.M. Paap, and S. Wiryadinata. Tecno-economic analysis: Best practices and assessment tools, 2020. Sandia National Laboratories. SAND2020-13473. Available from: https://www.osti.gov/servlets/purl/1738878. Access date: September 14, 2023.

[181] Köhler, T., S. Peterek, and T. Gries. Wet spinning PAN-fibres from aqueous solutions of ZnCl2 and NaSCN. 17th World Textile Conference AUTEX 2017. 2017. DOI: 10.1088/1757-899X/254/8/082016.

[182] L'Abbate, P., M. Dassisti, and A.G. Olabi. Small-size vanadium redox flow batteries: an environmental sustainability analysis via LCA. Life Cycle Assessment of Energy Systems and Sustainable Energy Technologies. 2018: Springer. pp. 61-78.

[183] Lakshmanan, V.I., I.A. Todd, and N. McQueen. Recovery of vanadium from Suncor flyash - flowsheet development. Presented at the Second International Conference on Separations Science and Technology. 1989. Ottawa, Ontario. **2**: pp. 525-531.

[184] Lavin, J.G. Chemical reactions in the stabilization of mesophase pitch-based carbon fiber. Carbon, 1992. **30**(3): 351-357.

[185] Le, M.N. and M.S. Lee. A review on hydrometallurgical processes for the recovery of valuable metals from spent catalysts and life cycle analysis perspective. Mineral Processing and Extractive Metallurgy Review, 2021 DOI: 10.1080/08827508.2020.1726914.

[186] Leal, G. and J. Penaloza. Production of carbon fibers from Castilla's crude-oil deasphalted bottoms. Ciencia, Tecnologia y Futuro, 2002. **2**(3): 41-47.

[187] Lee, F.M., R.D. Knudsen, and D.R. Kidd. Reforming catalyst made from the metals recovered from spent atmospheric residue of desulphurisation catalyst. Industrial & Engineering Chemistry Research, 1992. **31**: 487-490.

[188] Leistenschneider, D., P. Zuo, Y. Kim, Z. Abedi, D. Ivery, A. de Klerl, X. Zhang, and W. Chen. A mechanism study of acid-assisted oxidative stabilization of asphaltene-derived carbon fibers. Carbon Trends, 2021. **5**: 100090.

[189] Li, D., H. Gong, L. Lin, W. Ma, Q. Zhou, K. Kong, R. Huang, and Z. Hou. Selective aerobic oxidation of glycerol over zirconium phosphate-supported vanadium catalyst. Molecular Catalysis, 2019. **474**: 110404 DOI: https://doi.org/10.1016/j.mcat.2019.110404.

[190] Li, Y., G. Wang, Z. Li, J. Yuan, D. Gao, and H. Zhang. A life cycle analysis of deploying coking technology to utilize low-rank coal in china. Sustainability, 2020. **12**: 4884-4901 DOI: doi.org/10.3390/su12124884.

[191] Liu, Q., Z. Cui, and T.H. Etsell. Characterization of Athabasca oil sands froth treatment tailings for heavy mineral recovery. Fuel, 2006. **85**: 807-814.

[192] Llanos, Z. and W. Deering. GCMC's integrated process for recovery of metals from spent catalysts. Air & Waste Management Association 90th Annual Meeting & Exhibition. 1998. Toronto, Canada.

[193] Llanos, Z.R., G.F. Provoost, W.G. Deering, and F.J. Debaene. Integrated process for the recovery of metals and fused alumina from spent catalysts. US 5702500 A. US Patent and Trademark Office. December 30, 1997.

[194] Lourenssen, K., J. Williams, F. Ahmadpour, R. Clemmer, and S. Tasnim. Vanadium redox flow batteries: A comprehensive review. Journal of Energy Storage, 2019. **25**: 100844 DOI: https://doi.org/10.1016/j.est.2019.100844.

[195] Lowe, J. Aerospace applications, in Design and Manufacture of Textile Composites, A.C. Long, Editor. 2005. CRC Press.

[196] Lundberg, M. Environmental analysis of zirconium alloy production, 2011. Master. Uppsala Universitet.

[197] Macleod, G.D. Consider wet scrubbers for pollution control. 2018 [cited 2022 October, 1st]; Available from: https://www.aiche.org/resources/publications/cep/2018/october/consider-wet-scrubbers-pollution-control.

[198] Malone, D.P. and T. Holcombe. Recovering vaandium from petroleum coke as dust. US 6,241,806 B1. US Patent and Trademark Office. June 05, 2001.

[199] Maples, R.E. Petroleum refinery process economics. 1993. Tulsa, Oklahoma: PennWell Books.

[200] Marafi, M., E.K.T. Kam, A. Stanislaus, and M. Absi-Halabi. Rejuvenation of residual oil hydrotreating catalysts by leaching of foulant metals: modelling of the metal leaching process. Applied Catalysis A: General, 1996. **147**: 35-46.

[201] Marafi, M. and A. Stanislaus. Options and processes for spent catalyst handling and utilization. Journal of Hazardous Materials, 2003. **B101**: 123-132.

[202] Marafi, M., A. Stanislaus, and E. Furimsky. Handbook of Spent Hydroprocessing Catalyst. 2017: Elsevier.

[203] Marafi, M., A. Stanislaus, and E. Kam. A preliminary process design and economic assessment of a catalyst rejuvenation process for waste disposal of refinery spent catalysts. J Environ Manage, 2008. **86**(4): 665-81 DOI: 10.1016/j.jenvman.2006.12.017.

[204] Marufuzzaman, M., S.D. Eksiog˘lu, and R. Hernandez. Truck versus pipeline transportation cost analysis of wastewater sludge. Transportation Research Part A, 2015. **74**: 14-30.

[205] Maxwell, C. Cost Indices. 2022 [cited 2022 March 4]; Available from: https://toweringskills.com/financial-analysis/cost-indices/.

[206] McCorriston, L.L. Process using carbonate reagent for recovering vanadium from cokes and ashes derived from heavy oils. US 4,472,360 A. US Patent and Trademark Office. September 18, 1984.

[207] McCosh, R. Geology executive summary from mineral development agreement. Final report, 1996. Alberta Chamber of Resources.

[208] Meisen, A. Bitumen beyond combustion (BBC) project. Phase I report, 2017. Alberta Innovates. Available from: https://albertainnovates.ca/wp-content/uploads/2018/04/BBC-Report-1.pdf. Access date: December 10, 2021.

[209] Michaud, D. Flotation reagents. 2016 [cited 2023 May 4]; Available from: https://www.911metallurgist.com/blog/flotation-reagents.

[210] Mineral Technologies. Magnetic separators. 2023 [cited 2023 May 23]; Available from: https://mineraltechnologies.com/what-we-do/our-products/magnetic-separation/.

[211] Mining Technology. Moma titanium minerals mine, Mozambique. 2021 [cited 2023 December, 12]; Available from: https://www.mining-technology.com/projects/moma-titanium-minerals-mine-mozambique/?cf-view.

[212] Mirdehghan, S.A. 1- Fibrous polymeric composites, in Engineered polymeric fibrous materials, M. Latifi, Editor. 2021. Elsevier. pp. 1-58.

[213] Mohapatra, D. and K.H. Park. Selective recovery of Mo, Co and Al from spent Co/Mo/gamma-Al2O3 catalyst: effect of calcination temperature. J Environ Sci Health A Tox Hazard Subst Environ Eng, 2007. **42**(4): 507-15 DOI: 10.1080/10934520601188409.

[214] Montoya Sánchez, N. and A. de Klerl. Low-temperature oxidative asphaltenes liquefaction for petrochemicals: fact or fiction? Applied Petrochemical Research, 2016. **6**: 97-106.

[215] Morales-Mora, M.A., E. Rosa-Dominguez, N. Suppen-Reynaga, and S.A. Martinez-Delgadillo. Environmental and eco-costs life cycle assessment of an acrylonitrile process by capacity enlargement in Mexico. Process Safety and Environmental Protection, 2012. **90**: 27-37.

[216] Moran, K. and F. Chachula. Method for processing froth treatment tailings. US 8,852,429 B2. United States Patent and Trademark Office. 2014.

[217] Moran, K. and J. Doiron. A method for producing a zirconium concentrated product from froth treatment tailings. WO 2015/051435 A1. World Intellectual Property Organization. 2015.

[218] Moran, K., J. Doiron, F. Chachula, and M. Yakimchuck. Recovery of bitumen from froth treatment tailings. US 8,382,976 B2. United States Patent and Trademark Office. 2013.

[219] Moran, K., S. Nelson, and J. Oxenford. New oil sands technology to meet the challenges of climate change and tailings management. 2016 World Heavy Oil Congress. 2016. Calgary, Canada. Available from: https://cvwcleantech.com/titanium-corporations-technology-featured-at-2016-world-heavy-oil-congress/. Access date: February 13, 2019.

[220] Mordor Intelligence. Zirconium market - Segmented by ocurrence-type, application, and geography- Growth, trends, and forecast (2019-2024), 2018. Available from: https://www.marketresearch.com/Mordor-Intelligence-LLP-v4018/Zirconium-c1832/1.html. Access date: December 14, 2019.

[221] Morgan, P. Carbon Fibers and their Composites. 2005: Taylor & Francis Group. pp. 1131.

[222] Morris, E. Bench-scale, multifilament spinning conditions effect on the structure and properties of polyacrylonitrile precursor fiber, 2011. Master of Science in Mechanical Engineering. University of Kentucky.

[223] Moschopedis, S., S. Parkash, and J. Speight. Thermal decomposition of asphaltenes. Fuel, 1978. **57**: 431-434.

[224] Moskalyk, R.R. and A.M. Alfantazi. Processing of vanadium: a review. Minerals Engineering, 2003. **16**: 793-805.

[225] Mulak, W., A. Szymczycha, A. Lesniewicz, and W. Zyrnicki. Preliminary results of metals leaching from a spent hydrodesulphurization (HDS) catalyst. Physicochemical Problems of Mineral Processing, 2006. **40**: 69-76.

[226] Mular, A. and R. Poulin. CAPCOSTS: a handbook for estimating minig and mineral processing costs and capital expenditures and aiding mineral project evaluations. CIM special volume. 1998: Canadian Institute of MIning and Metallurgy. pp. 319.

[227] Nakano, J. and A. Nakano. Method for recovering target materials from source materials. US 10,323,298 B2. 2017.

[228] National Energy Technology Laboratory. Emissions advantage of gasification. Gasifipedia N.d. [cited 2022 December 20]; Available from: https://netl.doe.gov/carbon-management/energy-systems/gasification/gasifipedia.

[229] Netzer, D. Alberta bitumen processing integration study. Final report, 2006. The Province of Alberta, Department of Energy, The Alberta Energy Research Institute and Industry sponsors.

Available from: https://open.alberta.ca/publications/alberta-bitumen-processing-integration-study-final-report. Access date: May 15, 2019.

[230] Ni, G., W. Jiang, and W. Shen. Chemical modification of asphaltene with SEBS as presursor for isotropic pitch-based carbon fiber. Chemistry Select, 2019. **4**: 3690-3696.

[231] Nimana, B., C. Canter, and A. Kumar. Energy consumption and greenhouse gas emissions in the recovery and extraction of crude bitumen from Canada's oil sands. Applied Energy, 2015a. **142**: 189-199.

[232] Nimana, B., C. Canter, and A. Kumar. Energy consumption and greenhouse gas emissions in upgrading and refining of Canadas's oil sands products. Energy, 2015b. **83**: 65-79.

[233] Nimana, B., C. Canter, and A. Kumar. Life cycle assessment of greenhouse gas emissions from Canada's oil sands-derived transportation fuels. Energy, 2015c. **88**: 544-554.

[234] Nkosi, P., N. Dire, N. Nyambeni, and X.C. Goso. A comparative study of vanadium recovery from titaniferous magnetite using salt, sulphate, and soda ash roast-leach processes. 3rd Young Professionals Conference. 2017. Pretoria: pp. 191-200.

[235] Norris, G.A. and B.P. Weidema. Avoiding co-product allocation in the metals sector. ICMM International Workshop on Life Cycle Assessment and Metals. 2002. Montreal, Canada.

[236] Nunez, P. and S. Jones. Cradle to gate: life cycle impact of primary aluminium product. The International Journal of Life Cycle Assessment, 2015. **21**: 1594-1604.

[237] Nunna, S., P. Blanchard, D. Buckmaster, S. Davis, and M. Naebe. Development of a cost model for the production of carbon fibres. Heliyon, 2019. **5**: e02698.

[238] Oil Sands Magazine. Bitumen upgrading explained. 2020 [cited 2020 July 12th]; Available from: https://www.oilsandsmagazine.com/technical/bitumen-upgrading.

[239] Oil Sands Magazine. Oil and gas prices. 2024 [cited 2024 February 25]; Available from: https://www.oilsandsmagazine.com/energy-statistics/oil-and-gas-prices.

[240] Oil Sands Magazine. Products from the oil sands: dilbit, synbit and synthetic crude explained. N.d. [cited 2021 February 2]; Available from: Dilbit density

https://www.oilsandsmagazine.com/technical/product-streams.

[241] Omnia LLC. Assessment of carbon fiber manufacturing cost, 2012. Available from: https://www.invest.is/files/skjol/pdff/omnia_carbon_fiber_extract.pdf. Access date: February 4, 2022.

[242] Owen, M. and R. Tipman. Co-production of heavy minerals from oil sand tailings. CIM Bulletin, 1999. **92**(1030): 65-73.

[243] Oxenford, J., J. Coward, and S. Bulatovic. Heavy minerals from Alberta's oil sands, 2001. SGS Minerals Services. Available from: https://www.sgs.com/-/media/sgscorp/documents/corporate/brochures/sgs-min-tp2001-12-solutions-for-oil-sands-metallurgy.cdn.en.pdf. Access date: April 2nd, 2023.

[244] Pacheco, D., J. Bergerson, and H.L. MacLean. Modeling greenhouse gas emissions from oil sands partial upgrading technologies using a life cycle-based model. Energy & Fuels, 2020. **34**: 12757-12770.

[245] Park, M.-S., M.-J. Jung, and Y.-S. Lee. Significant reduction in stabilization temperature and improved mechanical/electrical properties of pitch-based carbon fibers by electron beam irradiation. Journal of Industrial and Engineering Chemistry, 2016. **37**(25): 277-287.

[246] Park, S.-J. and G.-Y. Heo. Precursors and Manufacturing of Carbon Fibers, in Carbon Fibers, S.-J. Park, Editor. 2015. Springer. pp. 31-66.DOI: 0.1007/978-94-017-9478-7_2.

[247] Pathak, A., M. Vinoba, and R. Kothari. Emerging role of organic acids in leaching of valuable metals from refinery-spent hydroprocessing catalysts, and potential techno-economic challenges: A review. Critical Reviews in Environmental Science and Technology, 2020: 1-43 DOI: 10.1080/10643389.2019.1709399.

[248] Pennington, J.W. Mercury. A materials survey, 1959. US Bureau of Mines. Information Circular 7941. Available from: https://digital.library.unt.edu/ark:/67531/metadc170716/.

[249] Perks, C. and G. Mudd. Titanium, zirconium resources and production: A state of the art literature review. Ore Geology Reviews, 2019. **107**: 629-646.

[250] Perles, T.T. Vanadium market structures and outlook. Presented at the Conference of Metallurgists. 2014. Vancouver, Canada. Available from: https://store.cim.org/Content/Images/uploaded/COM_2014_Conference_Guide_PROCEEDINGS.pdf.

[251] Perry, R.H., D.W. Green, and M.Z. Southard. Perry's Chemical Engineers' Handbook. 9th ed. 2018. New York: McGraw-Hill Education. pp. 2272.

[252] Peters, M.S., K.D. Timmerhaus, and R.E. West. Plant Design and Economics for Chemical Engineers. Fifth ed. 2003. New York.

[253] Petranikova, M., A.H. Tkaczyk, A. Bartl, A. Amato, V. Lapkovskis, and C. Tunsu. Vanadium sustainability in the context of innovative recycling and sourcing development. Waste Management, 2020. **113**: 521-544.

[254] Prophecy Development Corp. Gibellini (Vanadium) - Corporate presentation, 2019. Available from: https://www.prophecydev.com/projects/gibellini-vanadium/. Access date: July 10th, 2020.

[255] Purity Gas. Cost of nitrogen gas - how much should you be paying. 2017 [cited 2022 January, 4]; Available from: https://puritygas.ca/knowledge-center/nitrogen-gas-costs/.

[256] Qin, F., W. Jiang, G. Ni, J. Wang, P. Zuo, S. Qu, and W. Shen. From coal-heavy oil co-refining residue to asphaltene-based functional carbon materials. ACS Sustainable Chemistry & Engineering, 2019. **7**: 4523-4531.

[257] Queneau, P.B., R.F. Hogsett, L.W. Beckstead, and D.K. Huggins. Recovery of V_2O_5 and nickel values from petroleum coke. US Patent 4,443,415. United States Patent and Trademark Office. 1984.

[258] Rahman, M.M., C. Canter, and A. Kumar. Greenhouse gas emissions from recovery of various North American conventional crudes. Energy, 2014. **74**: 607-617.

[259] Rappas, A.S. and R.A. Spitz. Hydromethanation of a carbonaceous feedstock with vanadium recovery. US 8,557,878 B2. US Patent and Trademark Office. October 15, 2013.

[260] Redelius, P. Asphaltenes in bitumen, what they are and what they are not. Road Materials and Pavement Design, 2011. **10**(1): 25-43.

[261] Redick, H.E. Carbon fiber production. US 4,576,810. United States Patent and Trademark Office. 1986. Available from: https://patents.google.com/patent/US4576810A/en?oq=us+4576810+carbon+fiber+production. Access date: February 6, 2022.

[262] Reeves, R. Recovery of heavy minerals from a tar sand. US 7,341,658 B2. United States Patent and Trademark Office. 2008.

[263] Ren, T., M. Patel, and K. Blok. Olefins from conventional and heavy feedstocks: energy use in steam cracking and alternatives processes. Energy, 2006. **31**: 42-451.

[264] Ren, T., M.K. Patel, and K. Blok. Steam cracking and methane to olefins: energy use, CO2 emissions and production costs. Energy, 2008. **33**: 817-833.

[265] Roberts, D. Heats of polymerization. A summary of published values and their relation structure. Journal of Research of the National Bureau of Standards, 1950. **44**: 221-232.

[266] Roccheti, L., V. Fonti, F. Veglio, and F. Beolchini. An environmentally friendly process for the recovery of valuable metals from spent refinery catalysts. Waste Management & Research, 2013. **31**(6): 568-576 DOI: 10.1177/0734242X13476364.

[267] Rodby, K.E., R.L. Jaffe, E.A. Olivetti, and F.R. Brushett. Materials availability and supply chain considerations for vanadium in grid-scale redox flow batteries. Journal of Power Sources, 2023. **560**: 232605.

[268] Rogers, D.K. A study of the stabilization, carbonization, and graphitization of mesophase pitch-based carbon fiber, 1993. Doctoral Dissertation. Graduate School. PhD Ceramic Engineering. Clemson University.

[269] Roman-White, S., S. Rai, J. Littlefield, G. Cooney, and T. Skone. Life cycle greenhouse gas perspective on exporting liquiefied natural gas from the United States: 2019 update, 2019. National Energy Technology Laboratory. DOE/NETL-2019/2041. Available from:

https://www.energy.gov/sites/prod/files/2019/09/f66/2019%20NETL%20LCA-GHG%20Report.pdf. Access date: August 6, 2021.

[270] Rosental, M., T. Fröhlich, and A. Liebich. Life cycle assessment of carbon capture and utilization for the production of large volume organic chemicals. Frontier in Climate, 2020. **2**(586199) DOI: https://doi.org/10.3389/fclim.2020.586199.

[271] RZ Resources. Mineral separation plant. Proven MSP, located near key logistics infrastructure. 2023 [cited 2023 December, 12]; Available from: https://rzresources.com/operations/mineral-separation-plant/.

[272] Saad, S., A.S. Zeraati, S. Roy, M.A.S.J.R.R. Rahman Saadi, A. Rajeev, K.A. Miller, S. Bhattacharyya, S.R. Larter, G. Natale, U. Sundararaj, P.M. Ajayan, M.M. Rahman, and M.G. Kibria. Transformation of petroleum asphaltenes to carbon fibers. Carbon, 2022. **190**: 92-103.

[273] Saadi, M.A.S.R., P.A. Advincula, M.S.H. Thakur, A.Z. Khater, S. Saad, A. Shayesteh Zeraati, S.K. Nabil, A. Zinke, S. Roy, M. Lou, S.N. Bheemasetti, M.A.A. Bari, Y. Zheng, J.L. Beckham, V. Gadhamshetty, A. Vashisth, M.G. Kibria, J.M. Tour, P.M. Ajayan, and M.M. Rahman. Sustainable valorization of asphaltenes via flash joule heating. Science Advances, 2022. **8**(46): eadd3555 DOI: doi:10.1126/sciadv.add3555.

[274] Sakuma, A. and T. Kobori. Method for processing oil combustion ash. WO 2018211996 A1. World Intellectual Property Organization. November 22, 2018.

[275] Schmidt, R. and D.L. Denham Jr. Zircon-rutile-ilmenite froth flotation process. US5106489A. United States Patent and Trademark Office. 1991.

[276] Sharma, P., N. Berwal, N. Ahlawat, A.S. Maan, and R. Punia. Study of structural, dielectric, ferroelectric and magnetic properties of vanadium doped BCT ceramics. Ceramincs International, 2019. **45**(16): 20368-20378.

[277] Shimanoe, H., S. Ko, Y.-P. Jeon, K. Nakabayashi, J. Miyawaki, and S.-H. Yoon. Shortening stabilization time using pressurized air flow in manufacturing mesophase pitch-based carbon fiber. Polymers, 2019. **11**(12) DOI: https://doi.org/10.3390/polym11121911.

[278] Shlewit, H. and M. Alibrahim. Extraction of sulfur and vanadium from petroleum coke by means of salt-roasting treatment. Fuel, 2006. **85**: 878-880.

[279] Shwekat, K. Benefit-cost analysis of using class F fly ash-based green cement in masonry units, 2015. Graduate School of Wayne State University. Ph.D Civil Engineering.

[280] Singh, R., H. Mahandra, and B. Gupta. Optimization of a solvent extraction route for the recovery of Mo from petroleum refinery spent catalyst using Cyphos IL 102. Solvent Extraction and Ion Exchange, 2018. **36**(4): 401-419.

[281] Sinonine. Attrition scrubbers/cells. 2023a [cited 2023 April 1st]; Available from: https://www.9silica.com/PRODUCTS/Washing_and_classifing/54.html.

[282] Sinonine. Conditioning tank. 2023b [cited 2023 March 28th]; Available from: https://www.9silica.com/PRODUCTS/Silica_sand_beneficiation_equi/57.html.

[283] Sleep, S., I.J. Laurenzi, J.A. Bergerson, and H.L. MacLean. Evaluation of variability in greenhouse gas intensity of Canadian oil sands surface mining and upgrading operations. Environmental Science & Technology, 2018. **52**(20): 11941-11951.

[284] Small, C.C., S. Cho, Z. Hashisho, and A.C. Ulrich. Emissions from oil sands tailings ponds: Review of tailings pond parameters and emissions estimates. Journal of Petroleum Science and Engineering, 2015. **127**: 490-501.

[285] Snowden-Swan, L.J., K.A. Spies, G.J. Lee, and Y. Zhu. Life cycle greenhouse gas emissions analysis of catalysts for hydrotreating of fast pyrolysis bio-oil. Biomass and Bioenergy, 2016. **86**: 136-145.

[286] Sorrels, J.L., A. Baynham, D.D. Randall, and R. Laxton. Wet and dry scrubbers for acid gas control, in SO2 and acid gas control, EPA, Editor. 2021.

[287] Speight, J.G. The chemistry and technology of petroleum. 5th ed. 2014. Hoboken: CRC Press.

[288] Stantec Consulting Ltd. Bitumen beyond combustion - Phase 2 report, 2018. Alberta Innovates. Available from: https://albertainnovates.ca/wp-content/uploads/2020/07/Stantec-Bitumen-Beyond-Combustion-Phase-2-Report.pdf. Access date: January 4, 2022.

[289] Statista. Average price of crude gypsum on a free-on board (FOB) mine basis in the U.S. from 2007 to 2019. 2019 [cited 2020 July 7th]; Available from: https://www.statista.com/statistics/219363/wallboard-products-crude-price-in-the-us/.

[290] Stemerowicz, A., R.W. Bruce, G.V. Sirianni, and G.E. Viens. Recovery of vanadium and nickel from Athabasca tar sands fly ash. Canadian Institute of Mining and Metallurgy Bulletin, 1976: 102-108.

[291] Stone, D.K., S.K. Lynch, R.F. Pandullo, L.B. Evans, and W.M. Vatavuk. Flares. Part II. Capital and annual costs. Journal of the Air & Waste Management Association, 1992. **42**(4): 488-493 DOI: 10.1080/10473289.1992.10467008.

[292] Stry, B. Innovations in oxidation technology to enable market growth. Composites World. 2012. La Jolla, CA. Available from: https://www.harperintl.com/wp-content/uploads/2011/09/Composites-World-20121.pdf. Access date: March 05, 2022.

[293] Sun, D. A simple scheme for extraction of asphaltenes from asphalt at room temperature. Coatings, 2022. **12**(3) DOI: https://doi.org/10.3390/coatings12030407.

[294] Suncor Energy. Coke fired boiler replacement project. Project description summary, 2017. Available from: https://iaac-aeic.gc.ca/050/documents/p80144/121224E.pdf.

[295] Suzuki, T. and J. Takahashi. Prediction of energy intensity of carbon fiber reinforced plastics for mass-produced passenger cars. The Ninth Japan International SAMPE symposium. 2005. pp. 14-19.

[296] Tang, D.Z. The application of carbon fiber materials in sports equipment. Applied Mechanics and Materials, 2013. **443**: 613-616.

[297] Tang, S. and C. Hu. Design, preparation and properties of carbon fiber reinforced ultra-high temperature ceramic composites for aerospace applications: a review. Journal of Materials

Science & Technology, 2017. **33**(2): 117-130 DOI: https://doi.org/10.1016/j.jmst.2016.08.004.

[298] Tao, Y., Q. Ding, M. Deng, D. Tao, X. Wang, and J. Zhang. Electrical properties of fly ash and its decarbonization by electrostatic separation. International Journal of Mining Science and Technology, 2015. **25**(4): 629-633.

[299] Titanium Corporation Ltd. 2018 Annual general and special meeting: shareholder presentation. 2019 [cited 2023 March 29th]; Available from: http://www.titaniumcorporation.com/site/assets/files/6480/agm_presentation_2019-05-13.pdf.

[300] Toda, S. Alkaline roasting of spent catalyst containing molybdenumand vanadium. Journal of the Mining and Materials Processing Institute of Japan, 1989. **105**(3): 261-264.

[301] Toray. Carbon Fiber. N.d. [cited 2022 Jan 4]; Available from: https://www.toraycma.com/products/carbon-fiber/.

[302] Towler, G. and R. Sinnot. Chemical engineering design: Principles, practice and economics of plant and process design. 2nd ed. 2013: Elsevier.

[303] Towler, G. and R. Sinnot. Chemical engineering design: principles, practice and economics of plant and process design. 2008: Elsevier.

[304] Trading Economics. Molybdenum: 2005-2020 Data. 2020 [cited 2020 July 7th]; Available from: https://tradingeconomics.com/commodity/molybden.

[305] Trevoy, L., R. Schutte, and R. Goforth. Development of the heavy minerals potential of the Athabasca tar sands. CIM Bulletin, 1978. **71**(791): 175-180.

[306] Turton, R., R.C. Bailie, W.B. Whiting, J.A. Shaeiwitz, and D. Bhattacharyya. Analysis, synthesis, and design of chemical processes. 4th ed. 2012. United States: Prentice Hall.

[307] Turunga, A.S.S. Effect of solvent deasphalting process on the properties of deasphalted oil and asphaltenes from bitumen, 2017. MEng. Department of Chemical and Materials Engineering. University of Alberta.

[308] U.S. Environmental Protection Agency. Emission factors for greenhouse gas inventories. 2021 [cited 2021 May 21]; Available from: https://www.epa.gov/climateleadership/ghg-emission-factors-hub.

[309] U.S. Geological Survey. Mineral commodity summaries 2019, 2019. Available from: https://doi.org/10.3133/70202434. Access date: January 14th, 2020.

[310] U.S. Geological Survey. Mineral commodity summaries 2021. 2021 [cited 2022 March 9]; Available from: https://pubs.er.usgs.gov/publication/mcs2021.

[311] U.S. Geological Survey. Mineral commodity summaries 2022. , 2022. Available from: https://pubs.usgs.gov/periodicals/mcs2022/mcs2022.pdf. Access date: April 20th, 2023. https://doi.org/10.3133/mcs2022

[312] Ucore Rare Metals Inc. Ucore selects optimized oil sands concentrate and progresses to pre-MRT testing. 2017 [cited 2023 March 28th]; Available from: https://ucore.com/ucore-selects-optimized-oil-sands-concentrate-and-progresses-to-pre-mrt-testing.

[313] Ulrich, G.D. and P.T. Vasudevan. Chemical Engineering. Process Design and Economics A Practical Guide. Second ed. 2004: Process Publishing.

[314] Valeri, F., F. Girardier, and S. Abotteen. Minimizing catalyst costs by sound catalyst management. N.d. [cited 2022 April 15]; Available from: https://www.eurecat.com/pdf/minimize-catalyst-petrotech.pdf.

[315] van der Spek, M., A. Ramirez, and A. Faaij. Challenges and uncertainties of ex ante techno-economic analysis of low TRL CO_2 capture technology: Lessons from a case study of an NGCC with exhaust gas recycle and electric swing adsorption. Applied Energy, 2017. **208**: 920-934.

[316] Vanadium Price. 2020 [cited 2020 April 2nd]; Available from: vanadiumprice.com.

[317] vanadiumprice.com. V2O5 Vanadium Pentoxide Flake 98% Price USD / lb. 2022 [cited 2022 October 4]; Available from: https://www.vanadiumprice.com/.

[318] Vilaplana-Ortego, E., J. Alcañiz-Monge, D. Cazorla-Amorós, and A. Linares-Solano. Stabilization of low softening point petroleum pitch fibres by HNO_3. Carbon, 2003. **41**(5): 1001-1007.

[319] Villarreal, M.S., B.I. Kharisov, L.M. Torres-Martínez, and V.N. Elizondo. Recovery of vanadium and molybdenum from spent petroleum catalyst. Industrial & Engineering Chemistry Research, 1999. **38**: 4624-4628.

[320] Vishnyakov, A. Vanadium and nickel recovery from the products of heavy petroleum feedstock processing: A review. Metals, 2023. **13**(6): 1031 DOI: https://doi.org/10.3390/met13061031.

[321] Walker, A. and T. Wheelock. Separation of carbon from fly ash using froth flotation. Coal Preparation, 2006. **26**: 235-250.

[322] Wan, Y. and J. Takahashi. Development of carbon fiber-reinforced thermoplastics for mass-produced automotive applications in Japan. Journal of Composites Science, 2021. **5**(3): 86 DOI: https://doi.org/10.3390/jcs5030086.

[323] Wang, M., H. Lee, and J. Molburg. Allocation of energy use in petroleum refineries to petroleum products. Implications for life-cycle energy use and emission inventory of petroleum transportation fuels Internation Journal of Life Cycle Assessment, 2004. **9**(1): 34-44.

[324] Wang, Z., P.T. Benavides, J.B. Dunn, and D.C. Cronauer. Development of GREET catalyst module, 2015. Argone National Laboratory. Available from: https://greet.es.anl.gov/publication-catalyst-module. Access date: January 3, 2022.

[325] Warren, C.D. Carbon fiber. Precursors and conversion. N.d. October 15, 2020]; Available from: https://www.energy.gov/sites/prod/files/2016/09/f33/fcto_h2_storage_700bar_workshop_3_warren.pdf.

[326] Warren, C.D. Development of low-cost, high strength commercial textile precursor (PAN-MA), 2014. Oak Ridge National Laboratory. Available from: https://www-energy-gov.login.ezproxy.library.ualberta.ca/sites/prod/files/st099_warren_2014_o.pdf. Access date: July 12, 2023.

[327] Warren, C.D. Lower cost carbon fiber precursors, 2010. Oak Ridge National Laboratory. Available from: https://www.energy.gov/sites/prod/files/2014/03/f11/lm004_warren_2010_o.pdf. Access date: January 6, 2022.

[328] Wasajja, H., R. Lindeboom, J. van Lier, and P.V. Aravind. Techno-economic review of biogas cleaning technologies for small off-grid solid oxide fuel cell applications. Fuel Processing Technology, 2020. **197**: 106215.

[329] Watkinson, A.P., G. Cheng, and D.P.C. Fung. Gasification of oil sand coke. Fuel, 1989. **68**: 4-10.

[330] Witting, P., J. Fry, and C. Johnston. White paper: Maximizing the competitive benefits of low cost natural gas in the manufacturing of carbon fiber, n.d. Harper International. Available from: https://www.harperintl.com/wp-content/uploads/2016/02/White-Paper-Maximizing-the-Competitive-Benefits-of-Low-Cost-Natural-Gas-in-the-Manufacturing-of-Carbon-Fiber-Harper-International.pdf. Access date: August 1, 2021.

[331] Woods, D.R. Rules of Thumb in Engineering Practice. 2007: Wiley-VCH.

[332] Xiao, Y., C.R. Mambote, H. Jalkanen, Y. Yang, and R. Boom. Vanadium recovery as FeV from petroleum fly ash. The Twelfth International Ferroalloys Congress. Sustainable Future. 2010. Helsinki, Finland: pp. 177-188.

[333] Xu, Y., J. Wu, T. Dabros, P. Rahimi, and J. Kan. Investigstion on alternative disposal methods for froth treatment tailings-part 2, recovery of asphaltenes. The Canadian Journal of Chemical Engineering, 2013. **91**: 1358-1364 DOI: https://doi.org/10.1002/cjce.21822.

[334] Yadav, R., B. Nasri-Nasrabadi, and M. Naebe. Carbon fibre from Alberta oilsands asphaltenes (AOA), 2021. Carbon Nexus, Institute for Frontier Materials, Deakin University. Available from: https://albertainnovates.ca/app/uploads/2023/05/CFGC-Phase-I-Deakin-Naebe-Final-Public-Report.pdf. Access date: May 5, 2023.

[335] Yang, B., J. He, G. Zhang, and J. Guo, eds. Chapter 18 - Development of the vanadium industry. Vanadium. Extraction, manufacturing and applications. 2021. Elsevier. pp. 487-520. ISBN 9780128188989.

[336] Yang, Q.Z., G.J. Qi, H.C. Low, and B. Song. Sustainable recovery of nickel from spent hydrogenation catalyst: economics, emissions and wastes assessment. Journal of Cleaner Production, 2011. **19**: 365-375.

[337] Zachariah, A. and A. De Klerl. Partial upgrading of bitumen: impact of solvent deasphalting and visbreaking sequence. Energy & Fuels, 2017. **31**: 9374-9380.

[338] Zeng, L. and C.Y. Cheng. A literature review of the recovery of molybdenum and vanadium from spent hydrodesulphurisation catalysts. Part I: Metallurgical processes. Hydrometallurgy, 2009a. **98**(1-2): 1-9 DOI: 10.1016/j.hydromet.2009.03.010.

[339] Zeng, L. and C.Y. Cheng. A literature review of the recovery of molybdenum and vanadium from spent hydrodesulphurisation catalysts. Part II: Separation and purification. Hydrometallurgy, 2009b. **98**(1-2): 10-20 DOI: 10.1016/j.hydromet.2009.03.012.

[340] Zhang, J., G. Lin, U. Vaidya, and H. Wang. Past, present and future prospective of global carbon fibre composite developments and applications. Composites Part B: Engineering, 2023. **250**: 110463.

[341] Zhang, L., F. Yang, and Y. Tao. Removal of unburned carbon from fly ash using enhanced gravity separation and the comparison with froth flotation. Fuel, 2020. **259**.

[342] Zhang, P. and K. Inoue. Recovery of metal values from spent hydrodesulfurization catalysts by liquid-liquid extraction. Energy and Fuels, 1995. **9**: 231-239.

[343] Zhang, Y.L., X.G. Tian, L.Q. Yang, L.P. Zhang, D.G. Li, and P.P. Zhao. Improving the leaching of vanadium from petroleum coke. Petroleum Science and Technology, 2015. **33**: 765-772.

[344] Zhou, J., P. Bomben, M. Gray, and B. Helfenbaum. Bitumen beyond combustion. How oil sands can help the world reach net-zero emissions and create economic opportunities for Alberta and Canada, 2021. Alberta Innovates. Available from: https://albertainnovates.ca/wp-content/uploads/2023/06/AI-BBC-WHITE-PAPER_2022_WEB.pdf. Access date: September 16, 2023.

[345] Zhu, X., Y. Geng, Z. Gao, X. Tian, S. Xiao, and K. Houssini. Investigating zirconium flows and stocks in China: A dynamic material flow analysis. Resources Policy, 2023. **80**: 103139.

[346] Zircomet. Zircon sand - Historic pricing. 2023 [cited 2023 May 11]; Available from: http://www.zircomet.com/sec/11192/Zircon-Historic-Pricing/.

[347] Zuo, P., D. Leistenschneider, Y. Kim, Z. Abedi, D. Ivery, M. Zhang, and W. Chen. Asphaltene thermal treatment and optimization of oxidation conditions of low-cost asphaltene-derived carbon fibers. Journal of Industrial and Engineering Chemistry, 2021a. **104**: 427-436.

[348] Zuo, P., D. Leistenschneider, Y. Kim, D.G. Ivey, and W. Chen. The effect of thermal pretreatment temperature on the diameters and mechanical properties of asphaltene-derivated carbon fibers. Journal of Materials Science, 2021b. **56**: 14964-14977.

Appendix A: Discounted cash flow analysis and production cost

A.1 Present value of a future amount

An amount of money available at some time in the future worth less than the same amount in the present. The present value of a future amount is given by

$$P = F(1 + i)^{-N} \tag{A-1}$$

P: present value of a future amount, $

F: future amount, $

i: annual discount rate

N: discount periods

A.2 Net present value of an investment

The net present value of an investment is the total of the present value of all cash flows, i.e., revenue minus operating cost, minus the present value of all capital investments. Under the assumption that all capital investments are paid at year one, the NPV is calculated as

$$NPV = \sum_{j=1}^{N} \left(R_j - OPEX_j\right)(1 + i)^{-N} - CAPEX \tag{A-2}$$

NPV: net present value of an investment, $

R: annual revenue, $/y

$OPEX$: annual operating cost, $/y

$CAPEX$: capital cost, $

A.3 Internal rate of return

The internal rate of return is the return obtained from an investment in which all the cash flows and capital investments are discounted. It is calculated by setting the NPV given in Equation A-2 equal to zero and solving for the discount rate.

A.4 Production/recovery cost

In this study, the production/recovery cost of a product is defined as the minimum selling price at which the product should be sold to break even at a given discount rate. It is calculated by setting the NPV given in Equation A-2 equal to zero and solve for the selling price of the product (used to calculate the revenue), as shown in Equation A-3.

$$0 = \sum_{j=1}^{N} \left(sC_j - OPEX_j\right)(1 + IRR)^{-N} - CAPEX \tag{A-3}$$

s: selling price, i.e., production cost, \$/unit

C_j: annual production rate, unit/y

As the NPV was set equal to zero, the discount rate used in Equation A-3 corresponds to the desired IRR of the investment.

Appendix B: Morris method and Monte Carlo simulation

B.1 Morris method for sensitivity analysis

The Morris method, also known as the elementary effects method, is a global sensitivity analysis technique designed to identify the most influential input factors in a model. This method provides a balance between computational efficiency and the ability to explore the input space broadly.

B.1.1 Overview of the Morris method

The Morris method operates by perturbing each input factor across its range, one at a time, and measuring the resulting effect on the output. This approach yields a set of elementary effects for each factor, which represent the change in the output when the input is varied. The key innovation of the Morris method is the ability to assess both the magnitude and direction of the output's sensitivity to each input factor.

B.1.2 Implementation steps

- Sampling: the input space is divided into a grid, and a number of trajectories (or paths) are generated. Each trajectory involves systematically varying one factor at a time while keeping others fixed.
- Calculation of elementary effects: for each input factor in a trajectory, the elementary effect is calculated as:

$$EE_i = \frac{Y(X + \Delta e_i) - Y(X)}{\Delta} \tag{B-1}$$

EE_i: elementary effect of input i

X: input vector

$Y(X)$: model output

Δ: small change in the input

e_i: unit vector for the input i

- Statistical analysis: the elementary effects for each factor are analyzed to derive two metrics:

  Mean (μ): Represents the overall effect of the factor on the output, indicating the importance of the factor.

  Standard deviation (σ): Reflects the interaction effects and nonlinearity. A high σ suggests that the factor's effect on the output is highly variable, potentially due to interactions with other factors or nonlinear responses.

B.2. Monte Carlo simulation for uncertainty analysis

Monte Carlo simulation is a robust technique used to quantify uncertainty in model predictions by simulating many possible outcomes based on random sampling of input parameters.

B.2.1 Conceptual foundation

Monte Carlo simulation leverages the law of large numbers to approximate the probability distribution of an output variable. By randomly sampling inputs according to their probability distributions and repeatedly running the model, Monte Carlo simulation generates a distribution of possible outcomes that reflect the uncertainties in the input parameters.

B.2.2 Steps in Monte Carlo simulation

- Define input distributions: each uncertain input parameter is assigned a probability distribution based on empirical data, expert judgment, or assumptions.
- Random sampling: a large number of random samples are drawn from the input distributions. Each set of samples represents a possible scenario.
- Model execution: the model is run for each set of sampled inputs, producing a corresponding output. This process is repeated many times (typically thousands or millions) to capture the range of possible outcomes.
- Analysis of results: the resulting outputs are aggregated to form an empirical distribution, from which key statistics (mean, variance, percentiles) and probability density functions can be derived. This output distribution provides a comprehensive view of the uncertainty associated with the model predictions.

Appendix C: Chapter 6 – Additional information

C.1 Process modeling and equipment sizing

Table C-1 lists the process conditions used to complete the material and energy balance of each unit operation in both phases of the process.

Table C-2 presents the approach used to size the mean equipment required in each unit operation, as well as the operational parameters and their base-case values that were used to estimate the number of units, and energy and material consumptions.

Table C-1. Process conditions

Process phase	Unit operation	Process condition	Value	Reference
Heavy minerals concentration	Desliming	Underflow (coarse minerals fraction) composition	Relative to feed: Water: 3 wt.% Bitumen: 10 wt.% Diluent: 5 wt.% Solids: 42%	(Moran and Chachula 2014)
		Percentage of coarse minerals (>44 μm) in underflow	90%	(Erasmus et al. 2010)
		Recovery of Ti and Zr in underflow	88 wt.% Ti 90 wt.% Zr	(H.A. Simons Ltd. 1996)
		Temperature	25°C (ambient)	
	Froth flotation	Temperature	35°C	(Erasmus et al. 2010)

Process phase	Unit operation	Process condition	Value	Reference
Heavy minerals concentration		Rougher stage: overflow composition	Relative to feed: Water: 53 wt.% Bitumen: 98 wt.% Diluent: 60 wt.% Solids: 47%	(Moran and Chachula 2014)
Heavy minerals concentration	Froth flotation	Scavenger stage: overflow composition	Relative to feed: Water: 16 wt.% Bitumen: 100 wt.% Diluent: 0 wt.% Solids: 7.3%	(Moran and Chachula 2014)
		Percentage of coarse minerals (>44 µm) in underflow	95%	(Erasmus et al. 2010)

Process phase	Unit operation	Process condition	Value	Reference
		Recovery of Ti and Zr in underflow	97.5 wt.% Ti 99.1 wt.% Zr	(Moran and Chachula 2014)
		Conditioning time	12 min	(Moran and Doiron 2015)
		Flotation time	Rougher: 10 min Scavenger: 5 min	(Moran and Chachula 2014)
Heavy minerals concentration	Solvent extraction	1st stage overflow composition (to clarification)	Water: 0.4 wt.% Bitumen: 14.4 wt.% Diluent: 85.2 wt.% Solids: 0.1 wt.%	(Moran and Chachula 2014)
Heavy minerals concentration	Solvent extraction	3rd stage underflow (heavy mineral-rich slurry)	Water: 44.2 wt.% Bitumen: 0.20 wt.% Diluent: 5.95 wt.% Solids: 49.7 wt.%	(Moran and Chachula 2014)

Process phase	Unit operation	Process condition	Value	Reference
		Temperature	60°C	
		Retention time	20 min	(Reeves 2008)
Heavy minerals concentration	Diluent recovery	Hydrocyclone underflow (debituminized HMC) composition	Water: 8.2 wt.% Bitumen: 0.32 wt.% Diluent: 0.44 wt.% Solids: 91.0 wt.%	(Moran and Chachula 2014)
		Hydrocyclone overflow (to diluent recovery unit) composition	Water: 86.4 wt.% Bitumen: 0.06 wt.% Diluent: 12.4 wt.% Solids: 1.17 wt.%	
		Fraction of feed reporting to underflow	54 wt.%	
Heavy minerals concentration	Bitumen recovery	Temperature	204°C	

Process phase	**Unit operation**	**Process condition**	**Value**	**Reference**
Minerals separation	Zircon froth flotation	Temperature	90^{o}C	(Schmidt and Denham Jr. 1991)
		Conditioning time	12 min	(Moran and Doiron 2015)
		Flotation time	6 min	
		pH required	2	
		Solids concentration in product	35 wt.%	
		Minerals in feed reporting to overflow	Titanium minerals: 50.7% Zircon: 93.7% Silica: 41.7%	
Minerals separation	Primary gravity separation	Fraction of water reporting to underflow (zircon-rich stream)	6.5 wt.%	(H.A. Simons Ltd. 1996)

Process phase	**Unit operation**	**Process condition**	**Value**	**Reference**
		Minerals in feed reporting to underflow	Titanium minerals: 62.6% Zircon: 97.0% Silica: 54.5%	(Moran and Doiron 2015)
Minerals separation	Primary electrostatic and magnetic separation	Temperature	90°C	(Moran and Doiron 2015)
		Minerals in feed reporting to product	Titanium minerals: 5.8% Zircon: 90.0% Silica: 60.9%	(Moran and Doiron 2015)
Minerals separation	Finishing gravity separation	Solids concentration in feed	35 wt.%	(Moran and Doiron 2015)

Process phase	Unit operation	Process condition	Value	Reference
		Minerals in feed reporting to product	Titanium minerals: 48.5% Zircon: 95.9% Silica: 75.2%	
Minerals separation	Finishing electrostatic and magnetic separation	Temperature	90°C	(Moran and Doiron 2015)
		Minerals in feed reporting to product	Titanium minerals: 8.1% Zircon: 90.6% Silica: 71.6%	
Minerals separation	Titanium mineral separation (all operations)	Titanium minerals recovery efficiency	100%.	Assumption.

Table C-2. Sizing approach and operational parameters of main equipment

Process phase	Unit operation	Equipment	Sizing approach	Operational parameter	Value
Heavy mineral concentration	Desliming	Hydrocyclone	Mass flow as a function of diameter. Diameter based on the mean particle size separation (d50). Correlations from Aterburn (Aterburn N.d.) were used.	Pressure drop	70 kPa (Aterburn N.d.)

Process phase	**Unit operation**	**Equipment**	**Sizing approach**	**Operational parameter**	**Value**
		Reciprocating pump	Shaft power, based on pressure drop and volume flow rate	Hydraulic efficiency	55% for diaphragm pumps (Ulrich and Vasudevan 2004)
Heavy mineral concentration	Desliming	Tailings pump	Shaft power, based on head		
		Tailings piping	Length for a fixed diameter (20 in.). The number of pipes was calculated from the maximum flow capacity per pipe	Length	1,000 m
				Maximum flow capacity per pipe	3,960 m3/h (for a 20 in. diameter pipe)

Process phase	Unit operation	Equipment	Sizing approach	Operational parameter	Value
Heavy mineral concentration	Froth flotation	Conditioning tank	Volume, based on conditioning time and required flow rate	Power consumption (agitator)	Rated power of commercial equipment as a function of tank volume (Sinonine 2023b)
Heavy mineral concentration	Froth flotation	Flotation cell	Diameter, calculated from the required volume and a typical aspect	Fraction of air in aerated slurry	15 vol.%
				Number of cells	Rougher: 5 Scavenger: 4

Process phase	**Unit operation**	**Equipment**	**Sizing approach**	**Operational parameter**	**Value**
			ratio of 1.0 (Gorain et al. 2000)	Specific power consumption	2.5 kW/t solids (Ulrich and Vasudevan 2004)
				Air requirement	1.25 m^3/min-m^3 pulp (Gupta and Yan 2006)
				Glycol-based frother consumption	0.20 kg/t solid (Moran and Chachula 2014)
				Collector (naphtha) consumption	10.0 l/t solid (Moran and Chachula 2014)

Process phase	Unit operation	Equipment	Sizing approach	Operational parameter	Value
Heavy mineral concentration	Solvent extraction	Attrition cell	Cell volume, based on retention time and required flow.	Power consumption (agitator)	15 kW/cell for a cell volume of 2 m^3 (Sinonine 2023a)
Heavy mineral concentration	Solvent extraction	Settling chamber	Volume, calculated from the optimal aspect ratio and design diameter. Diameter estimated from terminal and superficial velocities calculated for a particle diameter of	Optimal aspect ratio	3 for cells operating at atmospheric pressure (Ulrich and Vasudevan 2004)

Process phase	Unit operation	Equipment	Sizing approach	Operational parameter	Value
			44 µm		

Process phase	**Unit operation**	**Equipment**	**Sizing approach**	**Operational parameter**	**Value**
Heavy mineral concentration	Diluent recovery	Hydrocyclone	Mass flow as a function of diameter. Diameter based on the mean particle size separation (d50). Correlations from Aterburn (Aterburn N.d.) were used	Pressure drop	70 kPa (Aterburn N.d.)
		Reciprocating pump (for slurry)	Shaft power, based on pressure drop and volume flow rate	Hydraulic efficiency	55% for diaphragm pumps (Ulrich and Vasudevan 2004)

Process phase	**Unit operation**	**Equipment**	**Sizing approach**	**Operational parameter**	**Value**
Heavy mineral concentration	Diluent recovery	Diluent recovery unit	Total height for a fixed diameter (modeled as a spray tower).	Recovery efficiency	92% (Kan 2011)
				Steam consumption	0.03 kg/kg feed (Kan 2011)
Heavy mineral concentration	Diluent recovery	Centrifugal pump (for diluent-rich stream)	Shaft power, based on pressure drop and volume flow rate	Hydraulic efficiency	70% (Ulrich and Vasudevan 2004)
Heavy mineral concentration	Bitumen recovery	Bitumen recovery unit	Total height for a fixed diameter	Natural gas consumption	53.9 scf/bbl feed (Gary and Handwerk 2001)
				Electricity consumption	0.5 kWh/bbl feed (Maples 1993)

Process phase	Unit operation	Equipment	Sizing approach	Operational parameter	Value
				Bitumen recovery efficiency	100%
Minerals separation	Zircon froth flotation	Conditioning tank	Volume, based on conditioning time and required flow rate		
Minerals separation	Zircon froth flotation	Flotation cell	Diameter, calculated from the required volume and a typical aspect	Fraction of air in aerated slurry	15 vol.%
				Number of cells	Rougher: 5 Scavenger: 4

Process phase	Unit operation	Equipment	Sizing approach	Operational parameter	Value
			ratio of 1.0 (Gorain et al. 2000)	Specific power consumption	2.5 kW/t solids (Ulrich and Vasudevan 2004)
				Air requirement	1.25 m^3/min-m^3 pulp (Gupta and Yan 2006)
				Frothing agent consumption rate	0.04 kg/t solid (Camachen N.d.)
				Collector consumption rate	0.56 kg/t solid (Michaud 2016)
				Activator consumption rate	0.56 kg/t solid (Michaud 2016)

Process phase	**Unit operation**	**Equipment**	**Sizing approach**	**Operational parameter**	**Value**
				Depressant consumption rate	2.25 kg/t solid (Michaud 2016)
Minerals separation	Primary gravity separation	Spiral separator	Nominal capacity per unit and number of units per circuit	Nominal capacity per unit	1.35 t/h (Perry et al. 2018)
				Number of units per circuit	7 (Moran and Doiron 2015)
				Pressure drop	0.34 m/turn (Perry et al. 2018)
				Number of turns per unit	5 (Perry et al. 2018)
				Water consumption per final spiral	1.8 l/s (Perry et al. 2018)

Process phase	**Unit operation**	**Equipment**	**Sizing approach**	**Operational parameter**	**Value**
Minerals separation	Dewatering and drying (zircon-rich stream)	Disk filter	Filtration area estimated after the method described by Perry et al. (Perry et al. 2018)	Moisture content in filtration cake	25% (Perry et al. 2018)
				Specific energy consumption	2.0 kWh/t (Cec Mining Systems 2017)
		Dryer	Evaporation rate from water content in feed and cake, and 100 °C		
Minerals separation	Primary electrostatic and	High tension roll		Number of rolls per unit	4 (Mular and Poulin 1998)

Process phase	Unit operation	Equipment	Sizing approach	Operational parameter	Value
	magnetic separation		Number of rolls times roll diameter times roll length	Roll diameter and length	270 x 1,800 mm (Mular and Poulin 1998)
Minerals separation	Primary electrostatic and magnetic separation	High tension roll		Capacity per effective roll length	1.6 t/h/m (Mular and Poulin 1998)
Minerals separation	Primary electrostatic and magnetic separation	High tension roll		No. of stages	7 (Moran and Doiron 2015)
				Rated power consumption	4 kW (Mineral Technologies 2023)
		Rare earth magnets	Sized by vendor	Roll length	1.0 m

Process phase	**Unit operation**	**Equipment**	**Sizing approach**	**Operational parameter**	**Value**
				Capacity per effective roll length	7 t/h/m (Mineral Technologies 2023)
				No. of stages	2 (Moran and Doiron 2015)
				Rated power requirement	1.4 kW (Mineral Technologies 2023)
Minerals separation	Finishing gravity separation	Shaking table	Deck area	Deck area	90 ft^2 (Mular and Poulin 1998)
				Power requirement	1.49 kW (Mular and Poulin 1998)
Minerals separation	Finishing electrostatic and	High tension roll		Number of rolls per unit	4 (Mular and Poulin 1998)

Process phase	Unit operation	Equipment	Sizing approach	Operational parameter	Value
	magnetic separation		Number of rolls times roll diameter times roll length	Roll diameter and length	270 x 1,800 mm (Mular and Poulin 1998)
				Capacity per effective roll length	1.6 t/h/m (Mular and Poulin 1998)
				No. of stages	4 (Moran and Doiron 2015)
				Rated power consumption	4 kW (Mineral Technologies 2023)
		Induced roll magnetic separator	Capacity	Nominal capacity per unit	11.50 t/h (Mular and Poulin 1998)

Process phase	Unit operation	Equipment	Sizing approach	Operational parameter	Value
Minerals separation	Finishing electrostatic and magnetic separation	Induced roll magnetic separator	Capacity	Rated power consumption	7.5 kW (Mineral Technologies 2023)
Minerals separation	Separation of titanium minerals from gravity separation tails	Disk filter	See Dewatering and drying (zircon-rich stream)		
		Dryer	See Dewatering and drying (zircon-rich stream)		
		Electrostatic plate separator	Sized by vendor	Nominal capacity per unit	2.00 t/h (Mineral Technologies 2023)
				No. of stages	4 (Erasmus et al. 2010)
				Power requirement	0.5 kW (Mineral Technologies 2023)
Minerals separation		Disk filter	See Dewatering and drying (zircon-rich stream)		

Process phase	**Unit operation**	**Equipment**	**Sizing approach**	**Operational parameter**	**Value**
	Conditioning of zircon flotation tails	Dryer	See Dewatering and drying (zircon-rich stream)		
Minerals separation	Separation of titanium minerals from conditioned zircon flotation tails	High tension roll	See Finishing electrostatic and magnetic separation		
Minerals separation	Separation of titanium minerals from conditioned zircon flotation tails	Electrostatic plate separator	Separation of titanium minerals from gravity separation tails		
		Induced roll separator	See Finishing electrostatic and magnetic separation		

Process phase	**Unit operation**	**Equipment**	**Sizing approach**	**Operational parameter**	**Value**
Minerals separation	Separation of titanium minerals from finishing ES & MS tails	Electrostatic plate separator	Separation of titanium minerals from gravity separation tails		

C.2 Sensitivity analysis

Table C-3 lists the inputs considered for the sensitivity analysis of scenario 1. The ranges of variation of the inputs were selected based on typical values found in the literature. If such typical values were not available, a ±30% variation respect to the base-case value was assumed.

Table C-3. Model inputs considered for the sensitivity analysis

Input	Units	Base case	Min	Max	Reference
Specific power consumption per flotation cell	kW/kg solid	0.0025	0.002	0.003	(Ulrich and Vasudevan 2004)
Flotation time – rougher stage	min	10	5	15	(Moran and Chachula 2014)
Flotation time – scavenger stage	min	5	2.5	7.5	(Moran and Chachula 2014)
Flotation temperature	°C	35	25	35	(Erasmus et al. 2010)

Input	Units	Base case	Min	Max	Reference
Consumption rate – glycol-based frothing agent	kg/t solid	0.2	0.015	0.2	(Moran and Chachula 2014)
Consumption rate – collector (naphtha)	l/t solid	10	1	10	(Moran and Chachula 2014)
Retention time – solvent extraction, 1st stage	min	20	15	25	(Reeves 2008)
Retention time – solvent extraction, 2nd stage	min	20	15	25	(Reeves 2008)
Retention time – solvent extraction, 3rd stage	min	20	15	25	(Reeves 2008)
Solvent extraction temperature	°C	60	30	90	(Moran and Chachula 2014)

Input	Units	Base case	Min	Max	Reference
Steam requirement	Kg/kg feed	0.03	0.02	0.04	(Kan 2011)
Recovery efficiency	-	0.92	0.85	0.99	(Kan 2011)
Specific energy consumption per flotation cell – zircon flotation	kW/kg solid	0.0025	0.002	0.003	(Ulrich and Vasudevan 2004)
Conditioning time – zircon flotation	min	12	6	18	(Moran and Doiron 2015)
Flotation time – zircon flotation	min	6	3	9	(Moran and Doiron 2015)
Consumption rate – frothing agent (GDSP-007)		0.04	0.028	0.052	(Camachen N.d.)
Consumption rate – collector (Flotigam 285)		0.56	0.392	0.728	(Michaud 2016)

Input	Units	Base case	Min	Max	Reference
Consumption rate – activator (sodium fluorosilicate)		0.56	0.392	0.728	(Michaud 2016)
Consumption rate – depressant (unmodified wheat starch)		2.25	1.575	2.925	(Michaud 2016)
Zircon flotation temperature	ºC	90	85	95	(Schmidt and Denham Jr. 1991)
Water consumption per final spiral – primary gravity separation	l/s	1.75	1	2.5	(Ulrich and Vasudevan 2004)
Nominal capacity per spiral	t/h	1.35	0.4	1.8	(Perry et al. 2018)
Moisture content in cake – dewatering of zircon stream	-	0.25	0.15	0.25	(Ulrich and Vasudevan 2004)

Input	Units	Base case	Min	Max	Reference
Specific energy consumption – disk filter, dewatering of zircon stream	kWh/t	2	0.69	3.26	(Cec Mining Systems 2017)
Specific energy consumption – separation of titanium minerals from gravity separation tails	kWh/t	2	0.69	3.26	(Cec Mining Systems 2017)
Cake moisture - separation of titanium minerals from gravity separation tails	-	0.25	0.15	0.25	(Ulrich and Vasudevan 2004)
Titanium recovery efficiency - separation of titanium minerals from gravity separation tails	-	1	0.95	1	Provided by vendors
Cake moisture – conditioning of zircon flotation tails	-	0.25	0.15	0.25	{Ulrich, 2004 #28

Input	Units	Base case	Min	Max	Reference
Specific energy consumption – disk filter, conditioning of zircon flotation tails		2	0.69	3.26	(Cec Mining Systems 2017)
Titanium recovery efficiency – separation of titanium minerals from conditioned flotation zircon tails	-	1	0.95	1	Provided by vendors
Titanium recovery efficiency- separation of titanium minerals from finishing ES & MS operations	-	1	0.95	1	Provided by vendors
Natural gas per bbl of feed – bitumen recovery unit	Scf/bbl	53.9	37.73	70.07	(Gary and Handwerk 2001)
Electricity consumption per bbl feed – bitumen recovery unit	Scf/bbl	0.50	0.35	0.65	(Maples 1993)

Input	Units	Base case	Min	Max	Reference
Bitumen recovery efficiency	-	1	0.95	1	Assumed to have the same efficiency of a solvent recovery unit
Solid waste disposal cost	$/t	55	38.5	71.5	(Towler and Sinnot 2013)
Boiler efficiency	-	0.88	0.85	0.95	(Cengel and Boles 2015)
Electricity price	$/kWh	0.04	0.03	0.05	(Canada Energy Regulator 2017)

Input	Units	Base case	Min	Max	Reference
Natural gas price	$/GJ	1.62	1.13	2.11	(Canada Energy Regulator 2017)
DSP 007 price	$/t	1,410	987	1,83	(Camachen N.d.)
Flotigam price	$/t	3,000	2,100	3,90	Provided by vendors
Glycol-based frother price	$/t	4,680	3,276	6,084	Provided by vendors
Naphtha price	$/l	0.11	0.08	0.14	(Government of Canada 2023a)
Process water price	$/t	0.53	0.37	0.69	(Peters et al. 2003)

Input	Units	Base case	Min	Max	Reference
Sodium fluorosilicate price	$/t	580	406	754	Provided by vendors
Sulfuric acid price	$/t	200	140	260	Provided by vendors
Unmodified wheat starch price	$/t	790	553	1,027	Provided by vendors
On-stream factor	-	0.8	0.7	0.9	Assumed
OSBL estimation factor	-	1.0	0.5	1.0	(Towler and Sinnot 2013)
Zircon selling price	$/t	1,000	700	1,500	(U.S. Geological Survey 2022)

Input	Units	Base case	Min	Max	Reference
Rutile selling price	$/t	738.00	664	792	(U.S. Geological Survey 2022)
Leucoxene selling price	$/t	198.00	173	219	(U.S. Geological Survey 2022)
Bitumen selling price	$/bbl	25.00	17.50	32.50	(Government of Alberta 2023)

Input	Units	Base case	Min	Max	Reference
Labor annual rate per operator	$/y	57,600	40,320	74,880	(Chemistry Industry Association of Canada 2021)

C.3 Results

Table C-4 presents the IRR, capital cost, operation cost, and revenue estimated for different plant capacities of scenario 1, and Table C-5 shows the same economic indicators but for the base case of scenario 2.

Table C-4. Breakdown of economic indicators for different plant capacities. Scenario 1

Capacity[a]	IRR (%)	Capital cost (million $)	Operating cost[b] (million $ per year)	Revenue (million $ per year)
25	0.0	218.0	14.9	25.0
50	4.3	278.6	24.5	50.0
75	8.3	338.8	34.2	74.9
100	9.8	419.1	44.5	99.9
125	12.1	467.2	53.9	124.9
150	13.8	518.5	63.6	149.9
175	14.4	591.0	73.4	174.8
200	14.7	668.0	83.7	199.8

a. Expressed as a percentage of the base case capacity (100% = 15.5 Mt/y).

b. At year one of operations.

Table C-5. Breakdown of economic indicators for the base case of scenario 2

<table>
<tr><th colspan="5">Heavy mineral concentration plant (15.5 Mt FTT per year)</th></tr>
<tr><th>IRR (%)</th><th>HMC production cost ($/t)</th><th>Capital cost (million $)</th><th>Operating cost[a] (million $/year)</th><th>Revenue (million $/year)</th></tr>
<tr><td>10.0</td><td>21.52</td><td>147.5</td><td>9.2</td><td>27.8</td></tr>
<tr><th colspan="5">Heavy mineral separation plant (0.57 Mt HMC per year)</th></tr>
<tr><th>IRR (%)</th><th>Feedstock cost ($/t)</th><th>Capital cost (million $)</th><th>Operating cost[a] (million $/year)</th><th>Revenue (million $/year)</th></tr>
<tr><td>7.6</td><td>21.52</td><td>271.7</td><td>49.2</td><td>84.6</td></tr>
</table>

a. At year one of operations.

Appendix D: Chapter 7 – Additional information

D.1 Sensitivity analysis

Table D-1 presents the list of inputs considered for the sensitivity analysis. It also shows the ranges of variation which were selected based on typical values found in the literature. If such typical values were not available, a ±30% variation respect to the base-case value was assumed.

Table D-1. Model inputs considered for the sensitivity analysis

Input	Units	Base case	Min	Max	Reference
Specific power consumption per flotation cell	kW/kg solid	0.0025	0.002	0.003	(Ulrich and Vasudevan 2004)
Flotation time – rougher stage	min	10	5	15	(Moran and Chachula 2014)
Flotation time – scavenger stage	min	5	2.5	7.5	(Moran and Chachula 2014)
Flotation temperature	ºC	35	25	35	(Erasmus et al. 2010)
Consumption rate – glycol-based frothing agent	kg/t solid	0.2	0.015	0.2	(Moran and Chachula 2014)
Consumption rate – collector (naphtha)	l/t solid	10	1	10	(Moran and Chachula 2014)

Input	Units	Base case	Min	Max	Reference
Retention time – solvent extraction, 1st stage	min	20	15	25	(Reeves 2008)
Retention time – solvent extraction, 2nd stage	min	20	15	25	(Reeves 2008)
Retention time – solvent extraction, 3rd stage	min	20	15	25	(Reeves 2008)
Solvent extraction temperature	°C	60	30	90	(Moran and Chachula 2014)
Steam requirement	kg/kg feed	0.03	0.02	0.04	(Kan 2011)
Recovery efficiency	-	0.92	0.85	0.99	(Kan 2011)
Specific energy consumption per flotation cell – zircon flotation	kW/kg solid	0.0025	0.002	0.003	(Ulrich and Vasudevan 2004)
Conditioning time – zircon flotation	min	12	6	18	(Moran and Doiron 2015)
Flotation time – zircon flotation	min	6	3	9	(Moran and Doiron 2015)
Consumption rate – frothing agent (GDSP-007)		0.04	0.028	0.052	(Camachen N.d.)

Input	Units	Base case	Min	Max	Reference
Consumption rate – collector (Flotigam 285)		0.56	0.392	0.728	(Michaud 2016)
Consumption rate – activator (sodium fluorosilicate)		0.56	0.392	0.728	(Michaud 2016)
Consumption rate – depressant (unmodified wheat starch)		2.25	1.575	2.925	(Michaud 2016)
Zircon flotation temperature	ºC	90	85	95	(Schmidt and Denham Jr. 1991)
Water consumption per final spiral – primary gravity separation	l/s	1.75	1	2.5	(Ulrich and Vasudevan 2004)
Nominal capacity per spiral	t/h	1.35	0.4	1.8	(Perry et al. 2018)
Moisture content in cake – dewatering of zircon stream	-	0.25	0.15	0.25	(Ulrich and Vasudevan 2004)
Specific energy consumption – disk filter, dewatering of zircon stream	kWh/t	2	0.69	3.26	(Cec Mining Systems 2017)

Input	Units	Base case	Min	Max	Reference
Specific energy consumption - separation of titanium minerals from gravity separation tails	kWh/t	2	0.69	3.26	(Cec Mining Systems 2017)
Cake moisture - separation of titanium minerals from gravity separation tails	-	0.25	0.15	0.25	(Ulrich and Vasudevan 2004)
Titanium recovery efficiency - separation of titanium minerals from gravity separation tails	-	1	0.95	1	Provided by vendors
Cake moisture – conditioning of zircon flotation tails	-	0.25	0.15	0.25	(Ulrich and Vasudevan 2004)
Specific energy consumption – disk filter, conditioning of zircon flotation tails		2	0.69	3.26	(Cec Mining Systems 2017)
Titanium recovery efficiency – separation of titanium minerals from conditioned flotation zircon tails	-	1	0.95	1	Provided by vendors
Titanium recovery efficiency- separation of titanium minerals from finishing ES & MS operations	-	1	0.95	1	Provided by vendors

Input	Units	Base case	Min	Max	Reference
Natural gas per bbl of feed – bitumen recovery unit	Scf/bbl	53.9	37.73	70.07	(Gary and Handwerk 2001)
Electricity consumption per bbl feed – bitumen recovery unit	Scf/bbl	0.50	0.35	0.65	(Maples 1993)
Bitumen recovery efficiency	-	1	0.95	1	Assumed to have the same efficiency as a solvent recovery unit
Solid waste disposal cost	$/t	55	38.5	71.5	(Towler and Sinnot 2013)
Boiler efficiency	-	0.88	0.85	0.95	(Cengel and Boles 2015)
Electricity price	$/kWh	0.04	0.03	0.05	(Canada Energy Regulator 2017)

Input	Units	Base case	Min	Max	Reference
Natural gas price	$/GJ	1.62	1.13	2.11	(Canada Energy Regulator 2017)
DSP 007 price	$/t	1,410	987	1,83	(Camachen N.d.)
Flotigam price	$/t	3,000	2,100	3,90	Provided by vendors
Glycol-based frother price	$/t	4,680	3,276	6,084	Provided by vendors
Naphtha price	$/l	0.11	0.08	0.14	(Government of Canada 2023a)
Process water price	$/t	0.53	0.37	0.69	(Peters et al. 2003)
Sodium fluorosilicate price	$/t	580	406	754	Provided by vendors
Sulfuric acid price	$/t	200	140	260	Provided by vendors
Unmodified wheat starch price	$/t	790	553	1,027	Provided by vendors
On-stream factor	-	0.8	0.7	0.9	Assumed
OSBL estimation factor	-	1.0	0.5	1.0	(Towler and Sinnot 2013)

Input	**Units**	**Base case**	**Min**	**Max**	**Reference**
Zircon selling price	$/t	1,000	700	1,500	(U.S. Geological Survey 2022)
Rutile selling price	$/t	738.00	664	792	(U.S. Geological Survey 2022)
Leucoxene selling price	$/t	198.00	173	219	(U.S. Geological Survey 2022)
Bitumen selling price	$/bbl	25.00	17.50	32.50	(Government of Alberta 2023)
Labor annual rate per operator	$/y	57,600	40,320	74,880	(Chemistry Industry Association of Canada 2021)

Appendix E: Chapter 8 – Additional information

E.1 Process modeling and equipment sizing and scaling

Table E-1. Main assumptions for the modeling of the ACF production process

Operation	Parameter	Assumption/reference
Thermal pre-treatment	Off-gas composition	Estimated from data from Moschopedis et al. (1978) corresponding to pyrolysis in the nitrogen of asphaltenes separated from Athabasca bitumen. These numbers were scaled to match the weight loss shown in Table 8-2.
	Nitrogen flow	It was assumed twice the flow of evolved gases for the base case, based on published experimental setups.
	Asphaltene apparent specific heat (endothermic)	Obtained from Bazyleva et al. (2011) on the apparent specific heat of asphaltene after one cycle of heating in a nitrogen atmosphere.
Melt spinning	Melt latent heat	Calculated from Bazyleva et al. (2011) on the apparent specific heat of asphaltene after two cycles of heating in a nitrogen atmosphere.
	Power consumption per position	20 kW (Das and Nagapurkar 2021)

Operation	Parameter	Assumption/reference
	Spinning speed	750 m/min (Morgan 2005)
	Fiber diameter	7 µm (Zuo et al. 2021b)
Pre-stabilization	HNO_3 (17%) consumption	In the production of PAN by wet spinning, the GF is spun into a coagulation bath. The amount of residual solvent within the fibers after the bath is about 1 wt.% (Morris 2011). As a rough approximation, it was assumed that the same amount of HNO_3 solution would remain in the GF after dipping into the acid bath.
Stabilization	Off-gases composition	It was assumed that the evolved gas consists of CO, CO_2, H_2O, (as in pitch (Lavin 1992)), and SO_2. The off-gas composition was calculated from the elemental composition of GF and stabilized fibers reported by Chen (2021).
	Air intake	Twice the amount of air required to provide oxygen for the stabilization reaction (Griffing and Overcash 2009), which was calculated from the elemental composition of GF and stabilized fibers reported by Chen (2021).
	Specific heat of GF	Assumed to remain constant during the operation and equal to the specific heat of asphaltene.

Operation	**Parameter**	**Assumption/reference**
	Heat of reaction (exothermic)	-1,219 kJ/kg. The same heat of reaction of the stabilization of mesophase pitch-CF (Rogers 1993) was assumed.
Carbonization	Off-gases composition	The operation yield was used to estimate the weight loss in the form of evolved gases. The composition of the off-gases is mainly the nitrogen used to purge the furnace atmosphere.
	Nitrogen consumption	6.00 kg N_2/kg CF. This value is between those of PAN-CF production at laboratory-scale (Griffing and Overcash 2009) and commercial plants (Harper International 2013).
	Heat of reaction (endothermic)	504 kJ/kg CF, assuming the same value as for PAN-CF.
	Specific heat of carbon fiber	0.70 kJ/kg K, assuming the same value as for pure carbon.
Surface treatment	Energy consumption	3.44 kWh/kg CF, assuming the same value as for PAN-CF (Ellringmann et al. 2016).
	Water consumption	2.0 kg H_2O/kg CF, assuming the same value as for PAN-CF (Ellringmann et al. 2016).
	Electrolyte consumption	0.05 kg NaOH/kg CF, assuming the same value as for PAN-CF (Ellringmann et al. 2016).

Operation	Parameter	Assumption/reference
Sizing	Energy consumption	3.60 kWh/kg CF, assuming the same value as for PAN-CF (Ellringmann et al. 2016).
	Water consumption	0.98 kg H_2O/kg CF, assuming the same value as for PAN-CF (Ellringmann et al. 2016).
	Epoxy consumption	0.02 kg epoxy/kg CF, assuming same value as for PAN-CF (Ellringmann et al. 2016).

Table E-2. List of main equipment and assumptions for sizing and scaling

Operation	Equipment	Sizing approach
Thermal pre-treatment	Stirred vessel	The total volume is calculated based on the required kg per batch and asphaltene density. The number of reactors was calculated based on the volume of each reactor (3.7 m^3, from Peters et al. (2003) and the total volume. The power required by the agitator is based on a diameter ratio of 0.89, the rotation speed of 50 rpm, and the power number of 0.50.
Spinning	Melt spinner	The required number of positions is based on the mass flow of spun fiber per position, which was calculated based on the equipment specifications.

Operation	Equipment	Sizing approach
		The power rating of each spinner is 20 kW (Das and Nagapurkar 2021).
Pre-stabilization	Open vessel	The volume is calculated based on the volume of a single spool and the number of spools per batch, plus an allowance.
Stabilization	Walk-in oven	The capacity of each piece of equipment was calculated using the dimensions of commercial equipment and the dimensions of a single spool. The required number of equipment depends on the oven capacity and the number of spools per batch.
Carbonization	Furnace	
Off-gas abatement	Flare	The diameter and height were calculated with the sizing method presented by Stone et al. (1992)
	Wet scrubber and reactor	Capacity is expressed in terms of the volume flow of treated gas, which was calculated from the material balance.

E.2 Assumptions for cost estimation

Table E-3. Assumption for the estimation of capital cost

Item	Value	Comments/remarks
CEPCI	776.9	Corresponding to 2021 USD
Location factor	1.43[a]	For Fort McMurray, Alberta

Item	**Value**	**Comments/remarks**
Inside battery limit investment (ISBL)	Depends on the equipment	From cost curves and manufacturers
Delivered cost of equipment	10% FOB	Recommended value for predesign estimates (Peters et al. 2003)
Installed cost equipment	40% delivered cost	Varies between 25% and 55% (Peters et al. 2003)
Outside battery limit investment (OSBL)	40% ISBL	Site conditions not specified (Towler and Sinnot 2008)
Engineering cost	20% (ISBL + OSBL)	30% for small projects, 10% for large projects (Towler and Sinnot 2008)
Contingency	30% (ISBL + OSBL)	Typical value for general projects (Towler and Sinnot 2008)
Fixed capital investment	(ISBL + OSBL) + engineering and construction + contingency	
Working capital (WC)	15% (ISBL + OSBL)	Typical value for general plants (Towler and Sinnot 2008)
Total capital cost	FCI + WC	

a- Based on the 2003 location factor (1.60) and exchange rate (1.40 CAD/USD) and updated with 2021 exchange rate (1.25 CAD/USD) (Towler and Sinnot 2008)

Table E-4. Data input for estimation of equipment cost

Operation	Equipment	Cost
Thermal pre-treatment	Stirred Vessel	Determined from cost curves as a function of its volume and power required by the agitator (Peters et al. 2003).
Spinning	Melt spinner	$358,000 per position (Das and Nagapurkar 2021).
Pre-stabilization	Open vessel	Determined from cost curves as a function of its volume (Peters et al. 2003).
Stabilization	Walk-in oven	$57,860 per set. Maximum temperature: 343°C; capacity: 6.1 m^3. Provided by vendors.
Carbonization	Furnace	$285,000 per set. Maximum temperature: 1,800°C; capacity: 3.6 m^3. Provided by vendors.
Surface treatment	Vessel, electrodes, and electric system	Goss (1986) provides the cost for a capacity of 56.3 kg/h, while Das and Nagapurkar (2021) did it for a capacity of 428 kg/h. This data was used to determine a scale factor for the cost at a different capacity.
Sizing	Vessel and drying system	
Off-gas abatement	Flare	Determined from Environmental Protection Agency (2019) data. The equipment cost is a function of diameter and height.
	Wet scrubber and reactor	Determined from cost curves as a function of the volume flow of the off-gases (Woods 2007).

Table E-5. Data for estimating operation costs

Category	Item	Cost	Comments
Feedstock	Asphaltene	\$44/t	Asphaltene is a residue of bitumen deasphalting, with no commercial application and a near-zero value (Stantec Consulting Ltd. 2018).
Consumable	Sorbent	\$0.26/kg	(Wasajja et al. 2020)
	Epoxy	\$0.18/kg	(Gill et al. 2016)
	Lime	\$203/kg	(ChemAnalyst 2022)
	Nitric acid	\$0.38/kg	(ChemAnalyst 2022)
	Nitrogen	\$0.18/m^3	Price for consumption over 80,000 m^3/mo (Purity Gas 2017).
	Process water	\$0.18/m^3	Ultra-pure water
	Sodium hydroxide	\$0.63/kg	(ChemAnalyst 2022)
Utility	Electricity	\$0.042/kWh	(Canada Energy Regulator 2017)
	Natural gas	\$1.32/GJ	(Canada Energy Regulator 2017)

Labor	Labor	Based on salary, number of workers per shift per operation, three 8 h/shifts, 5 days/week, and 48 weeks/year.	
Other costs	Maintenance	5% ISBL	(Towler and Sinnot 2008)
	Rent	2% (ISBL+OSBL)	
	Insurance	1% ISBL	
	Plant overhead	1% revenue (R&D) + 65% labor (G&A)	

E.3 Inputs considered for sensitivity analysis

Table E-6. Economic inputs considered for the sensitivity analysis using the Morris method

Input	**Units**	**Base case**	**Range**	**Comments/reference**
Price of nitrogen, nitric acid, sodium hydroxide, epoxy, lime, sorbent, and process water.	\$/kg, \$/m^3			A variation of ±30% of the prices listed in Table E-5 was assumed.
Price of asphaltenes.	\$/t	44	30.8-57.2	A variation of ±30% was assumed.

Input	Units	Base case	Range	Comments/reference
Price of natural gas.	$/kWh	0.0048	0.0033-0.0062	A variation of ±30% was assumed.
Price of electricity from the grid	$/kWh	0.04	0.03-0.05	A variation of ±30% was assumed.
Purchased-delivered cost (as a percentage of the equipment cost)	%	10	7-13	A variation of ±30% was assumed.
Installation cost (as a percentage of the purchased-delivered cost)	%	40	28-52	A variation of ±30% was assumed.

Table E-7. Process and operational conditions inputs considered for the sensitivity analysis using the Morris method

Input	Units	Base case	Range	Comments/reference
Spinning speed	m/min	750	370 - 750	Achievable after the thermal pre-treatment. Raw asphaltene can be spun at 125 m/min (Zuo et al. 2021b).
Stabilization time	h	6	6-16	(Zuo et al. 2021b) (Chen 2021)

Input	Units	Base case	Range	Comments/reference
Carbonization temperature	°C	1,500	1,500-1,800	The low-end value has been used at laboratory scale (Zuo et al. 2021b). The high-end value would be a modification to the process to improve the mechanical properties of the ACF.
Nitrogen-to-carbon fiber ratio in carbonization ovens	kg N_2/kg CF	0.646	0.646-6	
Nitrogen requirement-to-off gases production ratio in thermal pre-treatment		2	2-10	Assumption
Air requirement in stabilization ovens (modifier of rated requirement)		1	0.7-1.3	A variation of ±30% of the rated air consumption in commercial ovens was assumed.
Nitric acid consumption in pre-stabilization	kg/kg CF	0.01	0.01-0.02	Assumption

Input	Units	Base case	Range	Comments/reference
Electrolyte consumption (NaOH)	kg/kg CF	0.05	0.035-0.065	A variation of ±30% was assumed.
Water consumption – surface treatment	kg/kg CF	2.0	1.4-2.6	A variation of ±30% was assumed.
Epoxy consumption	kg/kg CF	0.02	0.014-0.026	A variation of ±30% was assumed.
Water consumption – sizing	kg/kg CF	0.98	0.69-1.27	A variation of ±30% was assumed.
Off-gas temperature in stabilization and	°C	300	260-350	In PAN-CF, an off-gas temperature lower than the stabilized fiber inside the oven has been reported (Fakhrhoseini 2018). For this reason, temperatures lower than the stabilization temperature were considered in the variation range.
Energy consumption in surface treatment	kWh/kg CF	3.44	2.41-4.47	A variation of ±30% was assumed.

Input	Units	Base case	Range	Comments/reference
Energy consumption in sizing	kWh/kg CF	3.60	2.52-4.68	A variation of ±30% was assumed.
Set-up time for stabilization and carbonization.	h	1	0.5-1.5	Assumption

Table E-8. Equipment performance inputs considered for the sensitivity analysis using the Morris method

Input	Units	Base case	Range	Comments/reference
Agitator power number	-	0.5	0.5 -4	
Boiler efficiency	-	0.80	0.80-0.90	
Indirect fire heater	-	0.80	0.80-0.90	
Electric heater efficiency	-	0.75	0.65-0.85	

Input	Units	Base case	Range	Comments/reference
Thermal resistance furnaces	Km^2 /W	0.159	0.111- 0.206	Data from Morgan was used to calculate the thermal resistance (Morgan 2005). Then, a variation of ±30% was considered.

Table E-9. Process yield, properties and product characteristics inputs considered for the sensitivity analysis using the Morris method

Input	Units	Base case	Range	Comments/reference
Overall yield		0.55	0.398 - 0.6	
Specific heat of green fibers	kJ/kg	2.10	1.47 - 2.73	A variation of ±30% was assumed.
Heat of reaction (stabilization)	kJ/kg	-1,219	-1,585 to -853	A variation of ±30% was assumed.
Specific heat of stabilized fibers	kJ/kg K	0.70	0.49 - 0.91	A variation of ±30% was assumed.

Input	**Units**	**Base case**	**Range**	**Comments/reference**
Heat of reaction (carbonization)	kJ/kg	504	353 - 655	A variation of ±30% was assumed.
Spool diameter	m	0.20	0.19 - 0.21	A ±5% variation was assumed based on the diameters of commercial PAN- and pitch-CF spools.

Appendix F: Chapter 9 – Additional information

F.1 PAN pathway description

F.1.1 Crude oil production

Conventional crude is produced by standard methods of removing oil from reservoirs via wells. These methods include gas lift, water flooding, and steam injection. In this study, Mars crude oil, a sour crude with 31.5° API produced offshore in the Gulf of Mexico 130 miles southeast of New Orleans, was considered. Crude extraction consumes energy to drive injection pumps, compressors, and lift equipment, depending on the production method. Usually, diesel is used as an energy source; however, natural gas can be used, depending on its availability.

F.1.2 Naphtha production

Naphtha is a light cut derived from crude oil distillation in a refinery. Depending on its boiling range, naphtha is classified as light (26-95°C) or heavy (95-175°C). Light naphtha is usually used as a petrochemical feedstock. The first step in crude oil refining is desalting, in which the crude oil is mixed with freshwater, heated to about 121°C, and pumped through the desalting system. The desalted crude oil is heated and fed into the atmospheric distillation column, where it is fractioned. The energy requirement for the distillation operation includes the fuel for heating the crude oil, steam injected into the atmospheric column, and power to pump the fluids. The full-range naphtha fraction is fed into a stabilizer to remove the light ends by steam stripping. The stabilized naphtha is separated into light naphtha and heavy naphtha by a splitter. Figure F-1 is a simplified process diagram of naphtha production.

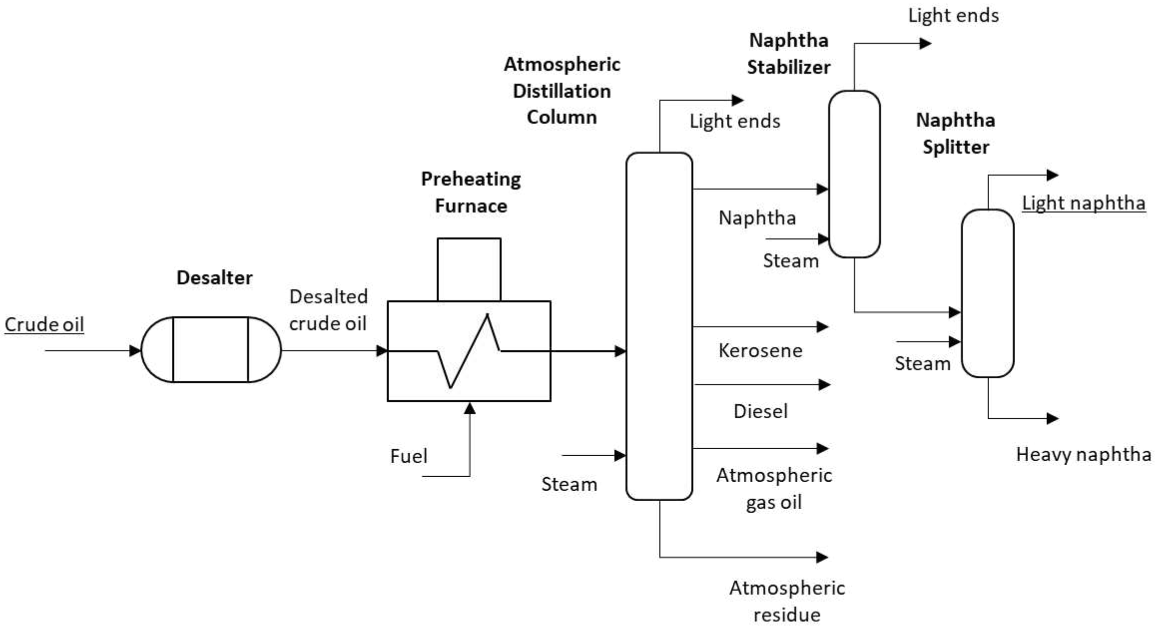

Figure F-1. Simplified light naphtha production process diagram

F.1.3 Propylene production

Propylene is produced as a by-product of ethylene production via steam cracking. The feedstock for steam cracking includes naphtha, gas oil, liquated petroleum gas, ethane, and propane. In general, ethane and naphtha produce more high-value chemicals (HVCs). The HVC yield is greater for ethane, but naphtha produces more propylene (Ren et al. 2006). For this reason, naphtha was considered as the feedstock for steam cracking.

A simplified process flow diagram of the SC process is presented in Figure F-2. Naphtha is preheated in the convective zone of the furnace to 650ºC, mixed with steam, and cracked in the radiant section at about 850ºC. The cracked gas is quenched in the transfer line exchangers (TLEs) to 400ºC to stop the reaction. In this step, heat is recovered by the production of high-pressure steam. The quenched gases are further fractioned to extract a liquid fraction rich in aromatics, while the gaseous fraction is de-superheated in a circulating quenching tower. The quenched gases are compressed, cleaned to remove acid gases and carbon dioxide, and dried to remove condensate. The dried gas is separated into different products through cryogenic separation and a series of distillation columns: a de-methanizer (to remove methane and lighter components), a de-ethanizer (to remove ethane and ethylene), a de-propanizer (to remove propane and propylene), and a final column to separate C4 and C5+.

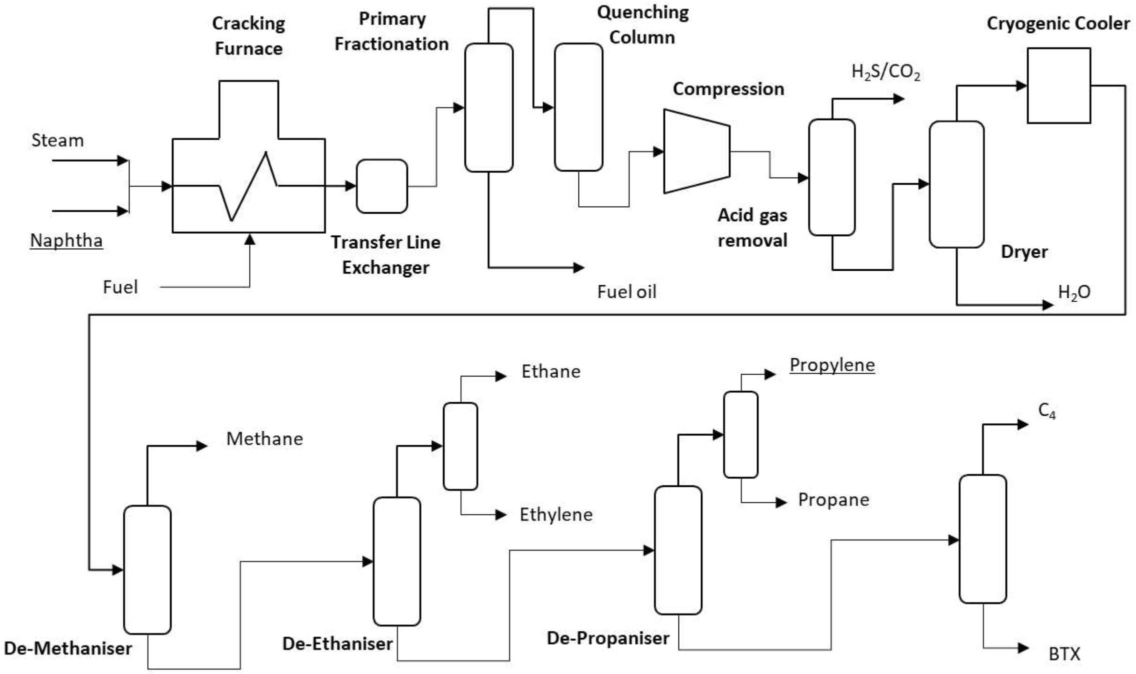

Figure F-2. Simplified naphtha steam cracking process diagram

F.1.4 Ammonia production

Ammonia is produced on a large scale through the Haber-Bosch process using natural gas and air (nitrogen) as the raw materials. Figure F-3 is a simplified process flow diagram of the

SMR-based (Haber-Bosch process) ammonia production process. Sulfur in the natural gas is removed by reacting it with zinc oxide. The treated natural gas is then fed into the reforming reactor to convert methane and light hydrocarbons into nitrogen, carbon monoxide, and carbon dioxide. This is a highly endothermic reaction for which heat is supplied by the combustion of natural gas as fuel. In a secondary reformer, the air is added to supply the nitrogen required for ammonia production, and additional heat energy is provided by combusting natural gas. To increase the yield of hydrogen, CO is converted into CO_2 via the water-gas shift reactor. CO_2 is removed by absorption, leaving a H_2- and N_2-rich process stream. CO and CO_2 deactivate the catalysts used for ammonia synthesis; for this reason, any traces of those gases are converted into CH_4 in a methanation process.

The synthesis of ammonia occurs at 100-250 bar and 350-550ºC. The reaction is exothermic and with an efficiency of 20-30% per pass. The ammonia is separated from the reactor output by cooling and condensing while the remaining is recycled to sustain the conversion loop. There are three main sources of GHG emissions from the ammonia production process: fuel combustion, electricity production, and the generation of process syngas in the reactors (Benchaita 2013; Boulamanti and Moya 2017).

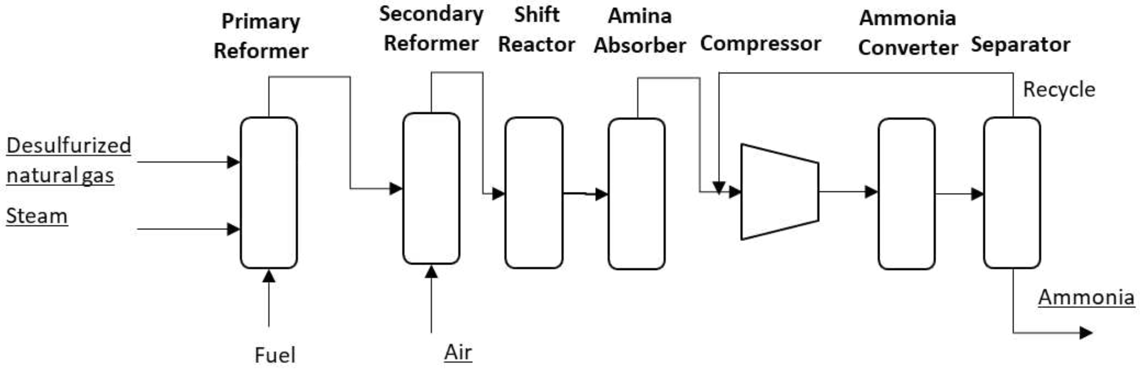

Figure F-3. Simplified ammonia production process diagram

F.1.5 Acrylonitrile production

The ammoxidation of propylene is the industrial route to produce acrylonitrile through the Standard Oil of Ohio (SOHIO) process. A simplified process flow diagram of this process is presented in Figure F-4. An approximately stoichiometric amount of propylene is reacted with excess ammonia and air (a 1.05:1.02 ammonia-to-propylene molar ratio and a 1.9:2.01 air-to-propylene molar ratio (Cespi et al. 2014)) in a fluidized bed reactor in the presence of catalysts at a temperature of 400-450ºC and 200 kPa. The conversion of propylene is around 98% and the molar yield of ACN is approximately 80%. Acetonitrile and hydrogen cyanide are also generated as by-products. The product yield depends on the performance of the catalysts. The reaction is highly exothermic, and the reactor temperature is maintained by the flow of cooling water. The energy required by the separation and purification steps is provided by the steam generated by cooling the reactor. Also, part of the steam is used to drive mechanical devices, like compressors.

The reactor product, at high temperature, is quenched with water. Sulfuric acid is used to neutralize the unreacted ammonia. Acrylonitrile and other organics are recovered from the quenched stream by water absorption, while the unreacted propylene is vented along the off-gas of this operation. Other species found in the off-gases are N_2, CO, and CO_2. The off-gas can be also burned in an incinerator to combust the hydrocarbons and CO, before venting. The stream containing acrylonitrile, acetonitrile, HCN, and some water undergoes a series of atmospheric distillations to obtain products and by-products of the desired purity. First, acrylonitrile and HCN are separated from the stream in the recovery column. The acetonitrile-rich bottoms are passed to the acetonitrile column to remove water. The remaining crude acetonitrile is usually incinerated. In the HCN column, ACN is separated from HCN by fractioning. The HCN-rich stream can be purified to obtain a saleable product, but it is usually incinerated. In the ACN column, heavy ends are removed to produce acrylonitrile with more than 99% purity.

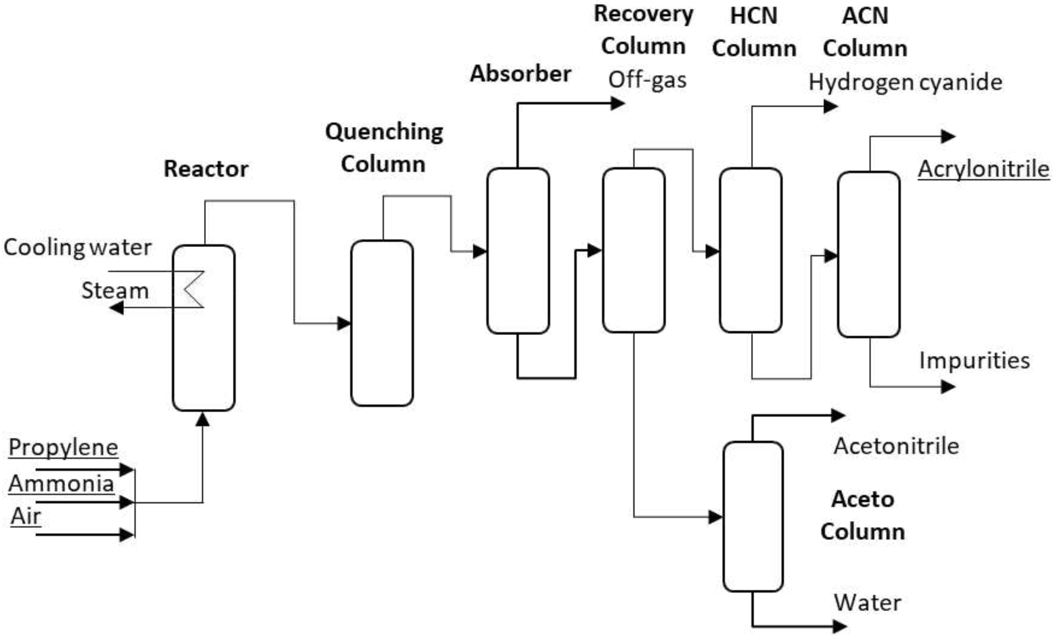

Figure F-4. Simplified SOHIO process diagram

F.1.6 PAN production

Figure F-5 presents a schematic of the PAN production process. In general, the process comprises the polymerization of acrylonitrile and the formation of dope, spinning the dope into fibers, and a series of washing, stretching, coating, and drying operations.

Acrylonitrile polymerization is based on free-radical polymerization and can be performed by one of the following methods (Park and Heo 2015): solution, bulk, emulsion, or aqueous dispersion polymerization. Among those, PAN is made by solution or emulsion polymerization at a commercial scale. The principal difference between these methods is how the dope for spinning is formed. In solution polymerization, the polymer, as it is formed, goes into a solution that can be used as dope after the unreacted ACN is removed. In emulsion polymerization, the spinning dope must be prepared separately after ACN polymerization. Solution polymerization was considered in this study because of its low complexity for the continuous process (Nunna et al. 2019).

The first step in the process is the polymerization of acrylonitrile with a comonomer, such as methacrylic acid (MA). For solution polymerization, a suitable solvent like dimethyl sulfoxide (DMSO) is also incorporated into the mixture. Precursors based on PAN consist of at least 5 mol% of comonomer to ease the processing for carbon fiber manufacturing. The mixture is continuously stirred to initiate the formation of free radicals in the acrylonitrile molecule. The reaction is exothermic, with the heat of polymerization equal to 17.3 kcal/mol of monomer (Roberts 1950). The polymer in the resulting dope is at least 85% ACN (Morgan 2005).

Spinning is the process of forming the dope into yarns or fibers. Wet spinning is used for most commercial processes. The dope is heated at a temperature in the range 25-120ºC and pushed through spinnerets with multiple holes. The spinnerets are immersed in a coagulation bath at 0-50ºC (Morgan 2005). The coagulant is water, with an amount of solvent lower than 40 wt.% in the case of organic solvents and lower than 14 wt.% in the case of aqueous solvents (Köhler et al. 2017). The resulting fibers are gradually subjected to tension to orient the molecular chains parallel to the fiber axis. (Morgan 2005).

After spinning, the spun fibers are either counter-current washed with hot water or heated to remove the remaining solvent and then are stretched by rollers at variable speeds. During this operation, the fiber temperature increases gradually, starting at 65°C, as residual solvent and washing water are removed from the pores of the fiber [8].

Preparation is the application of an aqueous emulsion on the surface of the fibers to act as lubricant, e.g., silicones (Morgan 2005). Next, residual water is removed from the fiber by drying. Finally, the PAN fibers are collected, and tows are wound directly onto spools using winders.

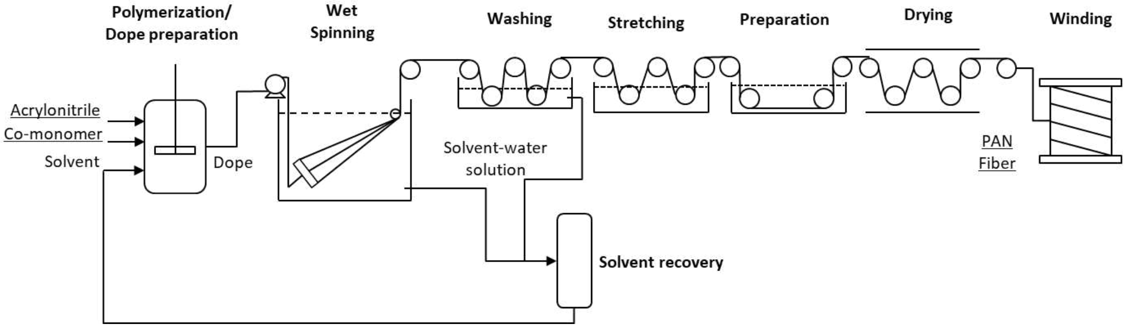

Figure F-5. Schematic of the PAN production process

F.1.7 PAN-based carbon fiber production

Figure F-6 shows a schematic of the PAN-CF production process. PAN fiber is stabilized by heating it to 200-300ºC in the air. The objective is to transform the precursor into a form that can be thermally treated at temperatures below the melting point. Stabilization is achieved by oxidation in multi-pass ovens with gradual increment of temperature. The flow of hot air into the ovens is controlled to heat the fiber and also to remove evolved gas components, avoid temperature build-up due exothermic reactions, and provide oxygen required for oxidation. Heat for stabilization is provided by electrical heaters.

The fibers are carbonized by heating in an oxygen-free atmosphere. Non-carbon molecules, such as HCN and volatile organic compounds, are removed, and the product is a fiber with >93% carbon content. The process has two parts: low-temperature carbonization and high-temperature carbonization. In the low temperature (LT) electrically heated furnace, temperature gradually increased to about 950-1,000°C. Purge nitrogen is fed to the oven to provide an oxygen-free atmosphere. The flow of nitrogen also contributes to evacuating evolved gases, tars, and particulates. The gases that evolve during LT carbonization include H_2O, CO_2, NH_3, HCN, H_2, CO, and CH_4. Further processing in a high temperature (HT) carbonization furnace induces the strength, modulus, electrical conductivity, and fiber density required for carbon fiber. LT carbonized fiber passes through the graphite muffle of the multi-zone furnace to be heated to 1,800°C at heating rates below 20°C/min. As in the LT furnace, purge nitrogen is used as inert gas.

Surface treatment is required to increase the adhesion between matrix resin and carbon fiber for manufacturing composite materials. Usually, an electrolytic surface treatment process is used. In such a case, sodium hypochlorite, nitric acid, or ammonium sulfate is used as the electrolyte, given their high solubility in water. The carbon fiber acts as the anode, while graphite cathodes are placed into the electrolyte tank. Residual electrolyte is removed from the carbon fiber by washing with warm water after surface treatment.

Sizing eases the handling of carbon fibers in further operations. The fibers are dipped in a dispersion of epoxy particles in water and then are subjected to drying to remove the water and leave the fibers coated with the epoxy. (Morgan 2005). Hereafter, the set of surface treatment, sizing, drying, and winding is referred to as finishing operations.

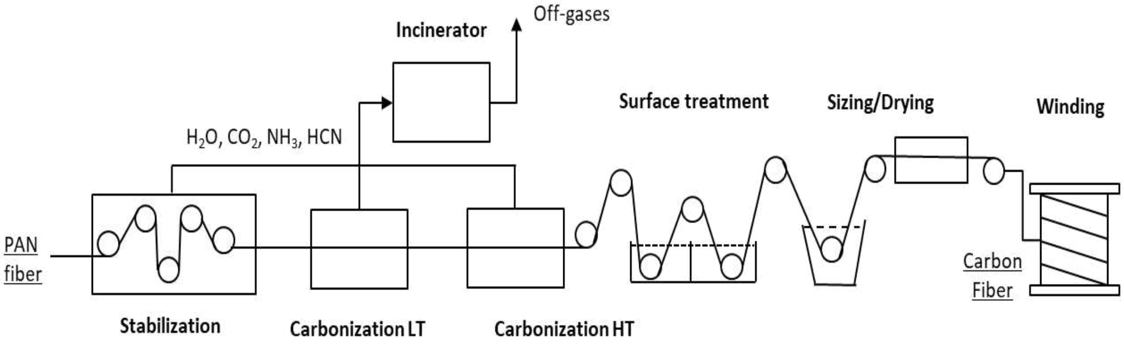

Figure F-6. Schematic of the PAN-based carbon fiber production process

F.2 Emission factors used for the estimation of PAN-CF life cycle GHG emissions

The emission factors for electricity production and fuel combustion for the PAN pathway were obtained from the US Environmental Protection Agency (EPA) Emission Factors for Greenhouse Gas Inventories, updated on April 1, 2021 (U.S. Environmental Protection Agency 2021), and presented in Table F-1 and Table F-2.

Table F-1. Emission factors for grid electricity production, US locations

Location	eGrid Subregion	CO_2 factor (kg/MWh)	CH_4 factor (kg/MWh)	N_2O factor (kg/MWh)
Houston, TX	ERCT	390.9	0.026	0.004
Port Arthur, TX	SRMV	363.1	0.019	0.003
Decatur, AL	SRTV	427.4	0.039	0.006

Table F-2. Emission factors for the combustion of natural gas, US

Location	CO_2 factor (kg/mmBtu)	CH_4 factor (g/mmBtu)	N_2O factor (g/mmBtu)
US	53.06	1.0	0.10

F.3 Data collection for the PAN pathway

Figure F-7 shows the system boundary for the crude oil production process. Aggregated energy consumption and GHG emissions data were taken from our research colleagues Rahman et al. specifically for Mars crude oil, a sour crude with 31.5° API produced offshore in the Gulf of Mexico 130 miles southeast of New Orleans (Rahman et al. 2014). In that study, it was assumed that the produced gas is sufficient to meet the onsite demand of heat and electricity. The latter was assumed to be produced in simple gas turbines with 32.6% efficiency. Flaring, venting, and fugitives were considered for the GHG emissions accounting. Rahman et al. took the emission factor for natural gas combustion from the GREET model. The GHG emissions reported by Rahman et al. are based on crude oil energy. For the purposes of this study, it is convenient to express those emissions on a volumetric basis by multiplying them by the lower heating value (LHV) and the density of the produced crude oil. The LHV of crude oil is about 90% of the higher heating value (HHV). The latter was correlated as a function of crude's specific gravity. The LHV in MJ/kg crude oil was then calculated using the formulae provided by Speight (Speight 2014).

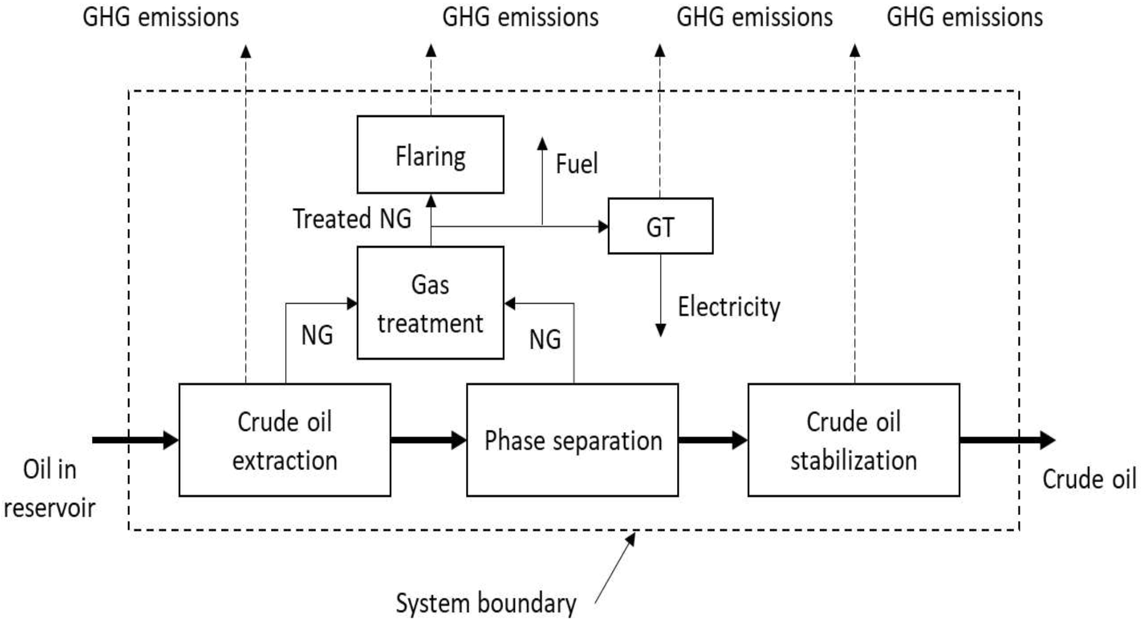

Figure F-7. System boundary for the crude oil production process

Figure F-8 shows the system boundary diagram for the naphtha production process. GHG emissions due to the combustion of natural gas as fuel in the crude furnace preheater and for steam production were considered for the inventory, as well as those emissions associated with the production of grid electricity. Data on electricity consumption was taken from the literature, while a rigorous process model was developed in Aspen HYSYS V10 to estimate the heat requirement. The atmospheric crude tower sample provided by the software was modified to consider the assay of Mars crude oil (BP 2021) and to incorporate the naphtha stabilization and splitting operations and the heating of the oil-water mixture fed to the desalter unit. From the simulation results, it is also observed that 10.48 kg naphtha is produced per bbl of crude oil.

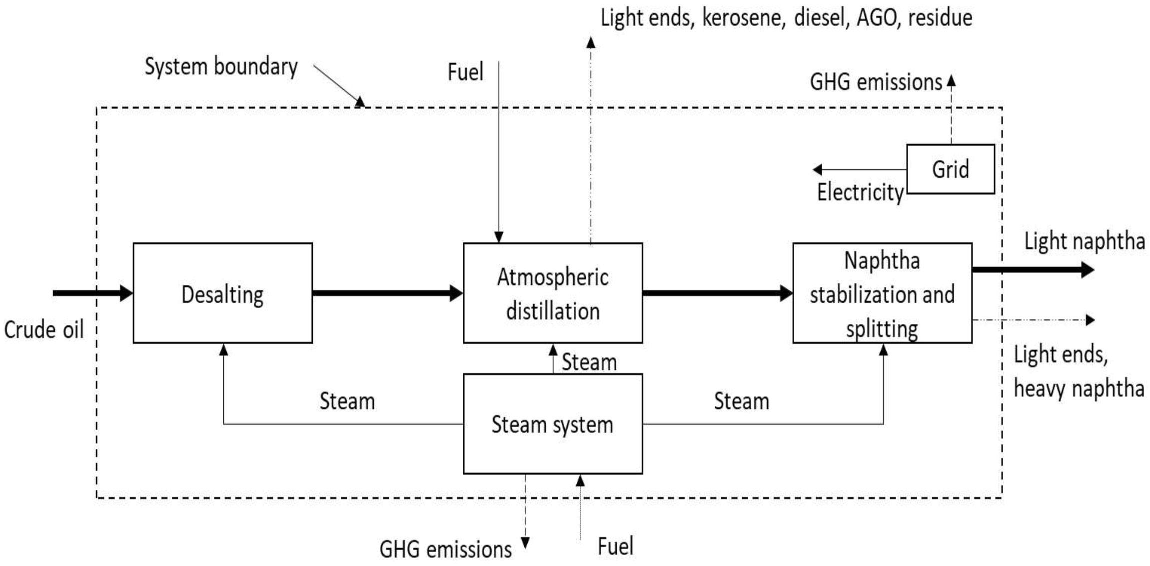

Figure F-8. System boundary for the naphtha production process

The product system shown in Figure F-8 is a multi-product system, therefore it is necessary to allocate energy consumption to the light naphtha stream. The allocation method proposed by Wang et al. (Wang et al. 2004) was used in this study. For any operation in the process, the cumulative energy consumed is allocated to stream p_1 as follows:

$$E_{p_1} = w_{p_1}\left(\sum H_{s_i} + E_p\right) \tag{D-1}$$

where:

E_{p_1}: cumulative energy consumption allocated to stream p_1
w_{p_1}: weight used to allocate the energy
H_{s_i}: incoming energy allocated to stream i
E_p: process energy

Mass-based allocation was used in this study. The reasons for this choice are twofold. First, energy consumption is usually proportional to the mass of the products processed (Wang et al. 2004), and second, the functional unit associated with the final product is mass-based; therefore, mass allocation seems to be a rational choice over an energy-content weighting approach. The weight for each operation in the process is defined as the ratio between the mass flow of the stream product associated with light naphtha production and the mass flow of all the product streams. The mass flows were obtained from the process simulation. The calculated weights are shown in Table F-3.

Table F-3. Allocation weight for each operation in the naphtha production process

Operation	Stream associated with light naphtha	Product streams	Weight
Desalting	Desalted crude oil	Desalted crude oil	1.00
Atmospheric distillation	Naphtha	Light ends, naphtha, kerosene, diesel, AGO, residue	0.20
Naphtha stabilization	Stabilized naphtha	Light ends, stabilized naphtha	0.71
Naphtha splitting	Light naphtha	Light naphtha, heavy naphtha	0.52

Figure F-9 shows the system boundary for the ammonia production process. GHG emissions from the combustion of natural gas fuel in the reformer, from electricity production, and generated in the process were accounted for in the inventory analysis. It is assumed that all the steam required in the process is generated by recovering waste heat; therefore, no emissions associated with steam production are included in the inventory. For the sake of completeness, the upstream emissions due to the production of natural gas used as feedstock for ammonia production were included.

The requirement of natural gas as feedstock in the ammonia production process used in this study was 0.56 kg natural gas/kg NH_3, according to data in Boulamanti et al. (Boulamanti and Moya 2017) (22-25 MJ/kg NH_3) and a heating value of natural gas of 42-55 MJ/kg.

The direct emissions from the ammonia production process and the methane requirement in the feedstock were estimated according to the overall reaction shown in Equation D-2. This reaction includes the primary and secondary reforming and the shift conversion.

$$0.88CH_4 + 1.26\,Air + 1.24H_2O \rightarrow 0.88CO_2 + N_2 + 3H_2 \qquad \text{(D-2)}$$

GHG emissions from the production of natural gas were retrieved from the literature. Roman-White et al. report the life cycle GHG emissions of natural gas (Roman-White et al. 2019). The system boundary includes all the value chains from extraction to export as liquid natural gas. In this study, the focus is extraction, gathering and boosting, processing, and domestic transportation. The emissions from these operations were estimated at 149 kg CO_2eq/MWh natural gas for production in the Gulf Coast. Considering a heat value of 50 MJ/kg, the GHG emissions are expressed as 2.07 kg CO_2eq/kg natural gas.

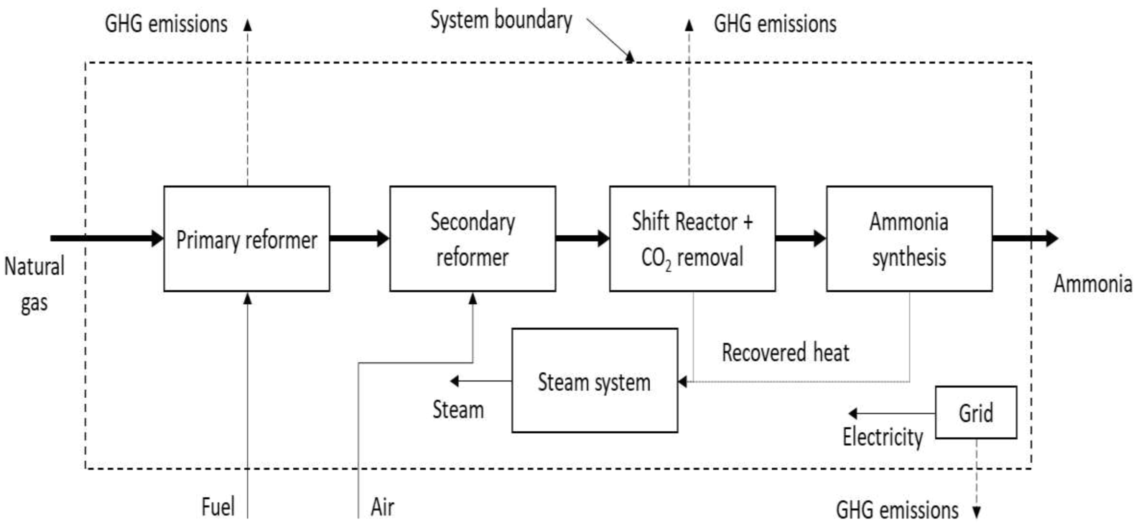

Figure F-9. System boundary for the ammonia production process

Figure F-10 shows the system boundary for the propylene production process. Note that only the GHG emissions from the combustion of fuel in the cracking furnace and those associated with electricity production were considered in the inventory analysis. This is because the process is energy-neutral in terms of thermal energy, e.g., no fuel is imported, either for process energy or steam generation (Ren et al. 2006; Ren et al. 2008).

In the naphtha steam cracking process, the methane-rich and hydrogen-rich streams and other fuel-grade by-products like ethane and propane are used as fuel in the furnace and boilers to provide the process energy. This energy accounts for 20-25% of the energy content of naphtha and is used to provide the energy for the endothermic cracking reaction, to produce steam to run the compressors, and to provide heat to the separation step (Ren et al. 2006). In this study, it was assumed that the energy provided by the combustion of fuel-grade by-products corresponds to 23% of the naphtha energy content, which was assumed to be 44.0 MJ/kg naphtha. Also, based on the process yield shown in Table F-4, the energy supplied by the combustion of the separated methane and hydrogen, e.g., the fuel gas in Figure F-10 was estimated. Then, we calculated the energy deficit that is supplied by the combustion of ethane and propane. The results are presented in Table F-5.

Once the energy supplied by ethane and propane was known, the required amount of each gas was calculated assuming they supply energy in the same proportion. Finally, the direct emissions of CO_2 from the combustion of methane, ethane, and propane were calculated.

Regarding electricity, Ren et al. reported a primary energy consumption of 1.0 MJ/kg ethylene, with a production efficiency of 40%. These values were used in this study but expressed in terms of produced propylene based on a propylene-to-ethylene ratio of 0.48 according to data in Table F-4. The energy consumption and GHG emissions were allocated to propylene on a mass basis. The aggregated data was allocated using the overall yield of propylene. The weight factor, i.e., 0.23, was calculated as the propylene-to-HVC mass ratio.

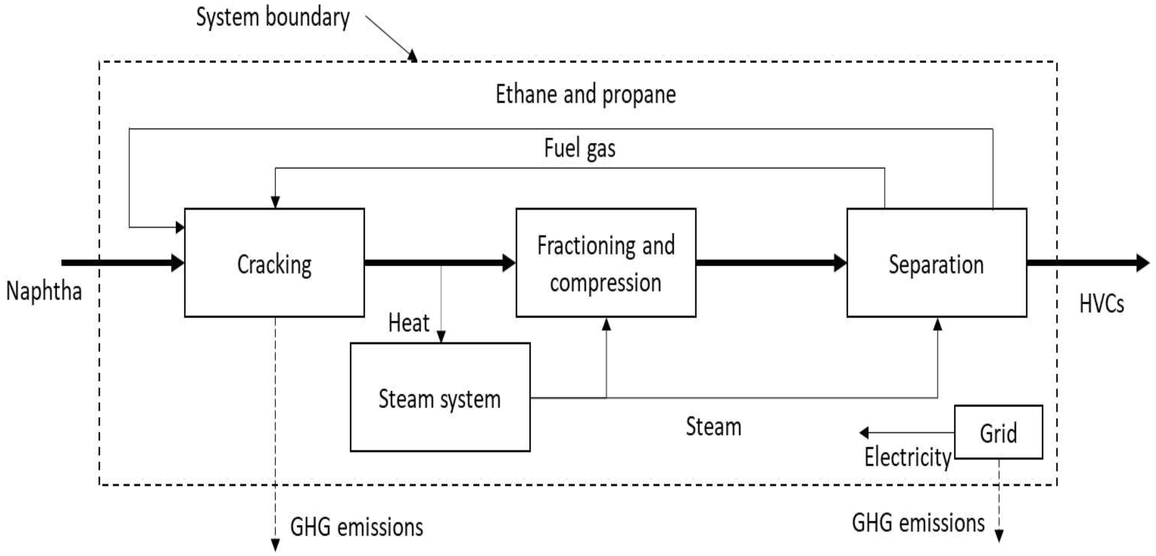

Figure F-10. System boundary for the propylene production process

Table F-4. The yield of the naphtha steam cracking process

Product	Yield (wt.%)	
	Ren et al. (Ren et al. 2006)	Used in this study
HVCs		
Ethylene	29-34	30
Propylene	13-16	14.5
Butadiene	4-5	4.5
Aromatics and C4+	10-16	13
Other		
Methane	13-14	13.5
Hydrogen	1	1

Table F-5. The energy supplied by the combustion of fuel-grade by-products

Energy	Value
The energy supplied by fuel-grade by-products	10.1 MJ/kg naphtha
The energy supplied by methane	6.8 MJ/kg naphtha
The energy supplied by hydrogen	1.2 MJ/kg naphtha
Energy deficit	2.1 MJ/kg naphtha

Figure F-11 presents the system boundary for the acrylonitrile production process. The GHG emissions accounted for in the analysis correspond to the combustion of fuel for the incineration of by-products, the production of electricity used in the process, and process emissions generated in the reaction.

According to Boulamanti et al, 1.09 kg propylene and 0.50 kg NH_3 are required to produce one kilogram of ACN; this is equivalent to an ammonia-to-propylene ratio of 0.46 (Boulamanti and Moya 2017).

The ammoxidation of propylene is a highly exothermic reaction, and the heat of the reaction produces enough steam to cover the needs of the plant (heat for the separation columns and to drive the reaction air compressor, for example) and for export. Moreover, the by-products acetonitrile and HCN are usually incinerated, and heat is recovered for preheating streams or steam production. For these reasons, the production of steam is not considered to generate GHG emissions.

The process emissions correspond to the CO_2 generated during the ammoxidation reaction, along with the emissions from the incineration of by-products and unreacted propylene (Hansora 2013). The propylene conversion to CO, CO_2, acetonitrile, and HCN, as well as the unreacted propylene, are shown in Table D-6.

To estimate the GHG emissions from the incineration of by-products, we need to quantify the amount of by-products generated. The Intergovernmental Panel on Climate Change (IPCC) reported a production of 18.5 kg acetonitrile/t ACN and 105 kg HCN/t ACN, based on process-specific acrylonitrile yield data (70%) and feedstock consumption (1.09 t propylene/t ACN) (IPCC 2006). With the propylene conversion data shown in Table D-6, a production of 33 kg acetonitrile/t ACN and 113 kg HCN/t ACN was estimated.

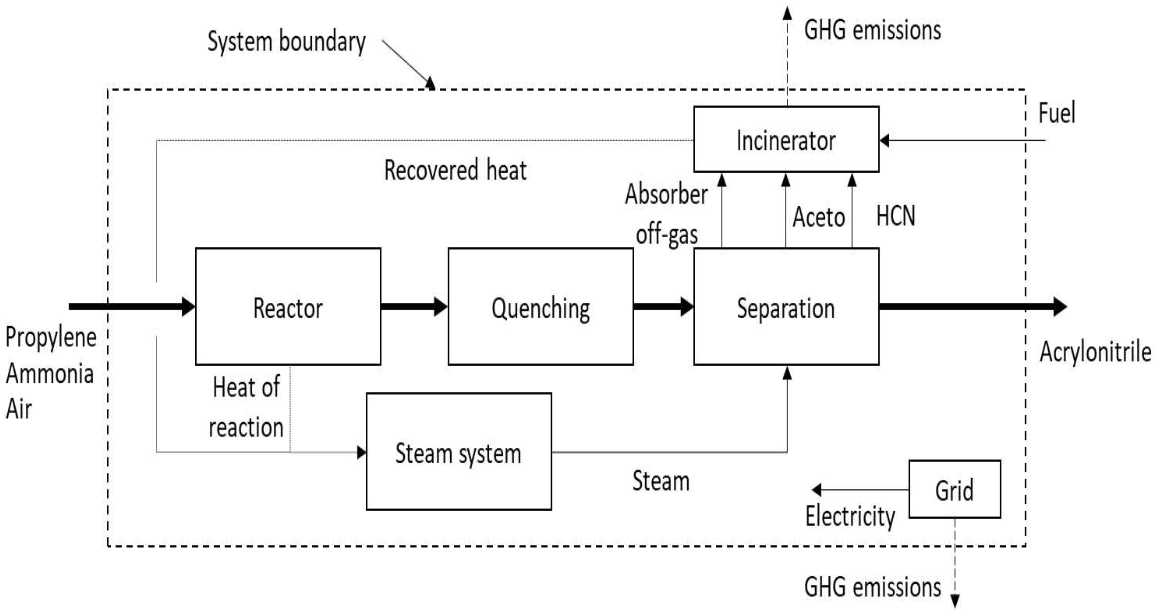

Figure F-11. System boundary for the acrylonitrile production process

Table F-6. Propylene conversion yield (Hansora 2013)

Product	Propylene conversion yield
ACN	80%
Acetonitrile	2.3%
HCN	5.9%
Acrylic acid	1.5%
Acrolein	0.7%
Acetic acid	0.2%
CO_2	5.1%
CO	2.9%
Unreacted propylene	1.4%

Regarding energy consumption in the production of PAN and PAN-CF, there is a wide variation in the results reported in the literature. The energy consumed by the manufacturing of PAN ranges from 10.84 to 65.87 kWh/kg PAN and for PAN-CF from 21.4 to 68.67 kWh/kg CF, as shown in Table F-7. For this study, the data provided by Das (Das 2011) was used because this author specified the unit operations considered in the production of PAN and PAN-CF. The PAN process includes continuous suspension polymerization followed by deaeration, filtration, and spinning of the dope into a coagulation bath. Following coagulation, the fiber is washed, stretched, lubricated, and dried. The solvent diffused into the coagulation bath is recovered by evaporation and recycled to the process. The PAN-CF process includes the stabilization of the PAN fibers, carbonization of the stabilized fibers, electrolyte surface treatment, and sizing of the carbon fibers. The off-gases of stabilization and carbonization operations are incinerated before venting to the atmosphere. The yield of the PAN process was considered 50 wt.%, that is, 2.00 kg of PAN are required to produce one kg of PAN-CF (Morgan 2005; Park and Heo 2015).

Table F-7. Literature data for energy consumption in the production of PAN and PAN-CF

Reference	PAN/CF production energy consumption kWh/PAN or kWh/kg CF	Comments
Suzuki and Takahashi (Suzuki and Takahashi 2005)	10.84 for PAN; 68.67 for CF	The authors reported 10.84 kWh/kg CF as the energy for raw material production. PAN was assumed as the raw material, but the system boundary is not clear.
Das (Das 2011)	65.87 for PAN; 21.4 for CF	From personal communication with MGA-Advanced Composites and Engineering.
Ghosh et al. (Ghosh et al. 2021)	15.15 for PAN; 44.59 for CF	PAN conversion efficiency from Das (Das 2011) and electricity data from Nunna et al. (Nunna et al. 2019); CF data from personal communication with Deakin University.

Reference	PAN/CF production energy consumption kWh/PAN or kWh/kg CF	Comments
Zanner	30-45	Includes PAN production. Personal communication with the production manager of EPC Engineering & Technology.
Harper International (Harper International)	68.52	Only CF production. Without heat recovery. Annual capacity: 1500 t CF.

F.4 Results of the PAN-CF life cycle GHG emissions estimation

Table F-8. Input-to-output ratio and output requirement per kg CF for each stage in the PAN pathway

Process	Input/output	Requirement per functional unit
Crude oil production	-	1.73 bbl crude oil/kg CF
Naphtha production	0.10 bbl crude oil/kg naphtha	18.2 kg naphtha/kg CF
Propylene production	6.89 kg naphtha/kg propylene	2.64 kg propylene/kg CF
Ammonia production	0.56 kg natural gas/kg ammonia	1.21 kg ammonia/kg CF 0.68 kg natural gas/kg CF
Acrylonitrile production	1.09 kg propylene/kg ACN	2.42 kg ACN/kg CF
	0.50 kg ammonia/kg ACN	
PAN production	1.21 kg ACN/kg PAN	2.00 kg PAN/kg CF
Carbon fiber production	2.00 kg PAN/kg CF	1.00 kg CF/kg CF

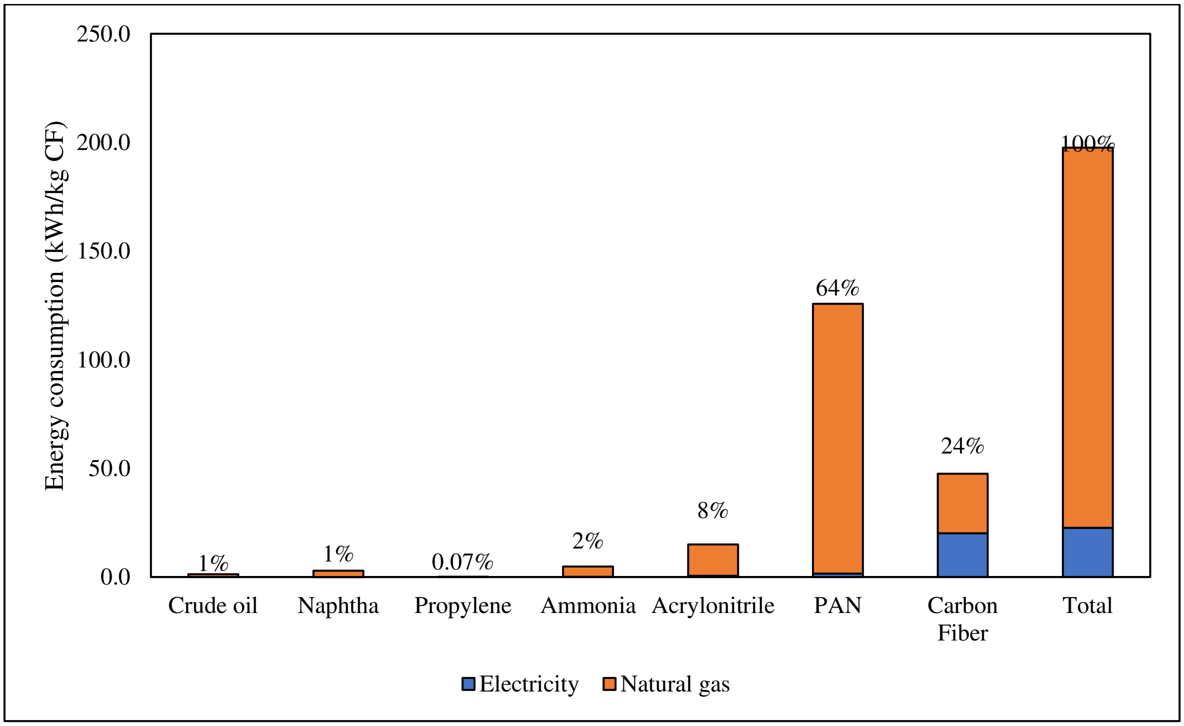

Figure F-12. Breakdown of the PAN-CF life cycle energy consumption

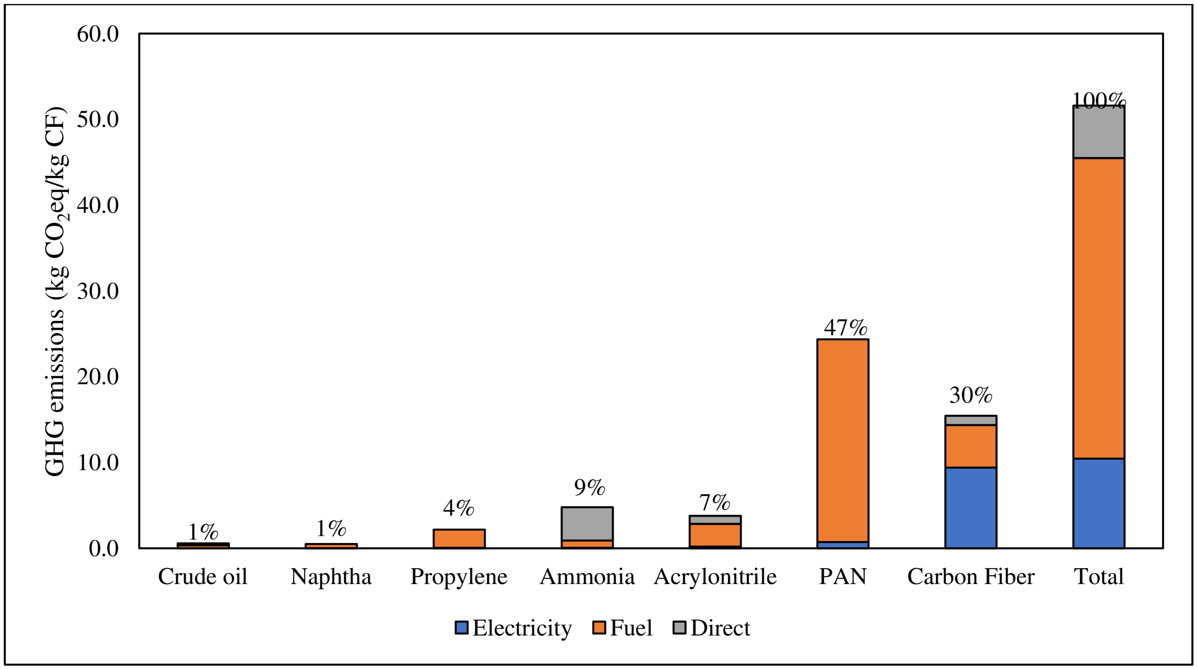

Figure F-13. Breakdown of the PAN-CF life cycle GHG emissions